

Removal of textile dyes from aqueous solution using reactive adsorption

Submitted in
fulfillment of the requirements for the degree of
Doctor of Philosophy

by

Komal Sharma
(ID No.: 2014RCH9051)

Under supervision of

Dr. Raj K. Vyas
Dr. Ajay K. Dalai



Department of Chemical Engineering
Malaviya National Institute of Technology Jaipur
Jaipur, India

March 2018

DECLARATION

I, **Komal Sharma**, declare that this thesis titled “**Removal of Textile Dyes from Aqueous Solution using Reactive Adsorption**” and the work presented in it, are my own. I confirm that:

- This work was done wholly or mainly while in candidature for a research degree at this university.
- Where any part of this thesis has previously been submitted for a degree or any other qualification at this university or any other institution, this has been clearly stated.
- Where I have consulted the published work of others, this is always clearly attributed.
- Where I have quoted from the work of others, the source is always given. With the exception of such quotations, this thesis is entirely my own work.
- I have acknowledged all main sources of help.
- Where the thesis is based on work done by myself, jointly with others, I have made clear exactly what was done by others and what I have contributed myself.

Date:

(Komal Sharma)
2014RCH9051

CERTIFICATE

This is to certify that the thesis entitled “**Removal of Textile Dyes from Aqueous Solution using Reactive Adsorption**” being submitted by **Ms. Komal Sharma (ID No.: 2014RCH9051)** is a bonafide research work carried out under my and Dr. Ajay K. Dalai’s supervision and guidance in fulfillment of the requirement for the award of the degree of **Doctor of Philosophy** in the department of Chemical Engineering, Malaviya National Institute of Technology Jaipur, India. The matter embodied in this thesis is original and has not been submitted to any other University or Institute for the award of any other degree.

Place: Jaipur

Date:

Dr. Raj K. Vyas

(Associate Professor)
Dept. of Chemical Engineering
M.N.I.T. Jaipur, India

Acknowledgement

It is a matter of pleasure for me to express my deep feelings of gratitude and sincere thanks to my guides **Dr. Raj K. Vyas**, MNIT Jaipur, India and **Dr. Ajay K. Dalai**, University of Saskatchewan, Canada for their inspiring guidance, ever enthusiasm and parental care have been an invaluable assets throughout my dissertation work. Their constant encouragement and valuable suggestion for my improvement have been of great help in preparing this report.

I am also thankful to **Dr. Kailash Singh** (Head of the Department) and all the faculty members of department for their invaluable guidance and encouraging me during my research work. I am especially desirous of acknowledging the entire **D.R.E.C. members, Dr. Kailash Singh, Dr. Prabhat Pandit, and Dr. V. K. Saharan**; for their inspiring advice, immense help, whole hearted support and constant encouragement throughout the tenure the research work.

I am very grateful to **Dr. A. B. Gupta** for making me aware about social problems and for addressing them in my research. I also want to give heartfelt thank to **Dr. Sumanta Kumar Meher**, Department of Chemistry, MNIT Jaipur for sharing knowledge. I am thankful to the Indian Institute of Chemical Technology (IICT), Hyderabad and Material Research Centre, MNIT Jaipur for their help in carrying out analysis.

I express my gratitude towards **Late Prof. S. N. Vyas** (IIT Bombay) for always being a guiding light to my path. I am also especially thankful to my **Parents, Mrs. Premlata Jangid, Mr. Mahesh Jangid and Mrs. Omana Vishwnathan, Mr. N. Vishwnathan** and my **Husband, Mr. Vishal Vishwnathan** for providing me the financial support, constant inspiration, enthusiasm and co-operation for my research work. I also thankful to my **Siblings, Ms. Saloni Sharma, Mr. Siddharth Jangid, and Ms. Vidhya Vishwnathan** for their regular suggestions and help made my work easy and proficient.

I am highly grateful to my **Landlord, Mrs. & Mr. Rajendra Kumar Sharma and their family**, who always made me feel like home. I am thankful to all my **Friends and colleagues, Mr. Ajay Sujana, Mr. Rakesh Baghel, Ms. Kritika Mathur, Ms. Swati Dubey, Ms. Akanksha Shukla, Ms. Jyoti Mev, Ms. Archana Dhakar, and Mr. Pankaj Kathania** for their help and suggestion during my research work. Last but not least I express gratitude all other people who knowingly, unknowingly helped me in this tenure.

I would like make a very special mention for a very special person who was the strongest force which encouraged me to complete my research work, **my daughter “Manaswini”**.

Komal Sharma

Abstract

In this study, granular activated carbon doped with iron (Fe-GAC) was prepared. Fe-GAC tested for removal of Methylene Blue and Safranin O in single and binary solute system from aqueous solution using reactive and plain adsorption processes. Fe-GAC was characterized by using transmission electron microscope coupled with energy dispersive spectroscopy (TEM) with EDS), X-ray diffraction (XRD) and BET surface area analysis.

For Methylene Blue, equilibrium adsorption isotherms, kinetics and thermodynamics were investigated for plain adsorption. The removal efficiencies of H₂O₂, Co-GAC, Co-GAC/H₂O₂, GAC, GAC/H₂O₂, Fe-GAC, Fe-GAC/H₂O₂ were observed as 6%, 8%, 13%, 40%, 41%, 25%, 94% respectively. Higher Methylene Blue removal was achieved due to the hydroxyl radical induced oxidative degradation in the presence of Fe-GAC / H₂O₂ at natural pH. Complete oxidative degradation of the dye was achieved in the presence of Fe-GAC / H₂O₂ catalyst in 3 h. Methylene Blue removal rate using reactive adsorption was almost four times faster than adsorption. Thermodynamic parameters revealed that enthalpy change for reactive adsorption was approximately one-third that of adsorption indicating reactive adsorption to be superior. Electrospray ionization mass spectroscopy (ESI-MS) analysis showed that reactive degradation of Methylene Blue molecule followed demethylation and hydroxylation processes. The process of reactive adsorption was further investigated by identifying compounds using desorption from spent Fe-GAC through ESI-MS. It is believed that the recovery and identification of such degraded compounds may be commercially attractive. Therefore, an oxidative degradation pathway and a reactive adsorption scheme have been proposed in this study.

In case of Safranin O, Fe-GAC and H₂O₂ doses were optimized to obtain maximum removal of Safranin O. Maximum removal was found to be 96.1% (initial Safranin O concentration: 10 mg/L) using 1.0 g/L Fe-GAC and 5.0 mM H₂O₂ doses for 5 h. Kinetic study revealed that pseudo-first-order kinetics explains the experimental data well for the reactive adsorption. Safranin O adsorption onto Fe-GAC was represented by Langmuir isotherm. Parallel pore reactive adsorption model has been applied for the reactive adsorption of Safranin O. For the purpose of model validation, adsorption and reactive adsorption predicted results were compared with experimental data. By fitting the experimental data to the model, it is observed that the surface reaction rate coefficient, k_r was found to be 5 times that of the apparent rate constant,

k_{app} . The requisite parameters such as the external liquid film mass transfer coefficient, macropore and micropore diffusivities were estimated by regression analyses. Furthermore, pore diffusion was found to be the rate controlling factor in pure adsorption whereas it was surface reaction in case of reactive adsorption. ESI-MS analysis showed that reactive degradation of Safranin O molecule followed hydroxylation and ring cleavage processes. An oxidative degradation pathway has also been proposed for Safranin O.

Simultaneous reactive adsorption of Methylene Blue and Safranin O was carried out from a binary mixture using Fe-GAC / H₂O₂. Fe-GAC and H₂O₂ doses were optimized to obtain maximum removal of Methylene Blue and Safranin O. Maximum simultaneous removal was found to be 96.2% and 90.2% for Methylene Blue and Safranin O respectively after 7 h of reactive adsorption using 0.5 g/L Fe-GAC and 2.0 mM H₂O₂ doses. Degradation activities of the dyes were accelerated by increasing temperature from 15 to 35 °C. Apparent kinetic reaction rate constant was also increased with increasing temperature and consequently, activation energies of the degradation of individual dyes present in the mixture were estimated and found to be 28.59 kJ mol⁻¹ and 32.53 kJ mol⁻¹ for Methylene Blue and Safranin O respectively. Thermodynamic parameters for Methylene Blue and Safranin O activation were also assessed for the degradation process. A thermodynamic study and ESI-MS analysis revealed that molecule of Safranin O is more difficult to remove than Methylene Blue. Degradation pathways for Methylene Blue and Safranin O have been proposed which indicate that the dyes were degraded via demethylation and hydroxylation processes.

The simultaneous adsorptive removal of Methylene Blue and Safranin-O was studied using iron oxide coated activated carbon. A statistical-based technique central composite design (CCD) using response surface methodology (RSM) was employed to evaluate the individual and synergetic effect of influence of the process key variables such as contact time (min), adsorbent dosage (g/L), Methylene Blue concentration (mg/L) and Safranin O concentration (mg/L), pH, on the removal percentages of Methylene Blue and Safranin-O as responses and optimized values were found to be 120 min, 1.2 g/L, 2 mg/L, 4 mg/L and 8.5 respectively. Pseudo-first-order model, Pseudo-second-order model and intraparticle diffusion models were studied. Kinetic study reveals that intraparticle diffusion model explains well the experimental data with 0.99 correlation coefficient value (R^2). The intraparticle diffusion model straight line intercept of

Methylene Blue was positive and Safranin O was negative suggesting that Methylene Blue adsorption occurs faster as compared to Safranin O diffusion. Extended Langmuir and Extended Freundlich isotherm models were studied out of which extended Freundlich model was found suitable due to higher R^2 (>0.985). A film solid pore diffusion model was developed and used to predict the surface mass transfer coefficient (k_L) and diffusion coefficient (D) for binary dye system containing Methylene Blue and Safranin O. The k_L values obtained were 5.9×10^{-5} m/s and 3.0×10^{-5} m/s and D were found to be 2.2×10^{-11} m²/s and 1.9×10^{-11} m²/s for Methylene Blue and Safranin-O respectively. k_L and D values were in agreement with the experimental data that suggested Methylene Blue removal is faster than Safranin O during binary dye adsorption. Film mass transfer coefficients, $k_{L,1}$ and $k_{L,2}$ for reactive adsorption were found to be 1.5 and 2 times respectively when compared to adsorption film mass transfer coefficient data. Surface reaction rate constants $k_{r,1}$ and $k_{r,2}$ were found to be 5 times of their corresponding k_{app} values in binary dye reactive adsorption.

Table of contents

Declaration	i
Certificate.....	ii
Acknowledgement	iii
Abstract	iv
Table of contents.....	vii
List of Figures.....	xiii
List of Tables	xvii
List of Abbreviations	xix
1 Introduction.....	1
1.1 Dyes and problems associated with dying effluents	1
1.2 Production of dyes and their discharge statistics	2
1.3 Fate of cationic dyes and their harmful effects	2
1.3.1 Methylene Blue.....	2
1.3.2 Safranin O.....	3
1.4 Available waste water treatment technologies.....	3
1.5 Brief statement of the problem.....	4
1.6 Brief accounts of existing knowledge and scope of work.....	4
1.7 Inadequacy in existing research knowledge.....	5
1.8 Research objectives	6
1.9 Research outline	6
1.10 Thesis organization summary.....	10
2 Literature review	12
2.1 Dyes.....	12
2.2 Classification of dyes	12

2.2.1	Classification based on the type of raw material	12
2.2.1.1	Natural dyes	12
2.2.1.2	Synthetic dye	12
2.2.2	Classification based on chemical structure	13
2.2.3	Classification of dyes based on their nuclear structure.....	14
2.2.3.1	Cationic dyes	14
2.2.3.2	Anionic dyes	14
2.2.4	Classification based on application of dyes	14
2.3	Multicomponent dye adsorption system	16
2.3.1	Quantitative determination of dyes in a multicomponent mixture	16
2.3.1.1	Derivative spectroscopy	17
2.3.1.2	Chemometric methods.....	19
2.3.2	Effects of various parameters on adsorptive removal of dyes from multicomponent systems	24
2.3.2.1	Adsorbent dose	30
2.3.2.2	Initial dye concentration	32
2.3.2.3	Molecular dimension of dye	33
2.3.2.4	Temperature.....	39
2.3.2.5	pH	39
2.3.2.6	Salt content	43
2.3.2.7	Presence of major cations and anions.....	44
2.3.3	Equilibrium relationship for dyes in multicomponent adsorption system	44
2.3.3.1	Extended Langmuir isotherm	45
2.3.3.2	Jain and Snoeyink modified extended Langmuir model	46
2.3.3.3	Extended Freundlich isotherm.....	46

2.3.3.4	Sheindorf-Rebuhn-Sheintuch equation.....	47
2.3.3.5	Ideal adsorbed solution theory.....	48
2.3.3.6	P-factor	48
2.3.3.7	Interaction factor.....	49
2.3.4	Mathematical modeling of multicomponent batch sorption	52
2.4	Reactive adsorption of organic pollutants.....	54
2.4.1	Brief account of existing work done on reactive adsorption	55
2.4.2	Reactive adsorption of dye using Fe-GAC/H ₂ O ₂ system	56
3	Materials and Methods.....	57
3.1	Materials.....	57
3.1.1	Synthesis of Fe-GAC	58
3.2	Methods and techniques	58
3.2.1	Details of instruments used during experiments and aqueous phase analysis	58
3.2.1.1	Analytical weighing balance	58
3.2.1.2	Oven.....	58
3.2.1.3	pH meter	59
3.2.1.4	Incubator shaker	59
3.2.1.5	UV-Vis spectrophotometer.....	60
3.2.1.6	Electrospray ionization coupled with mass spectroscopy (ESI-MS).....	60
3.2.2	Characterization techniques for adsorbent.....	61
3.2.2.1	Transmission electron microscope coupled with energy dispersive spectroscopy (TEM-EDS).....	61
3.2.2.2	BET surface area	61
3.2.2.3	X-ray diffraction (XRD).....	61
3.3	Batch reactive adsorption studies.....	61

3.4	Batch adsorption studies.....	62
3.5	Reactive adsorption	63
3.5.1	Kinetics	63
3.5.1.1	First order reaction kinetics	63
3.5.1.2	Second order reaction kinetics.....	63
3.5.2	Thermodynamics.....	63
3.6	Adsorption.....	65
3.6.1	Equilibrium isotherm for single component	65
3.6.1.1	Langmuir isotherm	65
3.6.1.2	Freundlich isotherm.....	66
3.6.2	Equilibrium isotherm for binary component.....	66
3.6.2.1	Extended Langmuir isotherm	66
3.6.2.2	Extended Freundlich isotherm.....	66
3.6.3	Kinetics	66
3.6.3.1	Pseudo-first-order kinetics.....	67
3.6.3.2	Pseudo second order	67
3.6.3.3	Intraparticle diffusion model	68
3.6.4	Thermodynamics.....	68
3.7	Error analysis - sum of squares of errors.....	68
4	Results and discussion	69
4.1	Catalyst characterization	69
Part I: Reactive adsorption and adsorption		73
4.2	MB removal efficiencies of different systems	73
4.3	Optimization of MB reactive adsorption conditions	74
4.4	Removal efficiencies of SO in single dye system	77

4.5	Removal efficiencies of MB and SO in binary dye system	78
4.6	Batch reactive adsorption studies.....	79
4.6.1	Kinetics of reactive adsorption decoloration	79
4.6.1.1	Methylene Blue in single dye system	79
4.6.1.2	Safranin O in single dye system	81
4.6.1.3	Methylene Blue and Safranin O in binary dye system	82
4.6.2	Thermodynamics of reactive adsorption.....	84
4.6.2.1	Methylene Blue in single dye system	84
4.6.2.2	Methylene Blue and Safranin O in binary dye system	85
4.7	Reaction mechanism	88
4.8	Oxidative degradation study using ESI-MS.....	89
4.8.1	Methylene Blue in single dye system	89
4.8.2	Safranin O in single dye system.....	97
4.8.3	Methylene Blue and Safranin O in binary dye system	100
4.9	Batch adsorption studies.....	105
4.9.1	Methylene Blue in single dye system	105
4.9.1.1	Equilibrium study of Methylene Blue	105
4.9.1.2	Kinetic study of Methylene Blue.....	107
4.9.1.3	Thermodynamic study of Methylene Blue	110
4.9.2	Safranin O in single dye system.....	112
4.9.2.1	Equilibrium study of Safranin O	112
4.9.3	MB and SO binary dye system	114
4.9.3.1	Equilibrium study of Methylene Blue and Safranin O in binary dye system	114
4.9.3.2	Kinetic study of Methylene Blue and Safranin O in binary dye system	117
Part II: Modeling.....		122

4.10	Central Composite Design (CCD) and response surface methodology (RSM)	122
4.11	SO adsorption and reactive adsorption modeling.....	128
4.12	Binary adsorption and reactive adsorption modeling.....	138
4.13	Economic analysis.....	151
5	Conclusions.....	153
	Future recommendations.....	155
	References.....	156
	Appendices.....	181

List of Figures

Figure 1.1: An overview of batch study for MB removal using adsorption and reactive adsorption	7
Figure 1.2: An overview of batch study for SO removal using adsorption and reactive adsorption	8
Figure 1.3: An overview of batch study for simultaneous MB and SO removal using adsorption and reactive adsorption	9
Figure 2.1: Spectral overlap of Acid Blue 25 (AB) and Direct Blue 86 (DB) in single and binary solutions (a) Zero order absorption spectra and (b) First order derivative spectra	19
Figure 2.2: Quantitative chemometric methods	20
Figure 2.3: Effect of initial dye concentration on dye removal from single and binary systems by PAN25% w/w EDA nanofiber ((A) Direct Red 80 (single), (B) Direct Red 23 (single), (C) Direct Red 80 (binary), (D) Direct Red 23 (binary))	33
Figure 2.4: Time-dependent UV–vis spectra of mixture of Methyl Orange (MO) / Methylene Blue (MB) in the presence of PANF-g-HPEI pretreated at pH (A) 5 and (B) 10	41
Figure 4.1: TEM of (a) GAC and (b) Fe-GAC	69
Figure 4.2: EDS analysis of (a) GAC and (b) Fe-GAC	70
Figure 4.3: XRD patterns of GAC and iron-loaded GAC after impregnation with solution of iron (III) chloride	71
Figure 4.4: Time profiles and removal efficiency of MB over H ₂ O ₂ , Co-GAC, Co-GAC/H ₂ O ₂ , GAC, GAC/H ₂ O ₂ , Fe-GAC, Fe-GAC/H ₂ O ₂	74
Figure 4.5: Effect of adsorbent dose on dye removal using Fe-GAC/H ₂ O ₂ at different time intervals	75
Figure 4.6: Effect of initial dye concentration on dye removal using Fe-GAC/H ₂ O ₂ at different time intervals	75
Figure 4.7: Effect of H ₂ O ₂ dose on dye removal using Fe-GAC/H ₂ O ₂ at different time intervals	76
Figure 4.8: % SO removal efficiencies in aqueous solution at pH 6.5 with various dosages of H ₂ O ₂ and Fe-GAC with C ₀ = 10 mg/L after 5 h at 30 °C	78
Figure 4.9: % dye removal efficiencies in binary mixture at pH 6.5 with various dosages of H ₂ O ₂ and Fe-GAC with C ₀ = 5 mg/L for each dye after 7 h	79
Figure 4.10: Pseudo-first-order plot for reactive adsorption kinetics of MB.	80

Figure 4.11: Pseudo-second-order plot for reactive adsorption kinetics of MB.....	80
Figure 4.12: Pseudo-first-order plot for reactive adsorption kinetics of SO.....	81
Figure 4.13: Pseudo-second-order plot for reactive adsorption kinetics of SO.....	82
Figure 4.14: Plots of MB (a) pseudo first-order-kinetics, (b) pseudo second-order-kinetics, during reactive adsorption of binary dye mixture.	83
Figure 4.15: Plots of SO (a) pseudo-first-order-kinetics, (b) pseudo-second-order-kinetics, during reactive adsorption of binary dye mixture.	83
Figure 4.16: Effect of temperature on the apparent rate constant of MB.	85
Figure 4.17: Effect of temperature on the apparent rate constant of MB for simultaneous reactive adsorption using Fe-GAC/H ₂ O ₂ system at pH 6.5.....	86
Figure 4.18: Effect of temperature on the apparent rate constant of SO for simultaneous reactive adsorption using Fe-GAC/H ₂ O ₂ system at pH 6.5.....	87
Figure 4.19: Oxidation-reduction process of GAC, iron and H ₂ O ₂	88
Figure 4.20. ESI-MS of (a) aqueous solution of MB before reaction (b) degradation products of MB using Fe-GAC after 1 h and (c) degradation products of MB using Fe-GAC after 3 h of reaction.....	91
Figure 4.21: Proposed oxidative degradation pathway of MB during reactive adsorption using Fe-GAC / H ₂ O ₂ system.	93
Figure 4.22: Changes in the UV–vis absorbance spectra of MB dye using Fe-GAC / H ₂ O ₂	94
Figure 4.23: Proposed scheme for MB reactive adsorption.....	95
Figure 4.24: ESI-MS of leached aqueous solution of spent Fe-GAC after MB reactive adsorption.	96
Figure 4.25: ESI–MS spectra of SO aqueous solution and its degradation products during reactive adsorption at (a) t = 0 h, (b) t = 1.5 h, and (c) t = 5 h.....	98
Figure 4.26: Proposed oxidative degradation pathways of SO in aqueous solution during reactive adsorption using Fe-GAC / H ₂ O ₂	99
Figure 4.27: ESI–MS spectra of binary mixture of MB and SO and its degradation products during reactive adsorption at (a) t = 0 h, (b) t = 2 h, and (c) t = 7 h.	102
Figure 4.28: UV–vis absorbance spectra of simultaneous removal of MB and SO using Fe-GAC / H ₂ O ₂	102

Figure 4.29: Proposed oxidative degradation pathways of MB and SO present in binary mixture during reactive adsorption using Fe-GAC / H ₂ O ₂	104
Figure 4.30. Langmuir isotherm of MB adsorption onto Fe-GAC.....	106
Figure 4.31: Freundlich isotherm of MB adsorption onto Fe-GAC.....	106
Figure 4.32: Pseudo-first-order kinetics of MB adsorption onto Fe-GAC.....	108
Figure 4.33: Pseudo-second-order kinetics of MB adsorption onto Fe-GAC.....	108
Figure 4.34: Intraparticle diffusion model of MB adsorption onto Fe-GAC.....	109
Figure 4.35. Plot of Gibbs free energy change, ΔG° versus temperature, T of MB adsorption onto Fe-GAC.....	110
Figure 4.36: Langmuir isotherm of SO adsorption onto Fe-GAC.....	113
Figure 4.37: Freundlich isotherm of SO adsorption onto Fe-GAC.....	113
Figure 4.38: Extended Langmuir isotherm fit for experimental versus model data of MB in binary dye adsorption onto Fe-GAC.....	114
Figure 4.39: Extended Freundlich isotherm fit for experimental versus model data of MB in binary dye adsorption onto Fe-GAC.....	115
Figure 4.40: Extended Langmuir isotherm fit for experimental versus model data of SO in binary dye adsorption onto Fe-GAC.....	116
Figure 4.41: Extended Freundlich isotherm fit for experimental versus model data of SO in binary dye adsorption onto Fe-GAC.....	116
Figure 4.42: Pseudo-first-order kinetics of MB in simultaneous binary dye adsorption.....	119
Figure 4.43: Pseudo-second-order kinetics of MB in simultaneous binary dye adsorption.	119
Figure 4.44: Intraparticle diffusion kinetics of MB in simultaneous binary dye adsorption.....	120
Figure 4.45: Pseudo-first-order kinetics of SO in simultaneous binary dye adsorption.	120
Figure 4.46: Pseudo-second-order kinetics of SO in simultaneous binary dye adsorption.	121
Figure 4.47: Intraparticle diffusion kinetics of SO in simultaneous binary dye adsorption.	121
Figure 4.48: Response surface contour plots of simultaneous MB decolorization (%) as the function of (a) Time and adsorbent and (b) SO and pH.	127
Figure 4.49. Response surface contour plots of simultaneous SO decolorization (%) as the function of (a) Time and adsorbent and (b) MB and pH.	127
Figure 4.50: SO concentration change in bulk during adsorption.	131
Figure 4.51: Concentration plots of SO in macropores during adsorption.	132

Figure 4.52: Concentration plots of SO in micropores during adsorption.....	132
Figure 4.53: SO concentration change in bulk during reactive adsorption.....	135
Figure 4.54: Concentration plots of SO reactive adsorption in macropores.....	136
Figure 4.55: Concentration plots of SO reactive adsorption in micropores.	137
Figure 4.56: Mechanisms of dye adsorption onto Fe-GAC.....	138
Figure 4.57: MB concentration change in bulk during adsorption and reactive adsorption of binary dyes.....	143
Figure 4.58: SO concentration change in bulk during adsorption and reactive adsorption of binary dyes.....	144
Figure 4.59: Concentration plots of MB in particle during binary dye adsorption.....	147
Figure 4.60: Concentration plots of SO in particle during binary dye adsorption.....	148
Figure 4.61: Concentration plots of MB in pores during reactive adsorption.	149
Figure 4.62: Concentration plots of SO in pores during reactive adsorption.	150

List of Tables

Table 2.1: Classification of dyes based on chromophoric groups	13
Table 2.2: Classification of dyes based on application.....	14
Table 2.3: Comparison between SVM and LS-SVM techniques	22
Table 2.4: Method used for simultaneous quantification of dyes.....	22
Table 2.5: Dyes and adsorbents studied in multicomponent adsorption systems.....	25
Table 2.6: Surface area of various adsorbents used in removal of mixture of dyes from wastewater.....	30
Table 2.7: General characteristics of various dyes.	35
Table 2.8: Effect of relative molecular volume of the constituents and the amount of sulfonic groups present in dye	37
Table 2.9: Favorable pH for dyes of different characteristics.	41
Table 2.10: Adsorption equilibrium of some dyes on various adsorbents.....	50
Table 3.1. Properties of dyes.....	57
Table 3.2: Specifications of electronic weighing balance	58
Table 3.3: Specifications of oven.....	58
Table 3.4: Specifications of pH meter	59
Table 3.5: Specifications of UV-Vis spectrophotometer.....	60
Table 3.6: Value of separation factor R_L	65
Table 4.1: Elemental analysis of GAC and Fe-GAC using EDS.....	71
Table 4.2: Thermodynamic parameters for reactive adsorption of MB.....	85
Table 4.3: Thermodynamic parameters for simultaneous reactive adsorption of MB and SO.....	87
Table 4.4: Related adsorption equilibrium parameters for the adsorption of MB on Fe-GAC at different temperatures.	107
Table 4.5: Kinetic parameters for the adsorption of MB onto the Fe-GAC at 30° C.....	109
Table 4.6: Thermodynamic parameters for adsorption of MB onto Fe-GAC.	111
Table 4.7: Comparison of the coefficients isotherm parameters for MB and SO adsorption onto Fe-GAC at optimum conditions.....	116
Table 4.8: Kinetic parameters for the simultaneous adsorption of MB and SO onto the Fe-GAC at 30° C.	118
Table 4.9: Process control variables and their limits	122

Table 4.10: Central composite design.....	123
Table 4.11: Analysis of Variance for the removal of MB (%R).....	124
Table 4.12: Analysis of Variance for the removal of SO (%R).....	125
Table 4.13: Parametric values of reactive adsorption model of SO.	131
Table 4.14: Parameters of pore surface diffusion model of binary dye mixture.	141
Table 4.15: Experimental particulars and Cost estimation of reactive adsorption and adsorption (Rs./mg of dye removal) for MB and SO dye removal.....	151

List of Abbreviations

k_{app}	Apparent rate constant, 1/min
A	Pre-exponential factor
E_a	Activation energy of reaction, kJ/mol
$\Delta G^\#$	Gibbs energy of reactive adsorption, kJ/mol
$\Delta H^\#$	Enthalpy of reactive adsorption, kJ/mol
$\Delta S^\#$	Entropy of reactive adsorption, kJ/mol K
C_0	Initial concentration of dye in liquid-phase, mg/L
C_e	Liquid-phase equilibrium concentration of dye, mg/L
q_e	Solid phase equilibrium concentration, mg/g
C_t	Liquid-phase concentration of dye at time t, mg/L
C_i	Liquid-phase concentration of dye at time t of i^{th} component, mg/L
q_t	Solid phase concentration at time t, mg/g
q_i	Solid phase concentration at time t of i^{th} component, mg/g
q_m	Maximum amount of dye per unit weight of adsorbent for complete monolayer coverage, mg/g
K_L	Equilibrium adsorption constant related to the affinity of binding sites, L/mg
K_F	Adsorption capacity of the adsorbent, (mg/g) (L/mg) ^{1/n}
k_1	First order rate constant, 1/min
k_2	Second order rate constant, g/mg min
n	Constant
R_L	Separation factor
k_{id}	Intra-particle diffusion rate constant, mg/g min ^{1/2}
C	Constant, mg/g
x_i, y_i, z_i	Multicomponent Freundlich adsorption constants, dimensionless
ΔG°	Gibbs energy of adsorption, kJ/mol
ΔH°	Enthalpy change of adsorption, kJ/mol
ΔS°	Entropy change of adsorption, kJ/mol K
K_e	Adsorption equilibrium constant

A	Total interfacial surface area, m^2
a	Interfacial surface area, m^2
C'	Molar liquid phase concentration, mol/m^3
C_s	Surface liquid phase concentration, mg/L
$C_{s,i}$	Surface liquid phase concentration of i^{th} component, mg/L
C_{sma}	Surface liquid phase concentration in macropore, mg/L
C_{smi}	Surface liquid phase concentration in micropore, mg/L
C_e	Liquid phase concentration at equilibrium, mg/L
D_i	Pore diffusivity coefficient of i^{th} component, m^2/s
D_{ma}	Macropore diffusivity coefficient, m^2/s
D_{mi}	Micropore diffusivity coefficient, m^2/s
f	Fraction of total adsorptive capacity in macropores
k_L	External liquid film mass transfer coefficient, m/s
$k_{L,i}$	External liquid film mass transfer coefficient of i^{th} component, m/s
k_r	Macropore surface reaction rate constant, $1/s$
$k_{r,i}$	Pore surface reaction rate constant of i^{th} component, $1/s$
N	Number of data points
q_{ma}	Solid-phase adsorbed concentration in macropores, mg/g
q_{mi}	Solid-phase adsorbed concentration in micropores, mg/g
$q_{s,ma}$	Solid-phase adsorbed concentration on macropores external surface, mg/g
$q_{s,mi}$	Solid-phase adsorbed concentration on micropores external surface, mg/g
$q_{s,i}$	Solid-phase adsorbed concentration of component i on pores external surface, mg/g
r	Radial variable, m
δ	Particle density, g/L
t	Time variable, s
V	Liquid phase volume, m^3
X	Experimental data

\bar{X}	Mean of experimental data
Y	Model simulated data
\bar{Y}	Mean of model simulated data

1.1 Dyes and problems associated with dying effluents

Dyes are organic entity which comprises of aromatic aryl rings that contain delocalized electron systems (Allen et al. 2004). Dyes are extensively used in textile, leather tanning, paper production, food, hair colorings industries, etc. (Gürses et al. 2016; Tan et al. 2007). Another application of these synthetic colored dyes is in ground water tracing to determine specific surface area of activated sludge, wastewater treatment, and sewage etc. (De Jesus da Silveira Neta et al. 2011; Yagub et al. 2014).

Chemical enters into natural aquatic systems by several means, viz. direct dumping of wastes coming from industries etc. and /or effluents from wastewater treatment plants with improper treatment. Moreover, huge quantities of these solutes are being found even after travelling long distances from their origin. Insufficient treatment of dyestuff containing effluents leads to color contamination of the environment such as soil and natural water bodies. Scarcity of potable water is one of the major threats for living beings due to chemical pollution of water which is caused by chemical contaminants from heavy metals, dyes, solvents, pesticides, etc. Even, low concentrated emissions lead to a considerable number of chronic effects that usually detected after a long period of time (Oller et al. 2011).

The presence of dye in water is prominently visible even at very low concentration. The intensity of color of a dye depends upon the number of functional groups present as its chromophore (Verma et al. 2012). The dye polluted wastewater is characterized by high biochemical and chemical oxygen demands (Ghaedi et al. 2015a; Liu et al. 2014). The presence of dyes in wastewater reduces sunlight penetration and resists photochemical action which creates problems in maintaining ecological balance. Their carcinogenic and toxic nature of chemical dyes causes damage to living organisms (Al et al. 2013; Sharma and Vyas 2015; Wong et al. 2004). Due to immense production, extensive application and uncontrolled discharge into water bodies, synthetic dyes create significant environmental pollution and may impact serious health-risk factors. Inflow of dye industrial effluents into the natural water bodies results in acute toxicity to

aquatic life (Verma 2008). The removal of these dyes from wastewater before discharging them into the mainstream is, therefore, essential.

1.2 Production of dyes and their discharge statistics

It has been predicted that the global textile market was worth 1557.1 billion USD with the production of more than 88.5 million tons per year till the end of 2015. The contribution of developing countries in the global textile market has reached to 58.6 % in terms of cost within last decade (Yacout et al. 2016). Most of the dyes used in textile processing are lacking in complete fixation of dyes to fabrics, and thus 20% of dyes enter the environment which produces dye-containing colored effluents (Nadejde et al. 2015; Rajoriya et al. 2017). The current world production of dyestuffs is about 10 million kg per year, approximately 2 million kg of active dye per year enter the biosphere, either in dissolved or suspended form in water (Allen et al. 2003).

1.3 Fate of cationic dyes and their harmful effects

Cationic or basic dyes come into category of toxic colorants. This class of dye can cause adverse effects like allergic dermatitis, skin irritation, mutations and cancer (Salleh et al. 2011). Among various classes of dyes, the highest toxicity is associated with the cationic dyes such as Methylene Blue and Safranin-O (Ghaedi et al. 2014).

1.3.1 Methylene Blue

Methylene Blue (MB) is a basic dye and numerous studies have considered MB (basic blue 9) as a model dye for the study of organic dye adsorption from aqueous solution. Caro discovered MB in 1878, MB is one of the most commonly used thiazine dyes (Almeida et al. 2009). It is a heterocyclic aromatic chemical compound with a molecular formula $C_{16}H_{18}N_3SCl$. The hydrated form contains 3:1 water and MB molecule respectively. In MB, positively charged nitrogen or sulfur centers are responsible for cationic nature of MB dye (Almeida et al. 2009). At room temperature, MB is a crystalline solid, odorless, dark green powder; it gives a blue solution on dissolving in water. It is very commonly used in biology and chemistry. In an aqueous solution, it dissociates into MB cation and its associated anion, chloride (El Qada et al. 2006).

MB is mostly found in textile dyeing industrial effluents. MB dye resists biological degradation even in the presence of sunlight and natural oxidizing agents (Hajjaji and El Arfaoui 2009). Furthermore, presence of MB in water bodies has harmful aesthetic effect. Contact of MB with skin due to chronic exposure may create effects like feeling of cold, redness or dryness. Ingestion through mouth may produce gastrointestinal irritation, discoloration of oral mucosa, mouth and throat, paleness of complexion, irritation of lips, lack of coordination or drowsiness (Anirudhan and Ramachandran 2015a; Ghosh and Bhattacharyya 2002). Accidental intake of large dose creates abdominal and chest pain, profuse sweating, severe headache, painful micturation, mental confusion, and methemoglobinemia (Ghosh and Bhattacharyya 2002). Acute exposure to MB may cause health problems like increased heart rate, vomiting, formation of Heinz bodies, shock, and cyanosis and tissue necrosis in humans (Özer et al. 2007; Verma 2008). For all mentioned reasons, effluents containing MB acquire environmental problem and therefore, it is important to develop proper and efficient treatment processes.

1.3.2 Safranin O

Safranin O (SO) (3,7-diamino-2,8-dimethyl-5 phenylphenazinium chloride) is among the oldest well known synthetic dyes and one of the most commonly used azine dye (El-Kemary and El-Shamy 2009). SO is a reddish brown powder and is water soluble. SO is generally used to dye wool, silk, tannin, fibers, cotton, leather, and paper. SO has extensive application in textile, trace, biological laboratory purpose (El-Kemary et al. 2011). The ingestion of Safranin O containing water causes distinct acute impact on health like irritation to mouth, throat, tongue, lips and pain in stomach which may lead to nausea, vomiting, and diarrhea (Hayat et al. 2011; Kaur et al. 2015). Therefore, it is highly desirable to treat and remove SO dye from the waste water.

1.4 Available waste water treatment technologies

Several, well-established conventional de-colorization methods involving physicochemical, chemical, and biological processes; and some of advanced processes such as sonochemical or advanced oxidation are discussed in the literature. These technologies include coagulation (Patel and Vashi 2012), flocculation and sand filtration (Zahrim and Hilal 2013), ultrafiltration (Zaghbani et al. 2008), adsorption (Tovar-Gómez et al. 2015), ozonation (Bessegato et al. 2016), photodegradation (Murcia et al. 2011), electrochemical oxidation (Faouzi Elahmadi et al. 2009), and microbiological treatment (Ng et al. 2014).

Among above mentioned techniques, adsorption is considered and found to be superior due to its simple operation, convenience, high efficiency, and economy. Adsorption is able to treat and remove different types of pollutants (Aksu 2005; Almeida et al. 2009; Ho and McKay 2003).

1.5 Brief statement of the problem

Dyes are classified as follows: anionic—direct, acid and reactive dyes; cationic—basic dyes; non-ionic—disperse dyes (Fu and Viraraghavan 2001). Among all types of dyes, cationic dyes have high brilliance and color tints; therefore, they give high visibility even at low concentrations (Aksu 2005). Thus decolorization of cationic dyes is very difficult. Carcinogenic effect could be produced by discharging an effluent which contains metal complex-based cationic dyes on release of metal (like chromium) into water supplies (Banat et al. 1997; Fu and Viraraghavan 2001). In an ETDA (Ecological and Toxicological Association of the dyestuff) survey of more than 90% of almost 4000 dyes tested and it was found that cationic dyes had LD₅₀ values greater than 200 mg/kg. Basic and diazo direct dyes produce highest toxicity rates (Garg et al. 2004). There is growing environmental concern over the contamination of wastewater by cationic dyes.

1.6 Brief accounts of existing knowledge and scope of work

Removal of Methylene Blue (Liu et al. 2015c; Yan et al. 2015) as well as Safranin O (Inbaraj et al. 2006; Mohammed et al. 2014; Rotte et al. 2014) has been attempted by various researchers in single dye adsorption system. Very limited research is available on Methylene Blue degradation using Fenton-like process (Mesquita et al. 2016; Oliveira et al. 2007; Pereira et al. 2011; Pinto et al. 2012). Degradation of Safranin O is also attempted by researchers using photocatalytic oxidation (Abdullah et al. 2007; Hayat et al. 2011). Removal of binary dyes Methylene Blue and Safranin O using adsorption system is reported in the literature (Ghaedi et al. 2015a; Ghaedi et al. 2015b).

It is observed by reviewing literature that there is still a need to develop some suitable methods for complete removal and / or degradation of harmful dyes. Commonly available adsorbents can be used for adsorption / reactive adsorption either in the raw form or by suitably modifying it. A number of studies are available on modification of adsorbents used for dye removal by adsorption (Bhatnagar et al. 2013; Chingombe et al. 2005; Figueiredo et al. 1999; Gong et al.

2015; Hadi et al. 2015; Orucoglu and Hacıyakupoglu 2015; Rivera-Utrilla et al. 2011; Shafeeyan et al. 2010; Shen et al. 2008; Trojanowicz 2006; Yin et al. 2007). Adsorbent modification needs to be explored in a better way in order to use effectively in a particular application. There is a need to use cheaper adsorbents with desired characteristics for potential applications.

In single dye system, a number of studies are available on dye degradation (Gupta et al. 2015; Khaksar et al. 2015; Oliveira et al. 2007). Dyes are present in wastewater usually in the form of mixture of dyes. Various studies on adsorptive removal of multi-component mixture of dyes have been reported in the literature (Allen et al. 2004; Kurniawan et al. 2012; Mahmoodi 2014a; Mahmoodi et al. 2010; Noroozi et al. 2008; Tovar-Gómez et al. 2015; Zolgharnein et al. 2015). The study on dyes present in a mixture is hardly attempted.

1.7 Inadequacy in existing research knowledge

Iron oxide modified granular activated carbon is a promising adsorbent for dye removal. Iron oxide modified granular activated carbon had been used for heterogeneous oxidation of Methylene Blue (Kim et al. 2013). However, this study (Kim et al. 2013) did not identify the reaction intermediates and the reaction pathways of MB degradation. To the best of knowledge, investigation on the kinetic and thermodynamic parameters of MB dye removal using reactive adsorption is not being attempted. No study is available in the literature identifying dye reactive adsorption products that are adsorbed on spent adsorbent. Recovery and identification of such degraded compounds may be commercially attractive obtained from dyes and other organic pollutants.

Safranin O oxidative degradation has not been attempted using iron oxide modified granular activated carbon. There is a need to identify the reaction intermediates along with the possible degradation pathways to obtain a better understanding of the mechanistic details of degradation of Safranin O dye. Literature also lacks in the data on surface mass transfer coefficient and diffusivity for Safranin O dye.

Degradation of binary dye is scarcely found in the literature (Gözmen et al. 2009; Juang et al. 2010). To my knowledge studies on reactive adsorption of mixture of dyes has not been reported in literature so far. Since mixture of dyes may yield several degradation products, it may be interesting to study degradation of mixture of dyes via reactive adsorption. Some of these

degradation products may have useful applications; that need to be identified. Surface mass transfer coefficients and diffusivities data on simultaneous adsorptive removal of Methylene Blue and Safranin O are also not available.

Keeping these inadequacies, below mentioned objectives were decided for this study:

1.8 Research objectives

1. Modification and characterization of a suitable adsorbent for reactive adsorption of dyes.
2. Removal of Methylene Blue and comparison of outcomes for batch studies on adsorption and reactive adsorption, identification of deposited oxidative degradation products on to reactive adsorbent, identification of Methylene Blue and its reactive degradation products and develop a degradation pathway.
3. Removal of Safranin O using adsorption and reactive adsorption and estimation of surface film mass transfer coefficient and diffusivity of Safranin O using surface - parallel pore diffusion model, identification of Safranin O and its reactive degradation products and to develop a degradation pathway.
4. Simultaneous removal of Methylene Blue and Safranin O using adsorption and estimation of surface film mass transfer coefficient and diffusivity of Methylene Blue and Safranin O during simultaneous removal using surface-pore-diffusion model.
5. Removal of Methylene Blue and Safranin O using adsorption and reactive adsorption, identification of Methylene Blue and Safranin O and their reactive degradation products during simultaneous oxidative degradation, and develop a simultaneous degradation pathway of both dyes.

1.9 Research outline

Figure 1.1, 1.2 and 1.3 show an overview of batch studies for MB removal, SO removal and simultaneous MB and SO removal using adsorption and reactive adsorption

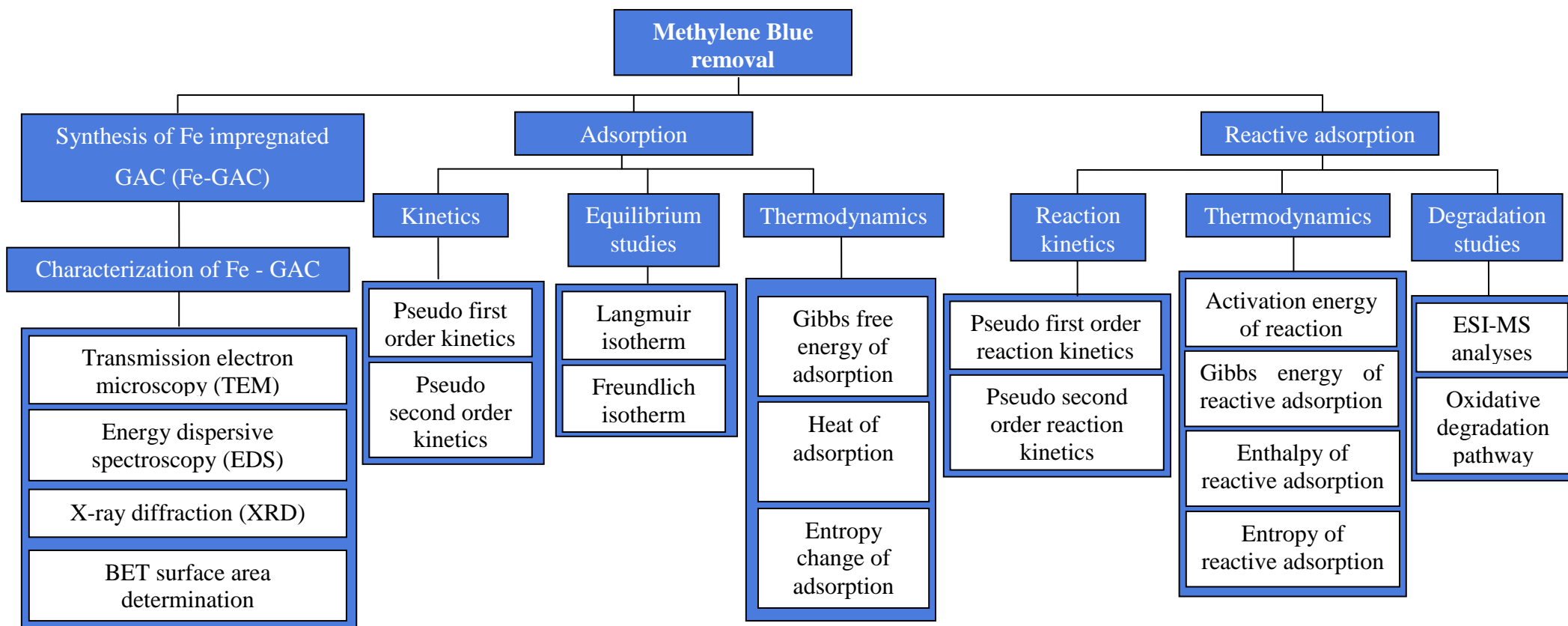


Figure 1.1: An overview of batch study for MB removal using adsorption and reactive adsorption

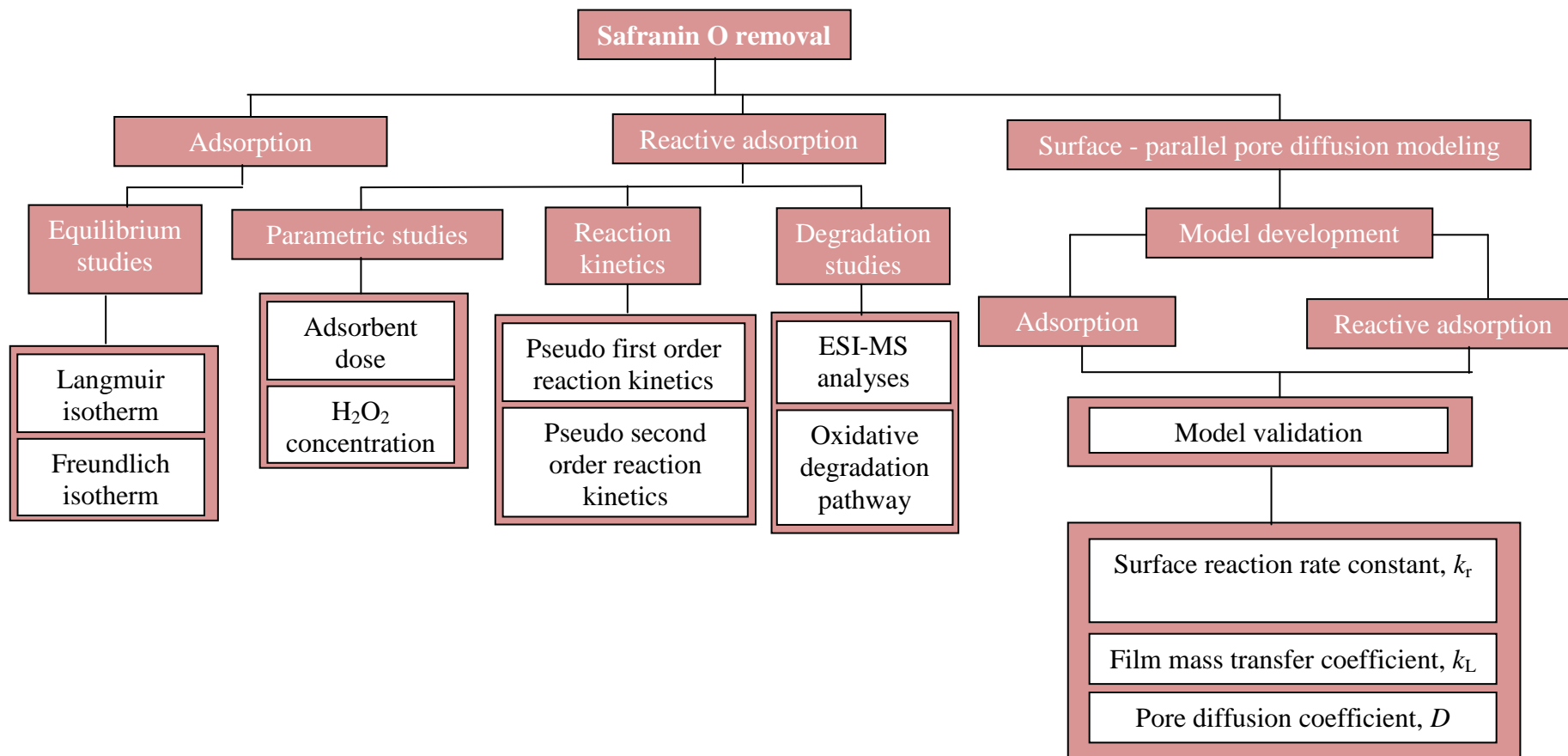


Figure 1.2: An overview of batch study for SO removal using adsorption and reactive adsorption

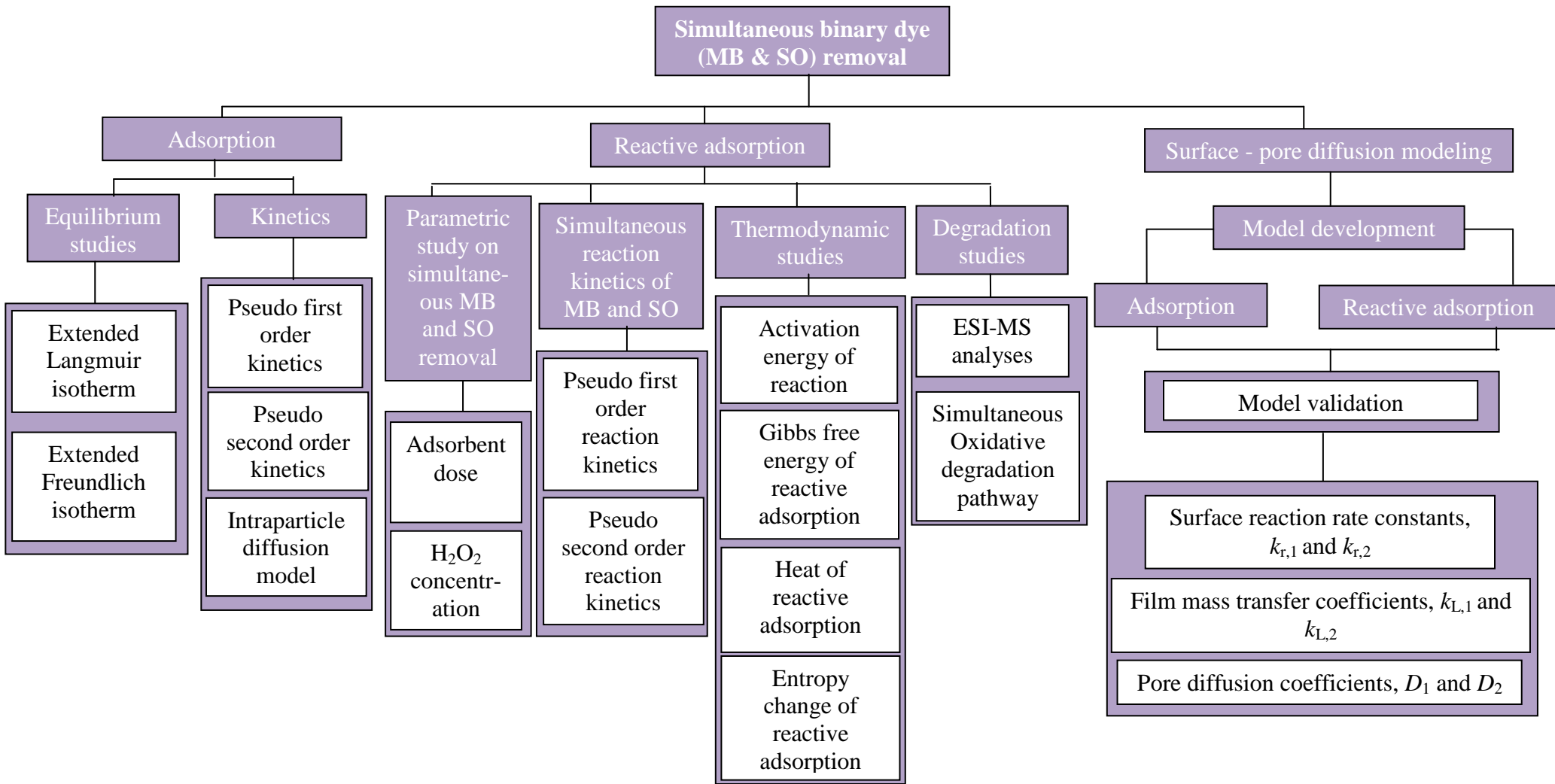


Figure 1.3: An overview of batch study for simultaneous MB and SO removal using adsorption and reactive adsorption

1.10 Thesis organization summary

The research work carried out has been organized into five chapters as shown below:

Chapter 1 discusses introduction to dyes and environmental problems associated with their discharge, dye production discharge statistics, fate of cationic dyes and their harmful effects and research objectives derived from the inadequacy found in the literature.

Chapter 2 presents the classification of dyes and multicomponent dye adsorption systems. Simultaneous quantification of dyes, effects of various parameters on adsorptive removal of dyes, different equilibrium adsorption isotherms, and mathematical modelling of batch sorption are discussed in multicomponent sorption section. Furthermore, reactive adsorption of organic pollutants is discussed. Reactive adsorption of dyes in single component system is also covered.

Chapter 3 describes the various chemicals used and synthesis procedure of reactive adsorbent. Equipments used and analytical instruments used are also summarized. Furthermore, experimental procedures adopted for adsorption and reactive adsorption are given in this chapter.

Chapter 4 has been divided into two sections. Section 1 shows the characteristics of synthesized reactive adsorbent. It also deals with the results obtained from adsorption and reactive adsorption studies for single and binary dye systems. Section 2 describes the modeling part. Central composite design and response surface methodology were applied to binary dye adsorption system. Surface mass transfer coefficients and diffusivities were calculated for single dye reactive adsorption and binary dye adsorption.

Chapter 5 provides summary, important outcomes of the thesis, and future recommendations which are helpful in treatment of dye-house wastewater.

In addition to the existing knowledge, the novelty and contribution of this research work are summarized as follows:

1. Kinetic and thermodynamic aspects of dye reactive adsorption have been studied for single and binary dye systems.
2. Formation of deposits on the surface of the reactive adsorbent was studied and identification of these deposited species for reactive adsorption of Methylene Blue dye has been reported.

3. Reactive adsorption of Safranin O was studied and an oxidative degradation pathway has been proposed.
4. External liquid film mass transfer coefficient, macropore and micropore diffusivities of Safranin O were estimated using surface - parallel pore reactive adsorption model.
5. Reactive adsorption of binary dye removal was studied and a simultaneous oxidative degradation pathway has been proposed.
6. A surface film solid pore diffusion model was developed and used to predict the surface mass transfer coefficients and diffusion coefficients for binary dye adsorption system.

2.1 Dyes

Dyes are colored moieties that have an affinity to color the substrate. The dye is generally applied in an aqueous medium, and use of a mordant may improve the dye's color fastness on the fiber. Generally, dyes used for coloring textile fibres have characteristics such as, get absorbed very strongly in the visible spectrum, are composed of polyaromatic compounds, are substantive to specific fibers (Christie 2007).

A dye structure contains – chromophore, chromogen and auxochrome. Chromophore consist of unsaturated group which absorbs light and reflects it at a particular angle to give the specific hue, e.g., azo, keto, nitro, nitroso, thio, ethylene etc; chromogen retains chromophore and determine the final hue and its affinity for fibre, fastness, stability etc. Auxochromes are substituted anionic or cationic groups in dye structure that intensify depth of shade, e.g. –OH, –COOH, SO₃H, –NH₂, –NH(CH₃) etc.

2.2 Classification of dyes

Dyes are classified as:

2.2.1 Classification based on the type of raw material

Based on raw material, it is further classified into two classes:

2.2.1.1 Natural dyes

The dyes are obtained from natural sources. Natural black 1 (hematein) is one of the most commonly used natural dye.

2.2.1.2 Synthetic dye

Synthetic dyes can be obtained using organic and/or inorganic elements. Examples are acid, basic, direct, reactive, vat, mordant, disperse, and sulphur etc.

2.2.2 Classification based on chemical structure

Dyes can be classified on the basis of their chromophoric groups, dyes can be defined (Hunger 2003) as shown in Table 2.1:

Table 2.1: Classification of dyes based on chromophoric groups (Hunger 2003)

S. No.	Chromophore group	Chemical group	Applications
1.	Acridine dyes, derivatives of acridine	$>C=N-$ and $>C=C$	Textiles
2.	Anthraquinone dyes, derivatives of anthraquinone	$>C=O$ and $>C=C$	Textiles
3.	Azo dyes	$-N=N-$	Textiles
4.	Nitro dyes	$-NO_2$	Textiles
5.	Phthalocyanine dyes, derivatives from phthalocyanine	$>C=N$	Paper
6.	Azin dyes	$-C=N=C-$ and $-C-N-C$	Leather and textiles
7.	Xanthene dyes, evolved from xanthene	$-O-C_6H_4$	Cotton, silk and wool
8.	Indophenol dyes, evolved from indophenols	$>C=N-$ and $>C=O$	Color photography
9.	Oxazin dyes, evolved from oxazin	$-C-N=C=C-O-C=$	Calico printing
10.	Thiazole dyes, evolved from thiazole	$>C=N-$ and $-S-O=$	Dye intermediates

2.2.3 Classification of dyes based on their nuclear structure

This classification can be done into two groups:

2.2.3.1 Cationic dyes

Basic dyes are water-soluble and mainly applied to acrylic, nylon, wool, and silk dyeing. Cationic dye includes different substituted aromatic groups that produce various chemical structures.

2.2.3.2 Anionic dyes

An anionic or acid dye is a dye that carries a salt of a sulfuric, carboxylic or phenolic organic acid. Anionic dye includes various compounds, which exhibit characteristic varieties in structure for example azo dyes, anthraquinone, triphenylmethane, nitro dyes, direct dyes, and reactive dyes. This class possess as characteristic of water solubility and ionic substituent. Acid dyes are applied to nylon, silk, wool, and modified acrylic fibers.

2.2.4 Classification based on application of dyes

Application based classification is shown in Table 2.2:

Table 2.2: Classification of dyes based on application (Hunger 2003)

Class	Chemical types	Properties	Principal substrates
Acid	Azo, anthraquinone, azine, triphenylmethane, xanthenes, nitro and nitroso	Water soluble and anionic	Nylon, wool, paper, silk, inks, and leather
Basic	Cyanine, hemicyanine, diphenylmethane, diazahemicyanine, triarylmethane, azo, azine, xanthenes, acridine, oxazine, and anthraquinone	Water soluble and cationic	Paper, polyacrylonitrile, modified nylon, polyester, polyester, and inks
Direct	Azo, oxazine, and	Water soluble and	Cotton, rayon, leather,

Class	Chemical types	Properties	Principal substrates
	phthalocyanine	anionic	paper, and nylon
Disperse	Azo, nitro, styryl, and anthraquinone, benzodifuranone	Water insoluble and non ionic dyes used to dye hydrophobic fibres from liquid dispersion	Polyester, acetate, polyamide, plastics, and acrylic
Reactive	Azo, phthalocyanine, anthraquinone, formazan, basic, and oxazine	Dyes form covalent bond with fibre	Cotton, nylon, silk, and wool
Solvent	Azo, anthraquinone, triphenylmethane, and phthalocyanine	Water-insoluble but solvent-soluble	Plastics, varnishes, gasoline, stains, fats, inks, waxes, and oils
Vat	Anthraquinone and indigoids	Water insoluble	Cotton, rayon, and wool

Industrial dye effluents usually contain a number of dyes. Simultaneous quantification and removal of dyes in an aqueous solution have remained a challenge. In a mixture of dyes, quantification of one dye is interfered by the presence of the other. Several studies are available in literature dealing with quantification of dyes in a mixture elucidating different aspects (Zeinali et al. 2014; Zolgharnein et al. 2015; Zolgharnein et al. 2014a). Therefore, quantification of an individual dye in a mixture is largely based on spectrophotometric technique (Azad et al. 2015; Liu et al. 2015b). In addition to quantification, removal of dyes from a mixture of multicomponent solutes is little less challenging but is needed. Due to simplicity of operation and cost together with availability of a wide variety of adsorbents, adsorption is one of the techniques, which has been largely practiced (Chan et al. 2012b).

2.3 Multicomponent dye adsorption system

A number of studies have focused on the sorption behavior of dyes in single component dye system by various sorbents (Isa et al. 2007; Olgun and Atar 2009). Multisolute sorption systems have received scarce attention compared to single solute systems due to complex behavior and competitive and/or synergic effect of solutes present in the system. First experimental results on removal of binary mixture were presented by Kolthoff and Groot (1929) and treatment of ternary system was reported by McKay and Al Duri (1987).

2.3.1 Quantitative determination of dyes in a multicomponent mixture

Dyes quantitative determination present in a multicomponent mixture is based on the theory that the absorbance at specific wavelength of a multicomponent solution is equal to the addition of their respective absorbance in the mixture at that wavelength. Analysis of solutes present in a multicomponent mixture is based on the measurements at a number of wavelengths equal to the number of solutes in the mixture. Usually, for measurement of solute concentration, that wavelengths are selected where absorbance is maximum of each component (Nateri and Ekrami 2009).

Measurement of dyes concentrations present in binary and ternary aqueous systems using spectrophotometry are reported in literature. Equations obtained with absorbance values and calibration constants at respective wavelengths of solutes can be solved easily in MATLAB by converting them into matrices (Mahmoodi 2014a; Mahmoodi et al. 2011a; Mahmoodi et al. 2010). Nevertheless, spectrophotometry is non-selective that requires the solutes present in a mixture should have different absorption spectrum with no or low overlapping (An et al. 2010; Issa et al. 2014).

Derivative techniques and multivariate methods in chemometrics are important aspects for analysis of solutes present in mixtures using ultraviolet-visible molecular absorption spectrophotometry. These approaches are very useful in the resolving the complexity of band overlapping in quantitative analysis. It has been proved that derivative technique is useful in the resolution of simple binary dye mixtures and multivariate calibration method has been mostly chosen for complex mixtures (Nevado et al. 1999).

2.3.1.1 Derivative spectroscopy

UV/Vis absorption spectrophotometry is a method which is most widely used technique for quantitative analysis, due to its low cost, speed and, simplicity of measurements. Though, this analytical technique has a limitation of measurement for solutes present in a given sample to have different absorption spectrum and low overlapping, as a consequence its applications in multi-analyte system is limited (An et al. 2010; Hemmateenejad et al. 2014). A number of studies are available in literature for measuring concentration of dyes present in multicomponent mixtures with simple (Al-Degs et al. 2007) to more advanced (Gao et al. 2011) spectrophotometric techniques. The selection of a method for analyzing solutes in a mixture depends on the factors viz. extent of spectral overlap between solutes and/or presence of a complex matrix. It is important to use a suitable method for accurate solute quantification in multi-solute systems due to complexity of real matrices or high spectral / chromatographic overlap (Issa et al. 2014). Figure 2.1 shows the spectral overlap of Acid Blue 25 and Direct Blue 86 (Douissa et al. 2014).

Derivative spectrophotometry resolves the problem of quantification of solutes present in a mixture due to overlapping. This advanced spectrophotometric technique is based on derivative spectra that are generated from originator zero-order spectrum. The derivatization of zero order spectra enhances the selectivity for a compound and reduces the disturbance created by the presence of other moieties in a sample. Therefore, concentrations of dye present in mixtures can be determined by measuring the absorbance signal at the successive nth order derivative wavelength. This method does not require any prior separation or purification step before carrying out quantification of analytes (Karpińska 2004).

The derivative form of Beer's law is as follows:

$$D^n = \frac{d^n A}{d\lambda^n} \quad \dots(2.1)$$

where D is the value of derivative of n-order at wavelength λ .

The derivative spectrum of a mixture is the addition of derivative spectra of each individual component as per the additivity law:

$$D_{mix}^n = D_1^n + D_2^n + \dots + D_x^n \quad \dots (2.2)$$

where the value of n-order derivative of mixture at analytical wavelength, $D_1^n, D_2^n, \dots, D_x^n$ are the values of nth order derivative at wavelength of 1st, 2nd, . . . , xth elements of mixture. This allows determination of multiple elements (x) present in a mixture by taking the amplitude of derivative spectrum of mixture at several (minimum value of x) wavelengths (Karpińska 2004).

According to the 'zero-crossing technique' for simultaneous determination of analytes present in a sample, the absorbance of an analyte is performed by measuring the height of derivative peak at the wavelengths at which spectra of other element has a zero or near zero value, the measured amplitude provides concentration of assayed compounds only (Turabik 2008). It is important to note that zero-crossing wavelengths do not vary with the different concentrations of related species (Zolgharnein et al. 2015). The best linear responses are obtained using zero-crossing technique and the calibration graphs are less affected by concentration of other components (Gao et al. 2010). Andronic and Duta (2012) developed a simple, sensitive and selective model for simultaneous analysis of two dyes in solutions using first order derivative spectrophotometric method that used to overcome the spectral overlapping.

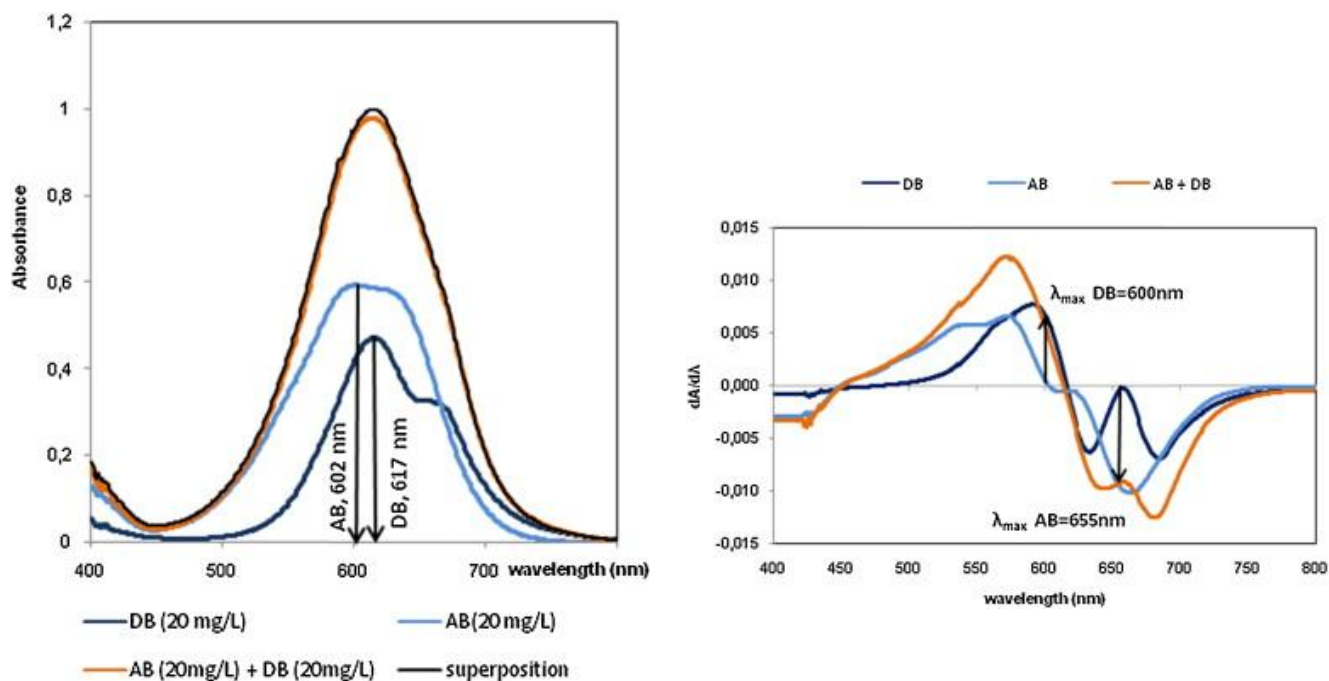


Figure 2.1: Spectral overlap of Acid Blue 25 (AB) and Direct Blue 86 (DB) in single and binary solutions (a) Zero order absorption spectra and (b) First order derivative spectra (Douissa et al. 2014)

Non-robust nature of the derivatization parameters, dependence on the instrumental features, and lack of homogeneous protocol of optimization of the parameters and production of results are disadvantages of derivative spectroscopy (Karpieńska 2004).

2.3.1.2 Chemometric methods

Incorporation of computer and statistical techniques with chemistry resolve analytical issues for sampling complex mixtures. Chemometrics combine chemistry with computer, which facilitates workers to resolve the components of a complex mixture without using a pre-separation step (An et al. 2010; Hemmateenejad et al. 2014). Chemometric methods provide analysis and quantification of solutes in complex matrices even without any prior knowledge about their chemical substances (Gholami et al. 2016). Figure 2.2 shows the flow chart of a quantitative chemometric method.

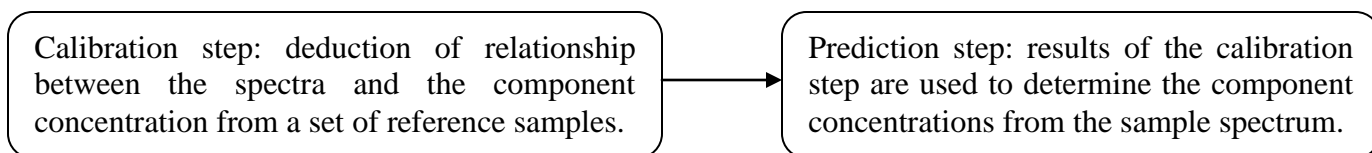


Figure 2.2: Quantitative chemometric methods (Nevado et al. 1999)

Chemometrics employ multivariate curve resolution–alternating least square (MCR–ALS) method to analyze spectroscopic data of evolutionary processes. MCR–ALS methods extract information about number of solutes involved in the system as well as their concentration profiles and pure spectra of species. This provides a platform to perform adsorption of multi solutes from wastewater systems (An et al. 2010; Hemmateenejad et al. 2014). Multivariate quantification method like multilinear regression (MLR), principal component regression (PCR), and partial least squares (PLS1) can resolve problem of spectrum overlapping or complex matrices which is normally observed in analytical chemistry (Al-Degs et al. 2008; Al-Degs and Sweileh 2012; Gholami et al. 2016). Issa et al. (2014) presented the algorithms for MLR, PCR, and PLS. Details on algorithms of MLR, PCR, and PLS1 could be found from literature (Brereton 2003). Multivariate calibration (MVC) methods minimize/eliminate sample preparation and avoid application of tedious chromatographic or electrochemical methods (Al-Degs et al. 2008; Al-Degs and Sweileh 2012). PLS is preferred over conventional PCR for data processing. The information from the calibration solution in case of PLS is better used as it reflects similarity of the sample to the calibration set. PLS uses both spectral and concentration data unlike PCR in which, the data decomposition is conducted only using the spectral information (An et al. 2010).

PLS can provide a robust regression model which requires a large number of calibration and test sets and, all solutes and interferences should be in the calibration set at the appropriate concentration level. PLS and related chemometric methods require previous knowledge of all species in the given samples, but identification of all species in a complex mixture is impractical and time consuming. 2nd order or higher order data analysis is capable for quantification of solutes even the data interferences are not modeled or calibrated. 2nd order multivariate calibration methods were successfully applied for three way array of data which is obtained by

stacking the data matrices of different samples under each other (Gholami et al. 2016). Al-degs and Sweileh (2012) developed a simple and sensitive spectrophotometric method for the simultaneous determination of five dyes using solid-phase extraction. They developed a model by using calibration set, while the effectiveness of the proposed model for prediction was tested in the validation set. A large number of calibration samples are necessarily required due to the high spectral overlap between the dyes present in mixture (Al-Degs and Sweileh 2012). PLS, PCR, and multiple least squares (MLS) methods often suffer in much more complex practice during calibration process.

Artificial neural network (ANN) is able to solve complex structure consists of highly nonlinear process. ANN is a flexible model and often robust with respect to input noise (Himmelblau 2008; Pirdashti et al. 2013). Zeinali et al. (2014) combined second order derivative spectrophotometry (SODS) and principal component–artificial neural network model (PCA–ANN) for accurate and reproducible determination of competitive nature of a binary dye mixture during adsorption process. PCA–ANN model minimizes the dimensionality of large data sets by reducing the number of spectral data which enables it to anticipate the concentrations of dyes in the mixtures (Zeinali et al. 2014). ANN models suffer with some problems like, over-fitting of data, requirements for selecting the number of hidden nodes hidden layers, adjustment of parameters containing weights and biases etc. which may lead to unreliability of the method. Support vector machine (SVM), a novel neural network algorithm, has distinct advantages when compared to ANN (Abdi et al. 2014). Problem of over-fitting is unlikely to occur with SVM as it provides global optimum solution rather than local as in other neural network models (Kim 2003). Concept of SVM was introduced by Vapnik in 2000 as a supervised learning algorithm.

Though SVM has outstanding performance for solving static function approximation problems, it has a higher computational load (Wang and Hu 2005). Suykens and Vandewalle (1999) proposed a modified version of SVM, called least squares support vector machine (LS-SVM), in order to minimize the complexity of SVM and to improve the speed of convergence. Abdi et al. (2014) compared SVM and LS-SVM. Table 2.3 shows some good features of LS-SVM over SVM. They found LS-SVM more reliable and applied it to predict dye removal efficiency in a ternary mixture of dyes. It is reported that the novel intelligent model (LS-SVM) was capable of

simulating the real physical trend of the removal efficiency of dyes with variation of sorbent dose and initial dye concentration in single and ternary mixture systems (Abdi et al. 2014).

Table 2.3: Comparison between SVM and LS-SVM techniques (Abdi et al. 2014)

Particulars	Support vector machine (SVM)	Least-squares support vector machine (LS-SVM)
Static function approximation problem solving	Higher computational burden, owing to required constraint optimization programming	Good speed of convergence
Formulation	Equality constraints	Inequality constraints
Optimum solution	Linear equations (linear programming)	Quadratic programming problem
Function approximation	Uses all samples	Selects some sparse support vectors

SVM-based methods also have some drawbacks. The limitation of an SVM-based method is that it is largely characterized by the choice of its kernel. Discrete data presentation and reduced speed and size, both in training and testing are also additional limitations (Burges 1998). Table 2.4 summarizes methods used by various researchers for simultaneous quantification of mixture of dyes present in wastewater system.

Table 2.4: Method used for simultaneous quantification of dyes

Dyes	Methods	Remark (s)	Reference
Methylene Blue and Malachite Green	Partial least squares as a multivariate calibration	Minimize/eliminate sample preparation and to avoid applying tedious chromatographic or electrochemical methods	(Issa et al. 2014)
Methylene Blue and Brilliant Green	1. Second order derivative spectrophotometric 2. Artificial neural network and principal component analysis	Results displayed that the performance of derivative spectrophotometric method was better than the PCA– ANN	(Zeinali et al. 2014)

		model	
Acid Blue 25 and Direct Blue 86	First order derivative spectrophotometric	-	(Douissa et al. 2014)
Acid Red 14 and Reactive Red 15	Partial least squares regression as a multivariate calibration	Partial least squares uses both spectral and concentration data but in principal component regression the data decomposition is conducted using only the spectral information	(Gao et al. 2011)
Direct Blue 78, Direct Red 79, and Direct Yellow 106	Colorimetric algorithm	Colorimetric algorithm achieves the lowest average ternary relative error when compared with Beer's law. Colorimetric algorithm decreases the effect of wavelength shifting on recipe prediction performance.	(Shams-Nateri 2011)
Brilliant Green and Methylene Blue	Fifth and fourth order derivative spectrophotometric	-	(Ghaedi et al. 2013)
Basic Yellow 28 and Basic Red 46	First order derivative spectrophotometric	-	(Turabik 2008)

Derivative techniques under computer-controlled instrumentation and MVC methods using chemometrics, both play very useful role in the resolution of band overlapping in quantitative analysis of multicomponent mixtures by UV-Vis molecular absorption spectrophotometry (Andronic and Duta 2012; Nevado et al. 1999). The derivative spectrophotometric method has been used due to its economic, facile and simple approach, whereas chemometric methods simultaneously determine components present in mixture with speed, precision and accuracy. Chemometrics avoid preliminary separation step (Ghaedi et al. 2014; Nevado et al. 1999; Zolgharnein et al. 2015).

A method impending should provide accuracy and precision to estimated experimental values in order to achieve the definite concentration of the solutes present in the mixtures. It has indicated that the method used for quantification of dyes should has minimum discrepancy (between the known and predicted concentration data) to propagate toward accurate experimental outcome (Zeinali et al. 2014). Apart from discrepancy, availability of compatible system and its thorough knowledge are also necessary criteria of selection of a suitable method.

2.3.2 Effects of various parameters on adsorptive removal of dyes from multicomponent systems

In practice, normally the wastewater is a mixture of several dyes rather than a single one and during adsorption the solutes compete with each other for adsorption. The interactions among these compounds may mutually enhance or mutually inhibit adsorption capacity (Ho and McKay 1999). Generally, a mixture of different solutes present in wastewater may exhibit three possible types of adsorption behavior: synergism (the effects of the mixture is to enhance the adsorption capacity than that of each of the individual sorbates in the mixture), antagonism (the effect of the mixture is to reduce the adsorption capacity than that of each of the individual adsorbates in the mixture) and non-interactive (neutral effect on the adsorption of each of the solutes in the mixture) (Srivastava et al. 2006). The knowledge of magnitude of such competitive interactions among the dyes needs to model adsorbate migration towards adsorbent surface in aqueous systems (Gutierrez and Fuentes 1993). A selected list of mixture of dyes and adsorbents studied are summarized in Table 2.5.

Table 2.5: Dyes and adsorbents studied in multicomponent adsorption systems

Dyes	Adsorbent (s)	Reference	Dyes	Adsorbent (s)	Reference
Acid Yellow 117 and Acid Blue 25	Bamboo derived activated carbon	(Chan et al. 2012a)	Methylene Blue and Rhodamine B	Modified waste sugarcane bagasse	(Yu et al. 2015)
Cibacron Black B and Cibacron Red RB	Phosphoric acid modified sawdust	(Chakraborty et al. 2006)	Methylene Blue and Brilliant Green	Graphite oxide nano particle	(Zeinali et al. 2014)
Polar Blue and Polar Yellow	Activated carbon	(Choy et al. 1999)	Methyl Orange and Methylene Blue	Polyacrylonitrile fiber hydrothermally treated with hyperbranched polyethylenimine	(Fan et al. 2015)
Methylene Blue and Malachite Green	Rarasaponin–bentonite	(Kurniawan et al. 2012)	Direct Blue 78 and Direct Red 31	Activated carbon	(Mahmoodi et al. 2011a)
Methylene Blue and Acid Orange 7	Methylene Blue and Acid Orange 7	(Liao et al. 2012)	Acid Blue 93 and Methylene blue	Cellulose based biosorbent	(Liu et al. 2015a)
C.I. Basic Blue 41 and C.I. Basic Red 18	Granular activated carbon and silkworm pupa	(Noroozi et al. 2008)	Acid Red 183 and Reactive Blue 4	Boron Industry Waste	(Atar et al. 2011)

Acid Blue 80 and Acid Yellow 117	Activated carbon	(Porter et al. 1999)	Disperse Red 60 and Disperse Blue 60	Granular activated carbon	(Sirianunta piboon and Srisornsak 2007)
Levafix Brilliant Red E-4BA and Levafix Brilliant Blue E-4BA	Microporous H-type activated carbon	(El-Barghouthi et al. 2007)	Reactive Blue 21 and Reactive Red 195	Clinoptilolite type natural zeolite	(Sismanoglu et al. 2010)
Methylene blue and Safranin-O	Nickel sulfide nanoparticles loaded on activated carbon	(Ghaedi et al. 2014)	Basic Red 46 and Basic Yellow 28	Bentonite	(Turabik 2008)
Reactive Blue 4 and Acid Red 183	Multiwall carbon nanotubes	(Wang et al. 2012b)	Methylene Blue and Acid Red 183	Multiwalled carbon nanotube	(Wang et al. 2012a)
Congo Red and Methyl Blue	Magnetic $MnFe_2O_4$	(Yang et al. 2014)	Reactive Yellow 86 and Reactive Red 2	Novel composite containing silver nanoparticles (AgNPs) and colemanite ore waste (COW)	(Yola et al. 2014)
Methyl Orange and	Nanostructured mesoporous	(Yahyaoui	Reactive Blue 4 and	Polysulfone-immobilized	(Vijayarag

Bromothymol Blue	alumina	and Azizian 2014)	Reactive Red 4	protonated Corynebacterium glutamicum	havan and Yun 2008)
Methyl Orange and Reactive Yellow 17			Reactive blue 4 and Reactive orange 16		
Methyl Orange and Methyl Violet			Reactive blue 4 and Basic blue 3		
Direct Green 6 and Direct Red 31	Core-shell magnetic adsorbent nanoparticle	(Mahmoodi 2014b)	Acid Orange 10 and Acid Blue 80	Husk of the mango seed	(Dávila-Jiménez et al. 2009)
Direct Green 6 and Acid Red 18			Acid Orange 7 and Acid Blue 324		
Acid Blue 80 and Acid Red 114	Activated carbon, Filtrasorb 400	(Choy et al. 2000)	Acid Orange 8 and Acid Green 25		
Acid Blue 80 and Acid Yellow 117			Acid Red 1 and Acid Green 27		
Acid Red 114 and Acid			Methylene Orange, Rhodamine	Mesoporous Cu ₂ O submicro-	(Liu et al.

Yellow 117			B and Methylene Blue	spheres	2012)
Congo Red and Acid Violet, and Rhodamine-B	Waste banana pith	(Namasivayam and Kanchana 1992)	Remazol Reactive Yellow, Remazol Reactive Black, and Remazol Reactive Red	Activated carbon Filtrasorb 400	(Al-Degs et al. 2000)
Acid Scarlet GR, Acid Turquoise Blue 2G, and Indigo Carmine	Poly-diallyldimethylammonium modified bentonite	(Shen et al. 2009)	Direct Fast Scarlet, Eosin Y, and Reactive Violet K-3R	Poly-(epichlorohydrin dimethylamine) modified bentonite	(Kang et al. 2009)
Remazol Reactive Yellow, Remazol Reactive Black, and Remazol Reactive Red	Filtrasorb 400 activated carbon (FS400)	(Al-Degs et al. 2007)	Acid Blue 92, Direct Green 6, and Direct Red 31	Gemini polymeric nanoarchitecture	(Mahmoodi et al. 2013)
Acid Green 25, Acid Black 26, and Acid Blue 7	Date stones	(Mahmoodi et al. 2010)	Alizarin Red and Alizarin Yellow	γ -alumina	(Zolgharnein et al. 2014a)
Direct Red 31, Direct Green 6, and Acid Blue	Gemini polymeric Nano architecture	(Abdi et al. 2014)	Basic Blue 3, Basic Red 22, and Basic Yellow 21	Peat	(Al-Duri and McKay 1991)

The adsorption capacity of each dye generally reduced in multisolute mixtures with the presence of another solute, however the extent of reduction depends on the type of dyes investigated (Al-Degs et al. 2007). This can be explained by the interaction among the dyes on the adsorbent surface; this non-equal competition leads to the heterogeneity of solid surface. Adsorption preference of a sorbent for various adsorbates affects by a number of factors such as; functional groups, structure, surface properties, etc. that are related to the characteristics of the adsorption sites, ionic weight, ionic size, molecular structure, ionic nature, etc. represents the properties of the adsorbates, and pH, ionic strength, etc. which are parameters of experimental conditions and solution chemistry (Allen et al. 1988; Turabik 2008).

To measure the extent of competition between dyes, El-Barghouthi et al. (2007) presented a parameter, known as competition factor. Competition factor is the ratio of the adsorption capacity for one dye in the presence of the other dye, to the adsorption capacity for the same dye from single solute solution. This factor can be used to evaluate extent of competition between solutes. Competition is positive if value of competition factor is greater than 1; the adsorption is synergistic in the presence of the other solute. No competition between adsorbates should exist at value of competition factor is equal to 1. Generally, the sorption capacity of one sorbate is reduced in the presence of another and for this case, the value of competition factor is less than 1 (El-Barghouthi et al. 2007). Competitiveness of the two dyes in binary system is also described by Yang et al. (2011) using a term inhibition percentage. Definition of inhibition percentage is given as the difference between adsorption capacities in single and that in binary systems.

On the contrary, some adsorbates show synergistic effect on the used adsorbent; electronic interactions, formation of any specific bond between dye and adsorbent surface and size of individual dye molecule may be responsible for such phenomenon (Wang et al. 2012a). Various factors affecting the dye adsorption in multisolute mixture systems are discussed in detail below.

2.3.2.1 Adsorbent dose

The adsorbent dose is an important parameter as it determines the capacity of adsorbent for a given initial concentration of dye solution and in turn shows whether the process is cost-effective or not (Hajati et al. 2014). Increase in adsorption with the dose can be attributed to increased surface area leading to the increased rate of mass transfer, the availability of more adsorption

sites for dye adsorption up to a certain limit and then it reaches a constant value. Decrease in adsorption capacity of adsorbent may be attributed to overlapping or aggregation of adsorption sites resulting in a decrease in total adsorbent surface area available to the dye (Mahmoodi et al. 2011b). The dye with a higher affinity would be preferentially removed by adsorption in case of limited dose of adsorbent (Shen et al. 2009). There is a critical adsorbent amount for which the removal percentage of dyes approaches a constant value (Ghaedi et al. 2013). Table 2.6 shows surface area of various adsorbents used in removal of mixture of dyes from wastewater.

Table 2.6: Surface area of various adsorbents used in removal of mixture of dyes from wastewater.

Adsorbent	Surface area (m²/ g)	Reference
CaFe ₂ O ₄ magnetic nanoparticles	42	(Liu et al. 2015b)
Clay	117	(Issa et al. 2014)
Zeolite	173	
Filtrisorb 400 activated carbon	1100	(Al-Degs et al. 2007)
Peat	32	(Allen et al. 2004)
Silica/chitosan hybrid	8	(Cestari et al. 2005)
Charred sawdust	559	(Chakraborty et al. 2006)
Bamboo derived activated carbon	2471	(Chan et al. 2012a)
Acid treated okara	1	(Gao et al. 2011)
Cadmium hydroxide nanowires loaded on activated carbon	1271	(Ghaedi and Mosallanejad 2014)
Hydroxy-aluminum pillared bentonite	200	(Hao et al. 2014)
Poly(epichlorohydrin dimethylamine) modified bentonite	27	(Kang et al. 2009)

Bamboo charcoal modified by microwave radiation	255	(Liao et al. 2012)
Mesoporous Cu ₂ O submicro-spheres	58	(Liu et al. 2012)
Cellulose-based Bioadsorbent	364	(Liu et al. 2015a)
Multiwall carbon nanotube	217	(Wang et al. 2012b)
Bentonite	72	(Turabik 2008)
Magnetic MnFe ₂ O ₄	156	(Yang et al. 2014)
Titanium peroxide	48	(Zhao et al. 2014)
Na-Bentonite and organoclay	36 and 28	(Anirudhan and Ramachandran 2015b)
Alumina nanoparticles	110	(Zolgharnein et al. 2015)

2.3.2.2 Initial dye concentration

Percentage dye adsorption decreases with increase in initial dye concentration in the dye solution as adsorption sites would be saturated and as a result adsorbent would give a lower yield for the adsorption at higher concentrations of dyes. But adsorbed amount per unit mass of adsorbent is increased in the case of sorbent dose is not changed. At the higher initial concentration of dye, the driving force is increased due to larger concentration gradient. Reduced percent adsorption at high dye concentration may sometimes be caused by the repulsion occurring between sorbed dye molecules on the adsorbent surface and remaining dye molecules in the solution (Almasian et al. 2015; An et al. 2015; Hajati et al. 2014). Figure 2.3 shows a comparative results of initial dye concentration on dye removal from single and binary systems using PAN25%w/w EDA (polyacrylonitrile 25%w/w ethylenediamine) nanofiber (Almasian et al. 2015).

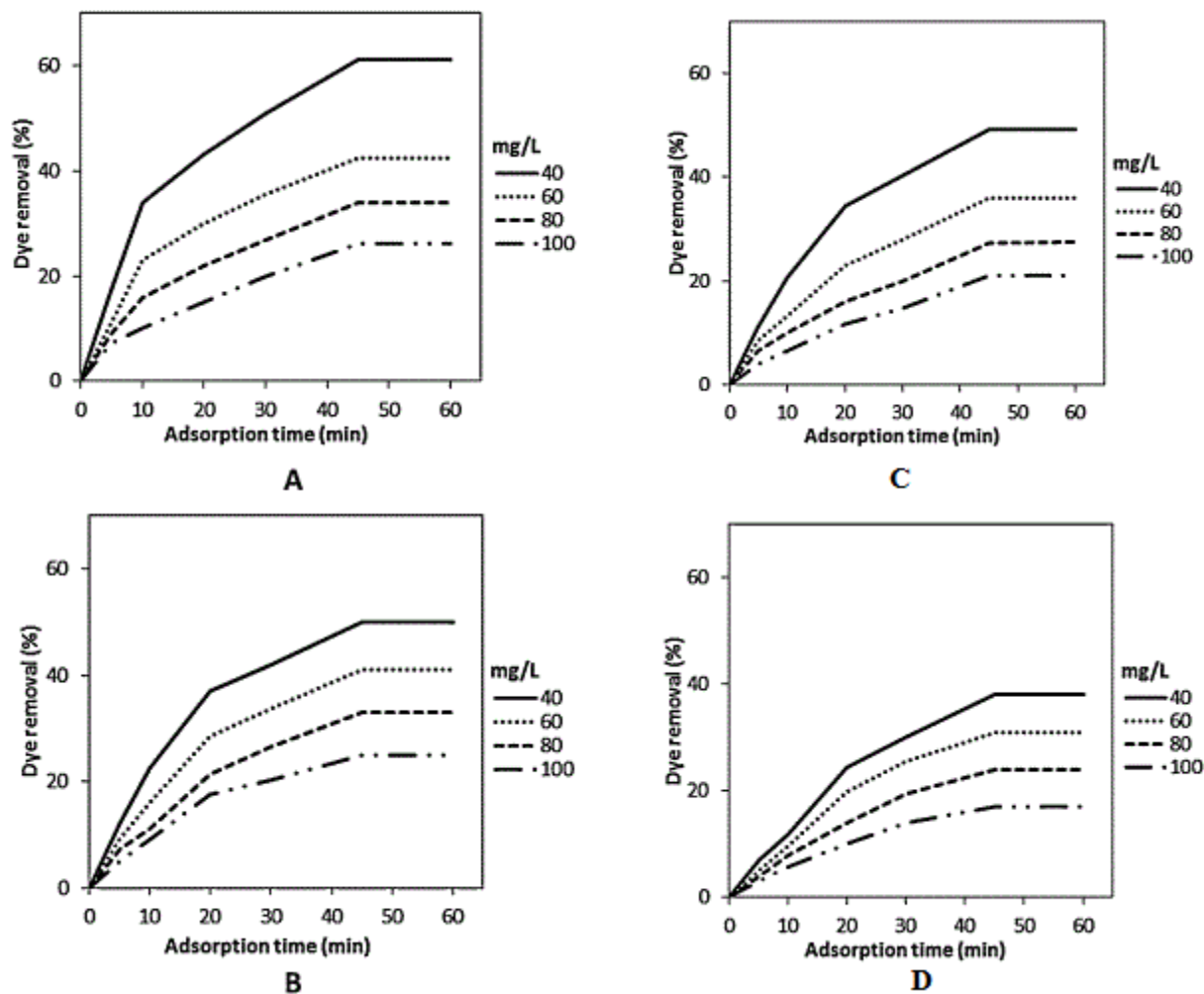


Figure 2.3: Effect of initial dye concentration on dye removal from single and binary systems by PAN25% w/w EDA nanofiber ((A) Direct Red 80 (single), (B) Direct Red 23 (single), (C) Direct Red 80 (binary), (D) Direct Red 23 (binary)) (Almasian et al. 2015).

Competitive adsorption was found to favor the adsorption of dye Reactive Blue 15 from the aqueous mixture solution at initial concentrations of Metanil Yellow = 1.34 mM and Reactive Blue 15 = 1.36 mM in the solution; while it favored the adsorption of dye Metanil Yellow from the mixture solution when initial concentrations of Metanil Yellow = 3.00 mM and Reactive Blue 15 = 1.34 mM. This indicates that an increase in initial dye concentration led to an increase in the adsorption trend of dye on the adsorbent (Chiou and Chuang 2006).

The binary solution exhibited inhibitory adsorption for each dye showing reduced yield of adsorption due to antagonistic effect. At lower initial concentrations of moieties in the solution,

all dye molecules get chance to interact with the binding sites and thus the higher percent removal are reported compared to higher initial concentrations of the binary mixture. At higher initial dye concentrations adsorption sites are saturated and lower adsorption yield is obtained. Competitive behavior exists in the presence of the other dye in the solution for adsorption sites on the sorbent surface, results in occupying some sites by the other sorbate, especially at relatively higher concentration (Turabik 2008).

2.3.2.3 Molecular dimension of dye

Ghaedi and Mosallanejad (2014) showed the kinetics of the competitive adsorption of Malachite Green and Sunset Yellow at their equal initial concentrations in mixture solution at 25°C. It is reported that the initial adsorption rate of Sunset Yellow onto Cadmium hydroxide nanowires loaded on activated carbon (Cd(OH)₂-NW-AC) was found faster than that of the Malachite Green. Therefore, the time required to reach adsorption equilibrium is shorter for Sunset Yellow than Malachite Green. The reason for this might be the unequal size of molecules of the two dyes. Molecule of dye Sunset Yellow is quite smaller as compared to Malachite Green molecule, hence it is easier for Sunset Yellow molecule to diffuse into adsorbent (Ghaedi and Mosallanejad 2014).

Pelekani and Snoeyink (2000) selected adsorbates of similar size and they investigated the effect of pore size distribution on competitive adsorption mechanism between Atrazine and Methylene Blue on a series of phenolic resin-based microporous activated carbon fibers. Adsorptive competition mechanism of a particular pore is controlled by the size of the adsorbate relative to both pore size and size of competing species. Primary micropores have ability of adsorption selectivity or molecular sieve ability which get reduced rapidly with increasing pore size and characteristics of selectivity is almost absent for the secondary micropore region. Competitive effect was more dominant in micropore region for the same sorption sites and the magnitude of the competition decreases with increase in the pore volume. This enables transfer of adsorbates from primary micropore region to the secondary micropores (8–20 Å) (Pelekani and Snoeyink 2000).

Chan et al. (2012b) demonstrated that it is difficult to predict the equilibrium behavior of multicomponent systems using single component parameters. The experimental data was best

fitted to the correlative extended Freundlich model, suggests that the non-ideal nature significantly affects the system due to the properties of adsorbate and heterogeneous surface of the tyre demineralised activated carbon. The multicomponent model based on the extended Langmuir and the ideal adsorbed solution theory (IAST) models provided a good prediction of adsorption behavior only for binary dyes having similar sizes and properties used in a system, because the similar adsorption behavior significantly reduced the adsorbate–adsorbate interaction. However, models on the removal of Acid Blue 25 and Acid Yellow 117 using tyre demineralised activated carbon were not a good fit compared to the empirical models, because the basic assumption of ideal system is not applicable as solutes exhibited non-ideal adsorption behavior particularly at high solution concentrations (Chan et al. 2012b). The efficiency and the kinetic results obtained in a study (Duta and Visa 2015) showed that the molecular flexibility, dye structure, and dye molecular dimensions differently influence the competition for sorption sites. Bemacid Blue dye molecule showed fast diffusion at easily accessible sites though it has large molecular size as the molecule consist of aromatic rings linked only by σ flexible bonds. The more rigid azo-bond containing Bemacid Red molecule has a slower diffusion that results in slower sorption but it is able to access a larger amount of sorption sites of adsorbent (e.g. inside the small micro-pores) (Duta and Visa 2015). So, molecular dimensions play an important role for describing behavior of adsorption system which contains mixture of dyes. Physical properties pertinent to the adsorption of few dyes are listed in Table 2.7 that can be used in future research to study the adsorption behavior of combinations of dyes in an aqueous solution.

Table 2.7: General characteristics of various dyes.

Dye	Chromophore	Mol.wt. in ionized form (g/mol)	λ_{\max} (nm)	Electrical charges	Length (Å)	Width (Å)	Depth (Å)	Reference
Methylene Blue	Thiazine	284.4	665	+1	16.34	7.93	4.00	(Zhao et al. 2013)
Sudan I	Azo	248.28	476	0	13.55	9.74	3.68	(Zhao et al. 2013)
Acid Orange 7	Azo	327.33	507.5	-1	15.67	10.03	5.44	(Zhao et al. 2013)
Orange G	Azo	406.33	512	-2	15.64	10.14	5.44	(Zhao et al. 2013)
New Coccine	Azo	535.49	536	-3	17.38	10.48	5.44	(Zhao et al. 2013)
Acid Red 88	Azo	377.39	503	-1	15.66	10.27	5.44	(Zhao et al. 2013)
Tropaeolin OO	Azo	352.39	529	-1	17.52	7.70	6.48	(Zhao et al. 2013)
Ponceau 6R	Azo	456.44	518	-2	17.09	10.41	5.44	(Zhao et al. 2013)
Croscin Scarlet 3B	Disazo	510.50	510	-2	21.81	10.61	5.44	(Zhao et al. 2013)
Croscin Scarlet 7B	Disazo	538.55	-	-2	22.17	10.24	5.44	(Zhao et al. 2013)

								al. 2013)
Acid Black 1	Disazo	570.51	330	-2	22.93	11.15	5.44	(Zhao et al. 2013)
Methyl Blue	Triarylmethane	753.82	602	-2	24.49	14.35	13.89	(Zhao et al. 2013)
Acid Blue 25	Anthraquinone	393.39	600	-1	15.518	12.573	5.413	(Aguayo-Villarreal et al. 2013)
Acid Green 25	Anthraquinone	576.60	642	-2	15	14.9	11.6	(Dávila-Jiménez et al. 2009)
Acid Yellow 117	Disazo	802.84	438	-2	29.1	20.2	4.01	(Chan et al. 2012b)
Malachite Green	Triarylamine-thane	329.46	618	+1	12	11	10	(Castellini et al. 2008)

The adsorption behavior of the dyes in binary mixtures was investigated by Dávila-Jiménez et al. (2009) based on the relative molecular volume of the constituents and the amount of sulfonic groups present in the dye. They reported that the amount of solute adsorption is directly proportional to the molecular volume difference. Large molecular volume difference produces a

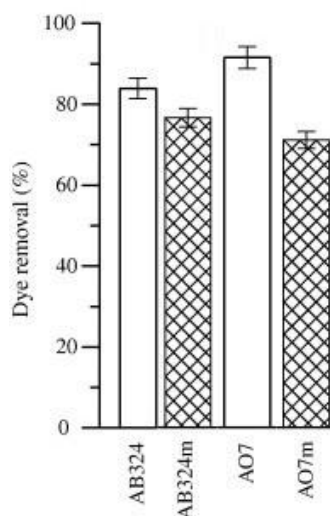
negligible diminution in the adsorption of the large molecule Acid Blue 80 from mixture and a considerable decrease in the adsorption of the small dye Acid Orange 10 from mixture vis-a-vis single component solutions. A great reduction of the removal capacity was observed for Acid Green 25 in presence of Acid Orange 8 and it amounts to 23%. Large molecular volume difference produces a negligible diminution of the adsorption of the large molecule Acid Green 27 in mixture and a considerable decrease of the adsorption of the small dye Acid Red 1 in mixture with respect to single component solutions. Table 2.8 shows the effects of relative molecular volume of the constituents and the amount of sulfonic groups present in the dye (Dávila-Jiménez et al. 2009).

Table 2.8: Effect of relative molecular volume of the constituents and the amount of sulfonic groups present in dye (Dávila-Jiménez et al. 2009)

Dyes in binary mixture	Relative molecular volume, ΔV (\AA^3)	Number of sulfonic groups on the dye moieties	Comparison of dyes adsorption in individual and in binary mixtures solutions (suffix 'm')	Effect
Acid Orange 10 + Acid Blue 80	214	2 and 2		The relative diminutions of the adsorbed amount are higher for the small molecules.

Acid Orange 90
7 + Acid Blue
324

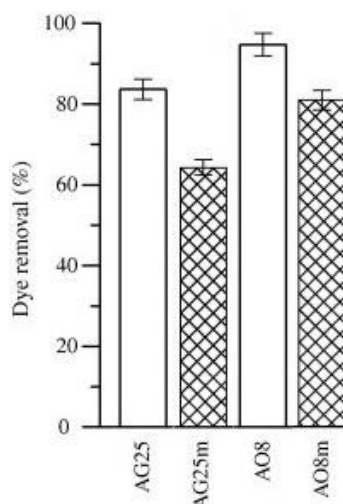
1 and 1



Removal of both dyes decreases in the mixture as compared to the single component solution.

Acid Orange 173
8 + Acid
Green 25

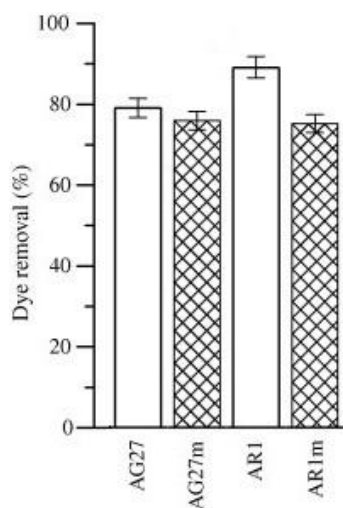
1 and 2



For this pair, competition of molecules with different bulkiness and different number of sulfonic functionalities play an important role.

Acid Red 1 + 199
Acid Green
27

2 and 2



Relative diminutions of the adsorbed amount are higher for the small molecules. Large molecular volume difference produces a negligible diminution of the adsorption of the large molecules.

2.3.2.4 Temperature

Issa et al. (2014) reported that the sorption of Methylene Blue and Malachite Green dyes was decreased with increase in temperature and this was evident from the maximum sorption values of solute, C_{sm} or equilibrium constants (K_L) for solutes as obtained from Langmuir equation. For both Methylene Blue and Malachite Green dyes, K_L values have been reduced by 60% and 40% respectively on increasing solution temperature by 20°C. This observation indicated that sorption of both dyes is sensitive to temperature and the sorption process is physically controlled (Issa et al. 2014).

Higher temperature is needed to obtain a higher dye removal by ZnS:Mn nanoparticles loaded on activated carbon (Hajati et al. 2014). Increased sorption at higher temperature in this case shows that large dye ion mobility was enhanced at higher temperature (Hajati et al. 2014; Mahmoodi et al. 2010; Turabik 2008), probably due to that an increasing number of molecules having sufficient energy at higher temperature interact with surface active sites (Mahmoodi et al. 2010).

2.3.2.5 pH

pH may play an important role in adsorptive removal of the target solutes by influencing the present state of solutes in solution. The dye adsorption capacity can be determined by the strength of ionic interaction between the adsorbent and the dyes (Ghaedi et al. 2012). Generally, high adsorption capacity is observed when anionic dyes are adsorbed on the adsorbent surface at acidic pH and cationic dyes at basic pH. This is by virtue of the strong electrostatic interaction between opposite charges that reside on the adsorbent surface and dye molecules (Kurniawan et al. 2012; Mahmoodi et al. 2011b).

Turabik (2008) studied the effects of pH (2–8) for the adsorption of Basic Yellow 28 and Basic Red 46 dyes from aqueous solution onto sorbent, bentonite. It was found that the sorption of these basic dyes on bentonite is mainly a pH-independent adsorption process. It takes place partly, by ion exchange and partly via non-coulombic interactions (Turabik 2008). Similarly, Zeinali et al. (2014) and An et al. (2015) also found that adsorption of dyes on the adsorbent is controlled by a adsorption mechanism which is pH-independent.

It is reported that free biomass of *Corynebacterium glutamicum* possesses excellent reactive dye binding capacity (Vijayaraghavan and Yun 2007). This specific characteristic of polysulfone-

immobilized protonated *Corynebacterium glutamicum* (PIPC) is used for biosorption of Reactive Blue 4 in the presence of Reactive Red 4, Reactive Orange 16, and Basic Blue 3 respectively in the competitive binary system. Among different values of initial pH (2–12), maximum 94% Reactive Blue 4 biosorption is reported between pH 2 and 3. In acidic pH, the biomass has net positive charge due to protonation of phosphonate, carboxyl, and amine functional groups (Won et al. 2005). Furthermore, reactive dyes release anions (ROSO^{3-}) in solution, which exhibits attraction due to electrostatic behavior towards positively charged biomass cell surface. Reactive dye biosorption was mainly occurred by the amino groups present in *Corynebacterium glutamicum* and the hydrogen ion present in *Corynebacterium glutamicum* acts as a bridging ligand between the bacterial cell wall and the molecule of dye (Vijayaraghavan and Yun 2008). At acidic pH, increased uptake of the anionic dyes due to electrostatic interactions between positive surface of a composite containing silver nanoparticles and colemanite ore waste (Ag-COW) was proclaimed as the surface charge of Ag-COW became more positive (Yola et al. 2014). Table 2.9 represents list of dyes and their suitable pH for maximum adsorption.

Fan et al. (2015) demonstrated that PANF-g-HPEIs (hydrothermally treated polyacrylonitrile fiber with hyperbranched polyethylenimine) adsorbent activated with different pH solutions effectively adsorb cationic and anionic dyes by applying a proper treatment. HPEI is a cationic polyelectrolyte, hence, PANFg-HPEIs may adsorb anionic Methyl Orange dye from aqueous solution. Capability of adsorbing cationic dye, Methylene Blue is due to the presence of COOH group on PANF-g-HPEIs. Figure 2.4 shows that adsorbent pretreated with pH = 5 solution adsorb the Methyl Orange molecules selectively from the Methyl Orange / Methylene Blue mixture. Adsorbent pretreated with pH = 10 solution adsorb selectively the cationic Methylene Blue molecules from the Methyl Orange / Methylene Blue mixture. The entire phenomena was studied using UV-vis spectrum of binary mixture as shown in Figure 2.4 (Fan et al. 2015).

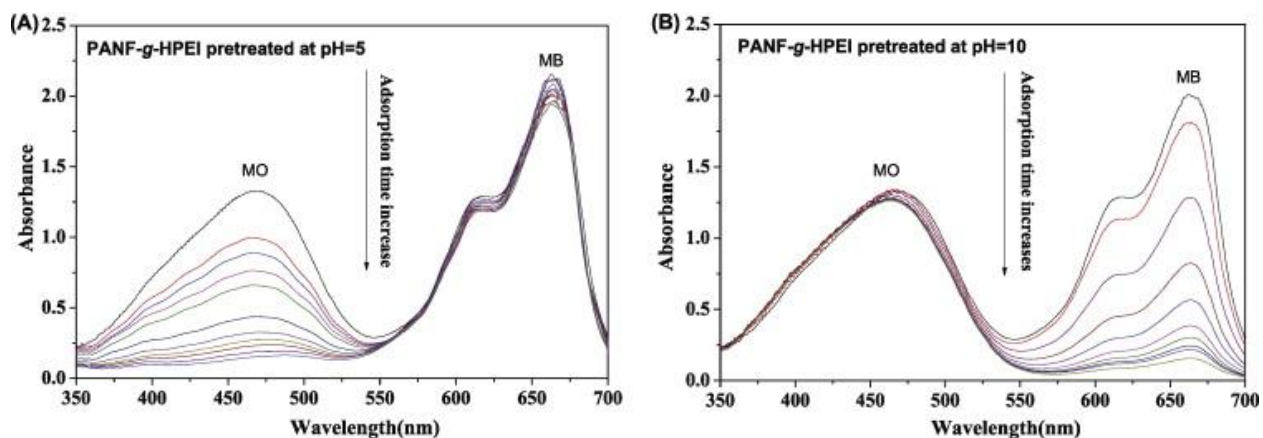


Figure 2.4: Time-dependent UV-vis spectra of mixture of Methyl Orange (MO) / Methylene Blue (MB) in the presence of PANF-g-HPEI pretreated at pH (A) 5 and (B) 10 (Fan et al. 2015).

Table 2.9: Favorable pH for dyes of different characteristics.

Dyes mixture	Nature of dye	Adsorbent	pH range	Favorable pH	Remarks	Reference
Brilliant green and Methylene blue	Cationic	Saccharomyces cerevisiae	1.0-8.0	6	Practically applicable for dye removal from natural aqueous dye solutions	(Ghaedi et al. 2013)
Direct Yellow 12 and Reactive Orange 12	Anionic	ZnS:Mn nanoparticles loaded on activated carbon	1.0-7.0	2	-	(Hajati et al. 2014)
Methylene Blue and Brilliant Green	Cationic	Graphite oxide nanoparticles	2.0-10.0	N.A.	Adsorption of dyes is controlled by a pH-independent adsorption mechanism	(Zeinali et al. 2014)

Basic Yellow 28 and Basic Red 46	Cationic	Bentonite	2.0 – 8.0	N.A.	pH-independent adsorption occurs by ion exchange and non-coulombic interactions	(Turabik 2008)
Direct Red 80 and Direct Red 23	Anionic	PAN-EDA nanofibers	2.1, 2.5, 3, 3.5, 6.5, and 9.1	3.5	-	(Almasian et al. 2015)
Crystal Violet and Congo Red	Cationic and anionic	CaFe ₂ O ₄ magnetic nanoparticles	4.0–10.0	N. A.	pH was not a critical limiting factor in a high efficiency of the dye removal using CaFe ₂ O ₄	(An et al. 2015)
Metanil Yellow and Reactive Blue 15	Anionic	Cross-linked chitosan beads	3.0–8.0	Metanil Yellow-4 Reactive Blue 15-3	Uptakes were much higher in acidic solutions than those in neutral and alkaline conditions.	(Chiou and Chuang 2006)
Direct Fast Scarlet, Eosin Y and Reactive Violet K-3R	Anionic	Poly-(epichlorohydrin dimethylamine) modified bentonite (EPIDMA/bentonite)	3.0–11.0	5	-	(Kang et al. 2009)
Reactive Yellow 86 and Reactive Red 2	Anionic	Silver nanoparticles and colemanite ore waste	2.0 – 9.0	2	Surface charge of Ag-COW became more positive that increased dye uptake	(Yola et al. 2014)

(Ag-COW)						
Methylene Blue and Malachite Green	Cationic	Rarasaponin-bentonite	3.0–10.0	8	-	(Kurniawan et al. 2012)
Reactive Red and Basic Red	Anionic and cationic	Water-compatible molecularly imprinted polymer	2.0–12.0	Reactive Red - 2 Basic Red - 10	-	(Kyzas et al. 2009)
Direct Red 23 and Acid Green 25	Anionic	Chitosan	2.0–10.0	2	High adsorption capacity due to the strong electrostatic interaction between –NH ³⁺ of chitosan and dye anions	(Mahmoodi et al. 2011b)
Alizarin Red S and Indigo Carmine	Anionic	Cetyltrimethylammonium bromide-modified TiO ₂	2.0–10.0	2.0	-	(Zolgharnein et al. 2014b)

2.3.2.6 Salt content

Dye industrial wastewater commonly contains dissolved inorganic ions. These ions may compete for the active sites on the sorbent surface because these salts have small molecular sizes and thus reduce the dye removal efficiency (Mahmoodi et al. 2011a; Mahmoodi et al. 2011b; Mahmoodi et al. 2010). A major disadvantage resulting of reactivity and non-selectivity of active sites on the sorbent is their reaction with non-target compounds, leading to dye auxiliaries in the exhausted dye bath present in the background water matrix. Thus, increased amount of adsorbent is needed to achieve the desired amount of dye removal (Mahmoodi et al. 2010).

2.3.2.7 Presence of major cations and anions

Liu et al. (2015b) investigated the effects of existing ions of inorganic salts on the selective sorption of dyes from industrial wastewater. In a ternary dye mixture system containing Congo Red, Methyl Orange, and Rhodamine B, effect of co-existing ions on the Congo Red uptake of in the presence of anions and cations viz. K^+ , NH_4^+ , Ni^{2+} , Mg^{2+} , Cu^{2+} , Pb^{2+} , Zn^{2+} , NO_3^- , CO_3^{2-} , PO_4^{3-} and SO_4^{2-} was studied. PO_4^{3-} and SO_4^{2-} creates a significant decrease in sorption of Congo Red. This was most likely occurred due to the formation of complexes inside the inner sphere surface on the adsorbent $CaFe_2O_4$ MNPs. However, the complexes of heavy metal ions along with other ionic species did not have negative impact on the sorption of Congo Red from wastewater (Liu et al. 2015b).

Apart from molecular dimension of dye; the effect of different parameters like sorbent dose, initial dye concentration, temperature, pH, salt content, and presence of major cations and anions on synergistic and antagonistic behavior of dyes during adsorption are extensively studied in a multicomponent dye system. It is reported that molecular dimension of each component differently affect the competition for the sorption sites and subsequently affect its rate and extent of adsorption during the treatment of mixture of dyes (Chan et al. 2012b; Duta and Visa 2015; Ghaedi and Mosallanejad 2014).

2.3.3 Equilibrium relationship for dyes in multicomponent adsorption system

Isotherms show the equilibrium relationship of a particular adsorbate-adsorbent system and these are basic requirement for any adsorption system design. Real industrial wastewater effluent contains mixture of several synthetic dyes, hence it is necessary to use isotherms that can express multicomponent adsorption, and competitive interaction among the participating adsorbates is taken into account. However, single solute isotherms would provide convenience to predict equilibrium of mixtures both from theoretical and practical applications of adsorption (Noroozi and Sorial 2013).

Presence of more than one solute in a system shows non-ideality. Multicomponent systems demonstrate many deviations from “ideal” adsorption due to sorbate - sorbate interactions in the solution. At sorption sites, alteration in sorbent affinity (or capacity) for one sorbate in the presence of the other, non-equal competition among sorbates, heterogeneity of the adsorbent

surface implies to have non-equal chances to be adsorbed for species (Al-Duri and McKay 1991).

Isotherm models that have been modified for multicomponent mixture of dyes are as follows:

2.3.3.1 Extended Langmuir isotherm

Butler and Ockrent (1930) extended the Langmuir model to explain the adsorption equilibrium in competitive adsorption systems. This empirical model assumes homogeneous adsorbent surface, sorbed species have no interaction, and sorption sites are uniformly available for all adsorbed species.

This model is applicable for ideal solutions. It is essential for applying extended Langmuir isotherm to an adsorption system that each solute obeys Langmuir behavior in a single solute system.

$$q_{e,i} = \frac{q_{m,i} K_{L,i} C_{e,i}}{1 + \sum_{i=1}^n K_{L,i} C_{e,i}} \quad \dots (2.3)$$

Kurniawan et al. (2012) proposed a revisited mathematical model for K_L and q_m parameters for sorption of binary system because the total or partial competitions between solutes for the sorption sites on the adsorbent surface occur. This may perform as the adsorption controlling factor. The lateral interaction or competitive behavior of dyes also affects adsorption potential. So, it could be remarked that adsorption behaviors in binary system cannot adequately described using both K_L and q_m parameters from single Langmuir model (Kurniawan et al. 2012).

The mathematical relationship between q_m and θ (each adsorbate's fractional loading on the sorbent surface) shows that the adsorbent surface was occupied with specific fractional loadings by solutes in binary system. The mathematical relationship between K_L and θ explains the adsorption potential for the adsorbate species which compete with each other for the sorption sites. The sorption affinity values for each component essentially lower as compared to single system due to the existence of competition between solutes of binary system (Kurniawan et al. 2012).

2.3.3.2 Jain and Snoeyink modified extended Langmuir model

Jain and Snoeyink (1973) developed a model to predict adsorption equilibrium for non-ideal systems. They extended Langmuir theory of multicomponent mixtures of binary adsorbates is thermodynamically consistent only if $q_{e,1} = q_{e,2}$. Jain-Snoeyink (JS) introduced an additional term in the extended Langmuir model which incorporates the competitive sorption behavior of binary organic sorbates on activated carbon from water solutions (Jain and Snoeyink 1973).

Sorption occurs without competition for different types of sites of sorbent along with adsorption with equal competition of solutes for sites in a binary organic system. In addition, the effects of competitive sorption became more significant with the increase in the number of solutes in solution (Martin and Al-Bahrani 1977). Choy et al. (2000) applied JS model to predict adsorption equilibrium of a binary dye system and found that this model cannot be used to predict the adsorption equilibrium of multicomponent acid dye on activated carbon. They found poor correlations between the predicted and experimental data (Choy et al. 2000).

2.3.3.3 Extended Freundlich isotherm

Extended Freundlich isotherm explains the reversible and non-ideal adsorption. The empirical isotherm model can be used for multilayer adsorption, where heat of adsorption and affinities are non-uniformly distributed over heterogeneous adsorbent surface (Adamson and Gast 1997). The total amount adsorbed solute on the adsorbent is the summation of sorption on all sites (Zeldowitsch 1934).

The equilibrium adsorption behavior of binary solute mixtures can be estimated by extended Freundlich model as mentioned below (Fritz and Schluender 1974):

$$q_{e,1} = \frac{K_{F,1} C_{e,1}^{n_1+x_1}}{C_{e,1}^{x_1} + y_1 C_{e,2}^{z_1}} \quad \dots (2.4)$$

$$q_{e,2} = \frac{K_{F,2} C_{e,2}^{n_2+x_2}}{C_{e,2}^{x_2} + y_2 C_{e,1}^{z_2}} \quad \dots (2.5)$$

Freundlich isotherm equations can be used to estimate $K_{F,1}$, $K_{F,2}$, n_1 and n_2 can be estimated from the and parameters (x_1 ; y_1 ; z_1 and x_2 ; y_2 ; z_2) are Freundlich adsorption constants in multi-component mixture of first and second solutes (McKay and Al-Duri 1989).

2.3.3.4 Sheindorf-Rebuhn-Sheintuch equation

Sheindorf et al. (1981) proposed Sheindorf-Rebuhn-Sheintuch (SRS) equation which is a Freundlich-type multicomponent adsorption isotherm. They employed Freundlich type multicomponent isotherm to describe sorption data of a variety of binary systems. In deriving SRS equation, the empirical model assumes that each moiety individually obeys Freundlich isotherm equation. Sorption energies exponentially distributed for each moiety in a multicomponent adsorption for available sorption sites and competitive Langmuir isotherm determines the coverage by each adsorbate at all energy level.

According to SRS equation, the isotherm coefficients are calculated from mono-component isotherm parameters except for the coefficients of sorption competition that should be determined through experiments for a multicomponent system. The i^{th} component sorption isotherm present in a k -component aqueous system can be expressed in terms of weight of sorbate is written as (Sheindorf et al. 1981):

$$q_i = K_{F_i} C_i \left(\sum_{j=1}^k \alpha_{ij} C_j \right)^{n_i-1} \quad \dots (2.6)$$

where α_{ij} is the competition coefficient for the sorption of solute i in the presence of solute j .

Sheindorf et al. (1982) applied SRS equation to the adsorption of organic pollutants on carbon from the aqueous solutions containing binary and ternary solutes. They reported that SRS equation is superior as compared to competitive Langmuir isotherm when the solutes in a system follow the Freundlich isotherm; however some parameters are needed for the Freundlich isotherm. The competition coefficients are obtained experimentally and these coefficients can be used in more complex systems ($k \geq 3$) (Sheindorf et al. 1982).

The competition coefficients of particular multicomponent systems are experimentally determined. One of the major advantages of the SRS equation is that it can predict the adsorption equilibrium of mixtures having three or more components by using values of a bi-component mixture in equation (2.6). This avoids performing a tiresome experiment containing three or

more solute in a mixture. α_{ij} could have value of zero (absence of competition) to value more than zero (< 10) shows a high degree of competition (Gutierrez and Fuentes 1993).

2.3.3.5 Ideal adsorbed solution theory

IAST is the most thermodynamically accepted model. It is originally proposed for mixtures of gas by Myers and Prausnitz (1965) and later it was used for dilute liquid solutions by Radke and Prausnitz (1972). IAST model predicts the adsorption equilibrium of ideal mixture from corresponding single solute isotherms as it assumes that the sorbed mixture forms an ideal solution (Myers and Prausnitz 1965).

Noroozi et al. (2008) applied IAST model on the basis of the theory which was presented by Lu and Sorial (2004) for the binary adsorption of dyes on GAC and silkworm pupa (SWP). They found that IAST gave good results for the binary dyes on GAC but it was found to be unsuccessful to predict the equilibrium of binary system on SWP. IAST can successfully used to study adsorption systems which are governed by physisorption. It is not suitable for systems governed by chemisorptions and therefore, it was observed to fail during adsorption study of the dye by silkworm pupa. Non-porosity in silkworm pupa limits the possibility to occur physisorption (Noroozi et al. 2008). Ho and McKay (1999) summarized the probable reasons for not getting satisfactory correlations of experimental data on application of the IAS model. No model has yet been proposed to predict chemisorption occurring because of chemical nature of dyes in multicomponent systems (Noroozi and Sorial 2013).

2.3.3.6 P-factor

This correlative technique was created by McKay and Al Duri (1987) and used for systems containing dye and carbon. It is based on a “lumped” capacity factor P_i is defined as follows (McKay and Al-Duri 1987):

$$P_i = \frac{q_{i,max, single}}{q_{i,max, multi}} \quad \dots (2.7)$$

Dimensionless capacity factor P correlates the equilibrium data of single component with the multi-component. This correlation model uses a ratio of $q_{i,max}$ i.e. monolayer capacity. Langmuir

isotherm model is used. Therefore, the multicomponent isotherm equation for each component i , is given as

$$q_{e,i,multi} = \frac{1}{P_i} \frac{q_{m,i} K_{L,i} C_{e,i}}{1 + \sum_{i=1}^n K_{L,i} C_{e,i}} \quad \dots (2.8)$$

Here, $q_{i,max,single}$ is a single component solid-phase concentration and $q_{i,max,multi}$ values are for the mixtures. Interaction and competition affects value of factor P and it likely depends on the relative concentrations of the dyes in the mixture, the sorbent surface sites coverage, the relative rates of each dye to approach equilibrium, and affinity and interactions (among dye-dye and dye-adsorbent) variations throughout the equilibrium isotherm. Choy et al. (2004) gave the values of P factor for different anionic dye systems.

2.3.3.7 Interaction factor

Schay (1956) first proposed η_i , interaction factor for i^{th} component in a N components system. It has a unique value for each component present in a mixture and is a function of all remaining components in an aqueous solution. It is difficult to predict the altered sorption capacity due to sorbent-sorbate interactions and competition of each component during sorption process. This correlative model incorporates various interactions in the solution and on the adsorbent surface (Choy et al. 2000). It assumes that interaction factor cannot be negative. It is based on minimizing the variance between measured and calculated multicomponent equilibrium data. η is calculated in order to minimize the hybrid fractional error function. The number of degrees of freedom of the systems is also taken into account (Choy et al. 2000).

$$\eta = \frac{100}{r-p} \sum_{i=1}^r \left[\frac{(q_{e,meas} - q_{e,calc})^2}{q_{e,meas}} \right]_i \quad \dots (2.9)$$

Where, r is the number of data points and p is the number of parameters of the isotherm equations. It has been reported that incorporation of interaction factor to extended Langmuir equation predicts good results in case of solutes have similar adsorbent affinities (Al-Duri and McKay 1991; McKay and Al-Duri 1989). Hence for the Langmuir isotherm:

$$q_{e,i} = \frac{q_{m,i} K_{L,i} (C_{e,i} / \eta_i)}{1 + \sum_{j=1}^r K_{L,j} (C_{e,j} / \eta_j)} \quad \dots (2.10)$$

Ho and McKay (1999) applied the concept of interaction factor to extended Langmuir equation to predict equilibrium data of copper and nickel ions in a competitive sorption system from aqueous solution using Peat. Furthermore, Mckay and Al-Duri (1989) and Al-Duri and Mckay (1991) found this model suitable for getting equilibrium isotherm data for multicomponent mixture of dyes with extended Langmuir equation. Chakraborty et al. (2006) studied the extended Langmuir isotherm modified with the interaction factors for adsorption of Reactive Red and Reactive Black on sawdust. They reported that it agrees well with the equilibrium data of dye mixtures.

Being simpler and relatively accurate approach, Choy et al. (2000) found that the application of the interaction factor does not provide a satisfactory correlation for their experimental data. The reason might be, this isotherm model neglects constant K for other components present in a system. They summarized the reasons for not getting satisfactory correlation using interaction factor. Table 2.10 summarizes adsorption equilibrium isotherms found suitable by various researchers for different systems consist of binary dye mixture.

Table 2.10: Adsorption equilibrium of some dyes on various adsorbents

Adsorbent	Adsorbates	Adsorption isotherm	Reference
Activated carbon	Direct Blue 78 and Direct Red 31	Langmuir	(Mahmoodi et al. 2011a)
Chitosan	Direct Red 23 and Acid Green 25	Temkin	(Mahmoodi et al. 2011b)
Cellulose extracted from Posidonia oceanica	Acid Blue 25 and Direct Blue 86	Extended Langmuir	(Douissa et al. 2014)
Granular activated carbon	C.I. Basic Blue 41 and C.I.	IAST	(Noroozi et al. 2008)

	Basic Red 18		
Natural kaolinitic-clay and philipsite-rich-zeolite tuff	Methylene blue and Malachite Green	Langmuir and competitive Langmuir	(Issa et al. 2014)
H-type activated carbon	Levafix Brilliant Red E-4BA and Levafix Brilliant Blue E-4BA	Competitive-Langmuir model	(El-Barghouthi et al. 2007)
Filtrisorb 400 activated carbon	Remazol reactive yellow, Remazol reactive black and Remazol reactive red	Langmuir	(Al-Degs et al. 2007)
Peat	Basic blue 3, Basic yellow 21, and Basic red 22	Extended Langmuir	(Allen et al. 2004)
Cationic surfactant (Hexadecyltrimethylammonium chloride) modified bentonite clay	Methylene blue, crystal violet and Rhodamine B	Extended Freundlich	(Anirudhan and Ramachandran 2015b)
Activated carbon from sawdust	Cibacron Red RB and Cibacron Black B	Langmuir isotherm modified with an interaction factor	(Chakraborty et al. 2006)
Activated carbon from waste bamboo	Acid Yellow 117 and Acid Blue 25	Redlich–Peterson	(Chan et al. 2008)
Activated carbon	Acid Blue and Acid Yellow	Extended Langmuir	(Choy et al. 1999)
Activated carbon	Acid Blue 80 and Acid Red 114	Langmuir isotherm modified with a P-factor	(Choy et al. 2004)
	Acid Blue 80 and Acid		

	Yellow 117		
	Acid Red 114 and Acid Yellow 117		
	Acid Blue 80, Acid Red 114 and Acid Yellow 117		
Acid treated okara	Acid Red 14 and Reactive Red 15	Partial competitive Langmuir, Langmuir– Freundlich and extended Freundlich	(Gao et al. 2011)
Clinoptilolite type natural zeolite	Reactive Blue 21 and Reactive Red 195	Extended Langmuir	(Sismanoglu et al. 2010)

2.3.4 Mathematical modeling of multicomponent batch sorption

Knowledge of the process behavior is needed before implementing it on a large scale. Mathematical modeling and simulation provide a complete knowledge of the process under different circumstances and enable a researcher to design a process without any prior experimental analysis. Literature is found rich with mathematical modeling considering continuous systems (Fernandez et al. 2015; Liapis and Rippin 1979; Ruthven et al. 1994) for removal of mixture of dyes due to their direct industrial application, whereas batch studies are helpful to facilitate necessary parameters in mathematical modeling (Al-Duri and McKay 1991). Only a limited number of batch studies to mixture of dyes sorption have been reported in the literature (Al-Duri and McKay 1992; Al-Duri and McKay 1991; Mckay and Al-Duri 1991). Chen et al. (2001) studied film-pore diffusion modeling for the sorption of metal ions from aqueous effluents onto peat in an agitated batch sorber (Chen et al. 2001).

Literature reveals that film-solid diffusion is appropriate to describe the adsorption of dyes (McKay and Al-Duri 1990). Film-solid diffusion can describe widest range of multicomponent solute systems and it is widely used model as it provided accurate results with similar diffusional

behavior of solutes (Liapis and Rippint 1977; Smith et al. 1987). The Freundlich extended empirical isotherm (Al-Duri and McKay 1991) and the modified extended Redlich-Peterson isotherm (Mckay and Al-Duri 1991) were used for solid solute equilibrium. The fundamental equations of single system were extended to binary (Al-Duri and McKay 1991; Mckay and Al-Duri 1991) and ternary (Mckay and Al-Duri 1991) dye systems. Following equations were developed based on non-idealities at the adsorbed phase, constant intraparticle diffusivity, absence of counterdiffusion and independent diffusion of components (Al-Duri and McKay 1991).

$$\frac{\delta u_j}{\delta t_j} = \frac{\delta^2 u_j}{\delta x^2} D_{sj} \quad \dots (2.11)$$

$$\frac{\delta u_j}{\delta t_j} x dx = \frac{k_{fj} R}{1000 \rho_s D_{sj} (1 - \varepsilon_p)} (C_{ij} - C_{sj}) \quad \dots (2.12)$$

$$q(t)_j = 3 \int_0^1 u_j x dx \quad \dots (2.13)$$

$$-V \frac{dC(t)_j}{dt} = m \frac{dq_j}{dt} \quad \dots (2.14)$$

where, dimensionless terms are

$$u_j = q(r, t)_j \cdot x \quad \dots (2.15)$$

$$\gamma_j = \frac{t D_{sj}}{R^2} \quad \dots (2.16)$$

$$x = r/R \quad \dots (2.17)$$

Initial and boundary conditions

$$u_j(0, \gamma_j) = 0 = u_j(x, 0) \quad \dots (2.18)$$

$$u_j(R, \gamma_j) = u_{sj}(\gamma_j) \quad \dots (2.19)$$

These equations can be solved numerically for t and analytically for x (McKay et al. 1984). Solid diffusivity showed as an increasing function of initial solute concentration of each in a multicomponent system and a single value of k_f described each component for specified conditions (Al-Duri and McKay 1991; McKay and Al-Duri 1991). However, D_{eff} was reduced with C_0 for multicomponent systems due to the increased internal resistance and competitive effects. Overall, it is reported that enhanced relative diffusion rate was found for the originally slower component and that inhibited the diffusion rate of faster one in the case of multisolute systems (Al-Duri and McKay 1992).

2.4 Reactive adsorption of organic pollutants

Adsorption has been found as one of the most efficient physicochemical processes for color removal, superior to many other processes used for recycling water in terms of the simplicity of operation (Almeida et al. 2009; Şahin et al. 2015). However, adsorption has some major hitches like spent adsorbent regeneration, cumbersome disposal of toxic species after adsorption, incomplete removal of contaminant, and slow adsorption rate. The enhancement in sorption capacity to improve the intake of adsorbate can be accomplished by considering a suitable and relevant modification method. Nevertheless, complete removal of contaminants and/or their alteration toward environmentally benign compounds are major concerns for long term solution (Gupta et al. 2016).

Reactive adsorption has emerged as an efficient process for dye removal due to the unique advantage of combining reactive degradation with adsorption in a single step (Gupta et al. 2015) and this leads to Process Intensification. It comprises concurrent reaction and separation of solute during adsorption in a single unit operation (Gupta et al. 2015). Reactive adsorption serves as a hybrid technology (Sharma et al. 2016). It is a viable alternative to adsorption that increases the degradation rate by a significant proportion when compared to simple adsorption with less frequency of regeneration (Shukla et al. 2010). The major component of organic pollutant consists of highly toxic colored dyes (Sharma et al. 2018). Reactive degradation may completely eradicate the color via degradation of dye molecules and may render the wastewater much less harmful (Nogueira et al. 2009).

2.4.1 Brief account of existing work done on reactive adsorption

Reactive adsorption has been studied by researchers in various fields like, desulphurization of petroleum streams (Ania and Bandosz 2006; Seredych et al. 2011), catalytic hydrodesulphurization (Bezverkhyy et al. 2008), removal of pharmaceuticals (Ania et al. 2011), heavy metal removal (Jia and Thomas, 2000), removal of Ammonia from food, rubber and fish processing, animal husbandry, composting plants etc. (Le Leuch and Bandosz 2007), removal of phenols and its derivatives (Matatov-Meytal and Sheintuch 1998; Shukla et al. 2010; Ania et al. 2002), and textile dyes (Nadejde et al. 2015) etc. Limited literature is available on removal of dyes by reactive adsorption.

Nogueira et al. (2009) studied reactive adsorption of Methylene Blue on clay montmorillonite using Electrospray Ionization Mass Spectrometry (ESI-MS) analytical technique and reported evidence of removal of organic substrate through reactive adsorption using ESI-MS data. Montmorillonite showed high activity for Methylene Blue oxidation in presence of H₂O₂. Results obtained from the study indicated that a highly reactive surface of montmorillonite which can be regenerated by hydrogen peroxide (by availing hydroxyl radicals) (Nogueira et al. 2009).

Gupta et al. (2015) studied the reactive adsorption of Methylene Blue using pretreated (hydrothermally modified) bentonite clay. The modified clay showed high efficacy for Methylene Blue removal via, reactive adsorption, which is supported by ESI-MS study. The results indicated that the crystalline structure of raw bentonite upon hydrothermal treatment transformed into amorphous nature. Pretreatment increased the concentration of OH surface functional groups pointing toward increased reactive behavior. Pretreated bentonite yielded a high degree of color removal rendering the Methylene Blue solution colorless with 100% Methylene Blue removal. Furthermore, ESI-MS analysis showed reactive degradation of Methylene Blue molecule by oxidation via hydroxylation of reaction intermediates. The degradation products of Methylene Blue were found environmentally benign (Gupta et al. 2015). Khaksar et al. (2015) studied green oxidative degradation of organic compound using Mn-doped ZrO₂ nanoparticles as an efficient catalyst. The catalytic degradation of Methylene Blue in the presence of these nanoparticles as catalyst in the presence of an oxidizing agent i.e. aqueous hydrogen peroxide has been studied (Khaksar et al. 2015).

2.4.2 Reactive adsorption of dye using Fe-GAC/H₂O₂ system

Granular activated carbon (GAC) has excellent adsorption capacity, chemical stability, mechanical strength and economic promise for the removal of dissolved organic matter (Chang et al. 2015; Rafatullah et al. 2010). Iron loading on GAC removes organic compounds through catalytic oxidation (Xu et al. 2015). The catalytic effect of Fe(III) and GAC as the electron donor (Xu et al. 2015) played an important role in the formation of hydroxyl radical from hydrogen peroxide.

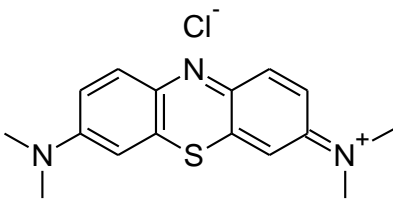
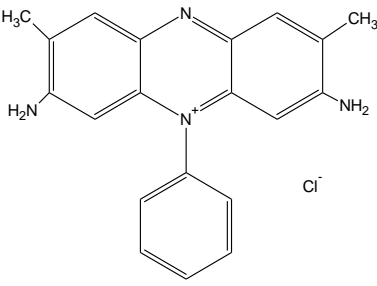
Reactive adsorption has offered a strong promise for wastewater treatment as it can catalyze the oxidative degradation of a wide range of compounds using Fe₂O₃/activated-carbon composites in the presence of H₂O₂ (Zazo et al. 2006) which produces hydroxyl radical ($\bullet\text{OH}$). $\bullet\text{OH}$ is a highly reactive specie ($E^0 = 2.80 \text{ V}$) (Pereira et al. 2011) that can quickly and non-selectively oxidize organic pollutants (Neamu et al. 2004). Furthermore, reactive adsorption of organic pollutant eradicates the limitation of sludge production in Fenton's process (Chen et al. 2011) and reduces the design complexity and capital investment.

3 Materials and Methods

3.1 Materials

MB from Fisher Scientific (India) and SO from Sigma Aldrich (India) were obtained and used as an adsorbate without further purification. Table 3.1 shows the characteristics of MB and SO dyes:

Table 3.1: Properties of dyes

Characteristics	Methylene Blue	Safranin O
Molecular formula	$C_{16}H_{18}N_3SCl$	$C_{20}H_{19}C_1N_4$
Molecular weight (g/mol)	319.85	350.84
λ_{max} (nm)	663	519
CAS number	61-73-4	477-73-6
Color index number	52015	50240
Water solubility	40 g/L (20 °C)	50 g/L (20 °C)
Molecular structure		

Granular activated carbon (CDH, India), hydrogen peroxide and ferric chloride were procured from Merck (India).

3.1.1 Synthesis of Fe-GAC

Fe-GAC was prepared using 2.5% Fe^{3+} solution using FeCl_3 (Mondal et al. 2007). A multiple times washing of GAC followed by drying at 105 °C until a constant weight was obtained. Afterwards, 10 g of GAC was used and further treated with 24 mL of FeCl_3 solution (2.5% Fe^{3+}) at its natural pH (2 – 4). Iron impregnation was carried out in an oven at 70°C until the complete drying of the solution. Unbounded iron of Fe impregnated GAC was removed by multiple washing using deionized water. Finally, Fe-GAC was dried at 110 °C till no change in weight loss was found and then it was stored for further use. Preparation method of Co-GAC is given elsewhere (Sharma et al. 2016).

3.2 Methods and techniques

3.2.1 Details of instruments used during experiments and aqueous phase analysis

3.2.1.1 Analytical weighing balance

A weighing balance was used for weighing chemicals for the experiments. The specifications of the same are given in Table 3.2:

Table 3.2: Specifications of electronic weighing balance

Instrument	Weighing balance
Manufacturer	Mettler Toledo, USA
Capacity	220 g
Model	ME204
Least count	0.1 mg

3.2.1.2 Oven

A hot air oven was utilized for drying and heating purposes. The specifications are given in Table 3.3:

Table 3.3: Specifications of oven

Instrument	Hot air oven
Manufacturer	Associated scientific technologies, Delhi

Model	Sonar
Temperature	0 – 500 °C
Display	Digital

3.2.1.3 pH meter

A pH meter was used to determine the pH of aqueous solutions. It consists of two major parts (i) temperature sensor and (ii) electrode for pH measurement. Buffer solutions of pH = 4.01, 7.01, 10.01 were used for instrument calibration. Other features are given in Table 3.4:

Table 3.4: Specifications of pH meter

Instrument	pH meter
Manufacturer	Hanna instruments, USA
pH range	2 – 14
Accuracy	±0.02
Temperature correction	Automatic
Display	LCD

3.2.1.4 Incubator shaker

Incubator shaker (Model: STI – 109) was used for the adsorption experiments in batch operations. The temperature can be varied from 20 – 60 °C. It contains a controller with an accuracy of ±0.5 °C and a dual display PID microprocessor and, digital temperature indicator. The shaker was provided preset controlled temperature and shaking speed. Aqueous solutions with desired initial concentration, measured amount of sorbent and H₂O₂ (in case of reactive adsorption) were put in a 250 mL borosil Erlenmeyer flask to put in the incubator grooves. The required shaking speed and temperature were maintained.

3.2.1.5 UV-Vis spectrophotometer

Dyes concentrations were measured using UV-Vis spectrophotometer with a double beam. The instrument measures absorbance according to Beer-Lambert law. The calibration curves were prepared using concentrations of the particular dye solutions so that these followed the linear plot. The specifications of the equipment are given in Table 3.5:

Table 3.5: Specifications of UV-Vis spectrophotometer

Instrument	UV-Vis spectrophotometer
Manufacturer	Shimadzu corporation analytical instruments, Japan
Model	UV – 1800
Light source	Deuterium and tungsten halogen lamp
Optics	Double beam
Source power	230 ± 10% AC three phase
Frequency	50 Hz
Wavelength range	190 – 1100 nm

3.2.1.6 Electrospray ionization coupled with mass spectroscopy (ESI-MS)

A Xevo G2-S Q ToF (Waters, USA) mass spectrometer is used to carry out ESI-MS analyses in the positive ion mode. The samples are analyzed by introducing aliquots into the ESI source via a syringe pump at 10–20 mL/min flow rate. ESI conditions are as follows: desolvation temperature: 350 °C; cone gas flow rate: 156 L/h; desolvation gas flow rate: 600 L/h; capillary voltage 3 kV. The isolated ions are excited using a supplementary ac signal. This whole process is brought about collision-induced dissociation (CID). The collision energy is set at a value at which product ions were produced in measurable quantities.

3.2.2 Characterization techniques for adsorbent

3.2.2.1 Transmission electron microscope coupled with energy dispersive spectroscopy (TEM-EDS)

Images of virgin GAC and Fe impregnated GAC particles were taken using a using TecnaiG² 20 (FEI) S- Twin 200 kV transmission electron microscope (TEM) coupled with energy dispersive spectroscopy (EDS).

3.2.2.2 BET surface area

The adsorbent surface area was obtained using BET method. QuadraSorb Station 2 BET surface area analyzer was used to conduct the nitrogen adsorption-desorption process at 77.35 K. The Multi-layer Brunauer–Emmett–Teller (BET) equation was used to obtain the surface area.

3.2.2.3 X-ray diffraction (XRD)

Structure of GAC and Fe-GAC were recorded by X'Pert Pro x-ray diffractometer (PAN analytical BV, The Netherlands) operated at a voltage of 45kV and current of 40mA with Cu $k(\alpha)$ radiation of wavelength 1.54059 Å, at grazing angle X-ray diffraction. Scanning was done in region of 2θ from 10° to 50°.

3.3 Batch reactive adsorption studies

Fe-GAC exhibit catalytic activity in the presence of H₂O₂ and this characteristic was used for the study of degradation of dyes in single and binary aqueous solutions. For MB removal in single solute system, an Erlenmeyer flask was charged with 100 mL of aqueous MB (10 mg/L) and 0.2 g/L of catalyst was added. 1.0 mM H₂O₂ was added to the flask and the reaction mixture was continuously agitated using shaker at 30 ± 1 °C at pH 6.5. For SO removal in single solute system, an Erlenmeyer flask was charged with 100 mL of aqueous SO (10 mg/L) and 1.0 g/L of catalyst were added. 5.0 mM H₂O₂ was added to the flask and the reaction mixture was continuously agitated using a shaker at 30 ± 1 °C at pH 6.5.

To study simultaneous dye removal in binary dye system, an Erlenmeyer flask was charged with 100 mL of aqueous MB and SO (5 mg/L each) and 0.5 g/L of adsorbent was added. 2.0 mM H₂O₂ was added to the flask and the reaction mixture was continuously agitated using a shaker at 30 ± 1 °C at pH 6.5. Batch experiments of reactive adsorption were carried out at different

temperatures (15 – 35 °C) for kinetic and thermodynamic studies. In MB and SO mixture solutions, the optimal wavelength of each dye was chosen using absorbance spectra where impact of the other dye was observed to be minimal. Individual maximum wavelengths of dyes were used to measure absorbance in the solution due to very low level of peak overlaps.

For a defined time interval, a sample was pipetted into a quartz cell, and its absorption spectrum was measured using UV–visible spectrophotometer. An ESI-MS analysis was carried out to identify the degradation intermediates during reactive adsorption of dyes in single and binary solute system at definite time intervals. The shaking speed was kept at maximum (150 rpm) throughout the batch adsorption studies to minimize the external mass transfer and diffusion resistances. Therefore, these resistances were not taken into account during kinetic studies.

3.4 Batch adsorption studies

Equilibrium batch experiments of MB were carried out using equal masses of 0.2 g/L of Fe-GAC in 100 mL of MB (10–50 mg/L). Kinetic batch studies were also carried out with initial MB concentration of 10 mg/L and dose of 0.2 g/L Fe-GAC. The Gibbs energy, enthalpy and entropy, (ΔG° , ΔH° , ΔS°), for the adsorption process were obtained from the experiments carried out at different temperatures (20 – 60 °C). Equilibrium batch studies of SO were conducted using equal masses of 1.0 g/L of Fe-GAC in 100 mL of SO (10–50 mg/L). Batch removal of SO was also studied with initial concentration of 10 mg/L and a dose of 1.0 g/L of Fe-GAC for 5 h. Batch equilibrium experiments for simultaneous MB and SO removal were carried out using equal masses of 0.1 g/L of Fe-GAC in 100 mL of MB (1–5 mg/L) and SO (1–5 mg/L). Kinetic batch studies were also carried out with initial MB and SO concentrations of 5 mg/L each and a dose of 0.4 g/L of Fe-GAC. Isothermal shaker incubator was used for 24 h at 30 ± 1 °C and 150 rpm to reach the equilibrium of the solid-solution mixture. Maximum shaking speed throughout the batch adsorption minimizes the external mass transfer and diffusion resistances and hence, these resistances were not taken into account during kinetic studies. The concentrations of MB and SO solution were analyzed by UV- Vis spectrophotometer-1800 (Shimadzu) at λ_{max} 663 and 519 nm respectively. The dye removal percentage and adsorption capacity, q_e (mg/g) were calculated using the following relationships:

$$\% \text{ dye removal} = \frac{C_0 - C_t}{C_0} \times 100 \quad \dots (3.1)$$

$$q_t = \frac{(C_0 - C_t) \times V}{W} \quad \dots (3.2)$$

3.5 Reactive adsorption

3.5.1 Kinetics

The kinetic analysis was carried out of decoloration of dye solutions.

3.5.1.1 First order reaction kinetics

It can be expressed as (Rauf et al. 2010)

$$-\ln \frac{C_t}{C_0} = k_{app} t \quad \dots (3.3)$$

A linear fitting of the data between $-\ln \frac{C_t}{C_0}$ and t for dye of the above equation was used to estimate the value of k_{app} .

3.5.1.2 Second order reaction kinetics

Second order reaction kinetics can be represented by below equation (Rauf et al. 2010)

$$\frac{1}{C_t} = \frac{1}{C_0} + k_{app} \times t \quad \dots (3.4)$$

A plot of $1/C_t$ versus t was plotted to obtain k_{app} value.

3.5.2 Thermodynamics

The dependence of apparent rate constant on temperature can be expressed by Arrhenius relation as follows:

$$k_{app} = Ae^{-E_a/RT} \quad \dots (3.5)$$

Simplified,

$$\ln k_{app} = \ln A - \frac{E_a}{RT} \quad \dots (3.6)$$

A linear plot between $\ln k_{app}$ and $1/T$ used to estimate activation energy.

Lonhienne et al. (2000) used an enzymatic reaction system for the determination of activation parameters. The temperature dependence of the catalytic rate constant is given by the relation:

$$k_{cat} = \frac{k_B T}{h} e^{-\Delta G^\ddagger / RT} \quad \dots (3.7a)$$

$$\Delta G^\ddagger = RT \times \left(\ln \frac{k_B T}{h} - \ln k_{cat} \right) \quad \dots (3.7b)$$

where, R is the gas constant ($8.314 \text{ J mol}^{-1} \text{ K}^{-1}$), k_B is the Boltzmann constant ($1.3805 \times 10^{-23} \text{ J K}^{-1}$), h the Planck constant ($6.6256 \times 10^{-34} \text{ J s}$) and ΔG^\ddagger the free energy of activation. After introduction of the constant values, above equation leads to equation 3.7. The thermodynamic properties (ΔG^\ddagger , ΔH^\ddagger and ΔS^\ddagger) of dye oxidative degradation using reactive adsorption can be determined using activation energy and apparent rate constant (Lonhienne et al. 2000) using below equations.

$$\Delta G^\ddagger = RT \times (23.76 + \ln T - \ln k_{app}) \quad \dots (3.7)$$

$$\Delta H^\ddagger = E_a - RT \quad \dots (3.8)$$

$$\Delta S^\ddagger = \frac{\Delta H^\ddagger - \Delta G^\ddagger}{T} \quad \dots (3.9)$$

3.6 Adsorption

3.6.1 Equilibrium isotherm for single component

Adsorption equilibrium is a dynamic equilibrium state where both adsorption and desorption rates are equal (Foo and Hameed 2010). The experimental data were analyzed using Langmuir and Freundlich isotherms to describe the nature of adsorption equilibrium.

3.6.1.1 Langmuir isotherm

This equilibrium isotherm model was developed based on the assumptions of ideal adsorption that uptake occurs on homogeneous surface by monolayer sorption, no interaction between sorbed molecules, uniform energies of adsorption onto the surface, no transmigration of adsorbate in the plane of the surface (Karagoz et al. 2008). Non-linear form of Langmuir isotherm can be given as:

$$q_e = q_m \frac{K_L C_e}{1 + K_L C_e} \quad \dots(3.10)$$

Above equation is simplified to linear form as below:

$$\frac{C_e}{q_e} = \frac{1}{q_m K_L} + \frac{C_e}{q_m} \quad \dots(3.11)$$

R_L , dimensionless separation factor is given as (Weber and Chakravorti 1974):

$$R_L = \frac{1}{1 + K_L C_0} \quad \dots(3.12)$$

The nature of the adsorption process can be identified using value of R_L and it is as given in Table 3.6.

Table 3.6: Value of separation factor R_L (Weber and Chakravorti 1974)

R_L value	Nature of adsorption process
$R_L > 1$	Unfavorable
$R_L = 1$	Linear
$0 < R_L < 1$	Favorable
$R_L = 0$	Irreversible

3.6.1.2 Freundlich isotherm

Freundlich isotherm assumed non-ideal sorption and heterogeneous sorption (Hameed et al. 2007a). Non-linear form of Langmuir isotherm can be given as:

$$q_e = K_F C_e^{1/n}$$

Above equation can be also written in linear form as below:

$$\ln(q_e) = \frac{1}{n} \ln(C_e) + \ln(K_F) \quad \dots (3.13)$$

3.6.2 Equilibrium isotherm for binary component

3.6.2.1 Extended Langmuir isotherm

Butler and Ockrent (1930) proposed the extended Langmuir model to describe the sorption equilibrium in competitive adsorption systems (Butler and Ockrent 1930).

$$q_{e,i} = \frac{q_{m,i} K_{L,i} C_{e,i}}{1 + \sum_{i=1}^n K_{L,i} C_{e,i}} \quad \dots (3.14)$$

3.6.2.2 Extended Freundlich isotherm

The equilibrium adsorption from binary mixtures can also be estimated by the extended Freundlich equation as given (Fritz and Schlunder 1974)

$$q_{e,i} = \frac{K_{F,i} C_{e,i}^{n_i+x_i}}{C_{e,i}^{x_i} + y_i C_{e,j}^{z_i}} \quad \dots (3.15)$$

Freundlich isotherm equations can be used to estimate $K_{F,1}$, $K_{F,2}$, n_1 and n_2 can be estimated from the and parameters (x_1 ; y_1 ; z_1 and x_2 ; y_2 ; z_2) are Freundlich adsorption constants in multi-component mixture of first and second solutes (McKay and Al-Duri 1989).

3.6.3 Kinetics

The prediction of batch sorption kinetics is essential for adsorption column design in industries. In order to investigate the adsorption kinetics of dyes on to Fe-GAC, pseudo-first-order, pseudo-second-order and intraparticle diffusion models were used.

3.6.3.1 Pseudo-first-order kinetics

The pseudo-first-order kinetics is based on following assumptions as sorption occurs only on localized sites, it involves no interaction between the sorbed ions, adsorption energy does not dependent on surface coverage, saturated monolayer corresponds to maximum adsorption of adsorbates on the sorbent surface, and uptake of metal ion on the activated carbons is followed

first-order-rate equation (Largitte and Pasquier 2016). Pseudo-first-order equation can be written as (Kumar 2006):

$$q = q_e (1 - \exp^{-k_1 t}) \quad \dots (3.16)$$

Integration of the above equation for the boundary conditions $t = 0$ to $t = t$ and $q_t = 0$ at $t = 0$, gives:

$$\log(q_e - q_t) = \log(q_e) - \frac{k_1 t}{2.303} \quad \dots (3.17)$$

A linear plot between $\log(q_e - q_t)$ versus t was used to predict the values of k_1 and q_e .

3.6.3.2 Pseudo second order

Pseudo-second-order adsorption mechanism explains that the overall rate of dye sorption process controlled by the chemisorption (Hameed et al. 2007b). Pseudo-second-order kinetic model can be written as (Rodríguez et al. 2009):

$$q = \frac{K_2 q_e^2 t}{1 + K_2 q_e t} \quad \dots (3.18)$$

A simplified form is given as below:

$$\frac{t}{q_t} = \frac{1}{k_2 q_e^2} + \frac{1}{q_e} t \quad \dots (3.19)$$

A linear plot between (t/q_t) versus t was used to predict the values of k_2 and q_e .

3.6.3.3 Intraparticle diffusion model

Intraparticle diffusion represents the experimental kinetics where the effect of film diffusion is expected to be negligible (Kumar 2006). It is expressed as:

$$q_t = k_{id} t^{1/2} + C \quad \dots (3.20)$$

A linear plot between (q_t) versus t was used to predict the values of k_{id} and C .

3.6.4 Thermodynamics

Thermodynamic parameters including Gibbs free energy change (ΔG°), enthalpy change (ΔH°) and entropy change (ΔS°) were calculated for the adsorption process from the following equations (Hong et al. 2009; Karagoz et al. 2008);

$$\Delta G^\circ = -RT \ln K_e \quad \dots (3.21)$$

$$K_e = \frac{q_e}{C_e} \quad \dots (3.22)$$

$$\Delta G^\circ = \Delta H^\circ - T\Delta S^\circ \quad \dots (3.23)$$

The negative values of Gibbs free energy change (ΔG°) confirmed the feasibility of the process and the spontaneous nature. Plot of ΔG° versus T was used for estimation of thermodynamic parameters (ΔH° and ΔS°) for the adsorption of dye onto Fe-GAC. The positive value of ΔH° suggests the endothermic nature of adsorption for the Fe-GAC. The positive value of ΔS° reflects the affinity of the Fe-GAC for the dye (Bhattacharya and Sharma 2005).

3.7 Error analysis - sum of squares of errors

In the binary dye adsorption system, the optimum isotherm parameters mentioned in isotherm equations were found by minimizing the difference between the experimental and model data of the equilibrium solid phase concentration, q_e , using the sum of the squares of the error (SSE) function.

$$SSE = \sum_{i=1}^n (q_{e,calc} - q_{e,exp})_i^2 \quad \dots (3.24)$$

4.1 Catalyst characterization

Figure 4.1a shows the TEM image of virgin GAC. Clusters of iron on GAC are visible in the TEM image (Figure 4.1b). Figure 4.1b demonstrates that Fe has been deposited into particles of GAC. Figure 4.1a shows the amorphous nature of GAC whereas Figure 4.1b indicates the crystallinity of the synthesized Fe-GAC. Elemental analysis of GAC by EDS was used for further confirmation of presence of Fe on GAC surface (Figure 4.2a and b), a considerable amount of Fe has been embedded on GAC surface (Table 4.1). It can be interpreted from Table 4.1 that GAC surface primarily consists of carbon and oxygen only while Fe-GAC has iron and chloride ions traces in addition to C and O elements. TEM analysis of Fe-GAC verified the presence of iron particle clusters in GAC. These iron particles were sizes ranging from 50 to 100 nm. This size of iron particles deposited in GAC was found consistent with literature (Hristovski et al. 2009).

The BET surface area was 657 and 450 m²/g of GAC and Fe-GAC respectively. The specific surface area of Fe-GAC was reduced than GAC because of impregnation of iron inside the GAC particle during modification.

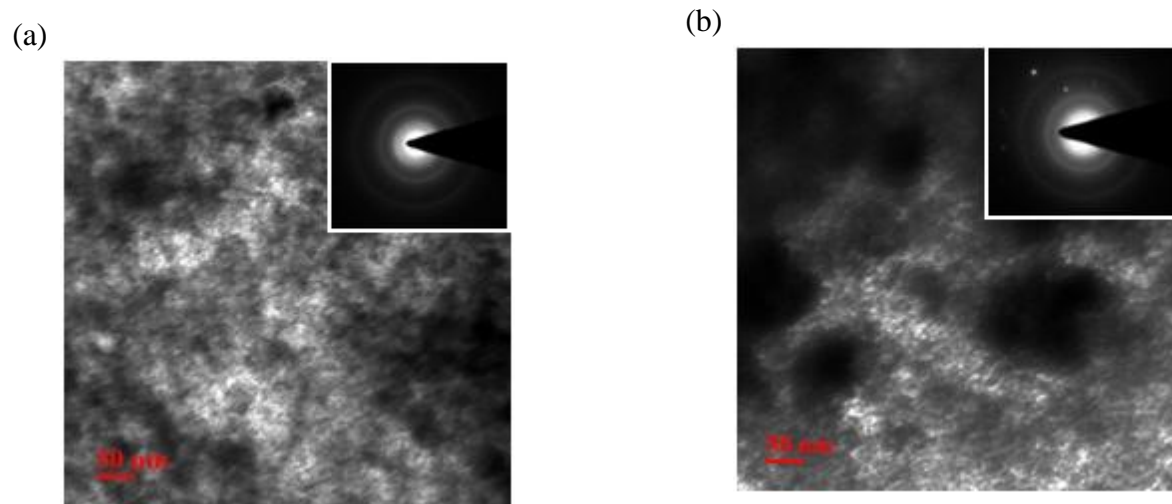
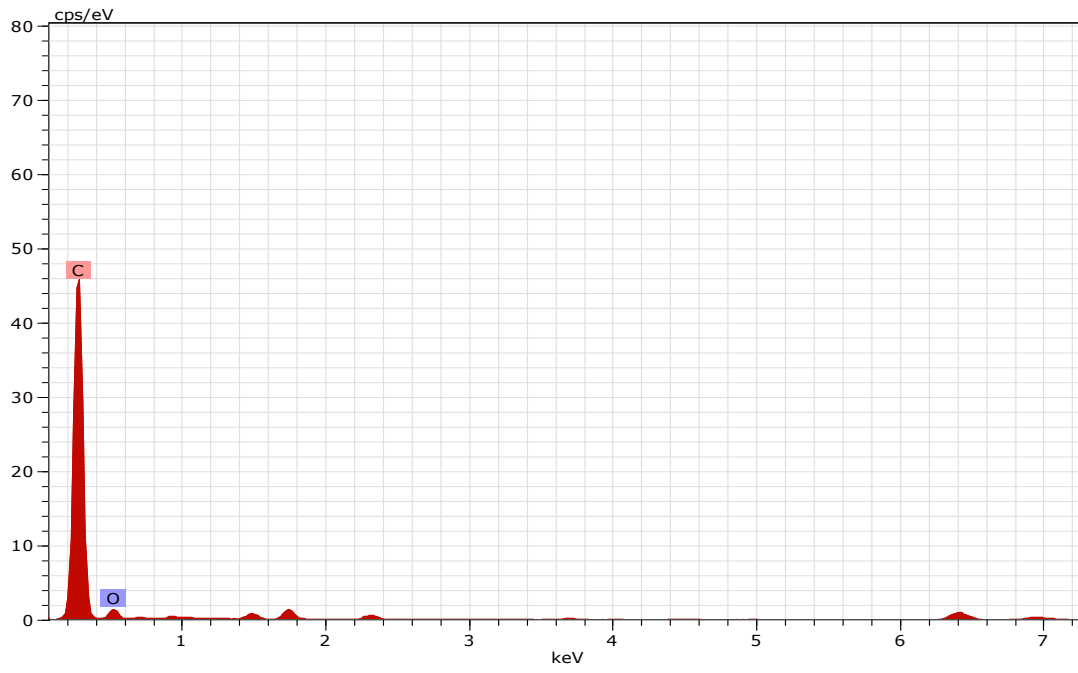


Figure 4.1: TEM of (a) GAC and (b) Fe-GAC

(a)



(b)

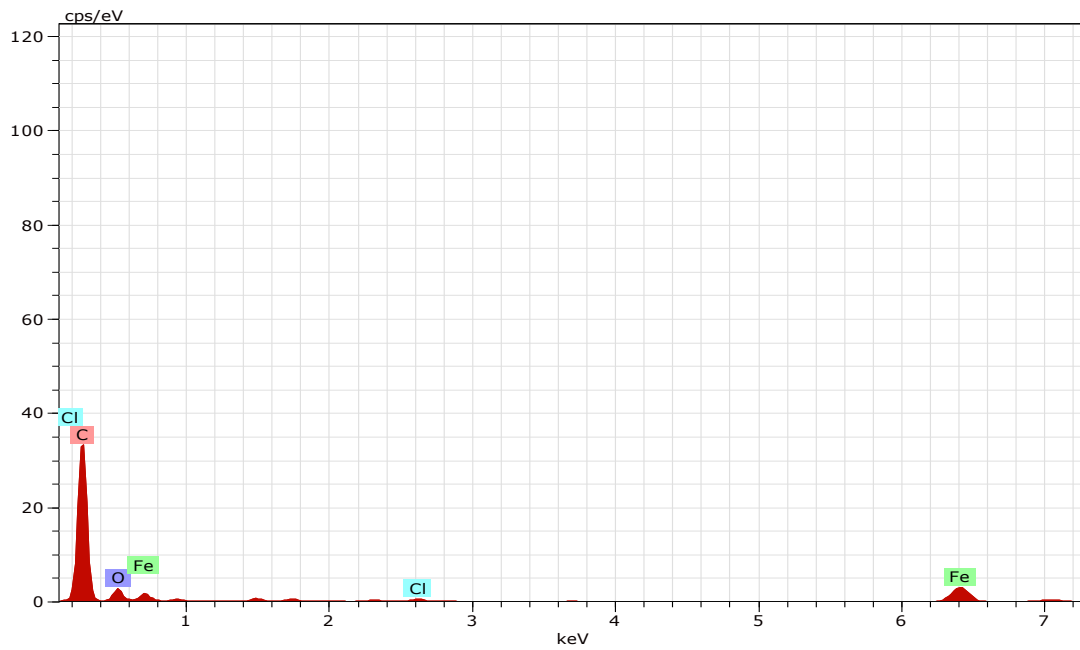
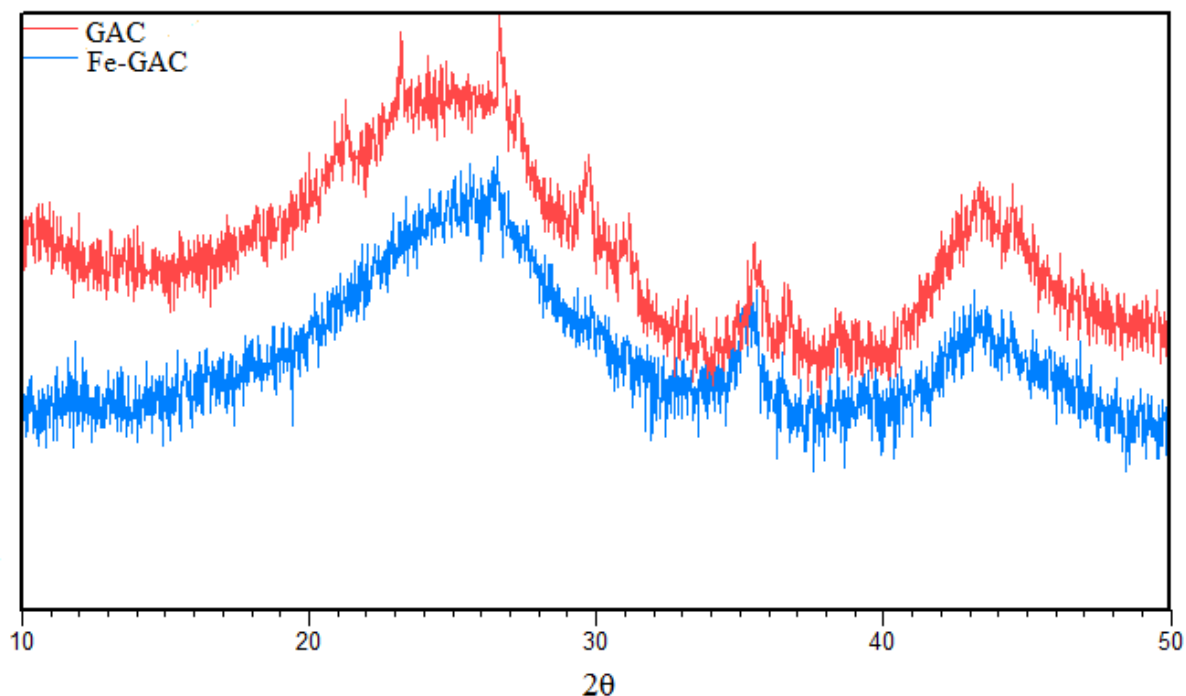


Figure 4.2: EDS analysis of (a) GAC and (b) Fe-GAC.

Table 4.1: Elemental analysis of GAC and Fe-GAC using EDS

Elemental analysis	GAC (wt %)	Fe-GAC (wt %)
C	99.60	96.56
O	0.40	1.06
Fe	-	2.17
Cl	-	0.21

**Figure 4.3:** XRD patterns of GAC and iron-loaded GAC after impregnation with solution of iron (III) chloride.

No significant difference was found between the XRD patterns of original and doped GAC apart from a peak in Fe-GAC sample at $2\theta = 26^\circ$ which was a broad halo for GAC (see Figure 4.3). The XRD pattern of Fe-GAC showed reflection corresponding to the crystalline phases, such as akaganeite (β -FeOOH) (Chang et al. 2010). XRD pattern of Fe-GAC showed presence of crystallinity, as its preparation involved drying at $70 - 80^\circ\text{C}$ for 8 h, during this period amorphous iron (hydr)oxides gradually converted to crystalline iron (III) oxides (Gu et al. 2005). Presence of crystalline phases in Fe-GAC could be confirmed using TEM diffraction pattern (see Figure 4.1).

Figure 4.3 shows that almost similar pattern obtained after impregnation may be due to that deposited Fe particles are very small to diffract, or may be also because of the concentration of sorbed iron is too low. It is reported that oxidizing activated carbons and their impregnation them with either iron (III) or (II) chloride solutions did not change the XRD patterns (Muñiz et al. 2009).

Part I: Reactive adsorption and adsorption

4.2 MB removal efficiencies of different systems

This study investigated the performance of Fe-GAC/H₂O₂ system for reactive adsorption of MB. λ_{\max} of dye was chosen for investigating removal of MB. A comparative evaluation was carried out for 7 systems (H₂O₂, Co-GAC, Co-GAC/H₂O₂, GAC, GAC/H₂O₂, Fe-GAC, Fe-GAC/H₂O₂). The MB removal efficiencies of H₂O₂, Co-GAC, Co-GAC/H₂O₂, GAC, GAC/H₂O₂, Fe-GAC, Fe-GAC/H₂O₂ were found to be 6%, 8%, 13%, 40%, 41%, 25%, and 94% respectively (Figure 4.4). It can be observed from Figure 4.4 that H₂O₂ alone and combined with GAC were not found effective for MB removal. Co-GAC and Co-GAC/H₂O₂ also showed very low MB removal efficiency. This could be due to the fact that Co-GAC/H₂O₂ could not generate enough hydroxyl radicals that can effectively oxidize MB (Bokare and Choi 2014; Burg et al. 2014; Ling et al. 2010).

Approximately, the same MB removal was obtained using GAC and GAC/H₂O₂ systems. It indicated that presence of GAC could not produce hydroxyl radicals using H₂O₂. Almost 15% less adsorptive MB removal was obtained using Fe-GAC than GAC may be due to reduction in availability of surface sites on GAC due to iron oxide coating. Furthermore, maximum MB removal was achieved using Fe-GAC/H₂O₂ system. Thus, Fe-GAC/H₂O₂ found most efficient system for MB removal probably due to impregnated iron oxides served as a catalyst for generation of hydroxyl radicals that removed MB via oxidative degradation.

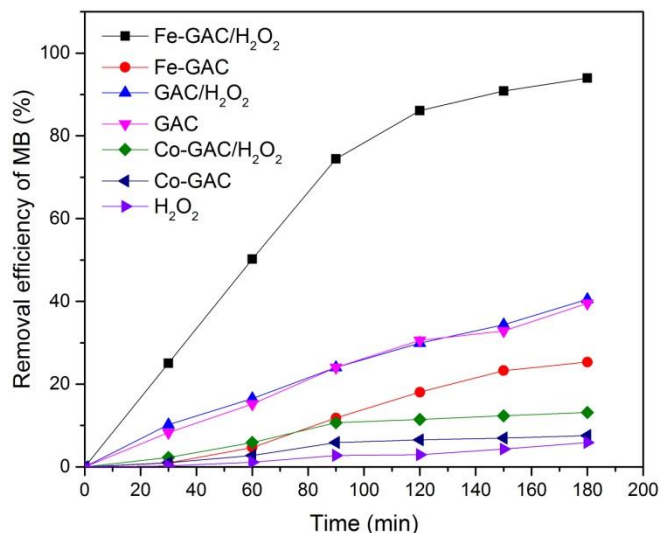


Figure 4.4: Time profiles and removal efficiency of MB over H₂O₂, Co-GAC, Co-GAC/H₂O₂, GAC, GAC/H₂O₂, Fe-GAC, Fe-GAC/H₂O₂

4.3 Optimization of MB reactive adsorption conditions

The effect of variation of adsorbent dose on the removal of MB by Fe-GAC/H₂O₂ is shown in Figure 4.5. Amount of Fe-GAC was varied from 0.10 g/L to 0.25 g/L for 240 min at an initial MB dye concentration of 10 mg/L. It is apparent that the dye concentration in solution decreases significantly up to 180 min with increasing Fe-GAC amount due to the availability of higher amount of Fe⁺³ which in further helps in producing larger amount of hydroxyl radicals (Neamu et al. 2004). Further increase in adsorbent dose (0.20 g/L to 0.25 g/L) did not improve the dye removal significantly. This may be due to the limitation of hydrogen peroxide availability.

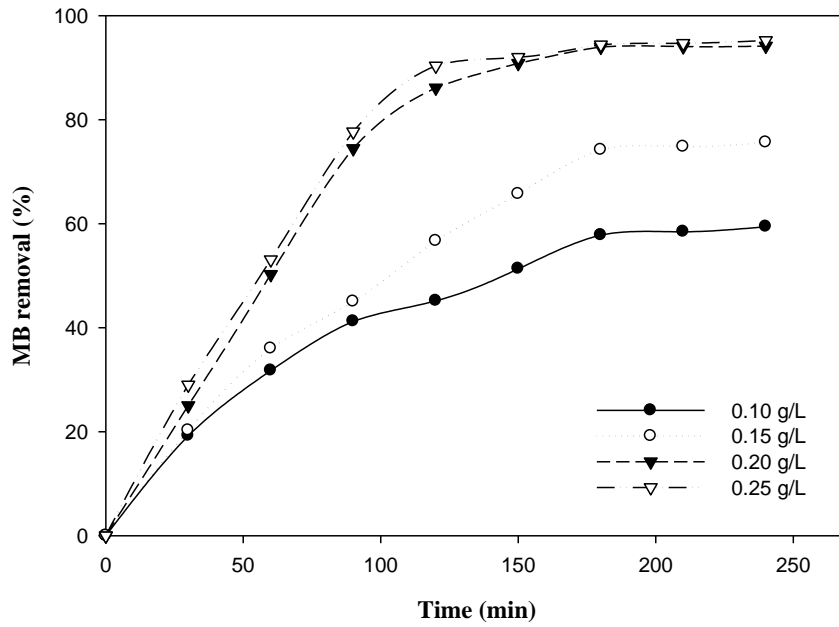


Figure 4.5: Effect of adsorbent dose on dye removal using Fe-GAC/H₂O₂ at different time intervals (Temp.: 30 °C, C₀: 10 mg/L, pH: 6.5, H₂O₂: 1.0 mM).

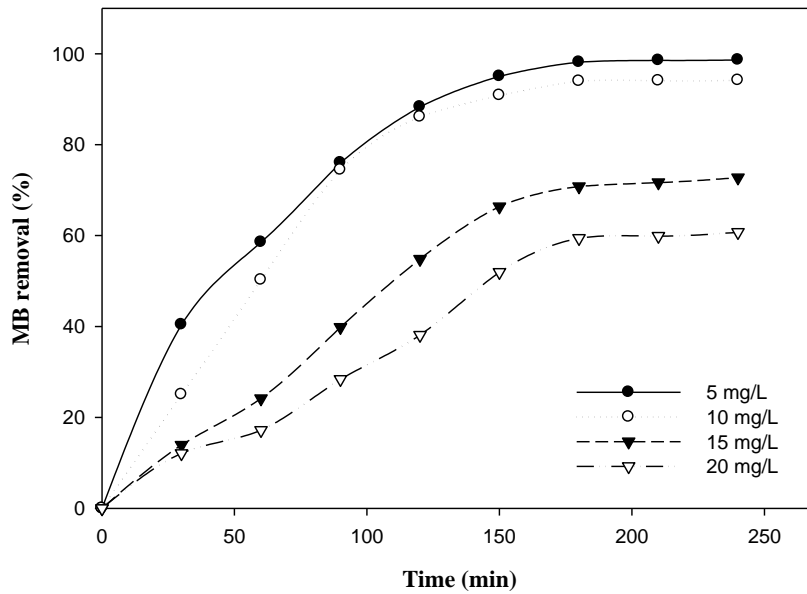


Figure 4.6: Effect of initial dye concentration on dye removal using Fe-GAC/H₂O₂ at different time intervals (Temp.: 30 °C, dose of Fe-GAC: 0.2 g/L, pH: 6.5, H₂O₂: 1.0 mM).

Figure 4.6 shows the effect of initial dyes concentration on the removal percentage. During the study, it was found that at lower concentration of MB, higher percent removal was observed due to low ratio of solute concentrations to adsorbent sites (Bagheri et al. 2016) and availability of ample amount of hydroxyl radicals. However, at higher dye concentrations, lower removal was found due to the saturation of sorption sites and shortage of hydroxyl radicals (Kasiri et al. 2008). There was no significant difference observed in dye removal for initial concentrations of 5 mg/L and 10 mg/L. This may be due to the availability of sufficient hydroxyl radicals for removal of MB at 10 mg/L concentration also. Therefore 10 mg/L dye concentration was chosen for further experiments.

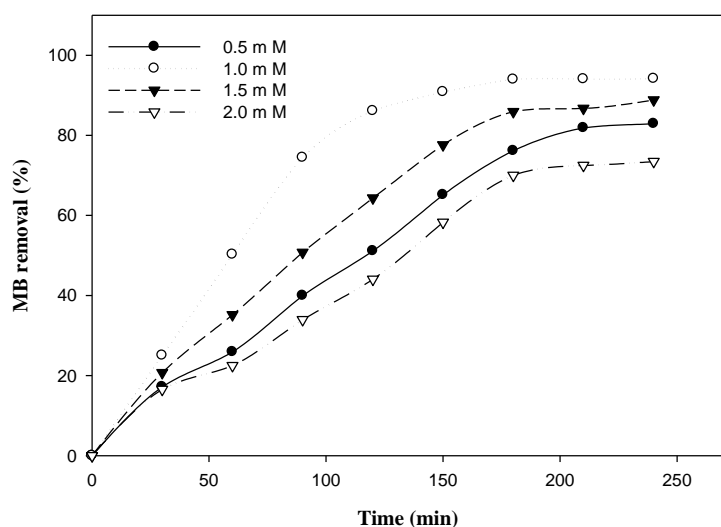


Figure 4.7: Effect of H₂O₂ dose on dye removal using Fe-GAC/H₂O₂ at different time intervals (Temp.: 30 °C, C₀: 10 mg/L, pH: 6.5, dose of Fe-GAC: 0.2 g/L).

Increase in hydrogen peroxide concentration from 0.5 to 1.0 mM accelerated the MB decolorization (Figure 4.7) due to the availability of higher amount of hydroxyl radicals for oxidative degradation of MB. However, when H₂O₂ concentration was increased from 1.0 to 2.0 mM, at the same operating conditions, the dye removal was decreased. This may be due to the production of hydroperoxyl radicals (HO₂[•]) by hydroxyl radicals in the presence of a local excess of H₂O₂ that contributes to [•]OH-scavenging (Kasiri et al. 2008; Neamu et al. 2004). The hydroperoxyl radicals are much less reactive than [•]OH with reaction rate constants lower than 2

$\times 10^4$ 1/M s in the presence of organic matter (Kasiri et al. 2008). HO_2^\bullet does not take part into the degradation by oxidation of the organic substrate (Neamu et al. 2004). Therefore, 1.0 mM H_2O_2 dose was considered optimum.

4.4 Removal efficiencies of SO in single dye system

SO removal efficiency was studied using reactive adsorption (Fe-GAC/ H_2O_2 system) at different Fe-GAC and H_2O_2 dosages. For the Fe-GAC/ H_2O_2 system, optimized dosage requirement of Fe-GAC for the catalytic reaction was found to be 1.0 g/L. Figure 4.8 indicates that higher Fe-GAC dose corresponds to the much more efficient use of H_2O_2 (Chen et al. 2011). The availability of ample amount of Fe^{+3} on adsorbent surface lead to the formation of sufficient $^\bullet OH$ radicals for oxidative degradation of SO.

Figure 4.8 also shows that the increase in hydrogen peroxide concentration from 1.0 to 5.0 mM accelerated the SO decolorization. However, when H_2O_2 concentration was increased from 5.0 to 7.0 mM, at the same operating conditions, the dye removal was decreased. This may be due to the $^\bullet OH$ generated, produced hydroperoxyl radicals (HO_2^\bullet) in the presence of a local excess of H_2O_2 (Eq. 4.1) that contributes to the $^\bullet OH$ -scavenging (Kasiri et al. 2008; Neamu et al. 2004).



HO_2^\bullet are much less reactive than $^\bullet OH$ with reaction rate constants lower than 2×10^4 1/M s in the presence of organic matter (Kasiri et al. 2008). At optimized conditions (1.0 g/L Fe-GAC and 5.0 mM H_2O_2), maximum 96.1% of SO removal was obtained for initial dye concentration of 10 mg/L and these conditions were used further for subsequent experiments.

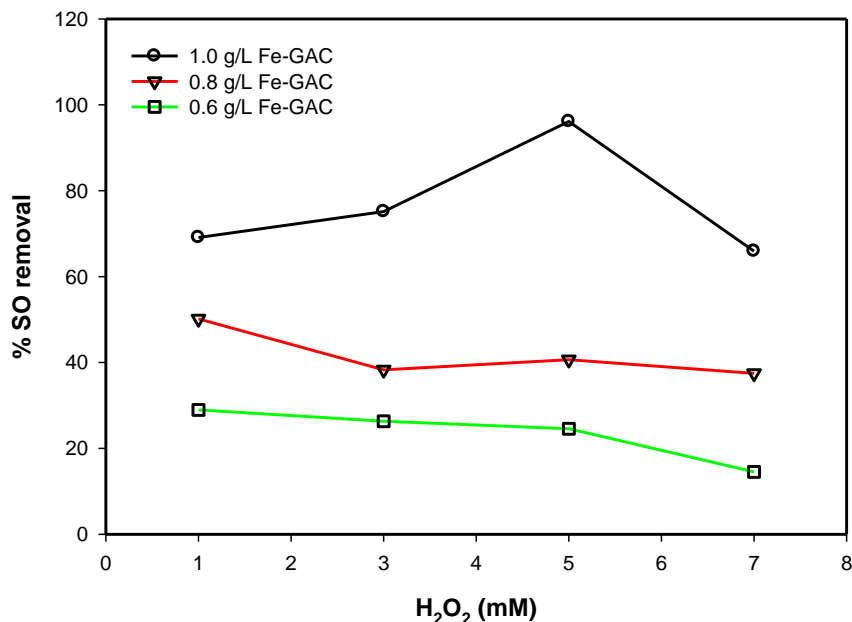


Figure 4.8: % SO removal efficiencies in aqueous solution at pH 6.5 with various dosages of H₂O₂ and Fe-GAC with C₀ = 10 mg/L after 5 h at 30 °C

4.5 Removal efficiencies of MB and SO in binary dye system

MB and SO removal efficiencies were studied in a binary mixture using the Fe-GAC/H₂O₂ process at different Fe-GAC and H₂O₂ dosages. For the Fe-GAC/H₂O₂ system, optimized dosage requirement of Fe-GAC for the catalytic reaction was found 0.5 g/L for both the dyes. Figure 4.9 indicates that higher Fe-GAC dose corresponds to the more efficient use of H₂O₂ (Chen et al. 2011). The availability of ample amount of Fe⁺³ on adsorbent surface lead to the formation of sufficient •OH radicals for oxidative degradation of MB and SO. Figure 4.9 shows that the increase in hydrogen peroxide concentration from 0.5 to 2.0 mM accelerated the MB and SO decolorization. However, when the H₂O₂ concentration was increased from 2.0 to 3.5 mM, at the same operating conditions, the dye removal was decreased. To the •OH-scavenging reduces the removal of dye (Eq. 4.1) (Kasiri et al. 2008; Neamu et al. 2004).

At optimized conditions (0.5 g/L Fe-GAC and 2.0 mM H₂O₂), maximum 96.2% of MB and 90.2% of SO removal were obtained for initial dye concentration of 5 mg/L each dye and these conditions were used further for subsequent experiments. The maximum removal of dyes present

in binary mixture was only 49.45% and 36.95% for MB and SO respectively obtained for initial dye concentration of 5 mg/L each dye for 7 h of adsorption process.

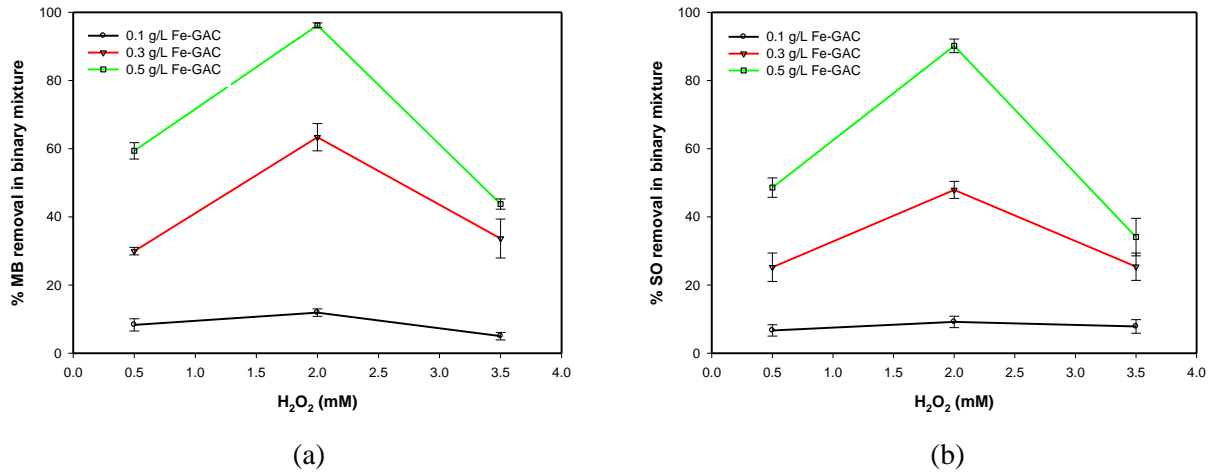


Figure 4.9: % dye removal efficiencies in binary mixture at pH 6.5 with various dosages of H₂O₂ and Fe-GAC with C₀ = 5 mg/L for each dye after 7 h

4.6 Batch reactive adsorption studies

4.6.1 Kinetics of reactive adsorption decoloration

4.6.1.1 Methylene Blue in single dye system

Experimental data between $\ln C_t$ and time (t) linearly fit for MB to the pseudo-first-order model which confirmed its applicability with R² value of 0.985 as shown in Figure 4.10. The apparent rate constant (k_{app}) obtained from the slope of the plot was 0.015 1/min. A plot of $1/C_t$ versus t was plotted as shown in Figure 4.11. Pseudo-second-order kinetics can be ruled out as upward concave curvature was found.

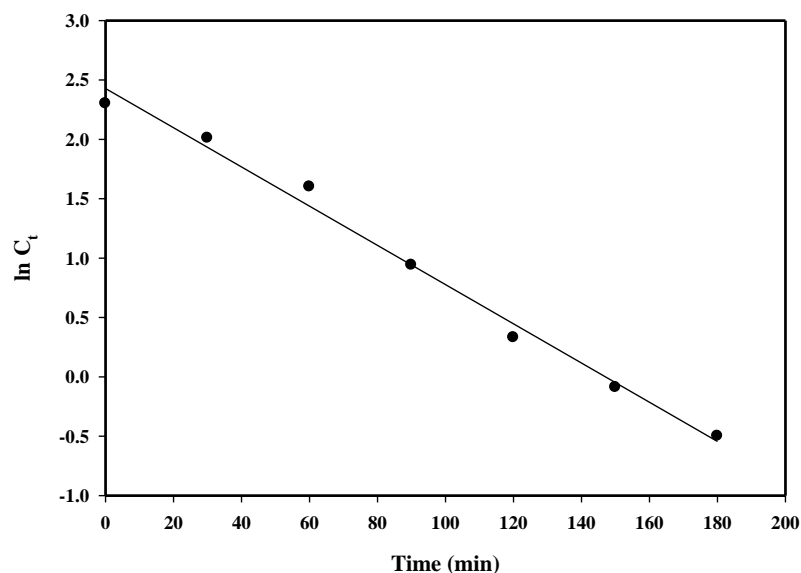


Figure 4.10: Pseudo-first-order plot for reactive adsorption kinetics of MB (Temp.: 30 °C, C₀: 10 mg/L, pH: 6.5, H₂O₂: 1.0 mM, dose of Fe-GAC: 0.2 g/L).

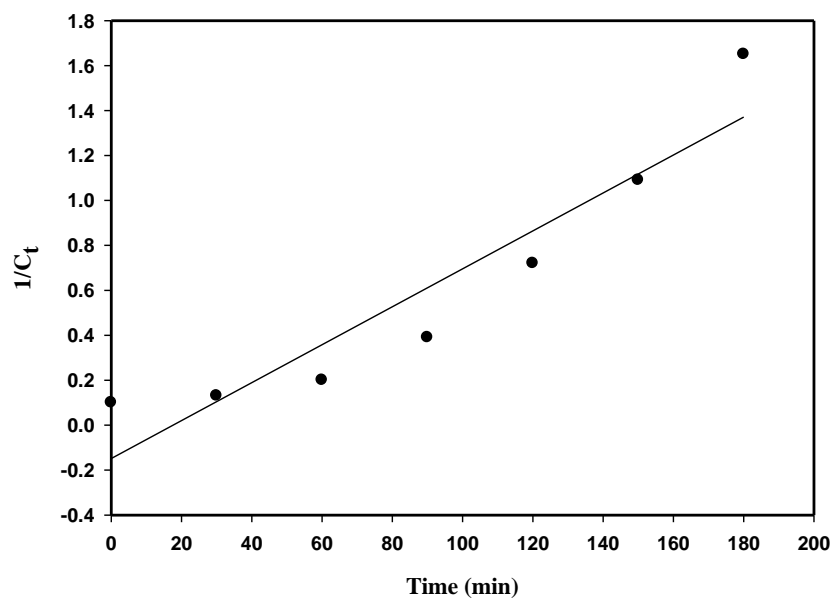


Figure 4.11: Pseudo-second-order plot for reactive adsorption kinetics of MB (Temp.: 30 °C, C₀: 10 mg/L, pH: 6.5, H₂O₂: 1.0 mM, dose of Fe-GAC: 0.2 g/L).

4.6.1.2 Safranin O in single dye system

A linear fitting of the data between $-\ln \frac{C_t}{C_0}$ and t for SO to the first-order-reaction-kinetics equation confirmed the applicability of pseudo first-order-kinetics model with a correlation coefficient of 0.982 as shown in Figure 4.12. k_{app} value 1.7×10^{-4} 1/s was obtained using pseudo-first-order-kinetics. A plot of $1/C_t$ versus t was plotted as shown in Figure 4.13 to check applicability of second order reaction systems. Pseudo-second-order kinetics can be ruled out as upward concave curvature (correlation coefficient value of 0.756) was found.

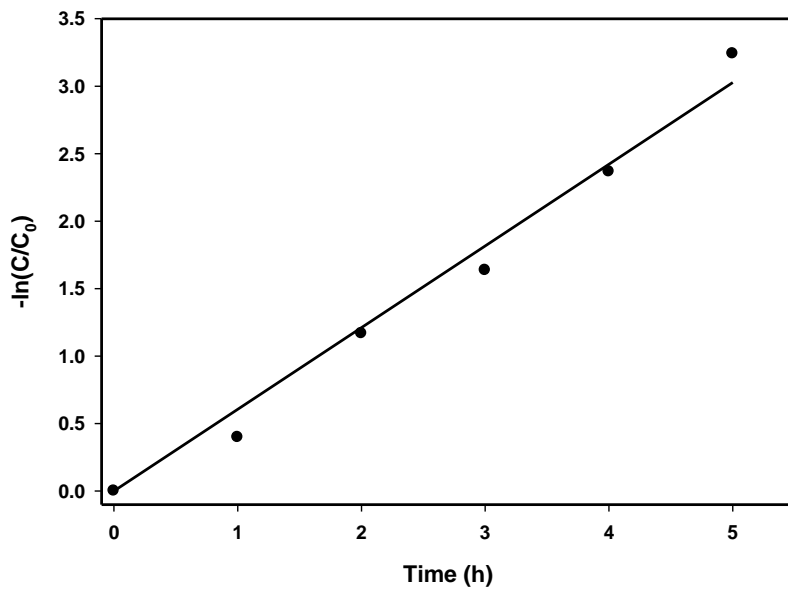


Figure 4.12: Pseudo-first-order plot for reactive adsorption kinetics of SO (Fe-GAC: 1.0 g/L, H_2O_2 : 5.0 mM, pH: 6.5, C_0 : 10 mg/L and Temperature: 30 °C).

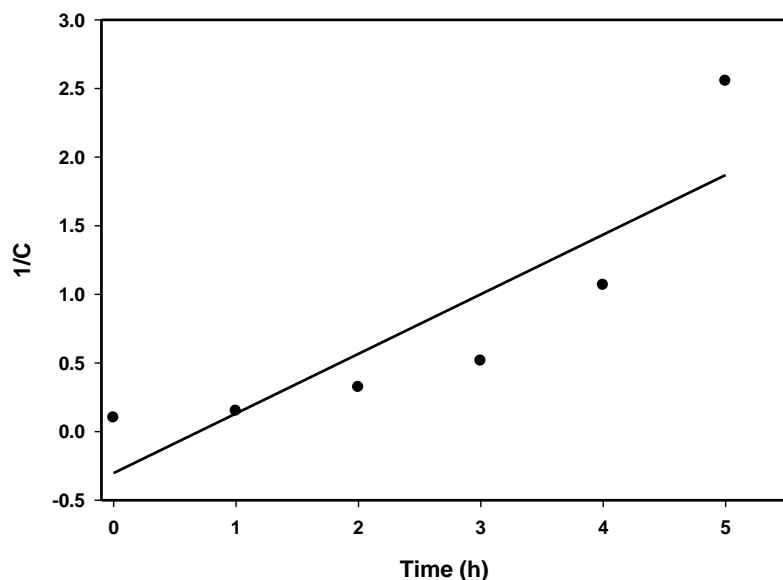
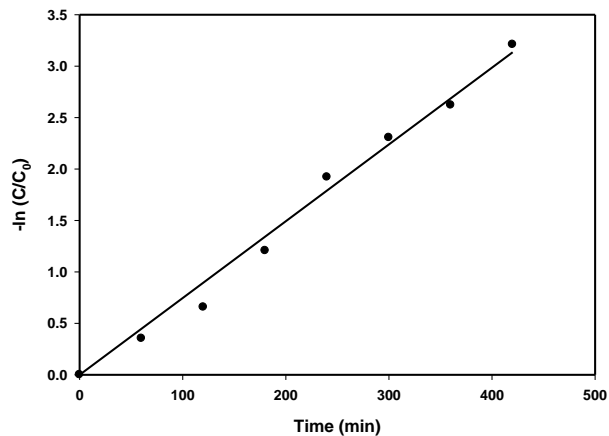


Figure 4.13: Pseudo-second-order plot for reactive adsorption kinetics of SO (Fe-GAC: 1.0 g/L, H₂O₂: 5.0 mM, pH: 6.5, C₀: 10 mg/L and Temperature: 30 °C).

4.6.1.3 Methylene Blue and Safranin O in binary dye system

A linear fitting of the data were plotted between $-\ln \frac{C_t}{C_0}$ and t for MB and SO confirmed the applicability of pseudo first-order-kinetics model with correlation coefficient values of 0.987 for MB and 0.985 for SO as shown in Figure 4.14(a) and Figure 4.15(a) respectively. k_{app} obtained for MB and SO at different temperatures are listed in Table IV.2 and Table IV.6 in appendix. Plot of $1/C_t$ versus t for pseudo-second-order reaction systems were plotted as shown in Figure 4.14(b) and Figure 4.15(b). An upward concave curvature is obtained which indicates that pseudo-second-order-kinetics should not be considered for the simultaneous oxidative degradation of MB and SO present in a binary mixture. k_{app} values for reactive adsorption of MB and SO at 30 °C were found to be 0.0074 and 0.0050 1/min, respectively. It can be seen that k_{app} values were always higher for MB in the presence of SO. This may be due to the fact that SO showed synergistic behavior for reactive adsorption of MB and consequently its degradation; whereas, MB showed antagonism for SO removal during reactive adsorption of this binary dye mixture.

(a)



(b)

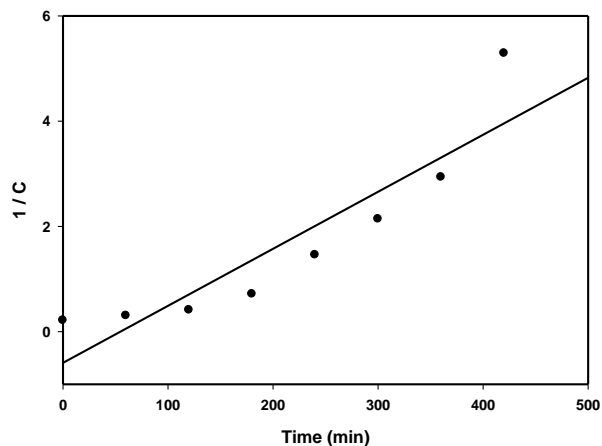
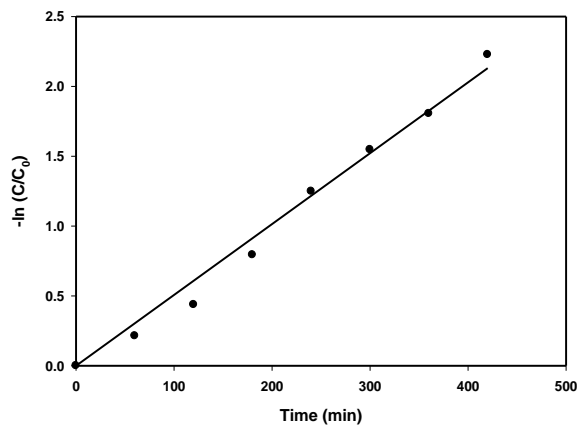


Figure 4.14: Plots of MB (a) pseudo first-order-kinetics, (b) pseudo second-order-kinetics, during reactive adsorption of binary dye mixture ($C_0 = 5$ mg/L each dye, Fe-GAC = 0.5 g/L, $H_2O_2 = 2.0$ mM, $T = 30^\circ C$, pH = 6.5).

(a)



(b)

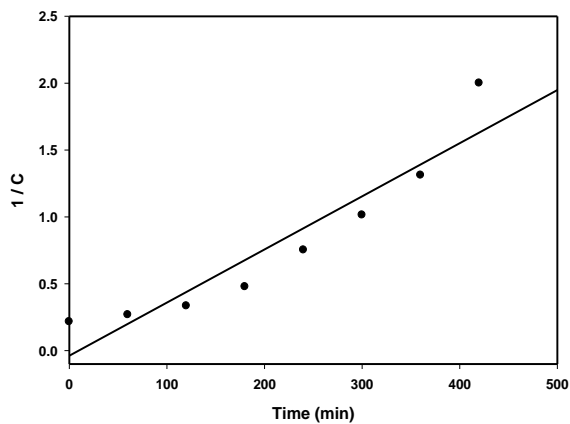


Figure 4.15: Plots of SO (a) pseudo-first-order-kinetics, (b) pseudo-second-order-kinetics, during reactive adsorption of binary dye mixture ($C_0 = 5$ mg/L each dye, Fe-GAC = 0.5 g/L, $H_2O_2 = 2.0$ mM, $T = 30^\circ C$, pH = 6.5).

4.6.2 Thermodynamics of reactive adsorption

4.6.2.1 Methylene Blue in single dye system

A linear plot between $\ln k_{app}$ and $1/T$ shows a straight line (Figure 4.16). Activation energy was estimated from equation (Eq. 3.6) and the value is given in Table 4.2. Higher MB degradation was achieved with increasing temperature as elevated temperatures enhanced the formation of $\bullet\text{OH}$ radicals in Fe-GAC/ H_2O_2 system (Lee and Yoon 2004). Table 4.2 presents the thermodynamic properties ($\Delta G^\#$, $\Delta H^\#$ and $\Delta S^\#$) of MB oxidative degradation using reactive adsorption which were determined using activation energy and apparent rate constant (Lonhienne et al. 2000).

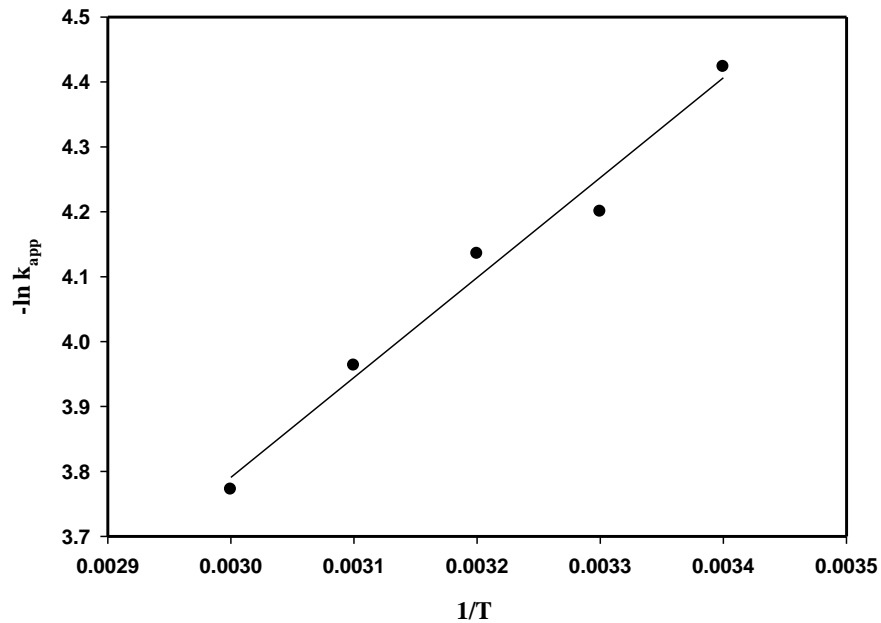
From Table 4.2, it can be seen that reactive adsorption of MB is not a temperature dependent process. However, an increase in temperature facilitates enhanced formation of $\bullet\text{OH}$ radicals that effectively degrade the dye. Similar results were reported for photodegradation of phenolics (Naeem et al. 2010).

The Gibbs free energy change (ΔG) indicates the degree of the spontaneity of the adsorption process. Gibbs free energy changes of adsorption must be negative for a better adsorption. The values of Gibbs free energy change of MB adsorption at temperature range of 20 – 60 °C were positive, which indicate that the adsorption process led to a decrease in Gibbs free energy. $\Delta G > 0$ means adsorption and desorption reactions are not in mutual thermodynamic equilibrium. Rather, the reverse reaction, that is desorption is taking place in reality. This way the direction of the reaction proceeds along the decreasing path of the Gibbs free energy (towards the direction of equilibrium). The positive values confirm the reactive adsorption process as it comprises concurrent reaction and separation of solute during adsorption.

The magnitude of activation energy gives an idea about the type adsorption, which is mainly physical or chemical. The physisorption processes usually have energies in the range of 5 – 40 kJ/mol, while higher activation energies (40 – 800 kJ/ mol) suggest chemisorption. It can be inferred from the present studies that interaction of dyes with the surface of Fe-GAC results in physical adsorption (Ma et al. 2012).

Table 4.2: Thermodynamic parameters for reactive adsorption of MB.

T (°C)	E _a (kJ/mol)	ΔG [#] (kJ/mol)	ΔH [#] (kJ/mol)	ΔS [#] (kJ/mol K)
20	12.46	82.53	10.03	-0.25
30		84.87	9.94	
40		87.59	9.86	
50		90.01	9.78	
60		92.35	9.69	

**Figure 4.16:** Effect of temperature on the apparent rate constant of MB.

4.6.2.2 Methylene Blue and Safranin O in binary dye system

The effects of temperature on reactive adsorption were studied by conducting batch experiments in the range of 15 to 35 °C. Table IV.2 and Table IV.6 in appendix list k_{app} values of MB and SO during simultaneous degradation at different temperatures. It can be observed from Table IV.2 and Table IV.6 in appendix that degradation of MB and SO were increased with increasing temperature.

A linear plot of dyes present in binary system between $\ln k_{app}$ and $1/T$ shows a straight line (Figure 4.17 and Figure 4.18) with correlation coefficient values of 0.990 for MB and 0.988 for

SO. Activation energy was estimated from above equation (Eq. 3.6) and the value is given in Table 4.3. Higher values of MB and SO degradation were achieved with increasing temperature as higher temperatures enhanced the formation of $\bullet\text{OH}$ radicals in Fe-GAC/ H_2O_2 system (Lee and Yoon 2004).

It can be seen from Table 4.3 that concurrent reactive adsorption of MB and SO was not a temperature dependent process. However, an increase in temperature facilitates enhanced formation of $\bullet\text{OH}$ radicals that effectively degraded the dyes. Similar results were earlier reported for photodegradation of phenolics (Naeem et al. 2010).

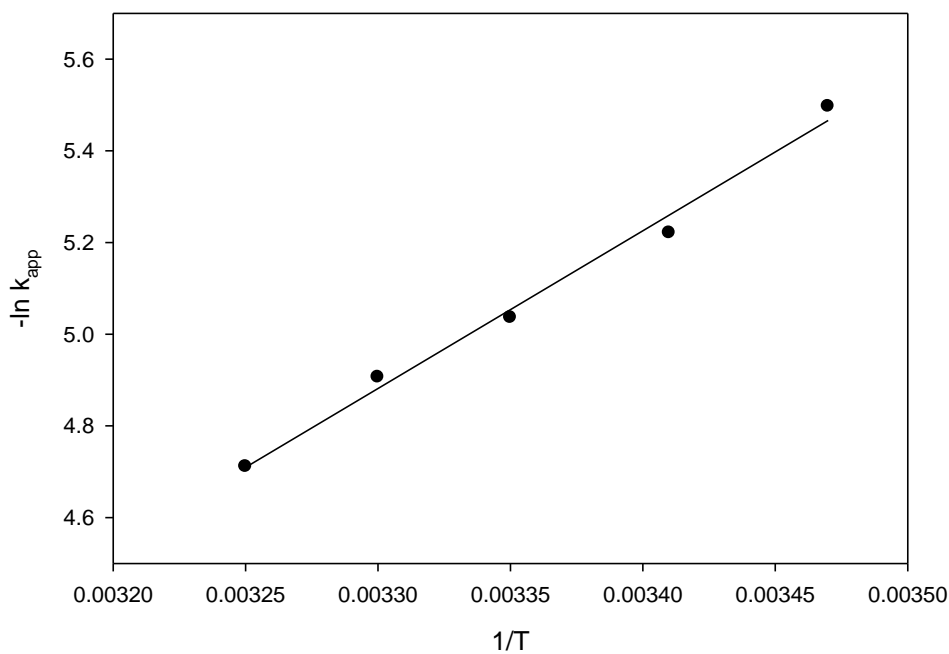


Figure 4.17: Effect of temperature on the apparent rate constant of MB for simultaneous reactive adsorption using Fe-GAC/ H_2O_2 system at pH 6.5.

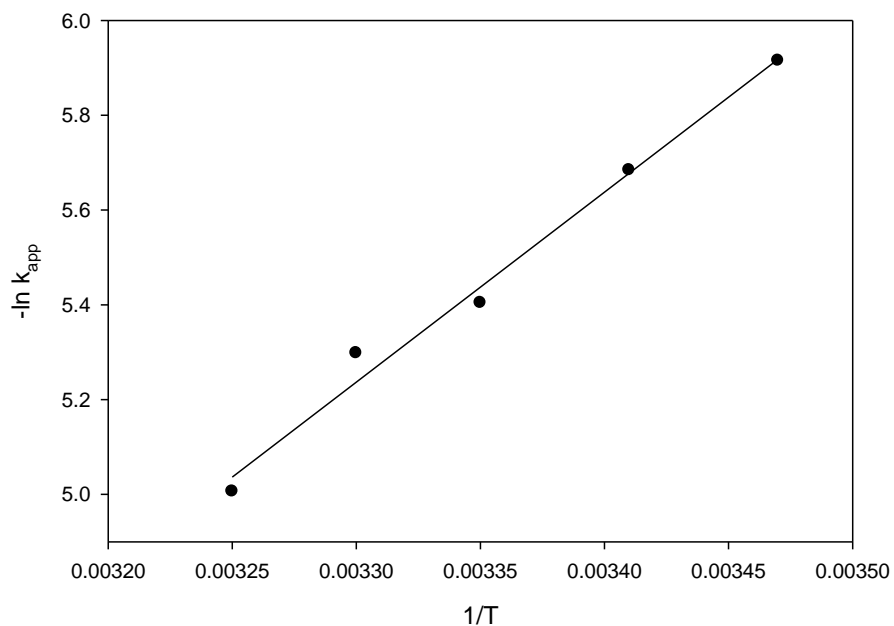


Figure 4.18: Effect of temperature on the apparent rate constant of SO for simultaneous reactive adsorption using Fe-GAC/H₂O₂ system at pH 6.5.

Table 4.3: Thermodynamic parameters for simultaneous reactive adsorption of MB and SO.

Dye in binary mixture	T (°C)	E _a (kJ/mol)	ΔG [#] (kJ/mol)	ΔH [#] (kJ/mol)	ΔS [#] (kJ/mol K)
MB	15	28.59	83.66	26.20	-0.20
	20		84.48	26.16	-0.20
	25		85.50	26.11	-0.20
	30		86.65	26.07	-0.20
	35		87.62	26.03	-0.20
SO	15	32.53	84.66	30.92	-0.19
	20		85.61	30.88	-0.19
	25		86.41	30.84	-0.19
	30		87.64	30.80	-0.19
	35		88.38	30.75	-0.19

4.7 Reaction mechanism

The loading of Fe^{+3} or Fe^{+2} on carbonaceous materials serve as catalyst in oxidative removal of the organic compounds (Xu et al. 2015). Degradation of MB using Fe-GAC / H_2O_2 system occurs through several parallel reactions. It is believed that the reaction with Fe-GAC is initiated by the activation of H_2O_2 in the presence of Fe^{+3} to produce an $\bullet OH$ radical via a Haber–Weiss mechanism (Pereira et al. 2011). During the reaction, $\bullet OH$ radicals are produced through a reaction between H_2O_2 and Fe^{+3} . $\bullet OH$ radical serves as reactive species in order to oxidize MB molecule and catalyst is regenerated to its original form through a number of reactions (Pereira et al. 2011; Pinto et al. 2012). Therefore, a possible reaction mechanism for oxidative degradation of MB is given as following in Eqs. (4.2) – (4.6)

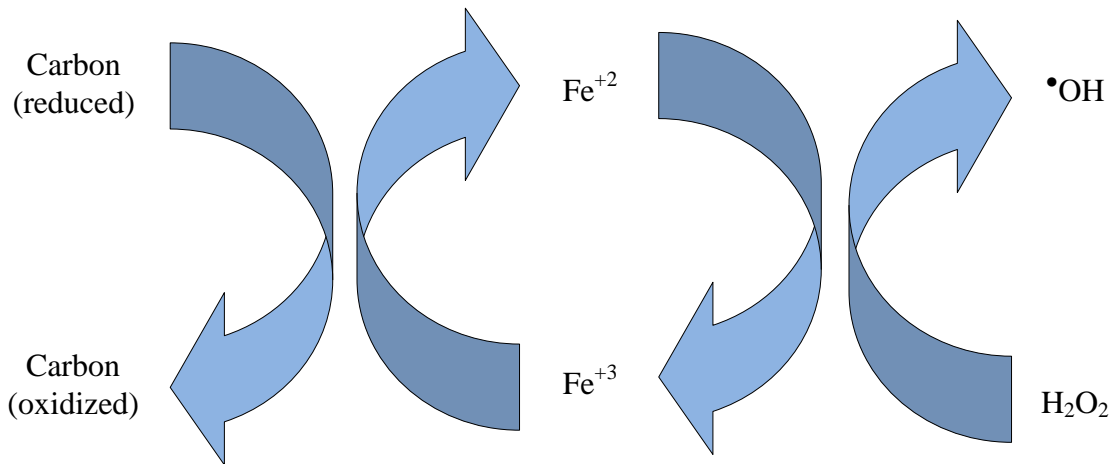
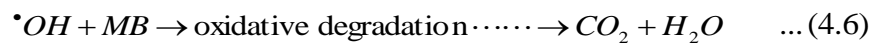
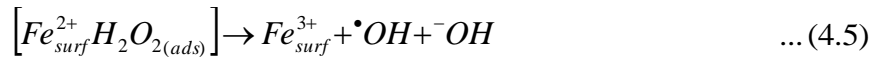
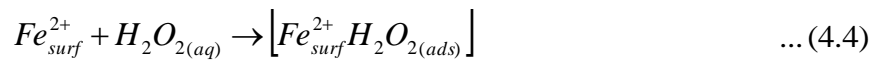
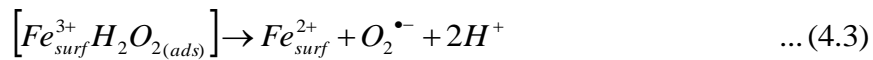
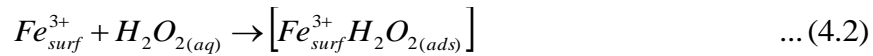


Figure 4.19: Oxidation-reduction process of GAC, iron and H_2O_2 .

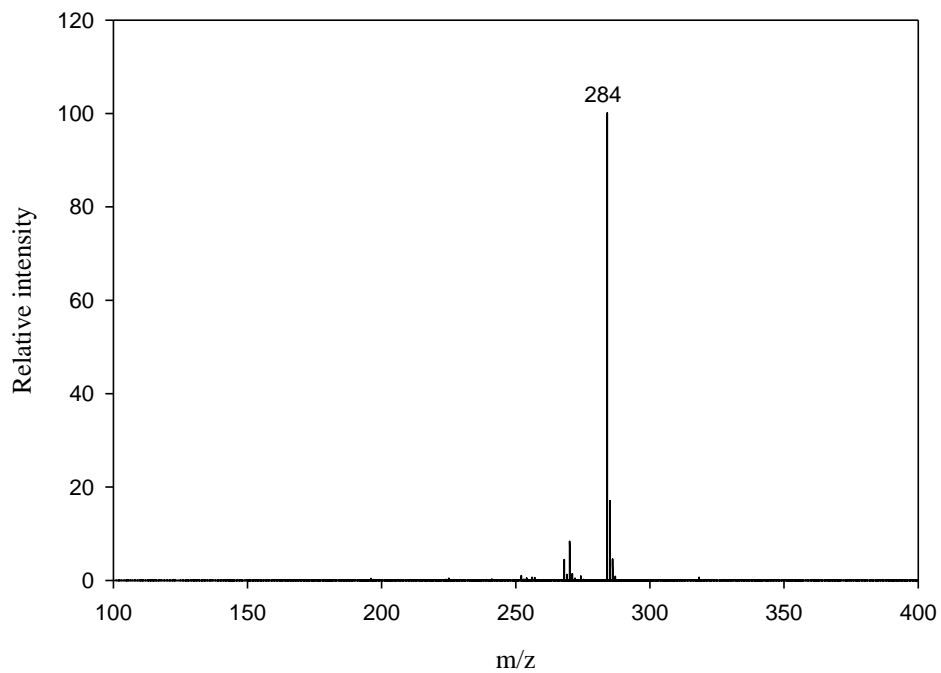
The reduction of hydrogen peroxide may involve transferring of electron from carbon surface to H_2O_2 , Fe^{+3} was reduced to Fe^{+2} that accelerated the H_2O_2 reduction rate by carbon of Fe-GAC. The hydroxyl radical is generated by a number of steps: initially, electrons are transferred from carbon to Fe^{+3} to form Fe^{+2} ; and then the Fe^{+2} donate electrons to H_2O_2 which results in the reduction of H_2O_2 . Fe^{+3} addition accelerates H_2O_2 reduction rate by carbon. The $\text{Fe}^{+3} / \text{Fe}^{+2}$ couple acts as a catalyst for degradation of MB via H_2O_2 reduction by GAC. The illustration of this process is given in Figure 4.19.

4.8 Oxidative degradation study using ESI-MS

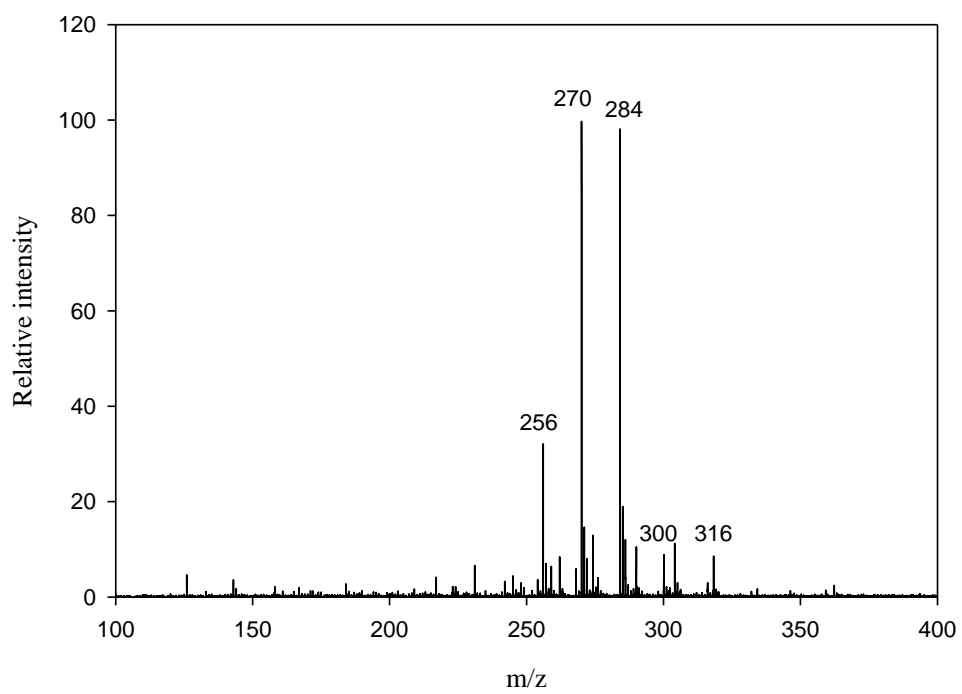
4.8.1 Methylene Blue in single dye system

The results obtained from ESI-MS study suggest that use of Fe-GAC as reactive adsorbent catalyzes the generation of hydroxyl radicals from H_2O_2 decomposition and promotes oxidative degradation of MB. The analysis of aqueous solution containing MB (Figure 4.20a – c) during batch study of reactive adsorption using ESI-MS showed oxidative degradation of MB in the solution due to occurrence of chemical reactions on Fe-GAC surface. Initially at $t = 0$, single peak at $m/z = 284$ shown in Figure 4.20a indicates presence of MB solely in the solution. Figure 4.22 shows UV-Vis spectra of MB with one main band in the visible region.

(a)



(b)



(c)

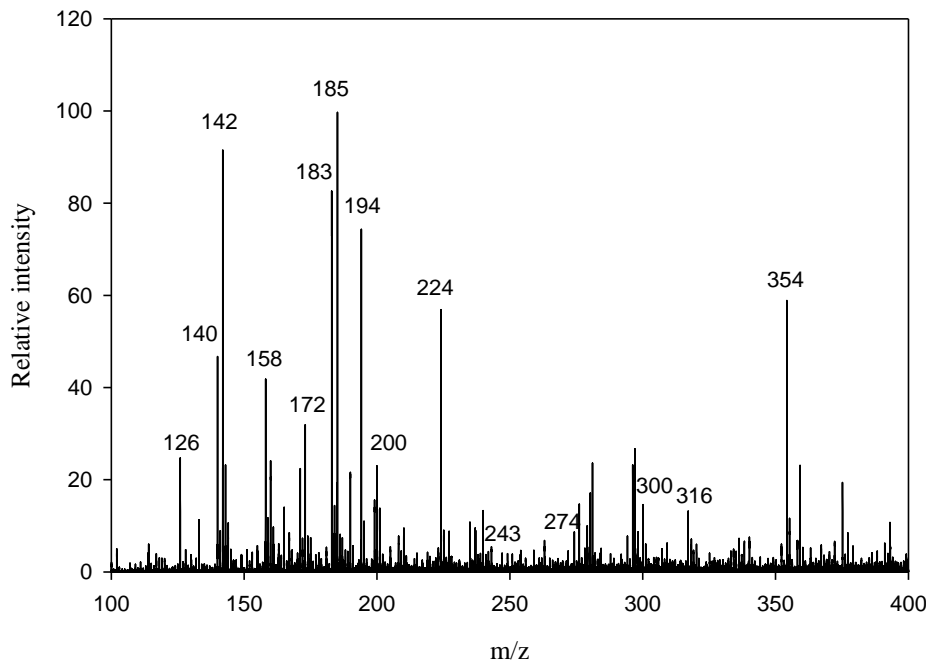


Figure 4.20. ESI-MS of (a) aqueous solution of MB before reaction (b) degradation products of MB using Fe-GAC after 1 h and (c) degradation products of MB using Fe-GAC after 3 h of reaction.

ESI-MS analysis for MB degradation using Fe-GAC / H₂O₂ system revealed that with the reaction period of 1 h, the intensity of signal at m/z = 284 decreased with the formation of intermediates (Figure 4.20b). It is reported that hydroxyl radicals facilitate demethylation of organic compounds (Behnajady et al. 2008; Chen et al. 2011; Rajoriya et al. 2017). It should be noticed that in the demethylation process, the shift of the absorption band is a characteristic phenomenon (Rauf et al. 2010; Wang et al. 2014). The structures of the intermediates are given in Figure 4.21. Absorbance peak due to formation of intermediate products of MB was shifted to 657 nm from 663 nm as the degradation time prolonged (Figure 4.22). Moreover, ESI-MS results obtained at 1 h of reaction period showed that the dye degradation is initiated by demethylation of the molecule. In reactive adsorption process, the generated •OH radicals may prefer to attack alkyl branch of MB to destruct the molecule structure and further degraded by N-demethylation process. The ESI-MS spectrum showed manifolds of peaks at m/z = 270 and 256 along with the parent peak m/z = 284, corresponding probably to the replacement of methyl groups with

protons. These are likely due to fragmentation of the parent molecule and the new peaks emerged in the spectra are the well-known homologues of MB such as Azure B ($m/z = 270$) and Azure A ($m/z = 256$) (Orendorz et al. 2008; Yogi et al. 2008).

After 3 h (Figure 4.20c) of reaction, the signal corresponding to MB ($m/z = 284$) was completely disappeared with the formation of different degradation products. MB absorbance peaks shifted to 652, 648, 639 and 637 nm as the reaction time proceeds (Figure 4.22). By observing shift in absorbance in the visible region of each MB spectra, it may be concluded that N-demethylation occurred throughout the reaction. Many peaks of different intensities were observed after 3 h in the mass spectra which indicate the variation in the composition and concentration of the degradation products. Furthermore, new compounds at $m/z = 300$, 316 and 354 found probably due to hydroxylation of the aromatic ring. These results indicated that the reactive degradation of MB molecule was initiated by demethylation which was facilitated by hydroxyl radicals, followed by hydroxylation. Inclusion of one, two and six hydroxylation stage to the MB molecule, due to the attachment of $\bullet\text{OH}$ to the aromatic ring of MB, produces three signal fragments at $m/z = 300$, 316 and 354 (Gupta et al. 2015; Oliveira et al. 2007). Additionally, after 180 min of reaction, the formation of intermediates with $m/z = 224$, $m/z = 200$, $m/z = 194$, $m/z = 185$, $m/z = 183$, $m/z = 172$ and $m/z = 158$ occurred due to over-oxidation of hydroxylated intermediates (Mesquita et al. 2016). Finally, the signal of $m/z = 142$ and $m/z = 140$ were indicative of the ring rupture (Souza et al. 2007). Therefore, reactive adsorption of dye solutions not only caused its discoloration (Figure 4.22), but also an appreciable degree of destruction in the dye molecule (Figure 4.20c). A degradation pathway for MB removal by reactive adsorption (Figure 4.21) with formation of different intermediate products corresponding to their individual m/z values has been proposed.

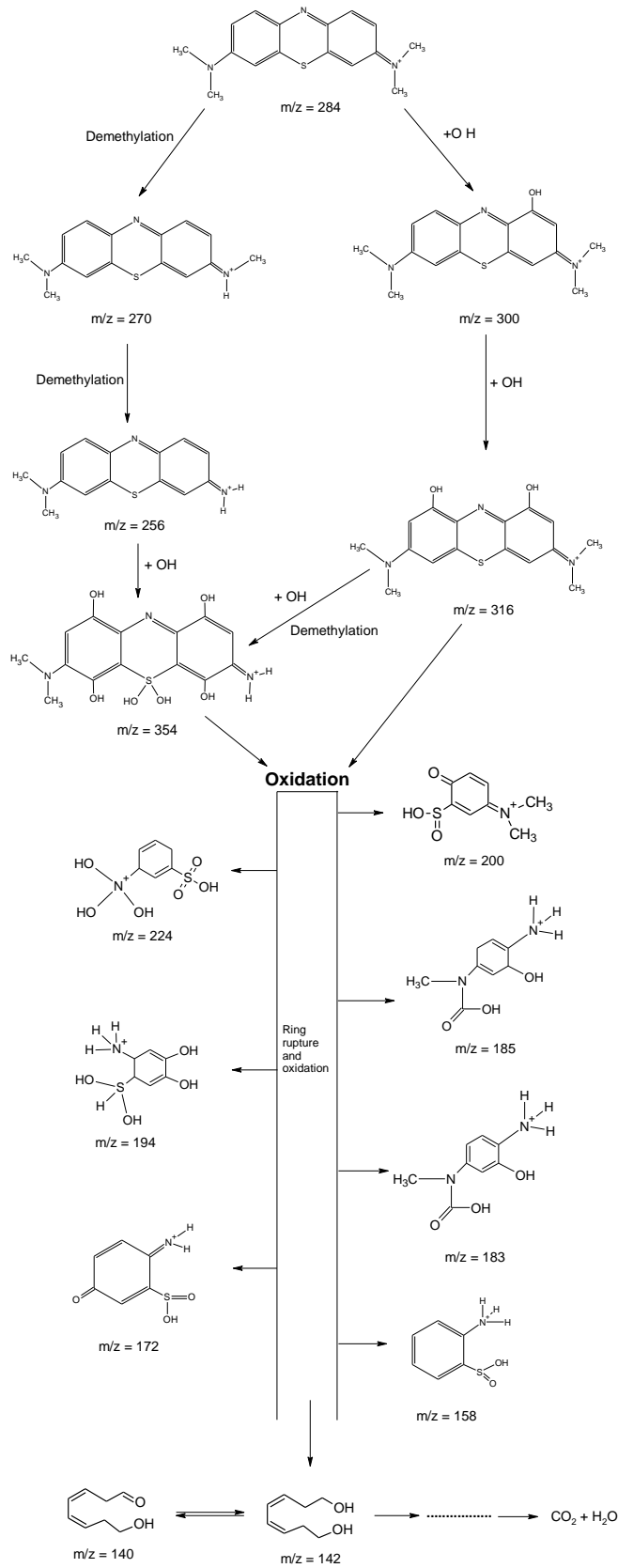


Figure 4.21: Proposed oxidative degradation pathway of MB during reactive adsorption using Fe-GAC / H₂O₂ system.

Reactive adsorption of MB using Fe-GAC / H₂O₂ renders the aqueous solution almost colorless. Figure 4.22 shows changes in absorption spectra during MB oxidative degradation in an aqueous solution with the Fe-GAC / H₂O₂ for 180 min. A decrease in the intensity of the maximum absorption peak at 663 nm was found due to MB degradation. It has been postulated that MB removal is occurred due to oxidative degradation. MB spectra show the maximum absorption in the UV-region at 291 nm due to the presence of poly-aromatic rings. It can be seen that almost complete mineralization of poly-aromatic rings occurred after 3 h of oxidative degradation of MB (see Figure 4.22).

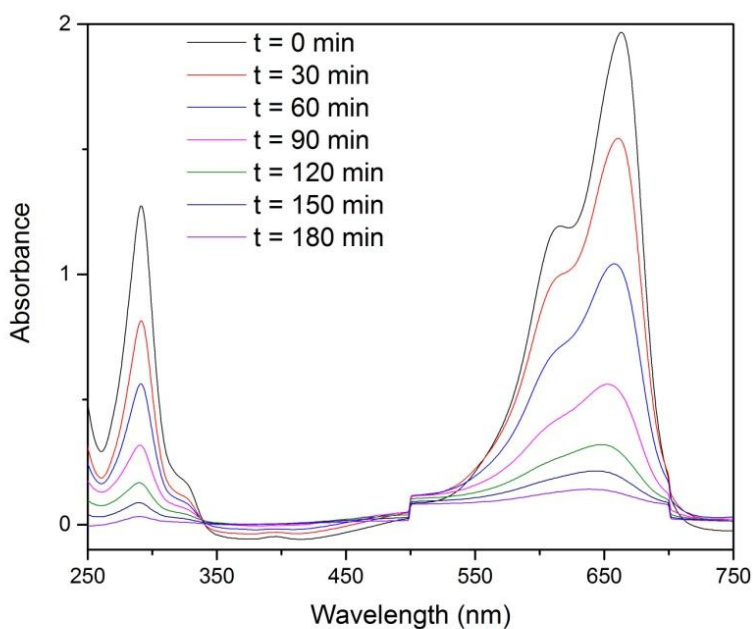


Figure 4.22: Changes in the UV–vis absorbance spectra of MB dye using Fe-GAC / H₂O₂.

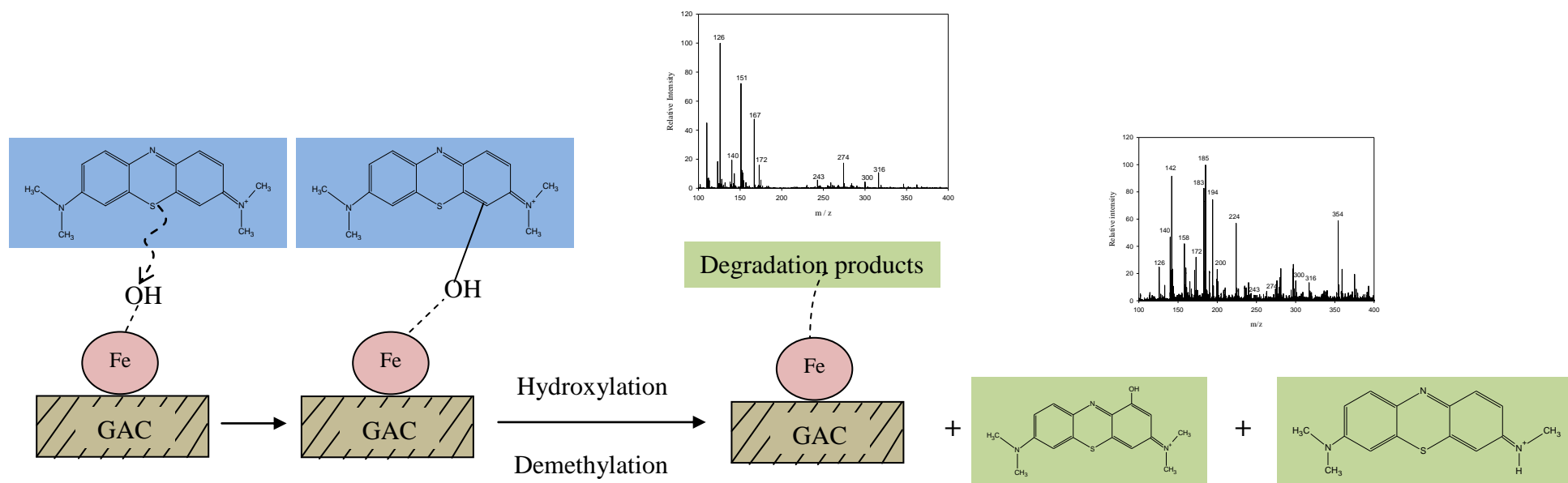


Figure 4.23: Proposed scheme for MB reactive adsorption.

According to reactive adsorption, one fragment of H_2O_2 gets attached to adsorbate (IUPAC 1997; Nogueira et al. 2009) and results into hydroxylated and demethylated product of MB. It has been already shown earlier in literature that the possible formation of some deposits on the surface of the adsorbent which occurs in the reactive adsorption process (Abecassis-Wolfovich et al. 2004; Zazo et al. 2006). In the present study, it was found that the degradation products of MB reactive adsorption get adsorbed on reactive adsorbent surface which was evident from the desorption study of spent Fe-GAC carried out using boiling process in distilled water for 15 min. The leachate was subsequently analyzed using ESI-MS analysis. ESI-MS spectra indicated the presence

of degradation products like $m/z = 316, 300, 274, 243, 172, 167, 151, 140, 126$ etc. (see Figure 4.23). The structures of these compounds were given in Figure 4.21. Ania et al. (2011) studied the existence of degraded compounds adsorbed on activated carbons surface after its exposure to antibiotic using thermal analysis (Ania et al. 2011).

MB retention on Fe-GAC seems to be take place due to reactive adsorption only. ESI-MS analysis showed absence of MB ($m/z = 284$) adsorption on carbon surface (see Figure 4.24). MB reactive adsorption relies on the chemical nature of either the carbon or the target probe (MB), and may provoke incomplete irreversible transformations of the adsorbate (Ania et al. 2011). The deposition of degradation products during the process of reactive adsorption found in line with the results reported earlier in literature (Zazo et al. 2006). MB solely found on the Fe-GAC surface in case of adsorption.

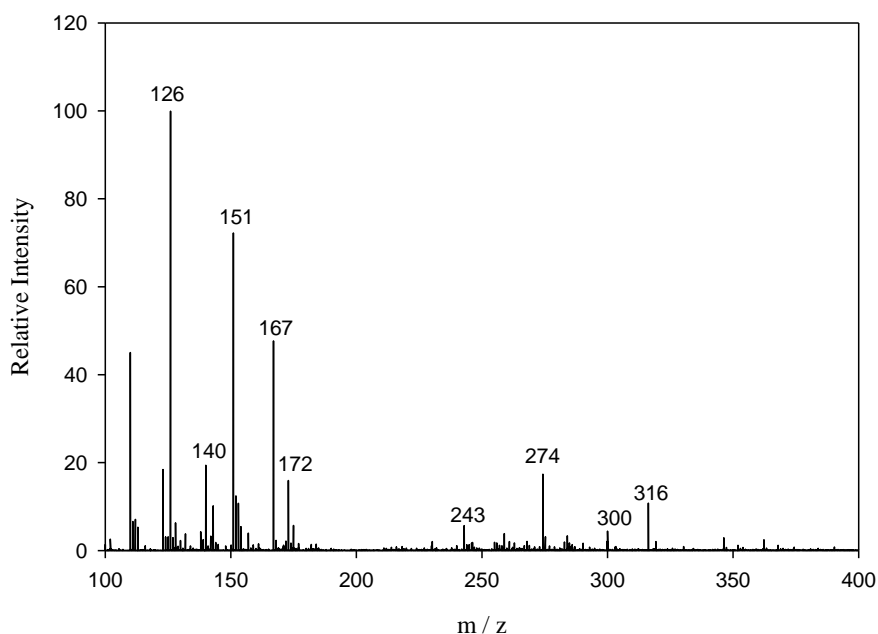
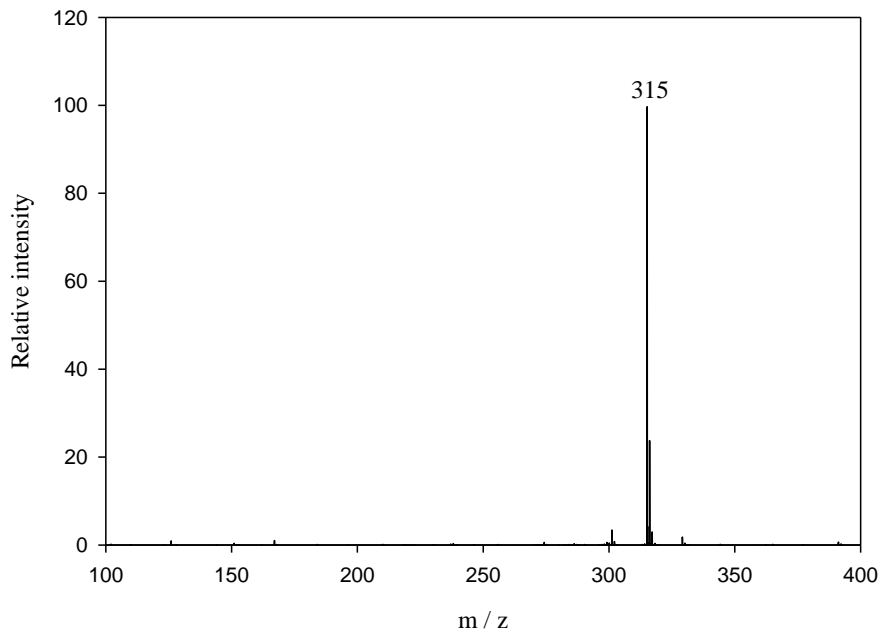


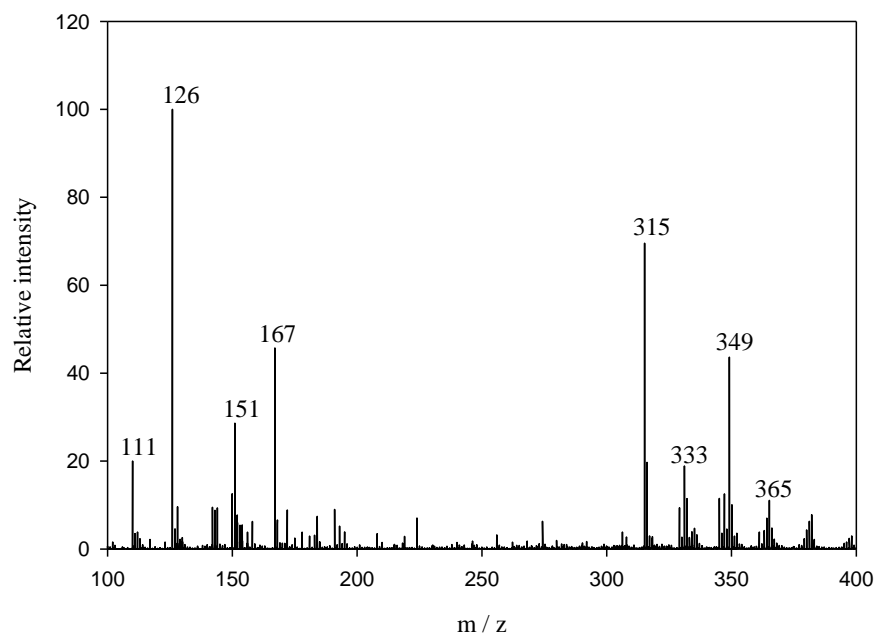
Figure 4.24: ESI-MS of leached aqueous solution of spent Fe-GAC after MB reactive adsorption.

4.8.2 Safranin O in single dye system

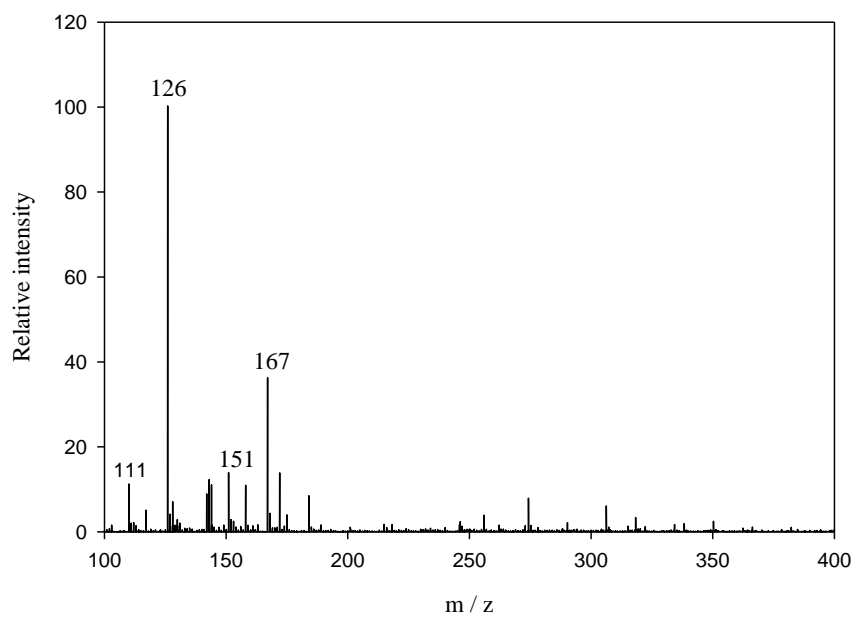
ESI-MS analyses were carried out for the identification of oxidative degradation intermediates formed during reactive adsorption of SO. The results obtained from ESI-MS study suggest that Fe-GAC catalyzed the generation of hydroxyl radicals by decomposition of H_2O_2 and promoted oxidative degradation of the dye. The analysis of aqueous solution (Figure 4.25a – c) during batch study of reactive adsorption using ESI-MS showed oxidative degradation of SO in the solution due to occurrence of chemical reactions on Fe-GAC surface in the presence of $\bullet\text{OH}$. Initially, peak corresponding to SO ($m/z = 315$) was present at $t = 0$ as shown in Figure 4.25a before any reaction took place.



(a)



(b)



(c)

Figure 4.25: ESI-MS spectra of SO aqueous solution and its degradation products during reactive adsorption at (a) $t = 0$ h, (b) $t = 1.5$ h, and (c) $t = 5$ h.

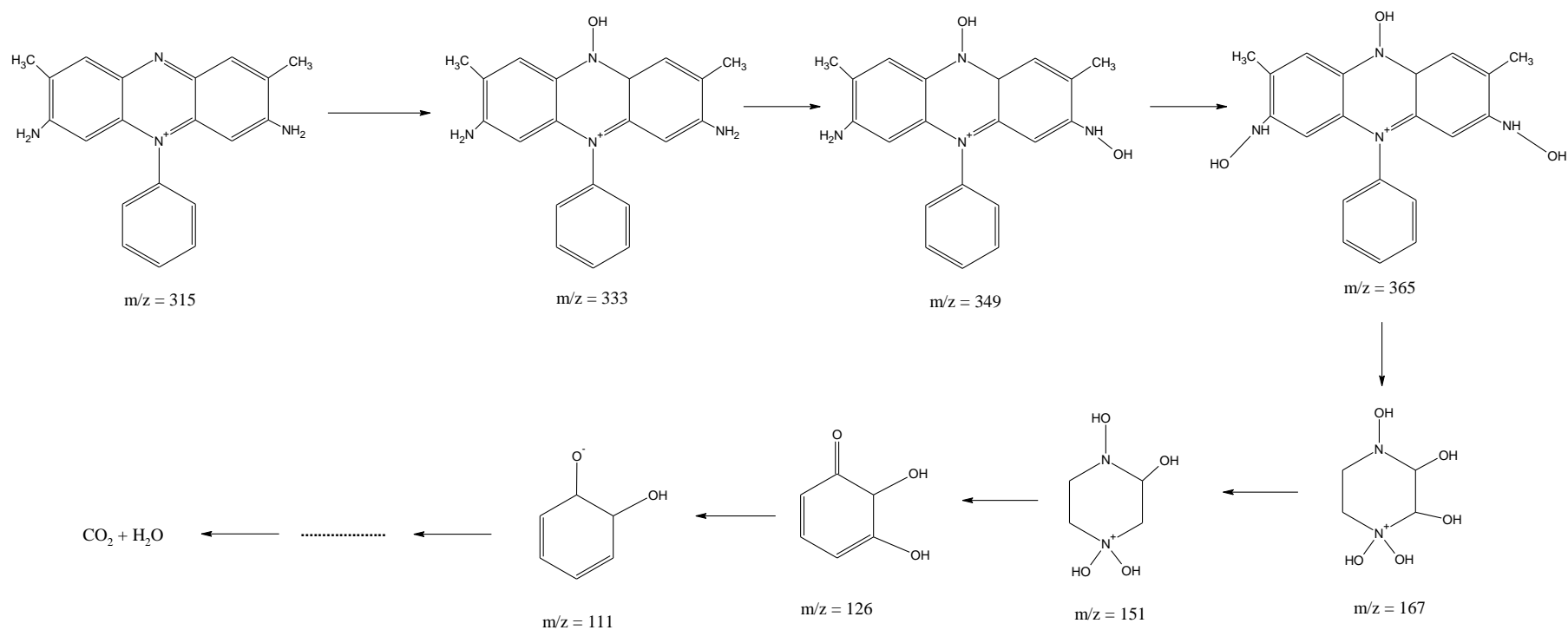


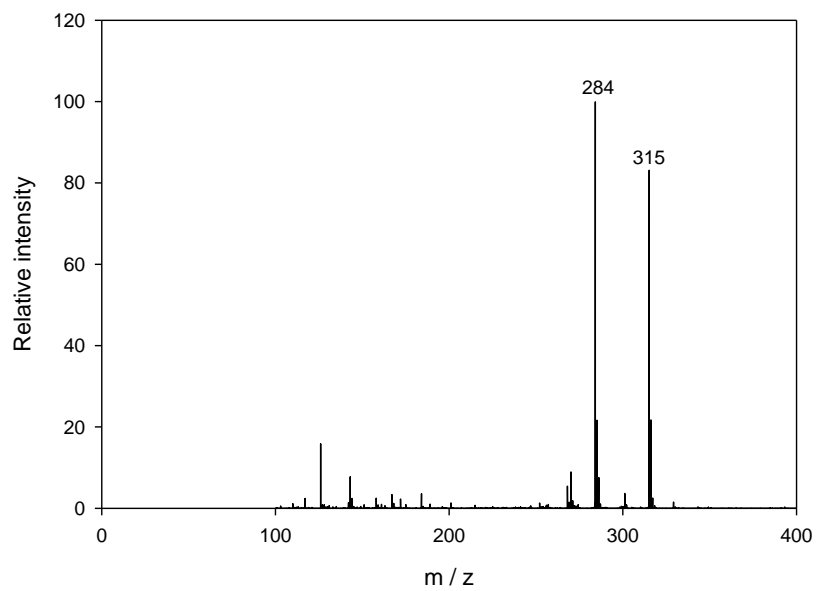
Figure 4.26: Proposed oxidative degradation pathways of SO in aqueous solution during reactive adsorption using Fe-GAC / H₂O₂.

The intensity of signal at $m/z = 315$ decreased with the formation of intermediates as can be seen in their ESI-MS analysis with the reaction period of 1.5 h (Figure 4.25b). There are two possible reaction pathways for dye degradation: (1) hydroxylation (Oliveira et al. 2007) and (2) ring cleavage (Chen et al. 2011). Direct attack of $\bullet\text{OH}$ on the organic moiety and the resulting reactions were responsible for the evolution of hydroxylated intermediates of SO. The hydroxylated intermediates formed can be observed in

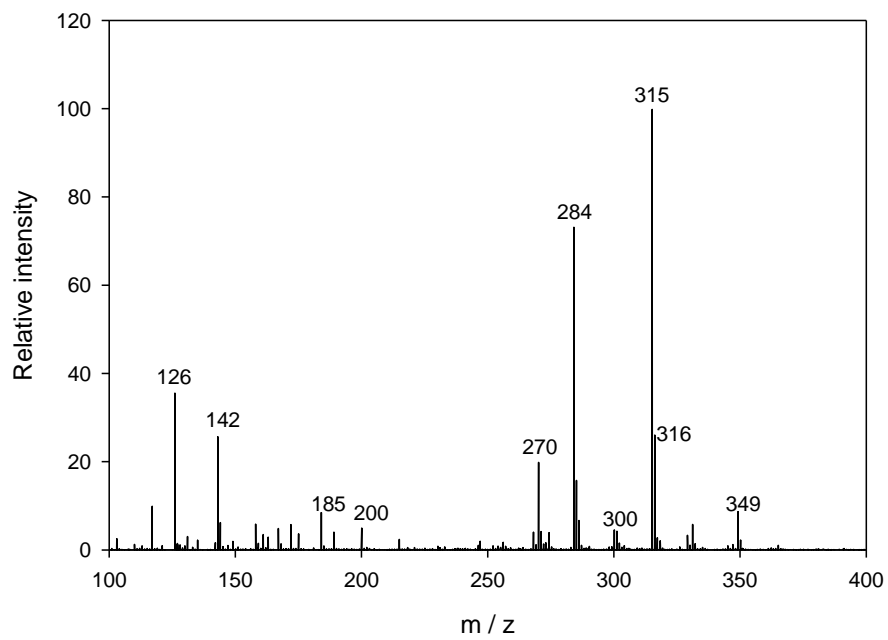
Figure 4.25b at $m/z = 333, 349, \text{ and } 365$. Ring cleavage of SO and hydroxylation result in the formation of intermediates at $m/z = 111, 126, 151, \text{ and } 167$ in 1.5 h. The intensity of hydroxylated intermediates of SO ($m/z = 333, 349, \text{ and } 365$) reduced and then completely vanished as reaction proceeded due to ring cleavage of SO chromophore and addition of OH group (Figure 4.25c). Intermediates at $m/z = 111, 126, 151, \text{ and } 167$ can be seen after 5 h of reaction. Furthermore, the presence of enough $\bullet\text{OH}$ radicals and adequate extent of time may result in complete mineralization of SO to CO_2 and H_2O . The entire oxidative degradation pathway is given in Figure 4.26.

4.8.3 Methylene Blue and Safranin O in binary dye system

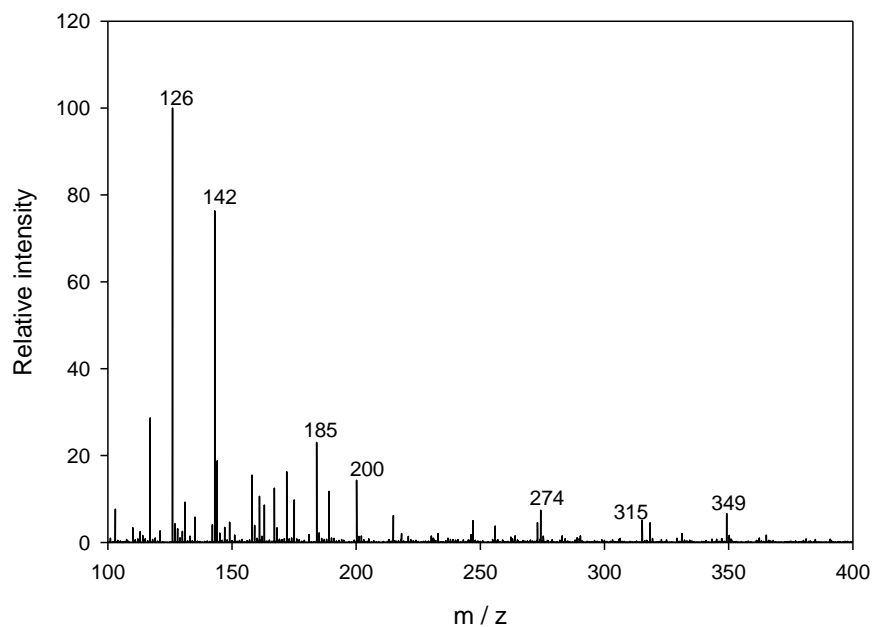
ESI-MS analyses were carried out for the identification of oxidative degradation intermediates formed during reactive adsorption of MB and SO. The results obtained from ESI-MS study suggest that Fe-GAC catalyzed the generation of hydroxyl radicals by decomposition of H_2O_2 and promoted oxidative degradation of the binary dye components. The analysis of aqueous solution (Figure 4.27a – c) during batch study of reactive adsorption using ESI-MS showed oxidative degradation of MB and SO in the solution due to occurrence of chemical reactions on Fe-GAC surface in the presence of $\bullet\text{OH}$. Initially, two peaks corresponding to MB ($m/z = 284$) and SO ($m/z = 315$) were present at $t = 0$ as shown in Figure 4.27a before any reaction took place. Figure 4.28 shows UV-Vis spectra of binary mixture of MB and SO in the visible region for $t = 0$ to $t = 7$ h at 1 h intervals.



(a)



(b)



(c)

Figure 4.27: ESI-MS spectra of binary mixture of MB and SO and its degradation products during reactive adsorption at (a) $t = 0$ h, (b) $t = 2$ h, and (c) $t = 7$ h.

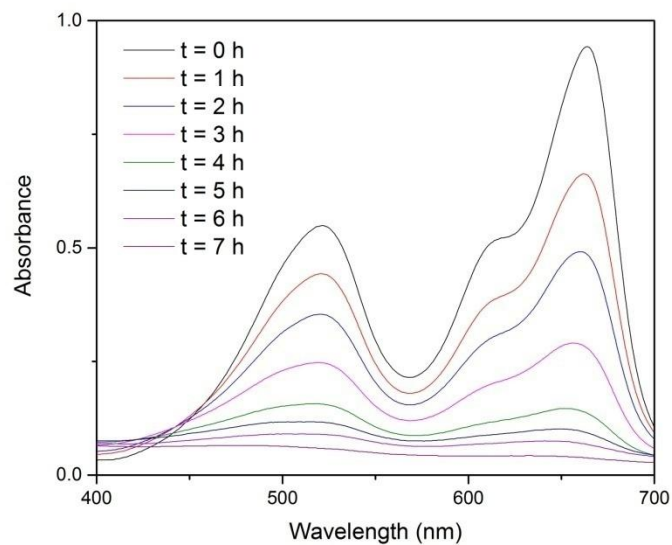


Figure 4.28: UV-vis absorbance spectra of simultaneous removal of MB and SO using Fe-GAC / H_2O_2 .

The intensity of signal at $m/z = 284$ and $m/z = 315$ decreased with the formation of intermediates as can be seen in their ESI-MS analysis with the reaction period of 2 h (Figure 4.27b). Direct attack of $\bullet\text{OH}$ on the organic moieties and the resulting reactions were responsible for the evolution of demethylated and hydroxylated intermediates of MB and SO (Behnajady et al. 2008; Oliveira et al. 2007; Rauf et al. 2010). Intensity of some intermediates formed at $m/z = 126, 142, 185,$ and 200 increased with reaction periods of 2 to 7 h, due to the further degradation of MB and SO in the mixture. The intermediates formed during reactive adsorption were also reactive towards $\bullet\text{OH}$ due to which intensity of some peaks like $m/z = 270$ etc. which were present after 2 h of reaction reduced and can be observed in Figure 4.27c. After 7 h of reactive adsorption, some new peaks of compounds which had lower values of m/z (i.e. 100 to 200) emerged and components at $m/z > 200$ disappeared due to reactive adsorption of MB and SO. It can be seen from Figure 4.27c that peak at $m/z = 284$ corresponding to MB disappeared completely whereas, peak at $m/z = 315$ corresponding to SO still remained after 7 h of reaction. These results explain that eradication of MB is easier than that of SO. It may be due to the presence of additional covalently bonded $-\text{NH}_2$ groups and a benzene ring other than the cyclic molecular structure of MB, making the SO molecular larger in size. Therefore, rate of diffusion of SO molecules is slower resulting in lower concentration available for reaction. Presence of MB molecules hindered the diffusion of SO molecules which are larger and hence antagonistic behavior of MB towards SO was observed during degradation. Furthermore, the presence of enough $\bullet\text{OH}$ radicals and adequate extent of time may result in complete mineralization of binary dye mixture to CO_2 and H_2O .

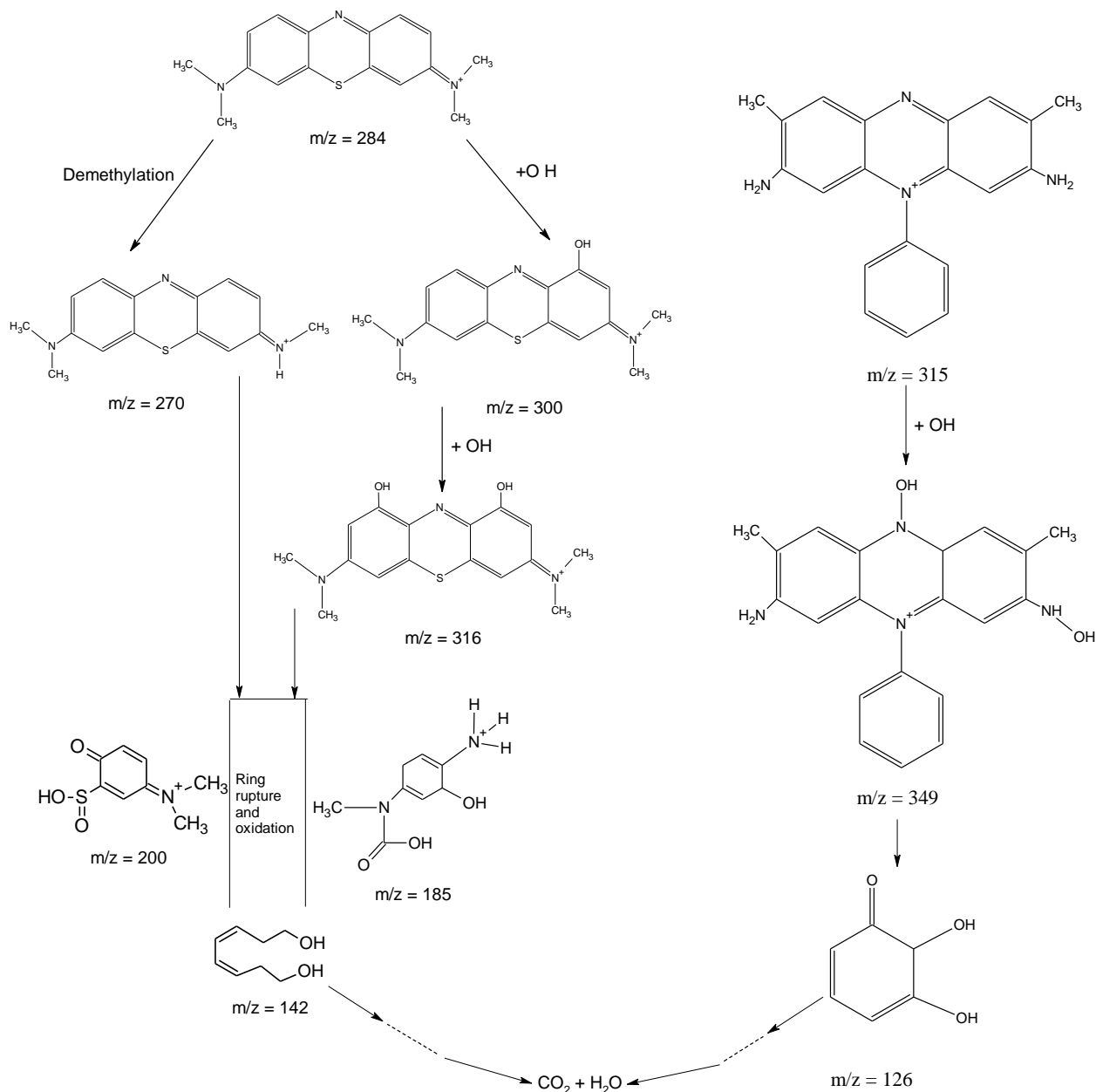


Figure 4.29: Proposed oxidative degradation pathways of MB and SO present in binary mixture during reactive adsorption using Fe-GAC / H₂O₂.

Figure 4.29 shows the proposed oxidative degradation pathways of MB and SO mixture during reactive adsorption using Fe-GAC / H₂O₂. The oxidative degradation intermediates formed during simultaneous reactive adsorption of MB and SO were found analogous to the intermediates formed when individual dye degradation was studied on the same system (Sharma et al. 2017a; Sharma et al. 2017c). Hence, it can be said that both dyes present in a mixture

degraded individually without occurrence of any reaction among the parent or intermediate compounds.

Reactive adsorption of MB and SO using Fe-GAC / H₂O₂ system rendered the aqueous solution almost colorless. Figure 4.28 shows absorption spectral changes when the MB and SO present in aqueous solution degraded by the Fe-GAC / H₂O₂ system for 7 h. The intensity of the maximum absorption at λ_{max} 663 nm and 519 nm decreased due to the degradation of MB and SO. It has been postulated that MB and SO removal occurred due to oxidative degradation (see Figure 4.29).

4.9 Batch adsorption studies

4.9.1 Methylene Blue in single dye system

4.9.1.1 Equilibrium study of Methylene Blue adsorption

Figure 4.30 shows Langmuir equilibrium isotherm of MB adsorption onto Fe-GAC. The isotherm equations applicability is compared using the Correlation coefficients (R^2 values). The results show in Table 4.4 that the Langmuir isotherm fits better than the Freundlich isotherm (Figure 4.31) as linear correlation coefficient, R^2 is higher for Langmuir isotherm. In the present study, R_L values were in the range of 0–1 which confirms that the Fe-GAC adsorbent is favorable for MB adsorption under the used experimental conditions (Table 4.4). Equilibrium study was not carried out for reactive adsorption, as MB molecule gets degraded during the process. Therefore, there is no possibility that MB equilibrium get established during reactive adsorption.

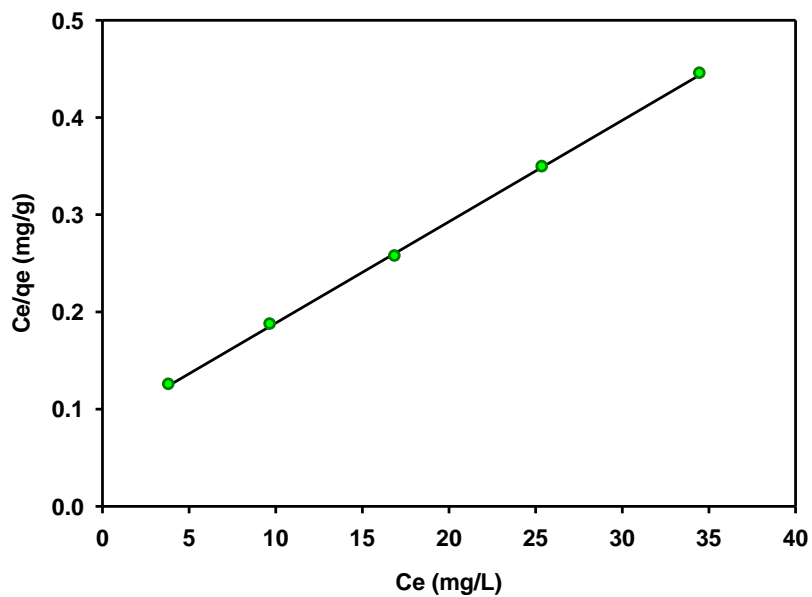


Figure 4.30. Langmuir isotherm of MB adsorption onto Fe-GAC (Adsorption conditions: Temp.: 30 °C, $C_0 = 10\text{-}50$ mg/L MB, adsorbent dose = 20 mg).

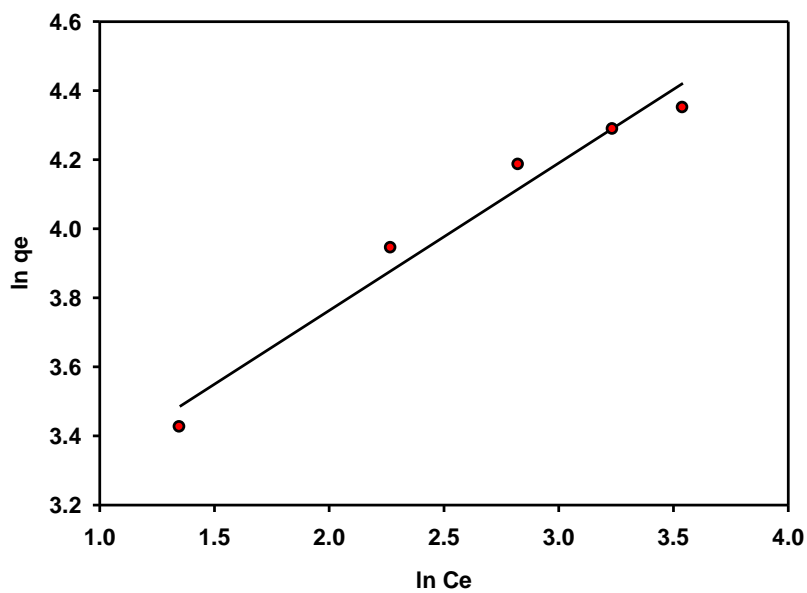


Figure 4.31: Freundlich isotherm of MB adsorption onto Fe-GAC (Adsorption conditions: Temp.: 30 °C, $C_0 = 10\text{-}50$ mg/L MB, adsorbent dose = 20 mg).

Table 4.4: Related adsorption equilibrium parameters for the adsorption of MB on Fe-GAC at different temperatures.

Adsorption isotherms	Adsorption isotherms constants	Temperature (°C)				
		20	30	40	50	60
Langmuir	q_m (mg/g)	90.91	100.00	111.11	125.00	142.86
	K_L (L/mg)	0.08	0.12	0.17	0.21	0.25
	R^2	0.991	0.999	0.994	0.998	0.995
	R_L	0.56	0.46	0.37	0.32	0.29
Freundlich	K_F (mg/g) (L/mg) ^{1/n}	12.13	18.34	24.48	30.36	37.79
	1/n	0.49	0.43	0.41	0.38	0.36
	R^2	0.974	0.968	0.903	0.915	0.881

4.9.1.2 Kinetic study of Methylene Blue adsorption

Figure 4.32 and Figure 4.34 show pseudo-first-order, pseudo-second-order kinetic and intraparticle diffusion models for MB adsorption onto the Fe-GAC. In the present work, higher value of correlation coefficient was found for pseudo-first-order as compared to pseudo-second-order kinetic and intraparticle diffusion models (see Table 4.5) indicate that the kinetic modeling of the MB adsorption onto the Fe-GAC adsorbent well followed the pseudo-first-order rate model. Rate constant values indicated that the removal efficiency of MB decreased significantly for adsorption ($k_1 = 0.004$, see Table 4.5) when compared with reactive adsorption ($k_{app} = 0.015$, see Table II.2 appendix). Therefore, MB removal rate constant was found almost four times for reactive adsorption than adsorption.

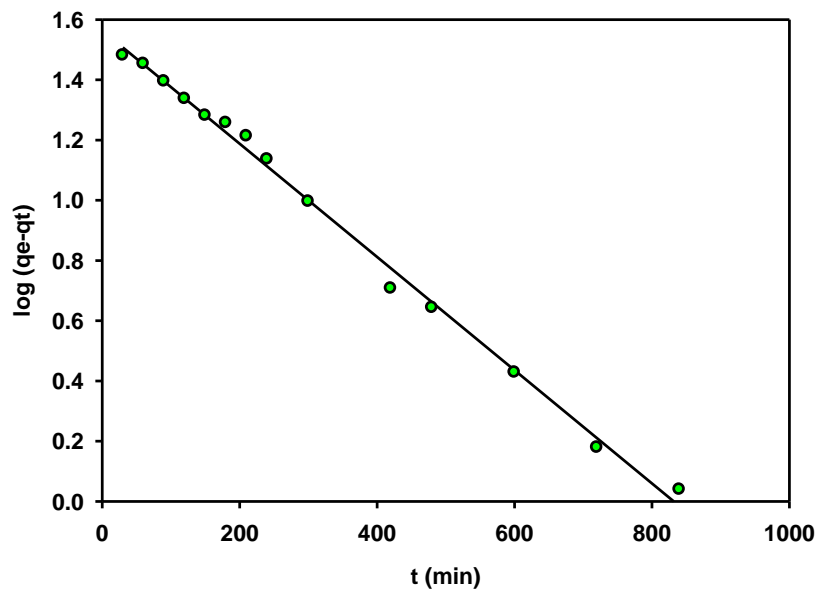


Figure 4.32: Pseudo-first-order kinetics of MB adsorption onto Fe-GAC (Adsorption conditions: Temp.: 30° C, C_0 : 10 mg/L MB, dose of Fe-GAC: 0.2 g/L).

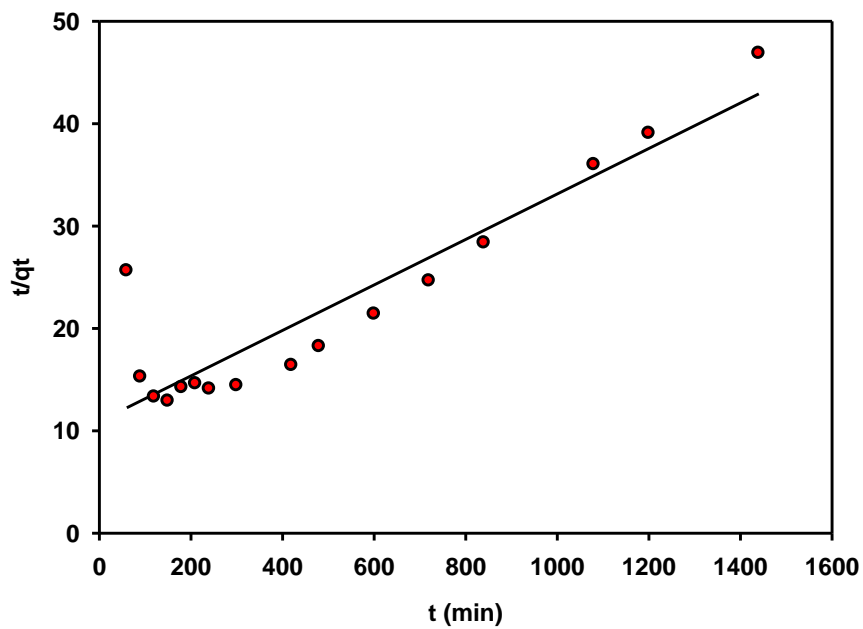


Figure 4.33: Pseudo-second-order kinetics of MB adsorption onto Fe-GAC (Adsorption conditions: Temp.: 30° C, C_0 : 10 mg/L MB, dose of Fe-GAC: 0.2 g/L).

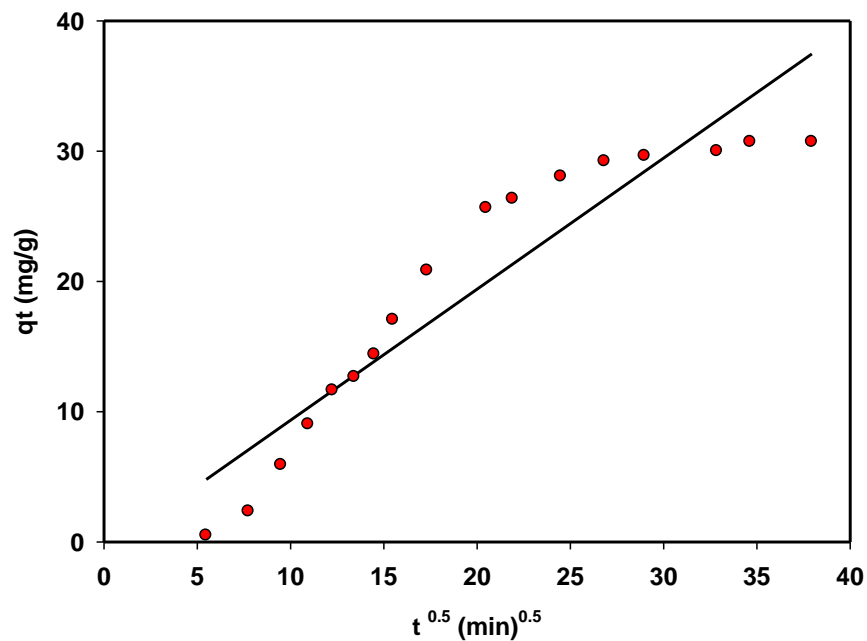


Figure 4.34: Intraparticle diffusion model of MB adsorption onto Fe-GAC (Adsorption conditions: Temp.: 30° C, C₀: 10 mg/L MB, dose of Fe-GAC: 0.2 g/L).

Table 4.5: Kinetic parameters for the adsorption of MB onto the Fe-GAC at 30° C.

Kinetic models	Parameters	
Pseudo first order	q _{e, exp} (mg/g)	34.8
	q _{e, calc} (mg/g)	36.56
	k ₁ (1/min)	0.004
	R ²	0.995
Pseudo second order	q _{e, calc} (mg/g)	45.46
	k ₂ (g/mg min)	4.44 × 10 ⁻⁵
	R ²	0.841
Intraparticle diffusion	k _{id} (mg/g min ^{1/2})	1.0
	C (mg/g)	-0.72
	R ²	0.877

The Weber-Morris theory was employed to identify the steps that occurred during the adsorption process (McKay et al. 1980). The intraparticle diffusion model attributed to initial surface sorption and consequent intraparticle diffusion phenomena. The intercept of the linear plot suggesting that intraparticle diffusion is not the only rate-controlling step (Chang et al. 2015) and the adsorption process is rather complex and involves more than one diffusion resistance (Rodríguez et al. 2009). It may be concluded that surface adsorption and intra-particle diffusion were concurrently operating during MB and Fe-GAC interactions (Bhattacharya and Sharma 2005).

4.9.1.3 Thermodynamic study of Methylene Blue adsorption

The negative values of Gibbs free energy change (ΔG°) confirm the feasibility of the process and the spontaneous nature. Plot of ΔG° versus T for estimation of thermodynamic parameters for the adsorption of MB onto Fe-GAC is shown in Figure 4.35. The positive value of ΔH° suggests the endothermic nature of MB adsorption onto Fe-GAC. The positive value of ΔS reflects the affinity of the Fe-GAC for MB (Bhattacharya and Sharma 2005).

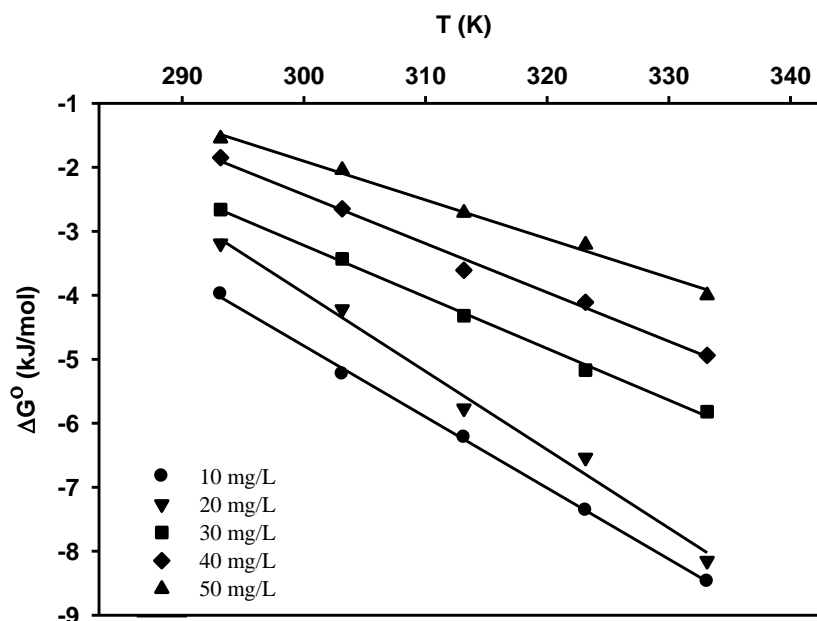


Figure 4.35. Plot of Gibbs free energy change, ΔG° versus temperature, T of MB adsorption onto Fe-GAC (Adsorption conditions: Temp.: 20-60° C, C_0 : 10-50 mg/L MB, dose of Fe-GAC: 0.2 g/L).

Table 4.6: Thermodynamic parameters for adsorption of MB onto Fe-GAC.

Dye conc. (mg/L)	ΔG° (kJ/mol)					ΔH° (kJ/mol)	ΔS° (kJ/mol K)	R^2
	Temperature ($^\circ\text{C}$)							
	20	30	40	50	60			
10	-4.12	-5.23	-6.02	-6.90	-7.71	28.53	0.111	0.999
20	-3.30	-4.22	-5.58	-6.14	-7.42	32.75	0.122	0.991
30	-2.75	-3.43	-4.18	-4.85	-5.30	20.96	0.081	0.998
40	-1.91	-2.65	-3.49	-3.86	-4.50	20.49	0.077	0.993
50	-1.60	-2.04	-2.63	-3.01	-3.64	16.30	0.061	0.994

Gibbs-free energy measures the spontaneity of the sorption system. The negative values of ΔG° indicate that the dye solubilization process is spontaneous and thermodynamically favorable. The increase in negative values of ΔG° with temperature implies the enhancement in the driving force of solubilization, which is confirmed by the greater extent of dye sorption with an increase in temperature. The decrease in ΔG° values with the increase in dye concentration is due to decrease in solubility of dye molecules (Appusamy et al. 2014).

It was found that the value of ΔH° decreases with the dye concentration. The positive value of ΔH° indicates that the solubility of dye is endothermic in nature. The increase in the amount of dye solubility with temperature also indicates the endothermic nature of adsorption. The decrease in ΔH° value with increasing dyes concentration at a fixed adsorbent dose may be due to decrease in the amount of dye solubility (Bingjia et al. 2007).

Monolayer adsorption is the predominant mechanism for dye accumulation on the adsorbent surface. Kinetic and equilibrium isotherm parameters explain that dye accumulated on the surface adsorbent via electrostatic force as the main contribution force in combination to other pathways like hydrogen bonding (Ansari et al. 2016). Thermodynamic data confirm that the interaction is through van der waes force as ΔH° values show physical adsorption (Bhattacharya and Sharma 2005; Dil et al. 2016; Postai et al. 2016). Binding of dye on to the adsorbent surface can be explained by the electrostatic interaction. Presence of akaganeite ($\beta\text{-FeOOH}$) may

produce negative charge (OOH^-) on the surface of GAC that attracts cationic dye MB towards the adsorbent surface and gives high monolayer adsorption capacity.

On comparing enthalpy values of MB removal obtained for reactive adsorption (Table 4.2) with adsorption (Table 4.6), it can be found that enthalpy value is almost one-third for MB removal using reactive adsorption. Hence, reactive adsorption for dye removal is an efficient method that completely removes the dye by degrading its molecule while consuming less energy. Reactive adsorption was found to be an efficient method for dye removal than adsorption may be due to the fact that reactive adsorption involves oxidative reaction of hydroxyl radicals and dye molecule. As fast as hydroxyl radical is formed, it reacts with dye molecule as this radical has a very short half-life. Gupta et al. (2016) reported that the oxidative reaction took place on external macropore surface only. The adsorbed concentration of organic moiety on macropores was rapidly degraded due to the formation of highly reactive OH free radicals on its surface that gives a high rate of the reaction. It was also reported that the overall resistance for reactive adsorption was much less as compared to pure adsorption. High pore diffusivity into Fe-GAC particle may be attributed to the rapid reactive adsorption (Gupta et al. 2016).

4.9.2 Safranin O in single dye system

4.9.2.1 Equilibrium study of Safranin O adsorption

Langmuir isotherm equation is also given by

$$q_e = \frac{kC_e}{1+bC_e} \quad \dots (4.7)$$

It is clear from Figure 4.36 and Figure 4.37 that both Langmuir ($R^2 = 0.996$) and Freundlich ($R^2 = 0.999$) isotherms are suitably explain the experimental data. Langmuir isotherm was used which assumes monolayer adsorption as reactive adsorption is a surface phenomenon in which hydroxyl radicals are formed on the adsorbent surface and oxidize the organic moieties. Parameters obtained for Langmuir isotherm are $k = 22.7 \text{ L/g}$ and $b = 0.909 \text{ L/mg}$.

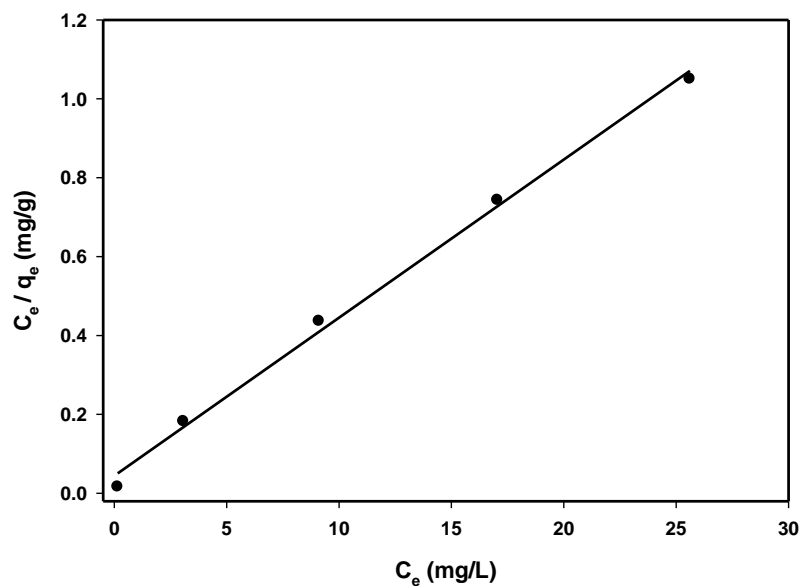


Figure 4.36: Langmuir isotherm of SO adsorption onto Fe-GAC (Adsorption conditions: Temp.: 30° C, C_0 : 10-50 mg/L MB, dose of Fe-GAC: 1.0 g/L).

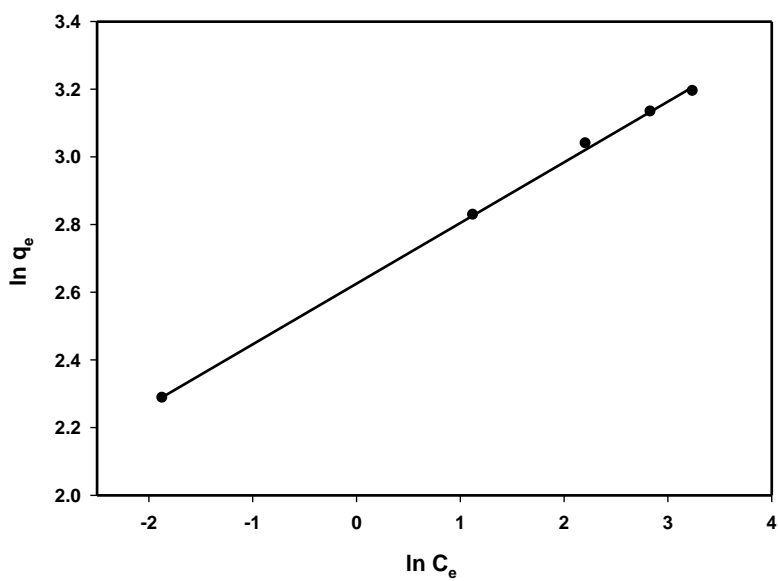


Figure 4.37: Freundlich isotherm of SO adsorption onto Fe-GAC (Adsorption conditions: Temp.: 30° C, C_0 : 10-50 mg/L MB, dose of Fe-GAC: 1.0 g/L).

4.9.3 MB and SO binary dye system

4.9.3.1 Equilibrium study of adsorption of Methylene Blue and Safranin O in a binary dye system

In this work, the optimum isotherm parameters for extended Langmuir and extended Freundlich isotherms were found by minimizing the difference between the experimental and model data of the equilibrium solid phase concentration, q_e , using the sum of the squares of the error (SSE) function. Figure 4.38 to Figure 4.41 show the fit of experimental versus model data for extended Langmuir and extended Freundlich isotherms. The parameters obtained for extended Langmuir and extended Freundlich isotherms, R^2 and SSE values are given in Table 4.7.

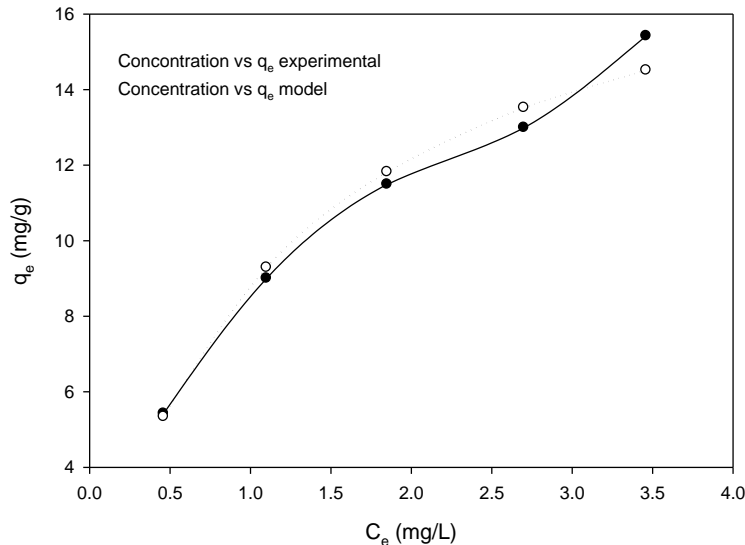


Figure 4.38: Extended Langmuir isotherm fit for experimental versus model data of MB in binary dye adsorption onto Fe-GAC (Adsorption conditions: Temp.: 30° C, C_0 : 1-5 mg/L MB and SO each, dose of Fe-GAC: 0.1 g/L, and pH 6.5).

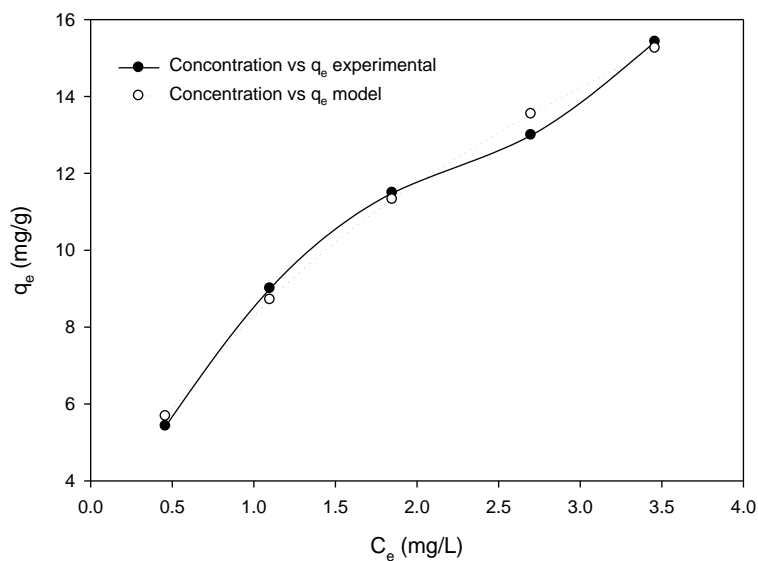


Figure 4.39: Extended Freundlich isotherm fit for experimental versus model data of MB in binary dye adsorption onto Fe-GAC (Adsorption conditions: Temp.: 30° C, C_0 : 1-5 mg/L MB and SO each, dose of Fe-GAC: 0.1 g/L, and pH 6.5).

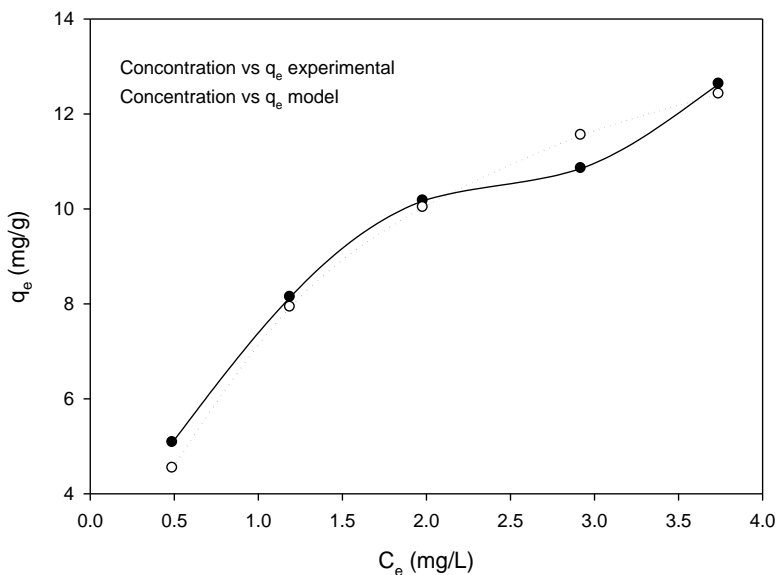


Figure 4.40: Extended Langmuir isotherm fit for experimental versus model data of SO in binary dye adsorption onto Fe-GAC (Adsorption conditions: Temp.: 30° C, C_0 : 1-5 mg/L MB and SO each, dose of Fe-GAC: 0.1 g/L, and pH 6.5).

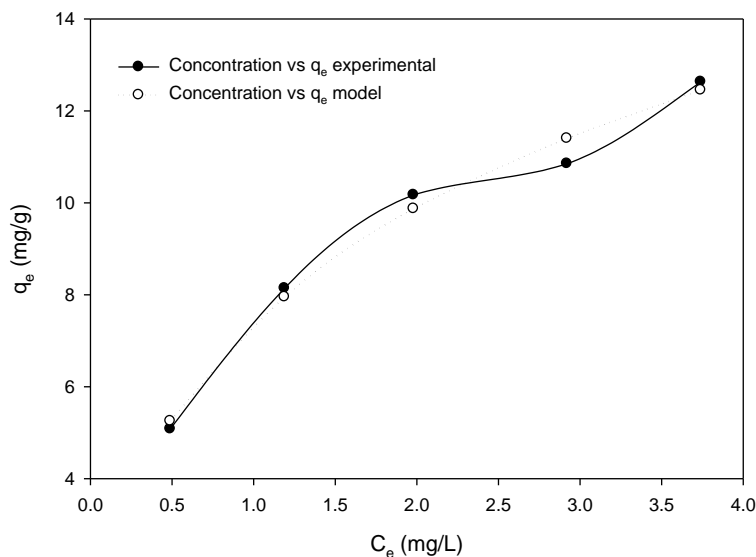


Figure 4.41: Extended Freundlich isotherm fit for experimental versus model data of SO in binary dye adsorption onto Fe-GAC (Adsorption conditions: Temp.: 30° C, C_0 : 1-5 mg/L MB and SO each, dose of Fe-GAC: 0.1 g/L, and pH 6.5).

Table 4.7: Comparison of the coefficients isotherm parameters for MB and SO adsorption onto Fe-GAC at optimum conditions.

Isotherm	Parameter	Value
Extended Langmuir	$K_{L,1}$	0.800
	$K_{L,2}$	0.012
	$q_{m,1}$	20.0
	$q_{m,2}$	1027.2
	SSE	2.20
	R^2 (MB)	0.978
	R^2 (SO)	0.984
Extended Freundlich	x_1	1.6
	y_1	1.0
	z_1	1.5
	x_2	-0.3
	y_2	0.8
	z_2	-0.9

SSE	1.00
R ² (MB)	0.991
R ² (SO)	0.985

The facts that by comparing values of SSE and R² of extended-Freundlich with extended Langmuir proved the greater validity of the extended-Freundlich to describe the simultaneous adsorption of MB and SO on the adsorbent.

4.9.3.2 Kinetic study of Methylene Blue and Safranin O adsorption in binary dye system

Figure 4.42, Figure 4.43, and Figure 4.44 show the pseudo-first-order, pseudo-second-order, and Intraparticle diffusion model for MB in binary dye system. Figure 4.45, Figure 4.46, and Figure 4.47 show the pseudo-first-order, pseudo-second-order, and intraparticle diffusion model for SO in binary dye system. Kinetic parameters of above three models are given in Table 4.8 and were obtained using well known straight line plots. The R² values and comparison of experimental adsorption capacity with values obtained from model pseudo-first and pseudo-second order for both dyes MB and SO suggest that adsorption of MB and SO does not follow these kinetic models.

In the case of intraparticle diffusion model, intraparticle diffusion may be responsible for the transportation of MB and SO from aqueous solution to the surface of adsorbent. It can be seen from Table 4.8 that R² values for both MB and SO were found to be higher than 0.99, so that intraparticle diffusion model fit to experimental data suitably. The intraparticle diffusion model attributed to initial surface sorption and consequent intraparticle diffusion phenomena. The intraparticle particle diffusion will be sole limiting in the case of constant is zero in the plot of q_t versus $t^{1/2}$, i.e. straight line pass through the origin (Ghaedi et al. 2014). Positive intercepts indicate that rapid adsorption occurs within a short period of time (Wu et al. 2009). In the present work intercept of MB is positive and SO is negative. Hence, MB adsorption occurs fast whereas SO diffused slowly into adsorbent.

Table 4.8: Kinetic parameters for the simultaneous adsorption of MB and SO onto the Fe-GAC at 30° C.

Kinetic models	Parameters	MB	SO
Pseudo-first-order	$q_{e, \text{exp}}$ (mg/g)	10.0	8.1
	$q_{e, \text{calc}}$ (mg/g)	17.1	12.0
	k_1 (1/min)	0.009	0.007
	R^2	0.773	0.886
Pseudo-second-order	$q_{e, \text{calc}}$ (mg/g)	13.3	25.6
	k_2 (g/mg min)	5.0×10^{-4}	4.4×10^{-5}
	R^2	0.963	0.851
Intraparticle diffusion	k_{id} (mg/g min ^{1/2})	0.478	0.495
	C (mg/g)	0.432	-2.264
	R^2	0.992	0.990

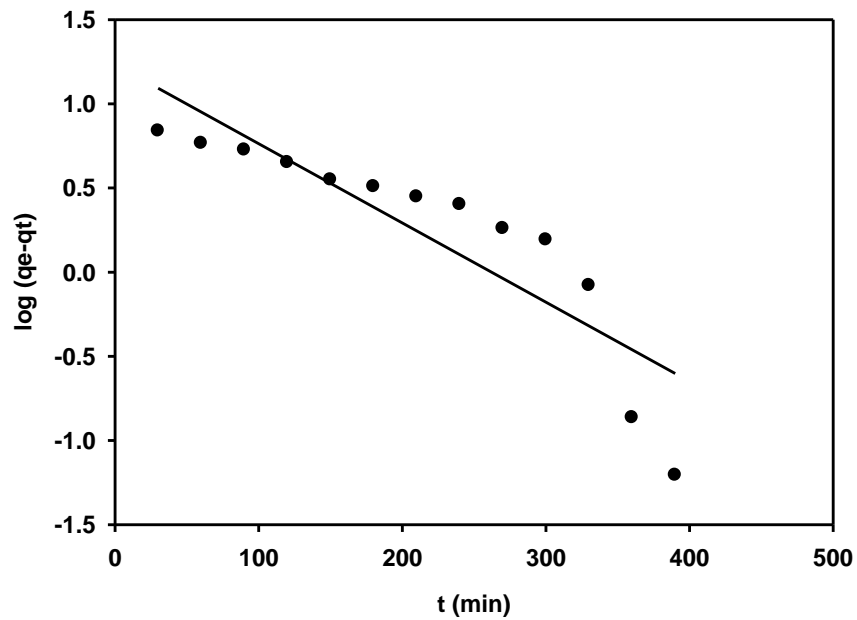


Figure 4.42: Pseudo-first-order kinetics of MB in simultaneous binary dye adsorption (Adsorption conditions: Temp.: 30° C, C_0 : 5 mg/L of MB and SO each, dose of Fe-GAC: 0.4 g/L).

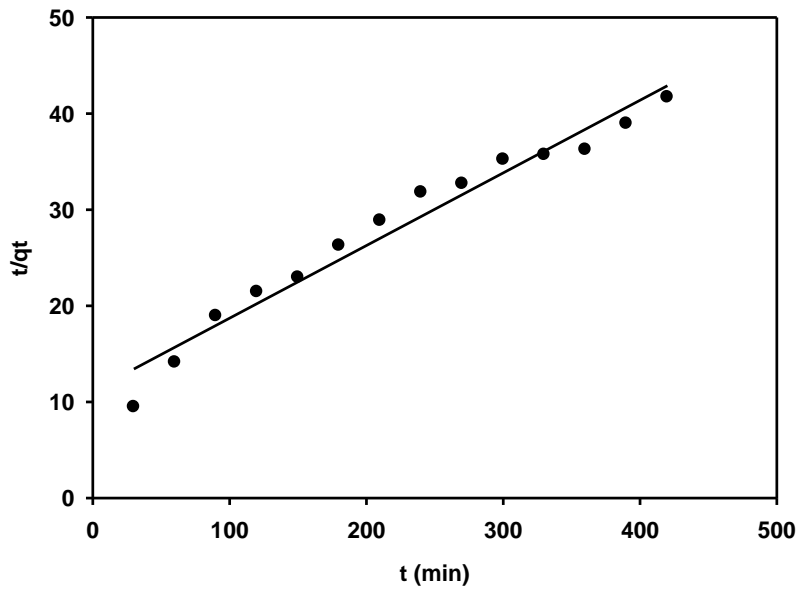


Figure 4.43: Pseudo-second-order kinetics of MB in simultaneous binary dye adsorption (Adsorption conditions: Temp.: 30° C, C_0 : 5 mg/L of MB and SO each, dose of Fe-GAC: 0.4 g/L).

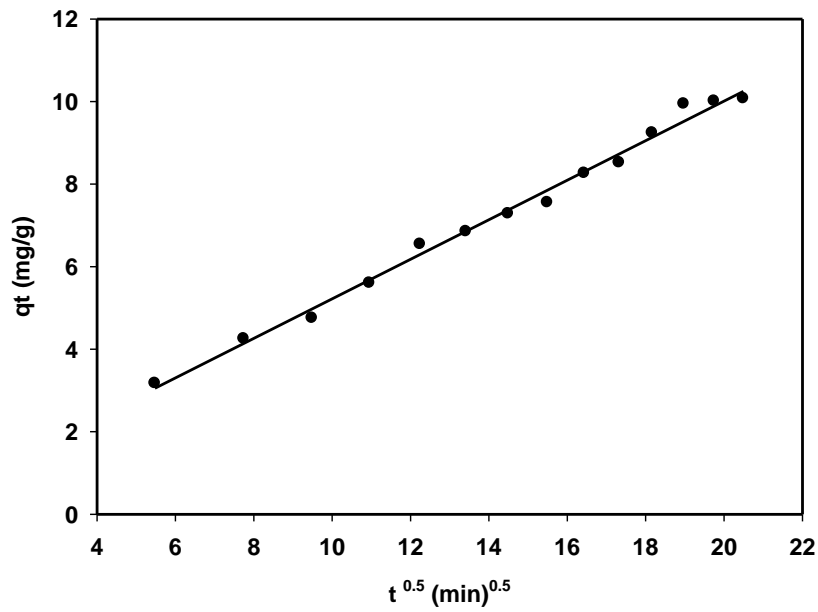


Figure 4.44: Intraparticle diffusion kinetics of MB in simultaneous binary dye adsorption (Adsorption conditions: Temp.: 30° C, C_0 : 5 mg/L of MB and SO each, dose of Fe-GAC: 0.4 g/L).

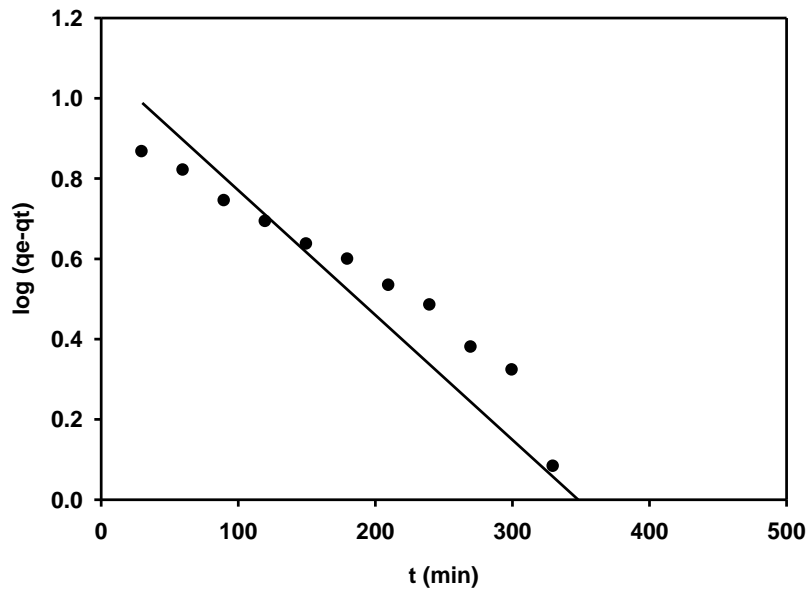


Figure 4.45: Pseudo-first-order kinetics of SO in simultaneous binary dye adsorption (Adsorption conditions: Temp.: 30° C, C_0 : 5 mg/L of MB and SO each, dose of Fe-GAC: 0.4 g/L).

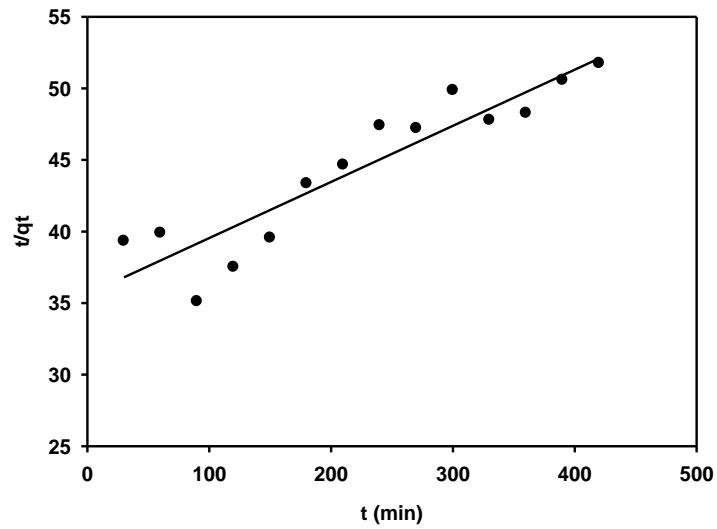


Figure 4.46: Pseudo-second-order kinetics of SO in simultaneous binary dye adsorption (Adsorption conditions: Temp.: 30° C, C_0 : 5 mg/L of MB and SO each, dose of Fe-GAC: 0.4 g/L).

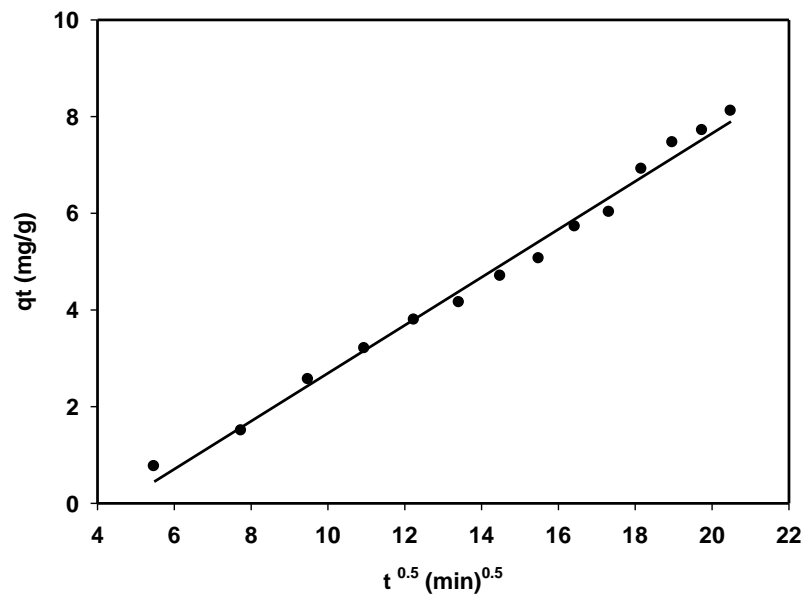


Figure 4.47: Intraparticle diffusion kinetics of SO in simultaneous binary dye adsorption (Adsorption conditions: Temp.: 30° C, C₀: 5 mg/L of MB and SO each, dose of Fe-GAC: 0.4 g/L).

Part II: Modeling

4.10 Central Composite Design (CCD) and response surface methodology (RSM)

The effect of factors on the responses was studied using central composite design (CCD). CCD helps to determine the synergies amongst the factors by doing minimum number of experiments. Table 4.9 shows the five process control variables; contact time, sorbent dose, MB concentration, SO concentration, and pH and their limits. Total 32 experiments for five factors were designed using half-fractional CCD. Responses were considered as MB and SO removal percentages. Factors and responses values are given in Table 4.10.

Table 4.9: Process control variables and their limits

Variable	Unit	Limits		
		-1	0	+1
Time	(min)	60	90	120
Adsorbent dose	(g / L)	0.8	1.0	1.2
Initial MB concentration	(mg / L)	2	3	4
Initial SO concentration	(mg / L)	2	3	4
Initial pH of solution	-	3.5	6.0	8.5

$$\%R = b_0 + \sum_{i=1}^5 b_i x_i + \sum_{i=1}^5 b_{ii} x_i^2 + \sum_{i=1}^4 \sum_{j=i+1}^5 b_{ij} x_i x_j \quad \dots (4.8)$$

where x_i , x_j are the factors values and b_0 , b_i , b_{ii} and b_{ij} are the constants, linear, quadratic, and interaction coefficients respectively. The model Eq. (4.8) was used to optimize and predict dye removal in percentage in terms of response (% R). Analysis of variance (ANOVA) determined significant and insignificant terms and afterwards, eq. (4.8) used to obtain predictive model. The ANOVA results are given in Table 4.11 and Table 4.12. ANOVA results shows that P-values for some terms are less than the confidence level (0.05) and the P-value is higher than 0.05 for lack of fit, indicate the adequacy and significance of the model. For the MB and SO removal time, adsorbent dosage, pH, initial MB concentration, and initial SO concentration were found to be significant.

Table 4.10: Central composite design

Run	Time (min)	Adsorbent dose (g/L)	MB concentration (mg/L)	SO concentration (mg/L)	pH	MB removal (%)	SO removal (%)
1	60	0.8	2	2	8.5	36.32%	37.29%
2	120	0.8	2	2	3.5	62.94%	53.81%
3	60	1.2	2	2	3.5	54.48%	48.31%
4	120	1.2	2	2	8.5	74.38%	71.61%
5	60	0.8	4	2	3.5	42.66%	33.05%
6	120	0.8	4	2	8.5	65.30%	54.24%
7	60	1.2	4	2	8.5	51.87%	39.41%
8	120	1.2	4	2	3.5	77.36%	65.68%
9	60	0.8	2	4	3.5	35.32%	37.71%
10	120	0.8	2	4	8.5	72.64%	66.95%
11	60	1.2	2	4	8.5	50.50%	50.42%
12	120	1.2	2	4	3.5	79.10%	76.48%
13	60	0.8	4	4	8.5	36.69%	31.78%
14	120	0.8	4	4	3.5	62.56%	57.20%
15	60	1.2	4	4	3.5	52.36%	45.76%
16	120	1.2	4	4	8.5	76.00%	70.76%
17	30	1.0	3	3	6	30.51%	27.12%
18	150	1.0	3	3	6	81.43%	77.12%
19	90	0.6	3	3	6	41.63%	43.50%
20	90	1.4	3	3	6	71.64%	66.67%
21	90	1.0	1	3	6	55.22%	53.67%
22	90	1.0	5	3	6	54.23%	43.22%
23	90	1.0	3	1	6	50.58%	36.44%
24	90	1.0	3	5	6	49.42%	44.41%
25	90	1.0	3	3	1	60.03%	57.06%
26	90	1.0	3	3	11	62.02%	59.04%
27	90	1.0	3	3	6	50.25%	49.44%

28	90	1.0	3	3	6	50.41%	48.59%
29	90	1.0	3	3	6	48.42%	48.87%
30	90	1.0	3	3	6	50.41%	47.74%
31	90	1.0	3	3	6	49.92%	48.59%
32	90	1.0	3	3	6	50.08%	48.87%

Table 4.11: Analysis of Variance for the removal of MB (%R)

Source	DF	Adj SS	Adj MS	F-Value	P-Value
Model	20	0.569222	0.028461	166.97	0.000
Linear	5	0.514277	0.102855	603.42	0.000
Time (min)	1	0.405337	0.405337	2377.98	0.000
Adsorbent (g / L)	1	0.108878	0.108878	638.75	0.000
MB (mg/L)	1	0.000034	0.000034	0.20	0.663
SO (mg/L)	1	0.000025	0.000025	0.15	0.709
pH	1	0.000003	0.000003	0.02	0.894
Square	5	0.041726	0.008345	48.96	0.000
Time (min)*Time (min)	1	0.008509	0.008509	49.92	0.000
Adsorbent(g/L)*Adsorbent (g/L)	1	0.010246	0.010246	60.11	0.000
MB (mg/L)*MB (mg/L)	1	0.005685	0.005685	33.35	0.000
SO (mg/L)*SO (mg/L)	1	0.000130	0.000130	0.76	0.401
pH*pH	1	0.025834	0.025834	151.56	0.000
2-Way Interaction	10	0.013218	0.001322	7.75	0.001
Time (min)*Adsorbent (g / L)	1	0.001369	0.001369	8.03	0.016
Time (min)*MB (mg/L)	1	0.001369	0.001369	8.03	0.016
Time (min)*SO (mg/L)	1	0.002697	0.002697	15.82	0.002
Time (min)*pH	1	0.001559	0.001559	9.15	0.012
Adsorbent (g / L)*MB (mg/L)	1	0.000005	0.000005	0.03	0.871
Adsorbent (g / L)*SO (mg/L)	1	0.000000	0.000000	0.00	0.981
Adsorbent (g / L)*pH	1	0.002033	0.002033	11.93	0.005
MB (mg/L)*SO (mg/L)	1	0.002263	0.002263	13.28	0.004
MB (mg/L)*pH	1	0.000314	0.000314	1.84	0.202
SO (mg/L)*pH	1	0.001609	0.001609	9.44	0.011
Error	11	0.001875	0.000170		
Lack-of-Fit	6	0.001589	0.000265	4.63	0.057
Pure Error	5	0.000286	0.000057		

Table 4.12: Analysis of Variance for the removal of SO (%R)

Source	DF	Adj SS	Adj MS	F-Value	P-Value
Model	20	0.521775	0.026089	308.43	0.000
Linear	5	0.471090	0.094218	1113.89	0.000
Time (min)	1	0.357725	0.357725	4229.21	0.000
Adsorbent (g / L)	1	0.084878	0.084878	1003.47	0.000
MB (mg/L)	1	0.017935	0.017935	212.03	0.000
SO (mg/L)	1	0.010258	0.010258	121.28	0.000
pH	1	0.000294	0.000294	3.48	0.089
Square	5	0.043334	0.008667	102.46	0.000
Time (min)*Time (min)	1	0.003369	0.003369	39.83	0.000
Adsorbent (g/L)* Adsorbent (g/L)	1	0.009644	0.009644	114.02	0.000
MB (mg/L)*MB (mg/L)	1	0.000069	0.000069	0.82	0.385
SO (mg/L)*SO (mg/L)	1	0.010062	0.010062	118.95	0.000
pH*pH	1	0.019145	0.019145	226.34	0.000
2-Way Interaction	10	0.007351	0.000735	8.69	0.001
Time (min)* Adsorbent (g / L)	1	0.000427	0.000427	5.04	0.046
Time (min)*MB (mg/L)	1	0.000047	0.000047	0.56	0.470
Time (min)*SO (mg/L)	1	0.002123	0.002123	25.10	0.000
Time (min)*pH	1	0.001663	0.001663	19.66	0.001
Adsorbent (g / L)*MB (mg/L)	1	0.000205	0.000205	2.42	0.148
Adsorbent (g / L)*SO (mg/L)	1	0.000063	0.000063	0.75	0.406
Adsorbent (g / L)*pH	1	0.000977	0.000977	11.55	0.006
MB (mg/L)*SO (mg/L)	1	0.000344	0.000344	4.06	0.069
MB (mg/L)*pH	1	0.001495	0.001495	17.67	0.001
SO (mg/L)*pH	1	0.000007	0.000007	0.08	0.779
Error	11	0.000930	0.000085		
Lack-of-Fit	6	0.000776	0.000129	4.19	0.069
Pure Error	5	0.000154	0.000031		
Total	31	0.522705			

The optimized values for the experimental factors contact time, sorbent dose, MB initial concentration, SO initial concentration and pH were found to be 120 min, 1.2 g/L, 2 mg/L, 4 mg/L, and 8.5 respectively. At this condition, the removal percentage for MB and SO were predicted to be 81.5% and 79.3%. In order to further confirm the reliability of the predicted results, an experiment was carried out at the obtained optimum conditions and the removal

percentage of MB and SO were obtained to be 80.72% and 78.92% respectively and obtained values of percentage dye removal are very close to the predicted values.

For both MB and SO dyes, removal was increased with sorbent dose and contact time as shown in Figure 4.48(a) and Figure 4.49(a). Removal of dyes was enhanced due to an increase in the number of sorption binding sites at Fe-GAC surface (Mahmoodi et al. 2010; Shen et al. 2009). It can be observed from Figure 4.48(b) and Figure 4.49(b) that removal of both dyes was increased with increase in pH. At basic pH of solution, the sorbent surface is negatively charged, resulting in the electrostatic forces between these groups and positively charged dye molecules which favor the adsorption of cationic dyes. With the increase in pH, the net positive charge of adsorbent decreases, consequently percentage removal of dyes increases (Kurniawan et al. 2012; Mondal et al. 2007; Sharma et al. 2018).

During the adsorption of binary mixture, removal of MB was not much affected by the presence of SO (see Figure 4.48(b)), whereas there was a significant reduction in the removal of SO when initial MB concentration was increased (see Figure 4.49(b)). The plausible reason may be the larger molecular size of SO than MB, due to the presence of additional covalently bonded $-NH_2$ groups and a benzene ring other than the cyclic molecular structure of MB. Presence of MB molecules hindered the diffusion of SO molecules which are larger and hence antagonistic behavior of MB towards SO was observed during adsorption (Sharma et al. 2017b).

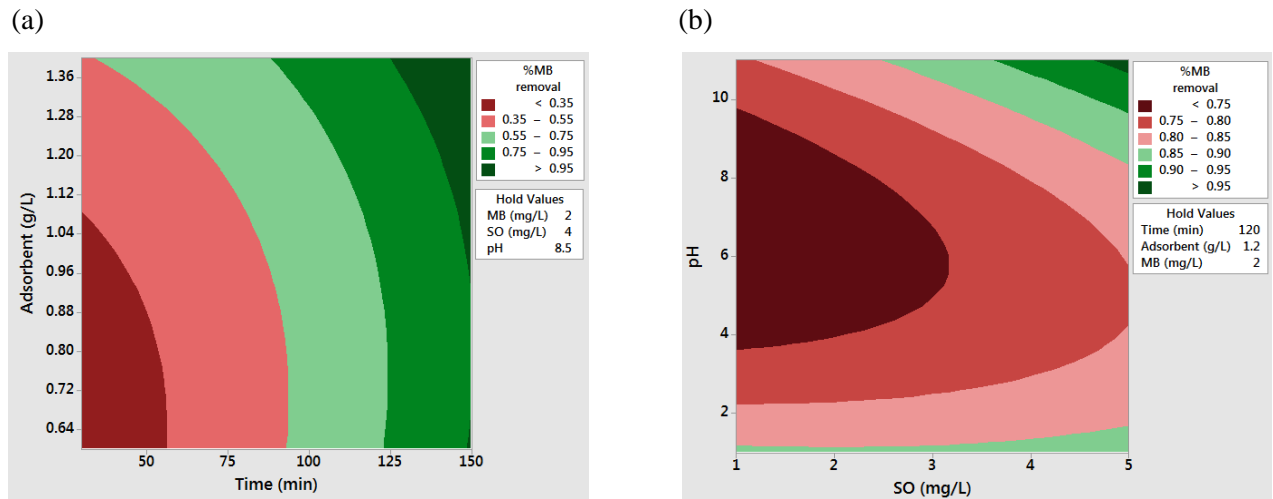


Figure 4.48: Response surface contour plots of simultaneous MB decolorization (%) as the function of (a) Time and adsorbent and (b) SO and pH.

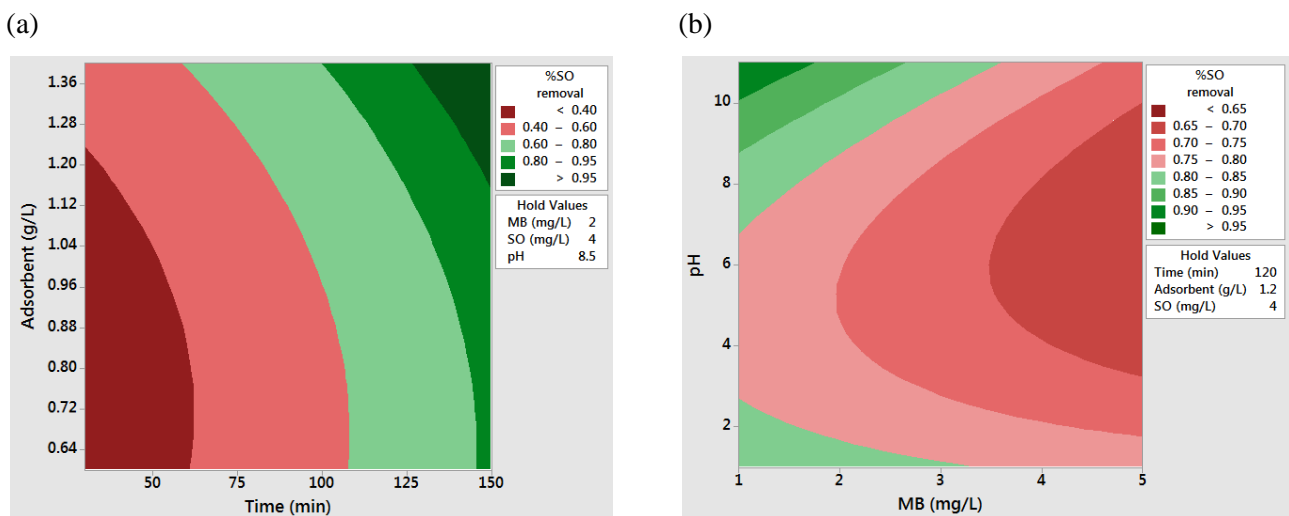


Figure 4.49. Response surface contour plots of simultaneous SO decolorization (%) as the function of (a) Time and adsorbent and (b) MB and pH.

4.11 SO adsorption and reactive adsorption modeling

A mathematical model was used (Gupta et al. 2016) for adsorption and reactive adsorption of SO. Porous GAC particle is visualized to contain two regions; consisting of macro-pores (f) and constituting the micro-pores ($1 - f$). Relatively fast sorption and diffusion take place in macro-pores when compared with micro-pores due to larger pore diameter. It was an assumption that the macro-pores and micro-pores are parallel to one another and distributed homogeneously within the particles and give radial transport. TEM analysis of used Fe-GAC verified the presence of iron particle clusters in GAC. These iron particles were sizes ranging from 50 to 100 nm. This size of iron particles deposited in GAC was found consistent with literature (Hristovski et al. 2009). For the modeling purpose micro-pores and meso-pores were clubbed together. Though, GAC particle consists of micro-pores (<2 nm), meso-pores (2–50 nm) and macro-pores (>50 nm) (Groen et al. 2003). Therefore, it was considered that iron particles' impregnation occurs in to macro-pores only. Thus, reactive sites are present on macro-pores only and micro-pores do not contain any reactive site due to absence of iron. However, it is believed that adsorption of SO occurs in macro-pores as well as micro-pores.

For a batch-wise removal of SO using reactive adsorption, mathematical model was employed. It is considered that molecules of SO pass through an aqueous film that lies outside particle surface and then these molecules further get adsorbed onto macro-pores and micro-pores surface of the particle. In reactive adsorption, dye molecules react with OH radicals generated on the surface of macro-pores as per pseudo-first-order reaction kinetics. The mechanism of reactive adsorption can be described by three resistances in series: (i) outer resistance across the film of liquid, (ii) resistance through macropore diffusion and (iii) surface reaction resistance. It is assumed that, at any moment, surface concentrations of dye are in equilibrium with the SO adsorbed amount on the particle surface. Following equations were presented this mathematical model:

External liquid phase mass balance:

$$V \frac{dC}{dt} = -k_L A(C - C_s) \quad \dots (4.9)$$

Macropore mass balance:

$$\frac{\partial q_{ma}}{\partial t} = \frac{\partial}{\partial r} \left(D_{ma} r^2 \frac{\partial q_{ma}}{\partial r} \right) - k_r q_{ma} \quad \dots (4.10)$$

Micropore mass balance:

$$\frac{\partial q_{mi}}{\partial t} = \frac{\partial}{\partial r} \left(D_{mi} r^2 \frac{\partial q_{mi}}{\partial r} \right) \quad \dots (4.11)$$

Initial and boundary conditions are:

$$C(0) = C_0 \quad \dots (4.12)$$

$$q_{ma}(r,0) = 0 \quad \dots (4.13)$$

$$q_{mi}(r,0) = 0 \quad \dots (4.14)$$

$$\frac{\partial q_{ma}}{\partial r}(0,t) = 0 \quad \dots (4.15)$$

$$\frac{\partial q_{mi}}{\partial r}(0,t) = 0 \quad \dots (4.16)$$

Solid-liquid interface relationship can be written as:

$$D_{ma} \frac{\partial q_{ma}}{\partial r}(R,t) = \frac{k_L}{\rho} (C - C_{s,ma}) \quad \dots (4.17)$$

$$D_{mi} \frac{\partial q_{mi}}{\partial r}(R,t) = \frac{k_L}{\rho} (C - C_{s,mi}) \quad \dots (4.18)$$

Surface concentrations of dye are in equilibrium with the SO adsorbed amount on the particle surface at any instant. Therefore,

$$C_{s,ma} = f(q_{s,ma}) \quad \dots(4.19)$$

$$C_{s,mi} = f(q_{s,mi}) \quad \dots(4.20)$$

$$C_s = f \times C_{s,ma} + (1-f) \times C_{s,mi} \quad \dots(4.21)$$

To evaluate fitness of experimental and the predicted data, below mentioned statistical indices was used for SO dye system.

$$RSQ = \frac{\sum (X - \bar{X})(Y - \bar{Y})}{\sqrt{\sum (X - \bar{X})^2} \sqrt{\sum (Y - \bar{Y})^2}} \quad \dots(4.22)$$

Adsorption and reactive adsorption studies

A MATLAB program was used for solving above equations. The program uses the factors viz. mass of sorbent, particle size and particle density of Fe-GAC, initial SO concentration, volume of aqueous solution, kinetic data and, Langmuir equilibrium constants, including time and intervals, apparent rate constant for reactive adsorption. Fraction of macropores, f was taken from literature (Peel et al. 1981). Primarily, values of k_L , D_{ma} , and D_{mi} were obtained for adsorption. These values do not change in case for reactive adsorption. Hence, using these values and k_{app} , further k_r was evaluated for reactive adsorption. The values of k_L , D_{ma} , D_{mi} , and k_r are given in Table 4.13. The program gives the results such as the theoretical kinetic data related to solute concentration in aqueous phase with time; solid-phase concentrations dye concentration at surface and time along with the dimensionless distance across the particles for macro- and micro-pore diffusion during adsorption and reactive adsorption. By fitting the experimental data to the model, it was found that the surface reaction rate constant, k_r is 5 times of apparent rate constant, k_{app} . This may be due to the fact that k_{app} values include the diffusional resistance along with reaction, which decreases the effective value of rate constant to be considered for surface reaction coefficient.

Table 4.13: Parametric values of reactive adsorption model of SO.

Parameters	Value
Film mass transfer coefficient, k_L	8.15×10^{-5} m/s
Macropore diffusivity, D_{ma}	1.1×10^{-12} m ² /s
Micropore diffusivity, D_{mi}	6.9×10^{-13} m ² /s
Surface reaction rate constant, k_r	8.5×10^{-4} 1/s
Macropore fraction, f	0.66

Adsorption

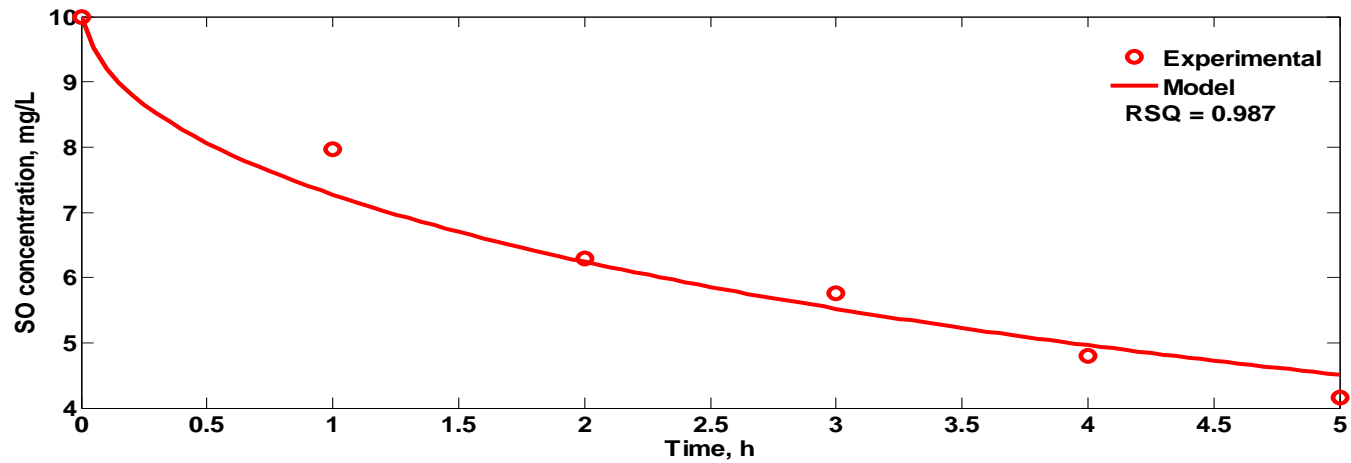


Figure 4.50: SO concentration change in bulk during adsorption.

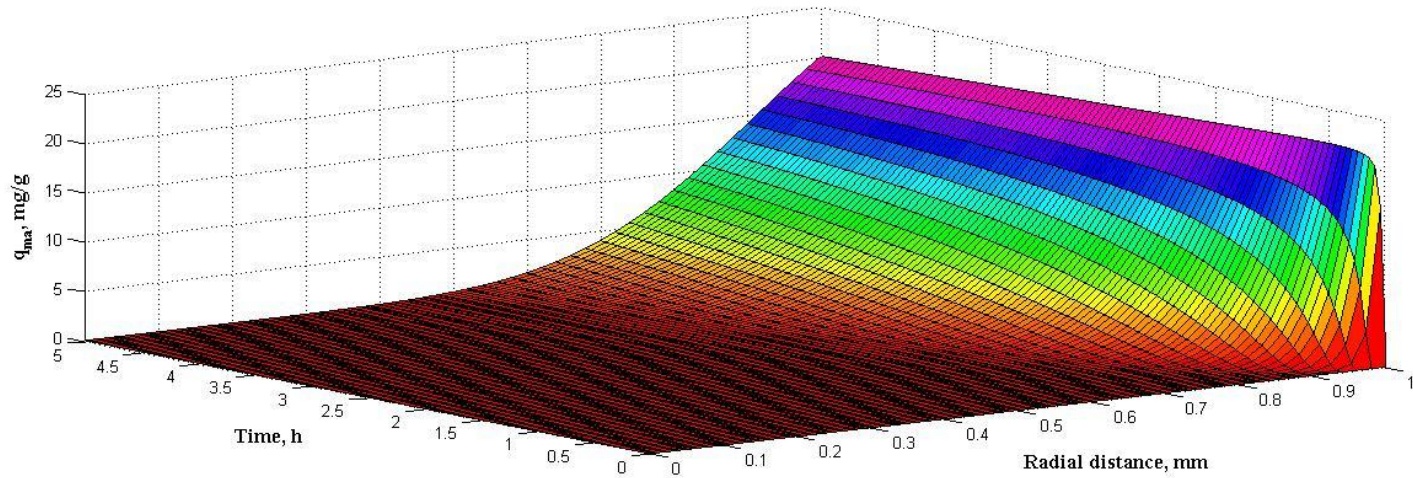


Figure 4.51: Concentration plots of SO in macro-pores during adsorption.

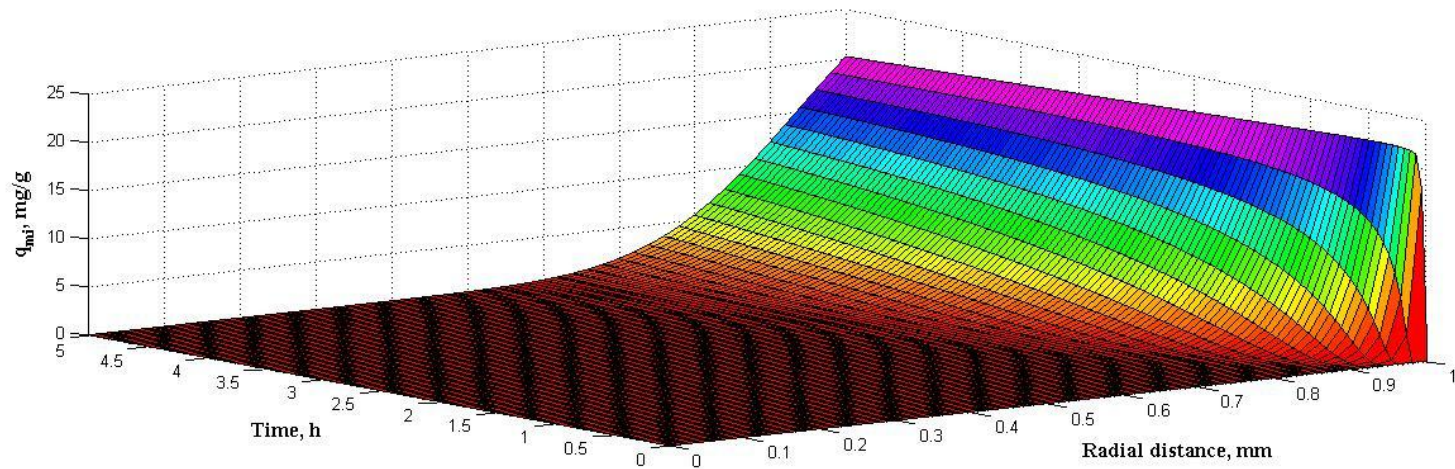


Figure 4.52: Concentration plots of SO in micro-pores during adsorption.

It can be seen from Figure 4.50 that predicted SO concentration in bulk using model are in accordance with experimental values for adsorption. However, the simulated values deviate from experimental values relatively higher for the first hour with negligible deviation later. This higher deviation may be due to the particle's surface hydrophobicity which results in initial slow film diffusion. After a certain period, the deviation is minimized as equilibrium is acquired across the film and only pore diffusion dominates. In addition, the SO concentration was reduced 58.4% only in 5 h from the bulk solution using adsorption.

Radial concentration profiles of SO, obtained from model, within the macropore and micropore regions of Fe-GAC particle during 5 h are presented in Figure 4.51 and Figure 4.52, respectively. The concentration profiles of SO in macro-pores of adsorbent particle (Figure 4.51) for 5 h, indicated that amount of SO diffused in Fe-GAC particle was up to 65% of the particle radius. Furthermore, adsorbate gets diffuse slowly towards center of the particle; possibly due to the smaller value of macropore diffusivity. Figure 4.52 indicates that the diffusion rate of SO is comparatively slow in micro-pores of the sorbent particle. It can be observed from concentration profiles that 51% of micro-pores have adsorbed SO via diffusion. Comparatively lower adsorption of SO in micro-pores than macro-pores, may be due to relatively smaller value of micropore diffusivity. The outer part of adsorbed concentration profile stipulates that the SO adsorbed concentration increased in a very short duration. Afterwards, SO concentration lowers down as time proceeds due to the diffusion in adjacent layers in macro- and micro-pore. Comparison of macro-pores and micro-pores profiles shows that the movement of concentration front towards the adsorbent center is almost similar in macro-pores and micro-pores.

Reactive Adsorption

The reactive adsorption experimental data of SO are found to be fit well to simulated values obtained from the parallel-pore-diffusion-model (Figure 4.53). During reactive adsorption, SO concentration reduces and was almost fully vanished (<0.5 mg/L) in 5 h. Therefore, this process is found much effective when compared to pure adsorption in terms of both time required for treatment as well as contaminant removal efficiency. Surface reaction dominates over pore diffusion in case of reactive adsorption. Sorbed concentration of SO in macro-pores depletes

rapidly due to oxidative degradation of SO in the presence of highly reactive OH^\bullet free radicals. Figure 4.54 and Figure 4.55 show the concentration profiles of SO within the reactive sorbent particle for a duration of 5 h in the macro-pores and micro-pores respectively. The adsorbed SO concentration profiles in the external part of macro-pores increases initially within a very short period due to high value of film mass transfer coefficient and then depletes rapidly due to chemical reaction. In 5 h, only 20% of the particle is diffused with SO diffused, indicating that a considerable part of sorbent is still vacant. However, the maximum amount of sorbed SO at the outer surface is same as simple adsorption. SO concentration depletes very fast due to high rate of reaction and it does not get enough time to move towards the center of the particle as macro-pores are highly reactive ($\text{Fe} / \text{H}_2\text{O}_2$). In case of reactive adsorption, the removal of SO dye was entirely occurring on external macro-pore surface only. This represents fast reaction of SO occurring in exterior surface of macro-pores and narrower pores offer strong diffusion resistances.

The maximum amount of adsorbed SO in the micro-pore is almost similar to pure adsorption. However, the concentration plots of adsorbed SO in micro-pores increase initially because of high value of film mass transfer coefficient but it decreases with time.

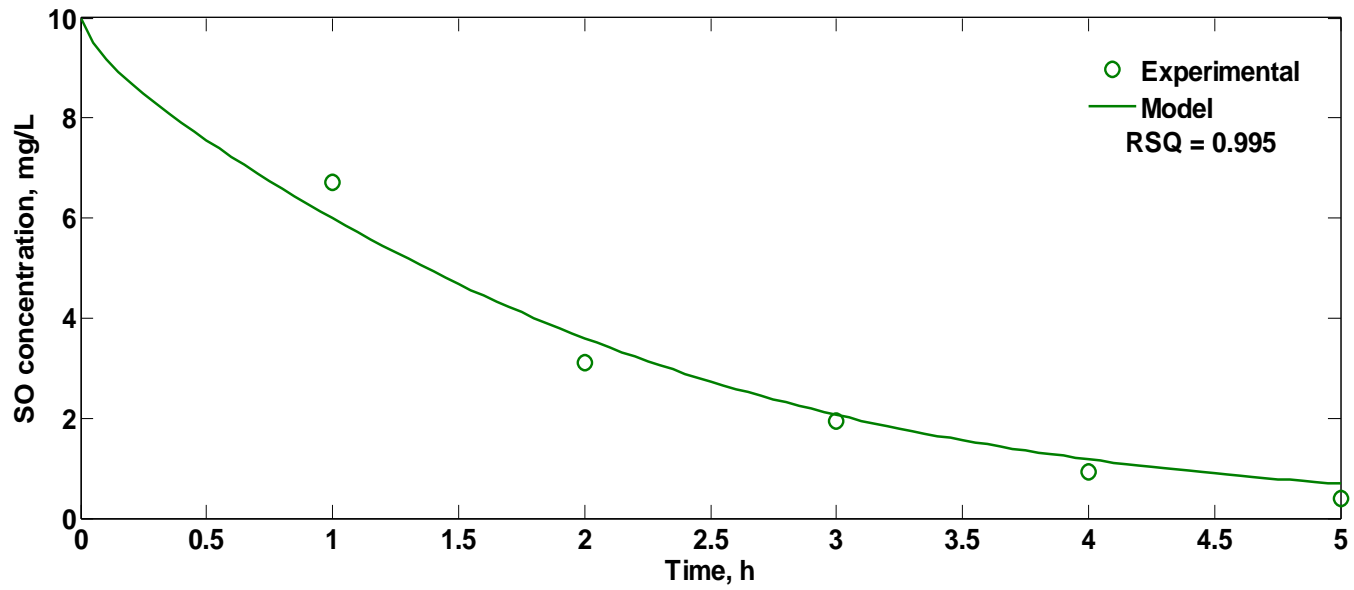


Figure 4.53: SO concentration change in bulk during reactive adsorption.

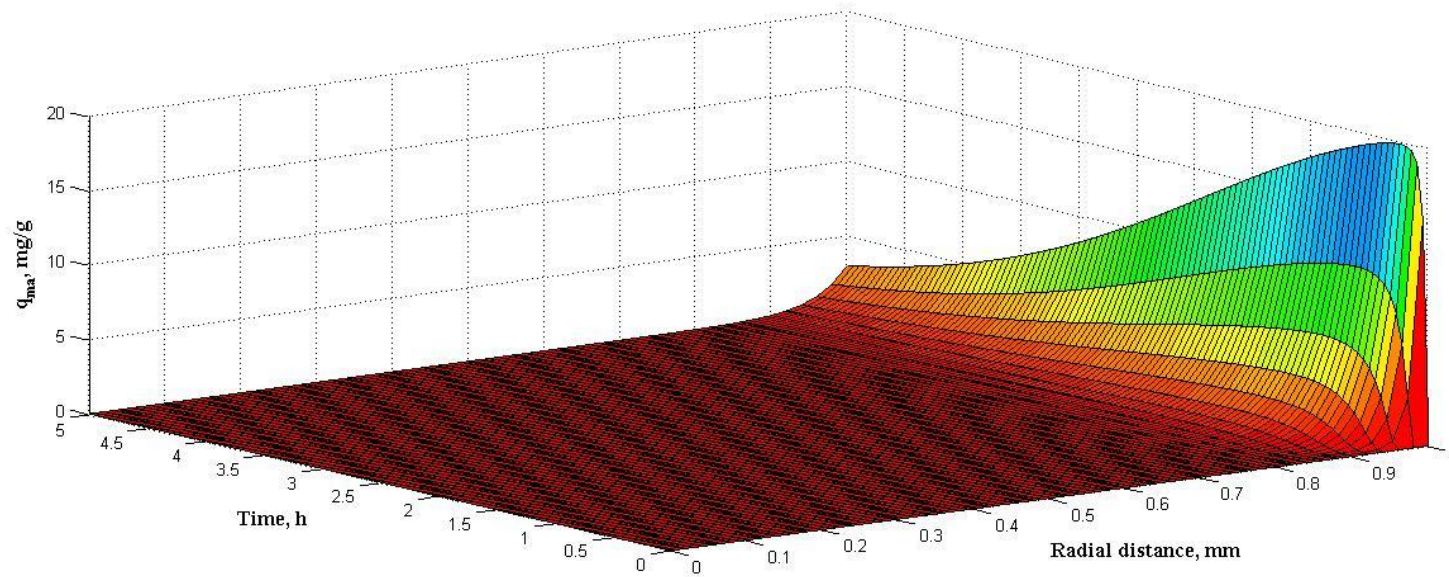


Figure 4.54: Concentration plots of SO reactive adsorption in macro-pores

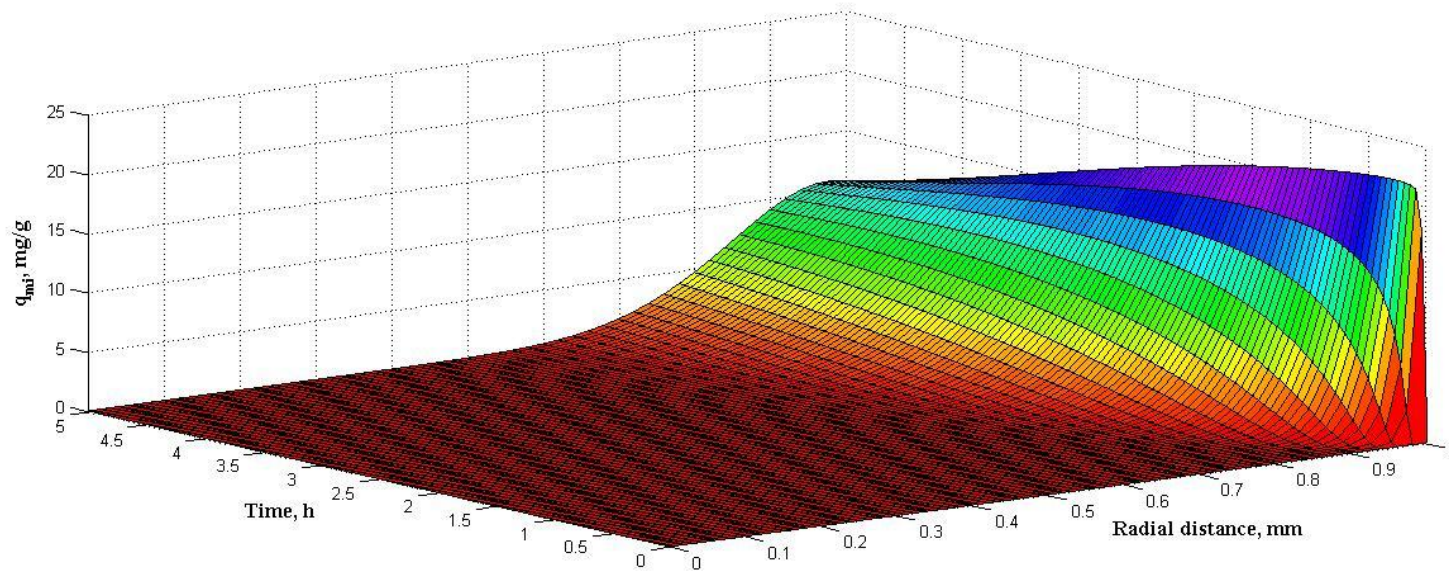


Figure 4.55: Concentration plots of SO reactive adsorption in micro-pores.

4.12 Binary adsorption and reactive adsorption modeling

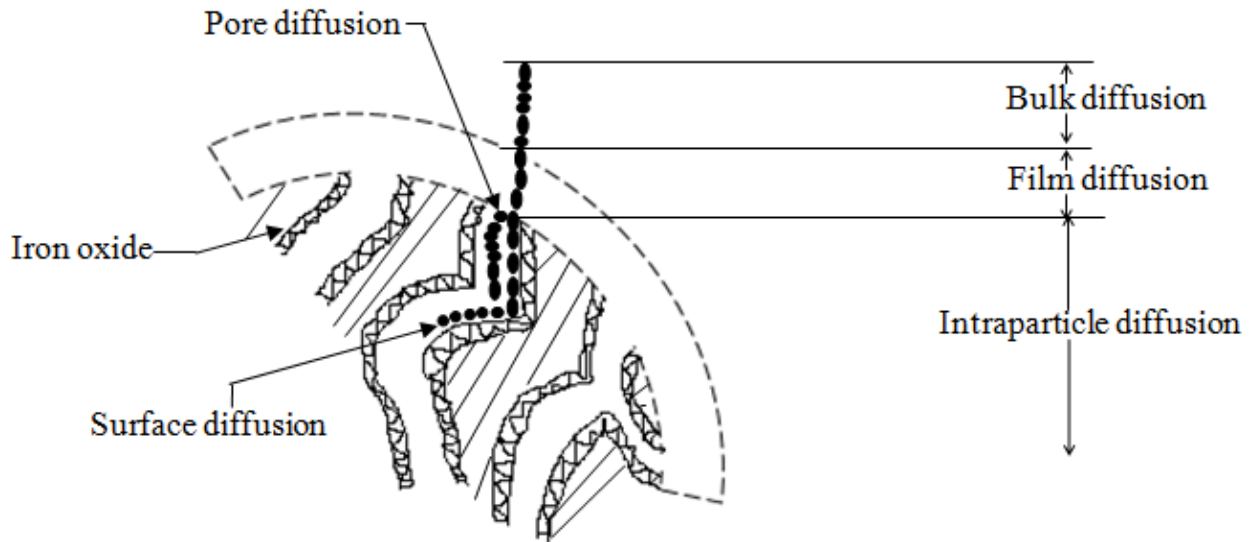


Figure 4.56: Mechanisms of dye adsorption onto Fe-GAC

The mass transfer mechanisms of dyes into the adsorbent include transport of the dyes from the bulk liquid to the liquid film, transport within liquid film, adsorption, and diffusion within the sorbent particle (Yan et al. 2013) as shown in Figure 4.56. This binary dye adsorption model includes diffusion through external film and consequent transport of dye within pore either through pore diffusion or surface diffusion. Two possible ways of mass transport mechanisms for dye diffusion into the sorbent particle are surface diffusion and pore diffusion. Surface diffusion involves migration of sorbate along the adsorbents pore surface and later involves diffusion in liquid-filled pores of the sorbent. Intraparticle diffusion is controlled by surface diffusion and / or pore diffusion. The type of diffusion to occur mainly depends on the molecular size of adsorbate and the mass adsorbed at equilibrium at a given temperature (Ocampo-Pérez et al. 2013). In the case of bi-dispersed adsorbents, surface diffusion may dominate in micro-pores and pore diffusion may be dominated in macro-pores (Tressaud 2006). In order to explain the type of diffusion involved in dye adsorption, Ocampo-Pérez et al. (2013) applied three models namely

(i) pore volume diffusion model (PVDM), (ii) pore volume and surface diffusion model (PVSDM), and (iii) surface diffusion model (SDM). They found that Methylene blue adsorption in activated carbon is controlled by pore volume and surface diffusion model (PVSDM). Surface diffusion dominates when the sorbent mainly consists of micro-pores and sorbate's molecular size is comparatively smaller (e.g. Phenol) (Ocampo-Pérez et al. 2013).

It is assumed that surface concentrations are always in equilibrium with the amount of sorbed solute on the sorbent surface. For the pore surface diffusion model, the mathematical model is developed using equations that are given as follows:

External liquid phase mass balance:

$$V \frac{dC_i}{dt} = -k_{L,i} A (C_i - C_{s,i}) \quad \dots (4.23)$$

Pore mass balance:

$$\frac{\partial q_i}{\partial t} = \frac{1}{r^2} \frac{\partial}{\partial r} \left(D_i r^2 \frac{\partial q_i}{\partial r} \right) - k_{r,i} q_i \quad \dots (4.24)$$

Initial and boundary conditions are:

$$C_i(0) = (C_0)_i \quad \dots (4.25)$$

$$q_i(r,0) = 0 \quad \dots (4.26)$$

$$\frac{\partial q_i}{\partial r}(0,t) = 0 \quad \dots (4.27)$$

Solid – liquid interface relationship can be written as:

$$D_i \frac{\partial q_i}{\partial r}(R,t) = \frac{k_{L,i}}{\rho} (C_i - C_{s,i}) \quad \dots (4.28)$$

Surface concentration of dye is considered to be in equilibrium with sorbed amount on the sorbent surface at any instant. Therefore,

$$C_{s,i} = f(q_{s1}, q_{s2}) \quad \dots (4.29)$$

Solution method

Finite difference technique was used to convert the above sets of differential equations to ordinary differential equations. The obtained ODEs were solved in MATLAB using inbuilt *ode15s* solver.

In order to appraise the fitness of experimental and predicted data, R^2 , a statistical index was used for the binary dye system.

$$RSQ = \frac{\sum (X - \bar{X})(Y - \bar{Y})}{\sqrt{\sum (X - \bar{X})^2} \sqrt{\sum (Y - \bar{Y})^2}} \quad \dots (4.30)$$

Since explicit function for calculating equilibrium values at pellet surface C_{s1} and C_{s2} could not be obtained using Freundlich isotherm for binary systems, Newton-Raphson technique was used for solving these equations:

$$C_s^{(k+1)} = C_s^{(k)} - \alpha [J^{(k)}]^{-1} F^{(k)} \quad \dots (4.31)$$

where F is the set of following equations:

$$F = \begin{bmatrix} f_1(C_{s1}, C_{s2}) - q_1 \\ f_2(C_{s1}, C_{s2}) - q_2 \end{bmatrix} \quad \dots (4.32)$$

Here, f_1 and f_2 are isotherm equations:

$$q_i = f_i(C_{s1}, C_{s2}) \quad \dots (4.33)$$

given by Eq (3.15).

J is the Jacobian matrix:

$$J = \begin{bmatrix} \frac{\partial f_1}{\partial C_{s1}} & \frac{\partial f_1}{\partial C_{s2}} \\ \frac{\partial f_2}{\partial C_{s1}} & \frac{\partial f_2}{\partial C_{s2}} \end{bmatrix} \quad \dots (4.34)$$

k is the iteration numbers and α is the damping factor in step size to avoid large step size. It was found that a value of 0.1 for α was appropriate.

A MATLAB program was used to solve the above equations. The program used the system variables, viz. mass, Fe-GAC particle size and its density, the initial MB and SO concentrations, volume of the solution, Freundlich equilibrium constants and kinetic data, including time and space intervals. Additionally, the system parameters, $k_{L,1}$, $k_{L,2}$, D_1 , and D_2 were supplied. These parameters were evaluated by the best fit method using program and the values were taken which can best describe the experimentally obtained concentration v/s time data. The program computes the theoretical kinetic data (i.e. liquid – phase concentration with time), the surface concentration q , the dimensionless distance r across the particles during adsorption. Table 4.14 gives the best-fit values of film mass transfer coefficients, diffusivities, and surface reaction rate constants.

Table 4.14: Parameters of pore surface diffusion model of binary dye mixture.

Dye	Parameters	Adsorption	Reactive adsorption
MB	Film mass transfer coefficient, $k_{L,1}$	5.9×10^{-5} m/s	8.85×10^{-5} m/s
	Diffusivity, D_1	2.2×10^{-11} m ² /s	2.2×10^{-11} m ² /s
	Surface reaction rate constant, $k_{r,1}$	-	6.1×10^{-4} 1/s
SO	Film mass transfer coefficient, $k_{L,2}$	3.0×10^{-5} m/s	6.0×10^{-5} m/s
	Diffusivity, D_2	1.9×10^{-11} m ² /s	1.9×10^{-11} m ² /s
	Surface reaction rate constant, $k_{r,2}$	-	4.1×10^{-4} 1/s

It can be seen from Figure 4.57 and Figure 4.58 that predicted MB and SO concentrations using model complies with the experimental values for binary dye adsorption and reactive adsorption with regression coefficients more than 0.98 and 0.99 for MB and SO, respectively. In addition, MB and SO concentration were reduced to 80.6% and 64.9%, respectively from the bulk solution

using adsorption of binary dyes. Maximum simultaneous removal was found to be 96.2% and 90.2% for MB and SO, respectively after 7 h of reactive adsorption using 0.5 g/L Fe-GAC and 2.0 mM H₂O₂ doses.

Table 4.14 shows that film mass transfer coefficients, $k_{L,1}$ and $k_{L,2}$ for reactive adsorption were found to be 1.5 and 2 times, respectively when compared with adsorption film mass transfer coefficient data. This may be due to the fact that during reactive adsorption, dyes come in to contact with hydroxyl radicals and do not get enough chance to cross the total path of external fluid film. Surface reaction rate constants $k_{r,1}$ and $k_{r,2}$ are 5 times of their corresponding k_{app} values, due to the fact that k_{app} values include the diffusional resistance along with reaction, which decreases the effective value of rate constant to be considered for surface reaction coefficient.

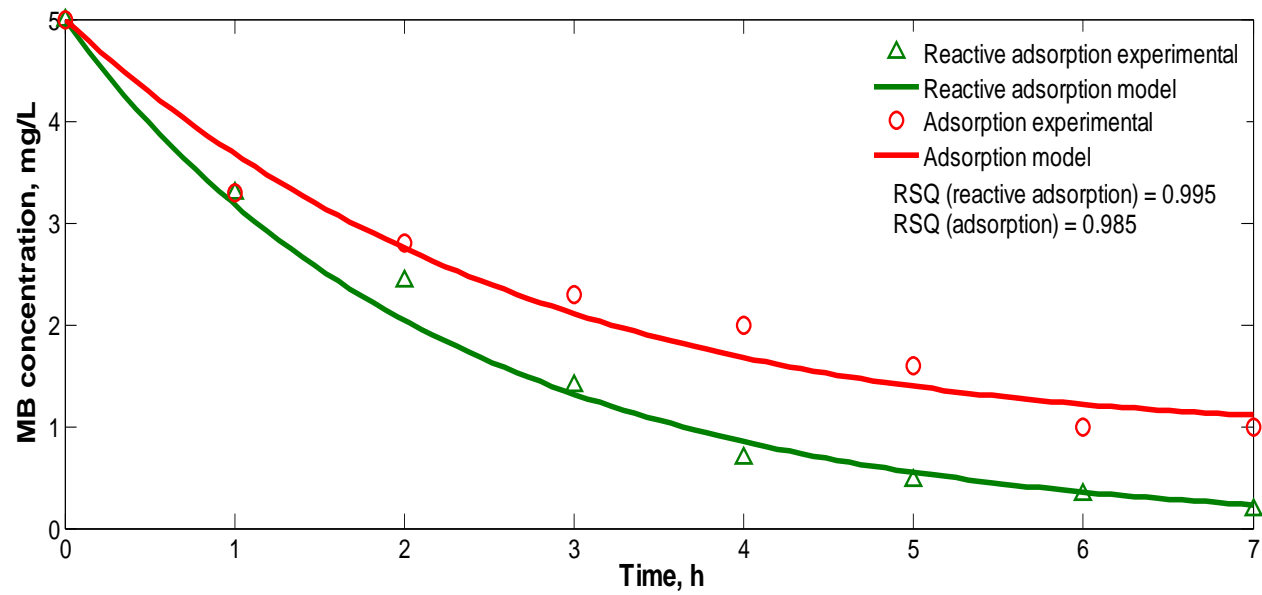


Figure 4.57: MB concentration change in bulk during adsorption and reactive adsorption of binary dyes.

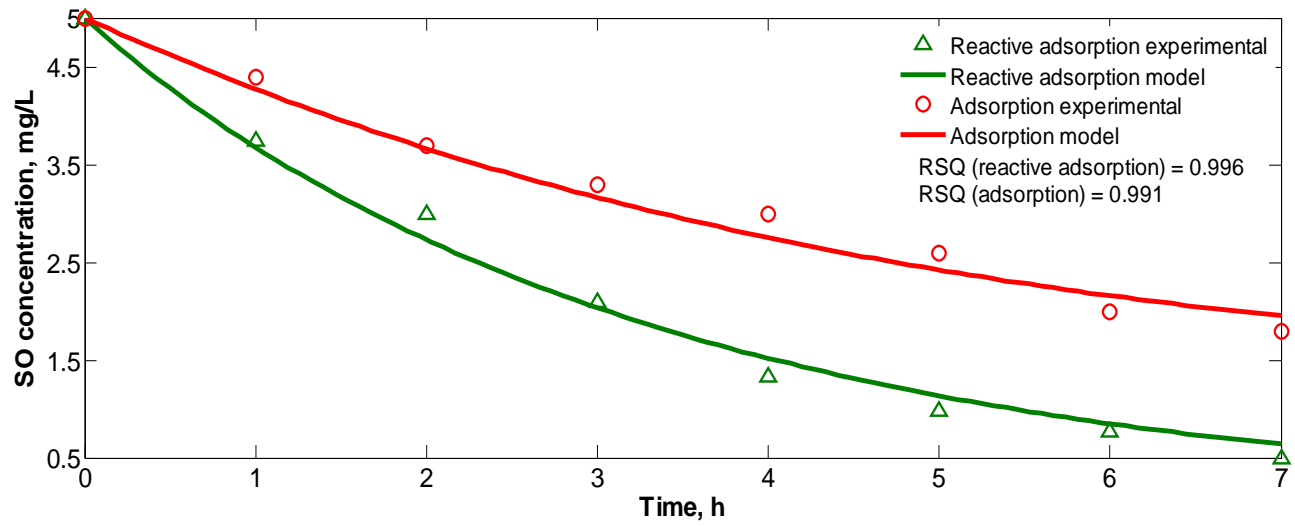


Figure 4.58: SO concentration change in bulk during adsorption and reactive adsorption of binary dyes.

It can be seen from Figure 4.59 that MB concentration during binary dye adsorption at the surface of adsorbent was almost 8.5 mg/g. As MB travels towards center of the particle from the surface, adsorption capacity for MB was 8.0 mg/g. It means that the molecular size of MB is lower than the particle diameter, so MB molecule could easily travel towards the particle center. Furthermore, it is important to observe that initially up to 3 h the concentration front of MB travels toward the particle center at a very fast rate and almost 85% of the total adsorption capacity of the particle was covered during this period. A high value of pore diffusion coefficient may be responsible for this aspect of adsorption.

Likewise, concentration plots of SO in particle during binary dye sorption is given in Figure 4.60. At the particle surface, SO concentration is 7 mg/g which reduced to almost 5.8 mg/g as dye travels from surface to center. This shows that SO molecule is comparatively difficult to diffuse toward the center of particle due to the larger size of the molecule. SO was diffused at a slow rate than MB in to the adsorbent particle, may be because of the lower diffusion coefficient value.

Concentration profile of MB in adsorbent particle during binary dye reactive adsorption is given in Figure 4.61. It can be seen from the figure that the maximum MB adsorption capacity was only less than 3.5 mg/g at the surface of the particle in contrast to plain adsorption. This maximum MB adsorption at particle surface decreased sharply to 0.2 mg/g as MB travels from surface to center of the particle. This may be due to the fact that reaction occurs in the presence of reactive species ($\text{Fe}/\text{H}_2\text{O}_2$) at particle surface which inhibit the dye to diffuse further. MB diffusion rate is very fast during initial 1 h of reactive adsorption, and then it falls abruptly as maximum amount of MB degrades at the adsorbent surface itself.

Figure 4.62 shows the concentration profile of SO with respect to reactive adsorption duration and particle radius. It can be seen from the figure that the maximum SO adsorption capacity was only 3.1 mg/g at the surface of the particle which almost 56% lesser than maximum SO adsorption capacity in plain adsorption. Only 0.25 mg/g maximum adsorption capacity of SO was found at the center of particle. Likewise MB, hindrance was observed during dye diffusion towards center of particle due to the reaction in the presence of reactive species ($\text{Fe}/\text{H}_2\text{O}_2$). Also,

SO degradation rate is very fast during initial 1 h of process as maximum amount of SO degraded at the adsorbent surface itself and then it falls abruptly.

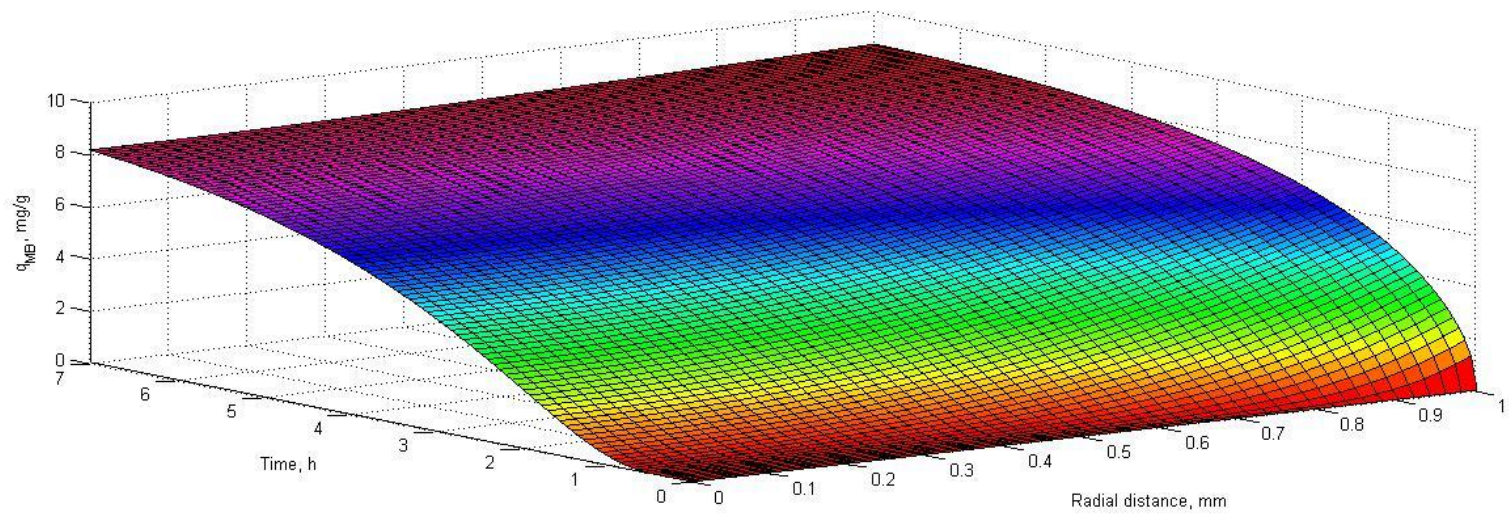


Figure 4.59: Concentration plots of MB in particle during binary dye adsorption.

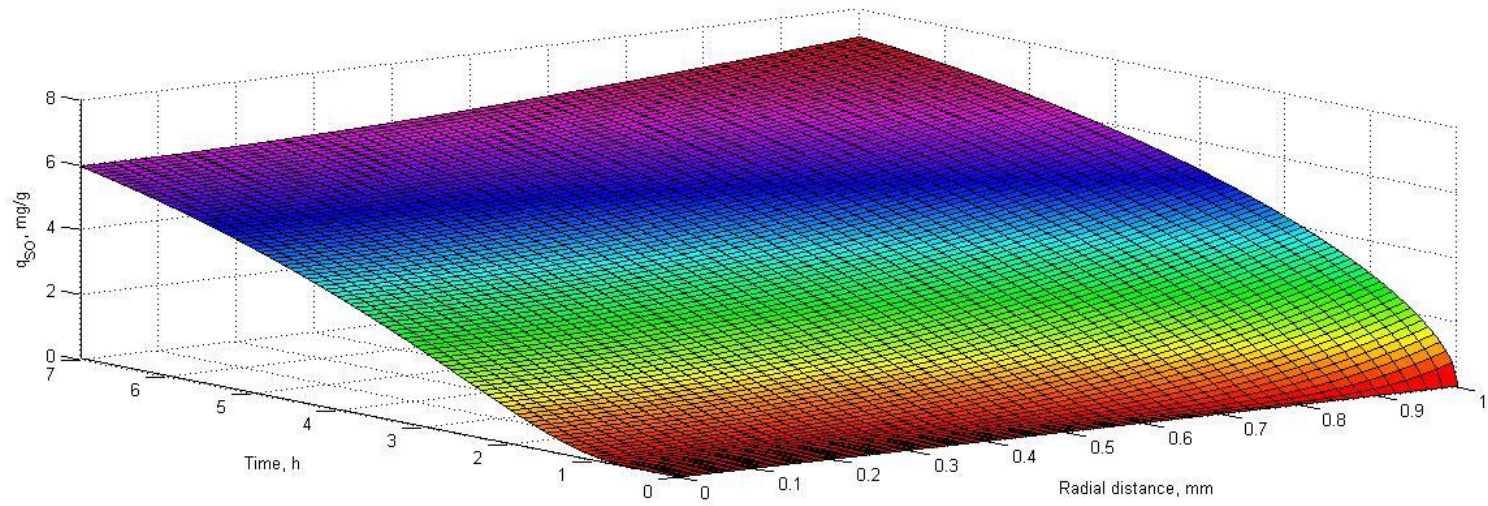


Figure 4.60: Concentration plots of SO in particle during binary dye adsorption.

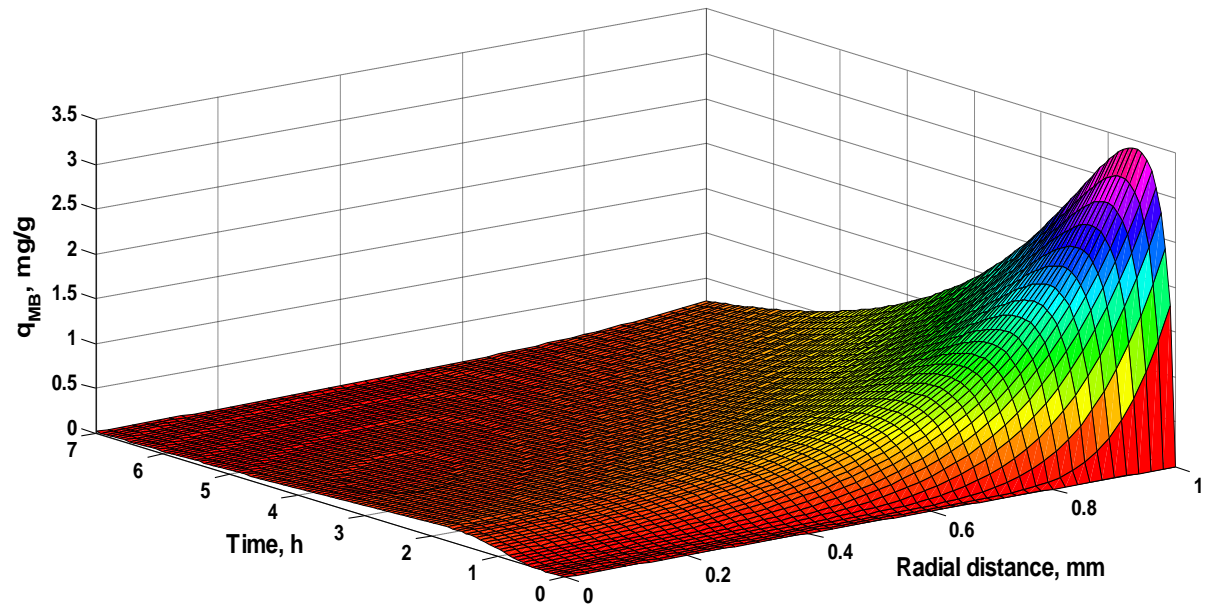


Figure 4.61: Concentration plots of MB in pores during reactive adsorption.

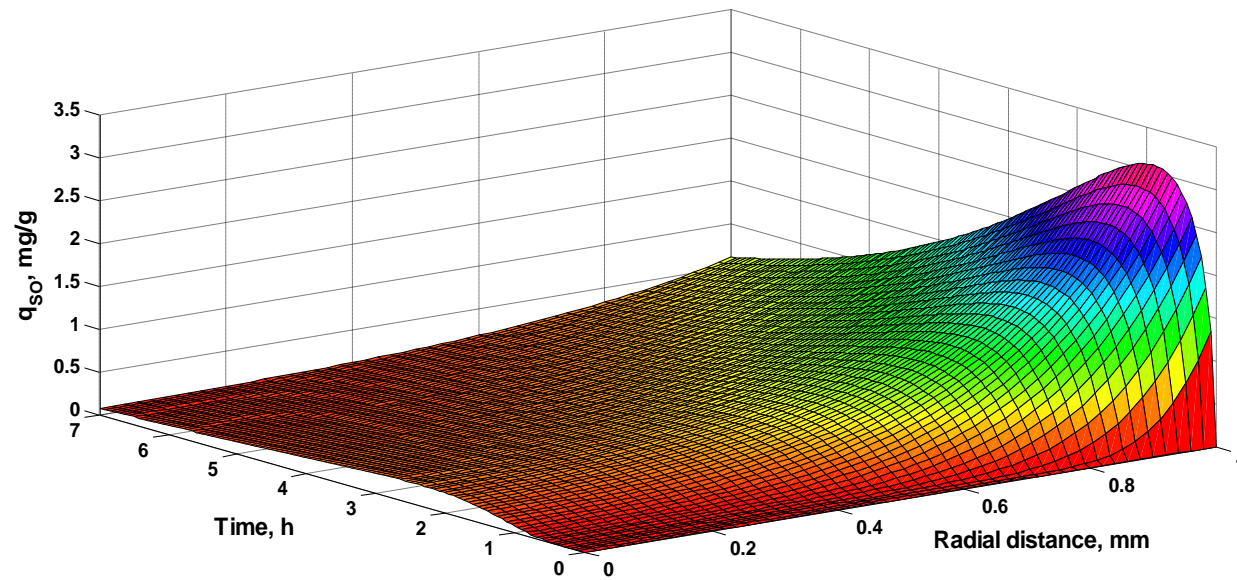


Figure 4.62: Concentration plots of SO in pores during reactive adsorption.

Economic analysis

Economic analysis provides a systematic approach to analyze and compare various alternatives available to achieve a particular objective. In order to carry out economic analysis, various experimental parameters used in reactive adsorption and adsorption for the removal of dye(s) present in single solute system and binary mixture are given in Table 4.15.

Table 4.15: Experimental particulars and Cost estimation of reactive adsorption and adsorption (Rs./mg of dye removal) for MB and SO dye removal

Particulars	MB		SO		MB + SO	
	Reactive adsorption	Adsorption	Reactive adsorption	Adsorption	Reactive adsorption	Adsorption
Initial dye concentration (mg/L)	10	10	10	10	5 MB 5 SO	5 MB 5 SO
Optimized adsorbent dose (g/L)	0.2	0.2	1.0	1.0	0.5	0.5
Contact time (h)	3	3	5	5	7	7
Optimized concentration of H ₂ O ₂ (mM)	10	-	50	-	20	-
% Removal obtained	94%	25%	96%	58%	96% MB 90% SO	49.45% MB 36.95% SO
Cost of adsorbent (Rs./mg of dye removal)	0.013	0.048	0.063	0.104	0.067	0.163
H ₂ O ₂ (Rs./mg of dye removal)	0.068	-	0.335	-	0.286	-
Cost of energy consumption (Rs./L of aqueous dye solution)	$0.21 \times 3 = 0.63$	$0.21 \times 3 = 0.63$	$0.21 \times 5 = 1.05$	$0.21 \times 5 = 1.05$	$0.21 \times 7 = 1.47$	$0.21 \times 7 = 1.47$
Total Cost (Rs./mg of dye removal)	0.711	0.678	1.448	0.154	1.823	1.633

A preliminary economic analysis was carried out for reactive adsorption and adsorption based on chemical requirements and consumption of electrical energy. Above Table 4.15 summarizes the cost involved in the reactive adsorption and adsorption for dye removal in the comparative manner.

It was found from Table 4.15 that the cost involved in Fe-GAC in the removal of MB, SO, and binary mixture of MB and SO was 73%, 39%, and 58% higher for adsorption than reactive adsorption, respectively. It can be concluded that cost associated with sorbent is always lesser in case of reactive adsorption in comparison to adsorption. Cost of electrical energy associated to stirring will be definitely higher for adsorption for the same amount of sorbent used as more time is required to reach equilibrium. However, the total cost is higher for reactive adsorption than adsorption in each case due to the cost of the hydrogen peroxide used. Reactive adsorption comprises simultaneous reaction and separation of solute during adsorption in a single unit operation. Unlike adsorption, reactive adsorption does not require cumbersome disposal of adsorbed species, which may be toxic also. Reactive degradation may completely eradicate the color via degradation of dye molecules and may render the wastewater much less harmful (Nogueira et al. 2009). Therefore, reactive adsorption is a potentially better method to remove organic compounds from waste water. Economic analysis for adsorption was found in-line with adsorption reported earlier (Bhatt 2014; Maheshwari 2014).

5 Conclusions

Granular activated carbon doped with iron (Fe-GAC) were effective for the removal of MB and SO in single and binary dye system in aqueous solution using reactive adsorption (Fe-GAC/H₂O₂) and adsorption (Fe-GAC). The synthesized reactive adsorbent (Fe-GAC) performed effectively with H₂O₂ for the degradation of MB in aqueous solution. Complete removal of MB was attained after 3 h of oxidative reaction. Kinetic studies showed that MB removal rate constant was almost four times for reactive adsorption than adsorption. It was found that enthalpy change was almost one-third for MB removal using reactive adsorption than adsorption. ESI-MS technique using (Fe-GAC/H₂O₂) revealed that reactive degradation of MB molecule was initiated by demethylation which was facilitated by hydroxyl radicals, followed by hydroxylation. Hence, reactive adsorption for dye removal is an efficient method that completely removes the dye by degrading its molecule while consuming less energy. Desorption studies of spent Fe-GAC further confirmed that MB molecule was degraded using reactive adsorption. A scheme for removal of MB using reactive adsorption was proposed.

Maximum optimized removal was found to be 96.1% (initial SO concentration: 10 mg/L) after 5 h of reactive adsorption using 1.0 g/L Fe-GAC and 5.0 mM H₂O₂ doses. Pseudo-first-order kinetics explained well the experimental data for reactive adsorption. Langmuir isotherm well presented the SO adsorption onto Fe-GAC. Parallel-pore-reactive-adsorption model was applied and it was validated using reactive adsorption and adsorption experimental data for SO. The surface reaction coefficient was 5 times of apparent rate constant. The external liquid film mass transfer coefficient, macropore and micropore diffusivities were estimated for SO reactive adsorption. Pore diffusion was rate controlling in adsorption and surface reaction was controlling factor in reactive adsorption. Reactive degradation of SO molecule followed hydroxylation and ring cleavage processes and an oxidative degradation pathway was proposed.

Batch experiments were conducted to study the kinetics and thermodynamics of simultaneous reactive adsorption of MB and SO using Fe-GAC / H₂O₂. Maximum simultaneous removal was found to be 96.2% and 90.2% for MB and SO respectively after 7 h of reactive adsorption using

optimized doses of Fe-GAC (0.5 g/L) and H₂O₂ (2.0 mM). The oxidative degradation of MB and SO followed pseudo-first order kinetics. Accelerative effect was found on kinetics of temperature increase that facilitates the process of degradation. During simultaneous reactive adsorption, value of apparent rate constant for MB was found higher than that of SO. This suggests that SO showed synergistic effect for MB removal. The effect of temperature variation from 15 to 35 °C showed that the apparent rate constants followed the Arrhenius relation. The activation energies for MB degradation was found comparatively lower (28.6 kJ/mol) than SO (32.5 kJ/mol). ESI-MS analyses of simultaneous oxidative degradation of MB and SO revealed that the dissociation of SO molecule is difficult as compared to that of MB molecule. MB and SO degradation pathways showed that dyes were degraded via demethylation and hydroxylation processes.

Simultaneous MB and SO adsorptive removal was carried out. Statistical technique revealed the effect of the variables such as contact time (min), sorbent dose (g/L), MB concentration (mg/L) and SO concentration (mg/L), pH on the removal of MB and SO as responses and optimized values were obtained to be 120 min, 1.2 g/L, 2 mg/L, 4 mg/L and 8.5, respectively. Intraparticle diffusion model fits suitable to the experimental data among pseudo-first-order model, pseudo-second-order model and intraparticle diffusion models. Extended Freundlich model was found suitable for simultaneous adsorption of MB and SO. A film solid pore diffusion model was developed and used to predict the surface film mass transfer coefficient (k_L) and diffusion coefficient (D) for binary dye system containing MB and SO. The k_L values obtained were 5.9×10^{-5} m/s and 3.0×10^{-5} m/s and D were found to be 2.2×10^{-11} m²/s and 1.9×10^{-11} m²/s for MB and SO, respectively. Film mass transfer coefficients, $k_{L,1}$ and $k_{L,2}$ for reactive adsorption were found to be 1.5 and 2 times, respectively when compared with adsorption film mass transfer coefficient data. $k_{r,1}$ and $k_{r,2}$ are 5 times of their corresponding k_{app} values for reactive adsorption.

Overall, the iron oxide loaded on GAC / H₂O₂ may serve as an effective and promising system for efficient removal and mineralization of organic compounds from waste water.

Future recommendations

1. Adsorbent modification needs to be explored in a better way in order to use it effectively in a particular application. There is a need to develop newer adsorbents with desired characteristics for potential applications. Moreover, novel applications of already developed adsorbents are to be found.
2. Degradation of dyes using reactive adsorption / catalytic wet oxidation has opened a new chapter by studying the degradation products. This presents a plethora of opportunities for research towards producing products through a newer route. The advantage of such a research is that it may provide an opportunity to utilize harmful components of wastewater having undesirable effects on environment for commercial purposes.
3. Newer pathways for the degradation of dyes are to be explored and theoretical interpretation of degradation pathway is to be further explored.
4. Since mixture of dyes may yield several degradation products, it may be interesting to study degradation of mixture of dyes via reactive adsorption. Some of these degradation products may have useful applications; these products need to be identified.
5. As a future research, it would be imperative to carry out detailed studies on separation schemes, utilization and production pathways for useful chemicals using degraded products of reactive adsorption.

References

- Abdi, J., Bastani, D., Abdi, J., Mahmoodi, N.M., Shokrollahi, A., Mohammadi, A.H.: Assessment of competitive dye removal using a reliable method. *J. Environ. Chem. Eng.* 2, 1672–1683 (2014).
- Abdullah, F.H., Rauf, M.A., Ashraf, S.S.: Photolytic oxidation of Safranin-O with H₂O₂. *Dye. Pigment.* 72, 349–352 (2007).
- Abecassis-Wolfovich, M., Landau, M. V., Brenner, A., Herskowitz, M.: Catalytic Wet Oxidation of Phenol with Mn–Ce-Based Oxide Catalysts: Impact of Reactive Adsorption on TOC Removal. *Ind. Eng. Chem. Res.* 43, 5089–5097 (2004).
- Adamson, A.W., Gast, A.P.: *Physical Chemistry of Surfaces*. Wiley Interscience, New York (1997).
- Aguayo-Villarreal, I.A., Hernández-Montoya, V., Bonilla-Petriciolet, A., Tovar-Gómez, R., Ramírez-López, E.M., Montes-Morán, M.A.: Role of acid blue 25 dye as active site for the adsorption of Cd²⁺ and Zn²⁺ using activated carbons. *Dye. Pigment.* 96, 459–466 (2013).
- Aksu, Z.: Application of biosorption for the removal of organic pollutants: a review. *Process Biochem.* 40, 997–1026 (2005).
- Al, G., Ozdemir, U., Aksoy, O.: Cytotoxic effects of Reactive Blue 33 on *Allium cepa* determined using Taguchi's L-8 orthogonal array. *Ecotoxicol. Environ. Saf.* 98, 36–40 (2013).
- Al-Degs, Y., Khraisheh, M. a. M., Allen, S.J., Ahmad, M.N., Walker, G.M.: Competitive adsorption of reactive dyes from solution: Equilibrium isotherm studies in single and multisolute systems. *Chem. Eng. J.* 128, 163–167 (2007).
- Al-Degs, Y., Khraisheh, M.A.M., Allen, S.J., Ahmad, M.N.: Effect of carbon surface chemistry on the removal of reactive dyes from textile effluent. *Water Res.* 34, 927–935 (2000).
- Al-Degs, Y.S., El-Sheikh, A.H., Al-Ghouti, M.A., Hemmateenejad, B., Walker, G.M.: Solid-phase extraction and simultaneous determination of trace amounts of sulphonated and azo sulphonated dyes using microemulsion-modified-zeolite and multivariate calibration. *Talanta.*

75, 904–915 (2008).

Al-Degs, Y.S., Sweileh, J.A.: Simultaneous determination of five commercial cationic dyes in stream waters using diatomite solid-phase extractant and multivariate calibration. *Arab. J. Chem.* 5, 219–224 (2012).

Al-Duri, B., McKay, G.: Prediction of binary systems for kinetics of batch adsorption using basic dyes onto activated carbon. *Chem. Eng. Sci.* 46, 193–204 (1991).

Al-Duri, B., McKay, G.: Pore diffusion: Dependence of the effective diffusivity on the initial sorbate concentration in single and multicomponent batch adsorption systems. *J. Chem. Technol. Biotechnol.* 55, 245–250 (1992).

Allen, S.J., Gan, Q., Matthews, R., Johnson, P. a.: Comparison of optimised isotherm models for basic dye adsorption by kudzu. *Bioresour. Technol.* 88, 143–152 (2003).

Allen, S.J., McKay, G., Khader, K.Y.H.: Multi-component sorption isotherms of basic dyes onto peat. *Environ. Pollut.* 52, 39–53 (1988).

Allen, S.J., McKay, G., Porter, J.F.: Adsorption isotherm models for basic dye adsorption by peat in single and binary component systems. *J. Colloid Interface Sci.* 280, 322–33 (2004).

Almasian, A., Mahmoodi, N.M., Olya, M.E.: Tectomer grafted nanofiber: Synthesis, characterization and dye removal ability from multicomponent system. *J. Ind. Eng. Chem.* 32, 85–98 (2015).

Almeida, C.A.P., Debacher, N.A., Downs, A.J., Cottet, L., Mello, C.A.D.: Removal of methylene blue from colored effluents by adsorption on montmorillonite clay. *J. Colloid Interface Sci.* 332, 46–53 (2009).

An, L., Deng, J., Zhou, L., Li, H., Chen, F., Wang, H., Liu, Y.: Simultaneous spectrophotometric determination of trace amount of malachite green and crystal violet in water after cloud point extraction using partial least squares regression. *J. Hazard. Mater.* 175, 883–888 (2010).

An, S., Liu, X., Yang, L., Zhang, L.: Enhancement removal of crystal violet dye using magnetic

calcium ferrite nanoparticle: Study in single- and binary-solute systems. *Chem. Eng. Res. Des.* 94, 726–735 (2015).

Andronic, L., Duta, A.: Photodegradation processes in two-dyes systems – Simultaneous analysis by first-order spectra derivative method. *Chem. Eng. J.* 198-199, 468–475 (2012).

Ania, C., Pelayo, J., TJ Bandosz: Reactive adsorption of penicillin on activated carbons. *Adsorption.* 17, 421–429 (2011).

Anirudhan, T.S., Ramachandran, M.: Adsorptive removal of basic dyes from aqueous solutions by surfactant modified bentonite clay (organoclay): Kinetic and competitive adsorption isotherm. *Process Saf. Environ. Prot.* 95, 215–225 (2015)(a).

Anirudhan, T.S., Ramachandran, M.: Adsorptive removal of basic dyes from aqueous solutions by surfactant modified bentonite clay (organoclay): Kinetic and competitive adsorption isotherm. *Process Saf. Environ. Prot.* 95, 215–225 (2015)(b).

Ansari, F., Ghaedi, M., Taghdiri, M., Asfaram, A.: Application of ZnO nanorods loaded on activated carbon for ultrasonic assisted dyes removal: Experimental design and derivative spectrophotometry method. *Ultrason. Sonochem.* 33, 197–209 (2016).

Appusamy, A., John, I., Ponnusamy, K., Ramalingam, A.: Removal of crystal violet dye from aqueous solution using triton X-114 surfactant via cloud point extraction. *Eng. Sci. Technol. an Int. J.* 17, 137–144 (2014).

Atar, N., Olgun, A., Wang, S., Liu, S.: Adsorption of anionic dyes on boron industry waste in single and binary solutions using batch and fixed-bed systems. *J. Chem. Eng. Data.* 56, 508–516 (2011).

Azad, F.N., Ghaedi, M., Dashtian, K., Hajati, S., Goudarzi, A., Jamshidi, M.: Enhanced simultaneous removal of malachite green and safranin O by ZnO Nanorod-loaded activated carbon; modeling, optimization and adsorption isotherm. *New J. Chem.* 39, 7998–8005 (2015).

Banat, I.M., Nigam, P., Singh, D., Marchant, R.: Microbial decolorization of textile dye - containing effluents: A review. 58, 217–227 (1997).

Behnajady, M.A., Modirshahla, N., Shokri, M., Vahid, B.: Effect of operational parameters on degradation of Malachite Green by ultrasonic irradiation. *Ultrason. Sonochem.* 15, 1009–1014 (2008).

Bessegato, G.G., Cardoso, J.C., da Silva, B.F., Zanoni, M.V.B.: Combination of photoelectrocatalysis and ozonation: A novel and powerful approach applied in Acid Yellow 1 mineralization. *Appl. Catal. B Environ.* 180, 161–168 (2016).

Bhatnagar, A., Hogland, W., Marques, M., Sillanpää, M.: An overview of the modification methods of activated carbon for its water treatment applications. *Chem. Eng. J.* 219, 499–511 (2013).

Bhatt, P.: Studies on removal of reactive blue 19 and direct red 81 dyes from wastewater using adsorption and electro coagulation, Ph.D. thesis, Chemical Engineering Department, Malaviya National Institute of Technology, Jaipur, (2014).

Bhattacharya, K.G., Sharma, A.: Kinetics and thermodynamics of Methylene Blue adsorption on Neem (*Azadirachta indica*) leaf powder. *Dye. Pigment.* 65, 51–59 (2005).

Bingjia, Y., Li, Y., Qiong, H., Shigendo, A.: Cloud Point Extraction of Polycyclic Aromatic Hydrocarbons in Aqueous Solution with Silicone Surfactants. *Chinese J. Chem. Eng.* 15, 468–473 (2007).

Bokare, A.D., Choi, W.: Review of iron-free Fenton-like systems for activating H₂O₂ in advanced oxidation processes. *J. Hazard. Mater.* 275, 121–135 (2014).

Brereton, R.G.: *Chemometrics: data analysis for the laboratory and chemical plant.* John Wiley & Sons (2003).

Burg, A., Shusterman, I., Kornweitz, H., Meyerstein, D.: Three H₂O₂ molecules are involved in the “Fenton-like” reaction between Co(H₂O)₆²⁺ and H₂O₂. *Dalt. Trans.* 43, 9111–9115 (2014).

Burges, C.J.: A tutorial on support vector machines for pattern recognition. *Data Min. Knowl. Discov.* 2, 121–167 (1998).

Butler, J.A. V., Ockrent, C.: Studies in electrocapillarity. III. *J. Phys. Chem.* 34, 2841–2859

(1930).

Castellini, E., Andreoli, R., Malavasi, G., Pedone, A.: Deflocculant effects on the surface properties of kaolinite investigated through malachite green adsorption. *Colloids Surfaces A Physicochem. Eng. Asp.* 329, 31–37 (2008).

Cestari, A.R., Vieira, E.F.S., Pinto, A. a., Lopes, E.C.N.: Multistep adsorption of anionic dyes on silica/chitosan hybrid: 1. Comparative kinetic data from liquid- and solid-phase models. *J. Colloid Interface Sci.* 292, 363–372 (2005).

Chakraborty, S., Basu, J.K., De, S., DasGupta, S.: Adsorption of Reactive Dyes from a Textile Effluent Using Sawdust as the Adsorbent. *Ind. Eng. Chem. Res.* 45, 4732–4741 (2006).

Chan, L.S., Cheung, W.H., Allen, S.J., McKay, G.: Error Analysis of Adsorption Isotherm Models for Acid Dyes onto Bamboo Derived Activated Carbon. *Chinese J. Chem. Eng.* 20, 535–542 (2012)(a).

Chan, L.S., Cheung, W.H., McKay, G.: Adsorption of acid dyes by bamboo derived activated carbon. *Desalination.* 218, 304–312 (2008).

Chan, O.S., Cheung, W.H., McKay, G.: Single and multicomponent acid dye adsorption equilibrium studies on tyre demineralised activated carbon. *Chem. Eng. J.* 191, 162–170 (2012)(b).

Chang, J., Ma, J., Ma, Q., Zhang, D., Qiao, N., Hu, M., Ma, H.: Adsorption of methylene blue onto Fe₃O₄/activated montmorillonite nanocomposite. *Appl. Clay Sci.* 119, 132–140 (2015).

Chang, Q., Lin, W., Ying, W.: Preparation of iron-impregnated granular activated carbon for arsenic removal from drinking water. *J. Hazard. Mater.* 184, 515–22 (2010).

Chen, B., Hui, C.W., McKay, G.: Film-pore diffusion modeling for the sorption of metal ions from aqueous effluents onto peat. *Water Res.* 35, 3345–3356 (2001).

Chen, C.C., Chen, W.C., Chiou, M.R., Chen, S.W., Chen, Y.Y., Fan, H.J.: Degradation of crystal violet by an FeGAC/H₂O₂ process. *J. Hazard. Mater.* 196, 420–425 (2011).

Chingombe, P., Saha, B., Wakeman, R.J.: Surface modification and characterisation of a coal-based activated carbon. *Carbon N. Y.* 43, 3132–3143 (2005).

Chiou, M.-S., Chuang, G.-S.: Competitive adsorption of dye metanil yellow and RB15 in acid solutions on chemically cross-linked chitosan beads. *Chemosphere.* 62, 731–40 (2006).

Choy, K.K.H., McKay, G., Porter, J.F.: Sorption of acid dyes from effluents using activated carbon. *Resour. Conserv. Recycl.* 27, 57–71 (1999).

Choy, K.K.H., Porter, J.F., McKay, G.: Langmuir Isotherm Models Applied to the Multicomponent Sorption of Acid Dyes from Effluent onto Activated Carbon. *J. Chem. Eng. Data.* 45, 575–584 (2000).

Choy, K.K.H., Porter, J.F., McKay, G.: Intraparticle diffusion in single and multicomponent acid dye adsorption from wastewater onto carbon. *Chem. Eng. J.* 103, 133–145 (2004).

Christie, R.M.: *Environmental aspects of textile dyeing.* (2007).

Dávila-Jiménez, M.M., Elizalde-González, M.P., Hernández-Montoya, V.: Performance of mango seed adsorbents in the adsorption of anthraquinone and azo acid dyes in single and binary aqueous solutions. *Bioresour. Technol.* 100, 6199–6206 (2009).

Dil, E.A., Ghaedi, M., Ghaedi, A., Asfaram, A., Jamshidi, M., Purkait, M.K.: Application of artificial neural network and response surface methodology for the removal of crystal violet by zinc oxide nanorods loaded on activate carbon: Kinetics and equilibrium study. *J. Taiwan Inst. Chem. Eng.* 59, 210–220 (2016).

Douissa, N. Ben, Dridi-Dhaouadi, S., Mhenni, M.F.: Study of antagonistic effect in the simultaneous removal of two textile dyes onto cellulose extracted from *Posidonia oceanica* using derivative spectrophotometric method. *J. Water Process Eng.* 2, 1–9 (2014).

Duta, A., Visa, M.: Simultaneous removal of two industrial dyes by adsorption and photocatalysis on a fly-ash-TiO₂ composite. *J. Photochem. Photobiol. A Chem.* 306, 21–30 (2015).

El-Barghouthi, M.I., El-Sheikh, A.H., Al-Degs, Y.S., Walker, G.M.: Adsorption Behavior of

Anionic Reactive Dyes on H-type Activated Carbon: Competitive Adsorption and Desorption Studies. *Sep. Sci. Technol.* 42, 2195–2220 (2007).

El-Kemary, M., Abdel-Moneam, Y., Madkour, M., El-Mehasseb, I.: Enhanced photocatalytic degradation of Safranin-O by heterogeneous nanoparticles for environmental applications. *J. Lumin.* 131, 570–576 (2011).

El-Kemary, M., El-Shamy, H.: Fluorescence modulation and photodegradation characteristics of safranin O dye in the presence of ZnS nanoparticles. *J. Photochem. Photobiol. A Chem.* 205, 151–155 (2009).

Fan, Y., Liu, H.-J., Zhang, Y., Chen, Y.: Adsorption of anionic MO or cationic MB from MO/MB mixture using polyacrylonitrile fiber hydrothermally treated with hyperbranched polyethylenimine. *J. Hazard. Mater.* 283, 321–328 (2015).

Faouzi Elahmadi, M., Bensalah, N., Gadri, A.: Treatment of aqueous wastes contaminated with Congo Red dye by electrochemical oxidation and ozonation processes. *J. Hazard. Mater.* 168, 1163–1169 (2009).

Fernandez, M.E., Bonelli, P.R., Cukierman, A.L., Lemcoff, N.O.: Modeling the biosorption of basic dyes from binary mixtures. *Adsorption.* 21, 177–183 (2015).

Figueiredo, J., Pereira, M.F., Freitas, M.M., Órfão, J.J.: Modification of the surface chemistry of activated carbons. *Carbon N. Y.* 37, 1379–1389 (1999).

Foo, K.Y., Hameed, B.H.: Insights into the modeling of adsorption isotherm systems. *Chem. Eng. J.* 156, 2–10 (2010).

Fritz, W., Schluender, E.U.: Simultaneous adsorption equilibria of organic solutes in dilute aqueous solutions on activated carbon. *Chem. Eng. Sci.* 29, 1279–1282 (1974).

Fu, Y., Viraraghavan, T.: Fungal decolorization of dye wastewaters: A review. *Bioresour. Technol.* 79, 251–262 (2001).

Gao, J.-F., Wang, J.-H., Yang, C., Wang, S.-Y., Peng, Y.-Z.: Binary biosorption of Acid Red 14 and Reactive Red 15 onto acid treated okara: Simultaneous spectrophotometric determination of

two dyes using partial least squares regression. *Chem. Eng. J.* 171, 967–975 (2011).

Gao, J.F., Zhang, Q., Su, K., Wang, J.H.: Competitive biosorption of Yellow 2G and Reactive Brilliant Red K-2G onto inactive aerobic granules: Simultaneous determination of two dyes by first-order derivative spectrophotometry and isotherm studies. *Bioresour. Technol.* 101, 5793–5801 (2010).

Garg, V.K., Kumar, R., Gupta, R.: Removal of malachite green dye from aqueous solution by adsorption using agro-industry waste: A case study of *Prosopis cineraria*. *Dye. Pigment.* 62, 1–10 (2004).

Ghaedi, M., Hajjati, S., Barazesh, B., Karimi, F., Ghezelbash, G.: *Saccharomyces cerevisiae* for the biosorption of basic dyes from binary component systems and the high order derivative spectrophotometric method for simultaneous analysis of Brilliant green and Methylene blue. *J. Ind. Eng. Chem.* 19, 227–233 (2013).

Ghaedi, M., Hajjati, S., Mahmudi, Z., Tyagi, I., Agarwal, S., Maity, A., Gupta, V.K.: Modeling of competitive ultrasonic assisted removal of the dyes - Methylene blue and Safranin-O using Fe₃O₄ nanoparticles. *Chem. Eng. J.* 268, 28–37 (2015)(a).

Ghaedi, M., Hajjati, S., Mahmudi, Z., Tyagi, I., Agarwal, S., Maity, A., Gupta, V.K.: Modeling of competitive ultrasonic assisted removal of the dyes - Methylene blue and Safranin-O using Fe₃O₄ nanoparticles. *Chem. Eng. J.* 268, 28–37 (2015)(b).

Ghaedi, M., Montazerzohori, M., Biyareh, M.N., Mortazavi, K., Soylak, M.: Chemically bonded multiwalled carbon nanotubes as efficient material for solid phase extraction of some metal ions in food samples. *Int. J. Environ. Anal. Chem.* 93, 528–542 (2012).

Ghaedi, M., Mosallanejad, N.: Study of competitive adsorption of malachite green and sunset yellow dyes on cadmium hydroxide nanowires loaded on activated carbon. *J. Ind. Eng. Chem.* 20, 1085–1096 (2014).

Ghaedi, M., Pakniat, M., Mahmoudi, Z., Hajjati, S., Sahraei, R., Daneshfar, A.: Synthesis of nickel sulfide nanoparticles loaded on activated carbon as a novel adsorbent for the competitive removal of Methylene blue and Safranin-O. *Spectrochim. Acta - Part A Mol. Biomol. Spectrosc.*

123, 402–409 (2014).

Gholami, A., Masoum, S., Mohsenikia, A., Abbasi, S.: Chemometrics-assisted excitation-emission fluorescence analytical data for rapid and selective determination of optical brighteners in the presence of uncalibrated interferences. *Spectrochim. Acta - Part A Mol. Biomol. Spectrosc.* 153, 108–117 (2016).

Ghosh, D., Bhattacharyya, K.G.: Adsorption of methylene blue on kaolinite. *Appl. Clay Sci.* 20, 295–300 (2002).

Gong, H., Chen, Z., Fan, Y., Zhang, M., Wu, W., Wang, W.: Surface modification of activated carbon for siloxane adsorption. *Renew. Energy.* 83, 144–150 (2015).

Gözmen, B., Turabik, M., Hesenov, A.: Photocatalytic degradation of Basic Red 46 and Basic Yellow 28 in single and binary mixture by UV/TiO₂/periodate system. *J. Hazard. Mater.* 164, 1487–1495 (2009).

Groen, J.C., Peffer, L.A.A., Perez-Ramirez, J.: Pore size determination in modified micro- and mesoporous materials. Pitfalls and limitations in gas adsorption data analysis. *Microporous Mesoporous Mater.* 60, 1–17 (2003).

Gu, Z., Fang, J., Deng, B.: Preparation and evaluation of GAC-based iron-containing adsorbents for arsenic removal. *Environ. Sci. Technol.* 39, 3833–3843 (2005).

Gupta, V.K., Sharma, M., Singh, K., Vyas, R.K.: Reactive adsorption of phenol onto Fe-GAC: Parallel pore batch modeling and experimental studies. *J. Taiwan Inst. Chem. Eng.* 0, 1–9 (2016).

Gupta, V.K., Sharma, M., Vyas, R.K.: Hydrothermal modification and characterization of bentonite for reactive adsorption of methylene blue: An ESI-MS study. *J. Environ. Chem. Eng.* 3, 2172–2179 (2015).

Gürses, A., Açıkyıldız, M., Güneş, K., Gürses, M.S.: Dyes and Pigments: Their Structure and Properties. In: *Dyes and Pigments*. pp. 13–29. Springer (2016).

Gutierrez, M., Fuentes, H.R.: Modeling adsorption in multicomponent systems using a

Freundlich-type isotherm. *J. Contam. Hydrol.* 14, 247–260 (1993).

Hadi, P., Xu, M., Ning, C., Sze Ki Lin, C., McKay, G.: A critical review on preparation, characterization and utilization of sludge-derived activated carbons for wastewater treatment. *Chem. Eng. J.* 260, 895–906 (2015).

Hajati, S., Ghaedi, M., Karimi, F., Barazesh, B., Sahraei, R., Daneshfar, A.: Competitive adsorption of Direct Yellow 12 and Reactive Orange 12 on ZnS:Mn nanoparticles loaded on activated carbon as novel adsorbent. *J. Ind. Eng. Chem.* 20, 564–571 (2014).

Hajjaji, M., El Arfaoui, H.: Adsorption of methylene blue and zinc ions on raw and acid-activated bentonite from Morocco. *Appl. Clay Sci.* 46, 418–421 (2009).

Hameed, B.H., Ahmad, a. L., Latiff, K.N. a: Adsorption of basic dye (methylene blue) onto activated carbon prepared from rattan sawdust. *Dye. Pigment.* 75, 143–149 (2007)(a).

Hameed, B.H., Ahmad, A.L., Latiff, K.N.A.: Adsorption of basic dye (methylene blue) onto activated carbon prepared from rattan sawdust. *Dye. Pigment.* 75, 143–149 (2007)(b).

Hao, Y., Yan, L., Yu, H., Yang, K., Yu, S., Shan, R., Du, B.: Comparative study on adsorption of basic and acid dyes by hydroxy-aluminum pillared bentonite. *J. Mol. Liq.* 199, 202–207 (2014).

Hayat, K., Gondal, M.A., Khaled, M.M., Yamani, Z.H., Ahmed, S.: Laser induced photocatalytic degradation of hazardous dye (Safranin-O) using self synthesized nanocrystalline WO₃. *J. Hazard. Mater.* 186, 1226–1233 (2011).

Hemmateenejad, B., Shadabipour, P., Khosousi, T., Shamsipur, M.: Chemometrics investigation of the light-free degradation of methyl green and malachite green by starch-coated CdSe quantum dots. *J. Ind. Eng. Chem.* 27, 384–390 (2014).

Himmelblau, D.M.: Accounts of Experiences in the Application of Artificial Neural Networks in Chemical Engineering. *Ind. Eng. Chem. Res.* 47, 5782–5796 (2008).

Ho, Y.S., McKay, G.: Competitive Sorption of Copper and Nickel Ions from Aqueous Solution Using Peat. *Adsorption.* 5, 409–417 (1999).

Ho, Y.S., McKay, G.: Sorption of dyes and copper ions onto biosorbents. *Process Biochem.* 38, 1047–1061 (2003).

Hong, S., Wen, C., He, J., Gan, F., Ho, Y.-S.: Adsorption thermodynamics of Methylene Blue onto bentonite. *J. Hazard. Mater.* 167, 630–3 (2009).

Hristovski, K.D., Westerhoff, P.K., Möller, T., Sylvester, P.: Effect of synthesis conditions on nano-iron (hydr)oxide impregnated granulated activated carbon. *Chem. Eng. J.* 146, 237–243 (2009).

Hunger, K.: *Industrial Dyes Further of Interest* : (2003).

Inbaraj, B.S., Chien, J.T., Ho, G.H., Yang, J., Hen, B.H.: Equilibrium and kinetic studies on sorption of basic dyes by a natural biopolymer poly(γ -glutamic acid). *Biochem. Eng. J.* 31, 204–215 (2006).

Isa, M.H., Lang, L.S., Asaari, F.A.H., Aziz, H.A., Ramli, N.A., Dhas, J.P.A.: Low cost removal of disperse dyes from aqueous solution using palm ash. *Dye. Pigment.* 74, 446–453 (2007).

Issa, A.A., Al-Degs, Y.S., Al-Ghouti, M.A., Olimat, A.A.M.: Studying competitive sorption behavior of methylene blue and malachite green using multivariate calibration. *Chem. Eng. J.* 240, 554–564 (2014).

IUPAC: *Compendium of Chemical Terminology*, 2nd ed. (the “Gold Book”). Compiled by A. D. McNaught and A. Wilkinson., <http://goldbook.iupac.org>.

Jain, J.S., Snoeyink, V.L.: Adsorption from bisolute systems on active carbon. *J. (Water Pollut. Control Fed.* 45, 2463–2479 (1973).

De Jesus da Silveira Neta, J., Costa Moreira, G., da Silva, C.J., Reis, C., Reis, E.L.: Use of polyurethane foams for the removal of the Direct Red 80 and Reactive Blue 21 dyes in aqueous medium. *Desalination.* 281, 55–60 (2011).

Juang, R., Lin, S., Hsueh, P.: Removal of binary azo dyes from water by UV-irradiated degradation in TiO₂ suspensions. *J. Hazard. Mater.* 182, 820–826 (2010).

Kang, Q., Zhou, W., Li, Q., Gao, B., Fan, J., Shen, D.: Adsorption of anionic dyes on poly(epichlorohydrin dimethylamine) modified bentonite in single and mixed dye solutions. *Appl. Clay Sci.* 45, 280–287 (2009).

Karagoz, S., Tay, T., Ucar, S., Erdem, M.: Activated carbons from waste biomass by sulfuric acid activation and their use on methylene blue adsorption. *Bioresour. Technol.* 99, 6214–6222 (2008).

Karpińska, J.: Derivative spectrophotometry - Recent applications and directions of developments. *Talanta.* 64, 801–822 (2004).

Kasiri, M.B., Aleboyeh, H., Aleboyeh, A.: Degradation of Acid Blue 74 using Fe-ZSM5 zeolite as a heterogeneous photo-Fenton catalyst. *Appl. Catal. B Environ.* 84, 9–15 (2008).

Kaur, S., Rani, S., Mahajan, R.K., Asif, M., Gupta, V.K.: Synthesis and adsorption properties of mesoporous material for the removal of dye safranin: Kinetics, equilibrium, and thermodynamics. *J. Ind. Eng. Chem.* 22, 19–27 (2015).

Khaksar, M., Amini, M., Boghaei, D.M., Chae, K.H., Gautam, S.: Mn-doped ZrO₂ nanoparticles as an efficient catalyst for green oxidative degradation of methylene blue. *Catal. Commun.* 72, 1–5 (2015).

Kim, J.R., Santiano, B., Kim, H., Kan, E.: Heterogeneous Oxidation of Methylene Blue with Surface-Modified Iron-Amended Activated Carbon. *Am. J. Anal. Chem.* 2013, 115–122 (2013).

Kim, K.: Financial time series forecasting using support vector machines. *Neurocomputing.* 55, 307–319 (2003).

Kolthoff, I.M., van der Goot, E.: The adsorption of hydroxybenzenes and other aromatic compounds and their replacing action upon each other at the interface water-charcoal. *Recl. des Trav. Chim. des Pays-Bas.* 48, 265–287 (1929).

Kumar, K.V.: Linear and non-linear regression analysis for the sorption kinetics of methylene blue onto activated carbon. *J. Hazard. Mater.* 137, 1538–1544 (2006).

Kurniawan, A., Sutiono, H., Indraswati, N., Ismadji, S.: Removal of basic dyes in binary system

by adsorption using rarasaponin–bentonite: Revisited of extended Langmuir model. *Chem. Eng. J.* 189-190, 264–274 (2012).

Kyzas, G.Z., Bikiaris, D.N., Lazaridis, N.K.: Selective separation of basic and reactive dyes by molecularly imprinted polymers (MIPs). *Chem. Eng. J.* 149, 263–272 (2009).

Largitte, L., Pasquier, R.: A review of the kinetics adsorption models and their application to the adsorption of lead by an activated carbon. *Chem. Eng. Res. Des.* 109, 495–504 (2016).

Lee, C., Yoon, J.: Temperature dependence of hydroxyl radical formation in the $h\nu/\text{Fe}^{3+}/\text{H}_2\text{O}_2$ and $\text{Fe}^{3+}/\text{H}_2\text{O}_2$ systems. *Chemosphere.* 56, 923–934 (2004).

Liao, P., Malik Ismael, Z., Zhang, W., Yuan, S., Tong, M., Wang, K., Bao, J.: Adsorption of dyes from aqueous solutions by microwave modified bamboo charcoal. *Chem. Eng. J.* 195-196, 339–346 (2012).

Liapis, A.I., Rippin, D.W.T.: The simulation of binary adsorption in continuous countercurrent operation and a comparison with other operating modes. *AIChE J.* 25, 455–460 (1979).

Liapis, A.I., Rippin, D.W.T.: A general model for the simulation of multi-component adsorption from a finite bath. *Chem. Eng. Sci.* 32, 619–627 (1977).

Ling, S.K., Wang, S., Peng, Y.: Oxidative degradation of dyes in water using $\text{Co}^{2+}/\text{H}_2\text{O}_2$ and $\text{Co}^{2+}/\text{peroxymonosulfate}$. *J. Hazard. Mater.* 178, 385–389 (2010).

Liu, J., Gao, Z., Han, H., Wu, D., Xu, F., Wang, H., Jiang, K.: Mesoporous Cu_2O submicrospheres, facile synthesis and the selective adsorption properties. *Chem. Eng. J.* 185-186, 151–159 (2012).

Liu, L., Gao, Z.Y., Su, X.P., Chen, X., Jiang, L., Yao, J.M.: Adsorption removal of dyes from single and binary solutions using a cellulose-based bioadsorbent. *ACS Sustain. Chem. Eng.* 3, 432–442 (2015)(a).

Liu, S., Ding, Y., Li, P., Diao, K., Tan, X., Lei, F., Zhan, Y., Li, Q., Huang, B., Huang, Z.: Adsorption of the anionic dye Congo red from aqueous solution onto natural zeolites modified with N,N-dimethyl dehydroabietylamine oxide. *Chem. Eng. J.* 248, 135–144 (2014).

Liu, X., An, S., Wang, Y., Yang, Q., Zhang, L.: Rapid selective separation and recovery of a specific target dye from mixture consisted of different dyes by magnetic Ca-ferrites nanoparticles. *Chem. Eng. J.* 262, 517–526 (2015)(b).

Liu, Y., Zheng, R., Han, Z., Gong, K., He, X., Zhai, X.: Supramolecular hybrids of polytungstates and their adsorption properties for methylene blue. *J. Solid State Chem.* 231, 169–174 (2015)(c).

Lonhienne, T., Gerday, C., Feller, G.: Psychrophilic enzymes: Revisiting the thermodynamic parameters of activation may explain local flexibility. *Biochim. Biophys. Acta - Protein Struct. Mol. Enzymol.* 1543, 1–10 (2000).

Lu, Q., Sorial, G.A.: Adsorption of phenolics on activated carbon - Impact of pore size and molecular oxygen. *Chemosphere.* 55, 671–679 (2004).

Maheshwari, M.: Studies on removal of Ciprofloxacin hydrochloride from aqueous solution using adsorption and advanced oxidation processes, Ph.D. thesis, Chemical Engineering Department, Malaviya National Institute of Technology, Jaipur, (2014).

Mahmoodi, N.M.: Dendrimer functionalized nanoarchitecture: Synthesis and binary system dye removal. *J. Taiwan Inst. Chem. Eng.* 45, 2008–2020 (2014)(a).

Mahmoodi, N.M.: Synthesis of core–shell magnetic adsorbent nanoparticle and selectivity analysis for binary system dye removal. *J. Ind. Eng. Chem.* 20, 2050–2058 (2014)(b).

Mahmoodi, N.M., Abdi, J., Najafi, F.: Gemini polymeric nanoarchitecture as a novel adsorbent: synthesis and dye removal from multicomponent system. *J. Colloid Interface Sci.* 400, 88–96 (2013).

Mahmoodi, N.M., Hayati, B., Arami, M.: Textile Dye Removal from Single and Ternary Systems Using Date Stones: Kinetic, Isotherm, and Thermodynamic Studies. *J. Chem. Eng. Data.* 55, 4638–4649 (2010).

Mahmoodi, N.M., Salehi, R., Arami, M.: Binary system dye removal from colored textile wastewater using activated carbon: Kinetic and isotherm studies. *Desalination.* 272, 187–195

(2011)(a).

Mahmoodi, N.M., Salehi, R., Arami, M., Bahrami, H.: Dye removal from colored textile wastewater using chitosan in binary systems. *Desalination*. 267, 64–72 (2011)(b).

Martin, R.J., Al-Bahrani, K.S.: Adsorption studies using gas-liquid chromatography—II. Competitive adsorption. *Water Res.* 11, 991–999 (1977).

McKay, G., Al-Duri, B.: Simplified model for the equilibrium adsorption of dyes from mixtures using activated carbon. *Chem. Eng. Process. Process Intensif.* 22, 145–156 (1987).

McKay, G., Al-Duri, B.: Prediction of multicomponent adsorption equilibrium data using empirical correlations. *Chem. Eng. J.* 41, 9 – 23 (1989).

McKay, G., Al-Duri, B.: Study of the mechanism of pore diffusion in batch adsorption systems. *J. Chem. Technol. Biotechnol.* 48, 269–285 (1990).

McKay, G., Al-Duri, B.: Multicomponent Dye Adsorption onto Carbon Using a Solid Diffusion Mass-Transfer Model. *Ind. Eng. Chem. Res.* 30, 385–395 (1991).

McKay, G., Allen, S.J., McConvey, I.F., Walters, J.H.R.: External mass transfer and homogeneous solid-phase diffusion effects during the adsorption of dyestuffs. *Ind. Eng. Chem. Process Des. Dev.* 23, 221–226 (1984).

McKay, G., Otterburn, M.S., Sweeney, A.G.: The removal of colour from effluent using various adsorbents-III. Silica: Rate processes. *Water Res.* 14, 15–20 (1980).

Mesquita, A.M., Guimarães, I.R., Castro, G.M.M. d., Gonçalves, M.A., Ramalho, T.C., Guerreiro, M.C.: Boron as a promoter in the goethite (α -FeOOH) phase: Organic compound degradation by Fenton reaction. *Appl. Catal. B Environ.* 192, 286–295 (2016).

Mohammed, M.A., Ibrahim, Shitu: Batch removal of hazardous safranin-O in wastewater using pineapple peels as an agricultural waste based adsorbent. *Int. J. Environ. Monit. Anal.* 2, 128–133 (2014).

Mondal, P., Balomajumder, C., Mohanty, B.: A laboratory study for the treatment of arsenic,

iron, and manganese bearing ground water using Fe³⁺ impregnated activated carbon: Effects of shaking time, pH and temperature. *J. Hazard. Mater.* 144, 420–426 (2007).

Muñiz, G., Fierro, V., Celzard, A., Furdin, G., Gonzalez-Sánchez, G., Ballinas, M.L.: Synthesis, characterization and performance in arsenic removal of iron-doped activated carbons prepared by impregnation with Fe(III) and Fe(II). *J. Hazard. Mater.* 165, 893–902 (2009).

Murcia, M.D., Gómez, M., Gómez, E., Gómez, J.L., Christofi, N.: Photodegradation of congo red using XeBr, KrCl and Cl₂ barrier discharge excilamps: A kinetics study. *Desalination.* 281, 364–371 (2011).

Myers, A.L., Prausnitz, J.M.: Thermodynamics of mixed-gas adsorption. *AIChE J.* 11, 121–127 (1965).

Nadejde, C., Neamtu, M., Schneider, R.J., Hodoroaba, V.-D., Ababei, G., Panne, U.: Catalytical degradation of relevant pollutants from waters using magnetic nanocatalysts. *Appl. Surf. Sci.* 352, 42–48 (2015).

Naeem, K., Weiqian, P., Ouyang, F.: Thermodynamic parameters of activation for photodegradation of phenolics. *Chem. Eng. J.* 156, 505–509 (2010).

Namasivayam, C., Kanchana, N.: Waste banana pith as adsorbent for color removal from wastewaters. *Chemosphere.* 25, 1691–1705 (1992).

Nateri, A.S., Ekrami, E.: Quantitative analysis of bicomponent dye solutions by derivative spectrophotometry. *Pigment Resin Technol.* 38, 43–48 (2009).

Neamu, M., Catrinescu, C., Kettrup, A.: Effect of dealumination of iron(III)—exchanged Y zeolites on oxidation of Reactive Yellow 84 azo dye in the presence of hydrogen peroxide. *Appl. Catal. B Environ.* 51, 149–157 (2004).

Nevado, J.J.B., Flores, J.R., Llerena, M.J. V, Fariñas, N.R.: Simultaneous spectrophotometric determination of tartrazine, patent blue V, and indigo carmine in commercial products by partial least squares and principal component regression methods. *Talanta.* 48, 895–903 (1999).

Ng, I.S., Chen, T., Lin, R., Zhang, X., Ni, C., Sun, D.: Decolorization of textile azo dye and

Congo red by an isolated strain of the dissimilatory manganese-reducing bacterium *Shewanella xiamenensis* BC01. *Appl. Microbiol. Biotechnol.* 98, 2297–2308 (2014).

Nogueira, F.G.E., Lopes, J.H., Silva, A.C., Gonçalves, M., Anastácio, A.S., Sapag, K., Oliveira, L.C.A.: Reactive adsorption of methylene blue on montmorillonite via an ESI-MS study. *Appl. Clay Sci.* 43, 190–195 (2009).

Noroozi, B., Sorial, G. a.: Applicable models for multi-component adsorption of dyes: A review. *J. Environ. Sci.* 25, 419–429 (2013).

Noroozi, B., Sorial, G.A., Bahrami, H., Arami, M.: Adsorption of binary mixtures of cationic dyes. *Dye. Pigment.* 76, 784–791 (2008).

Ocampo-Pérez, R., Leyva-Ramos, R., Sanchez-Polo, M., Rivera-Utrilla, J.: Role of pore volume and surface diffusion in the adsorption of aromatic compounds on activated carbon. *Adsorption.* 19, 945–957 (2013).

Olgun, A., Atar, N.: Equilibrium and kinetic adsorption study of Basic Yellow 28 and Basic Red 46 by a boron industry waste. *J. Hazard. Mater.* 161, 148–156 (2009).

Oliveira, L.C.A., Ramalho, T.C., Goncalves, M., Cereda, F., Carvalho, K.T., Nazzarro, M.S., Sapag, K.: Pure niobia as catalyst for the oxidation of organic contaminants: Mechanism study via ESI-MS and theoretical calculations. *Chem. Phys. Lett.* 446, 133–137 (2007).

Oller, I., Malato, S., Sánchez-Pérez, J.A.: Combination of Advanced Oxidation Processes and biological treatments for wastewater decontamination—A review. *Sci. Total Environ.* 409, 4141–4166 (2011).

Orendorz, A., Ziegler, C., Gnaser, H.: Photocatalytic decomposition of methylene blue and 4-chlorophenol on nanocrystalline TiO₂ films under UV illumination : A ToF-SIMS study. *Appl. Surf. Sci.* 255, 1011–1014 (2008).

Orucoglu, E., Hacıyakupoglu, S.: Bentonite modification with hexadecylpyridinium and aluminum polyoxy cations and its effectiveness in Se(IV) removal. *J. Environ. Manage.* 160, 30–38 (2015).

Özer, D., Dursun, G., Özer, A.: Methylene blue adsorption from aqueous solution by dehydrated peanut hull. *J. Hazard. Mater.* 144, 171–179 (2007).

Patel, H., Vashi, R.T.: Removal of Congo Red dye from its aqueous solution using natural coagulants. *J. Saudi Chem. Soc.* 16, 131–136 (2012).

Peel, R.G., Benedek, A., Crowe, C.M.: A Branched Pore Kinetic-Model for Activated Carbon Adsorption. *AIChE J.* 27, 26–32 (1981).

Pelekani, C., Snoeyink, V.L.: Competitive adsorption between atrazine and methylene blue on activated carbon: the importance of pore size distribution. *Carbon N. Y.* 38, 1423–1436 (2000).

Pereira, M.C., Cavalcante, L.C.D., Magalhães, F., Fabris, J.D., Stucki, J.W., Oliveira, L.C.A., Murad, E.: Composites prepared from natural iron oxides and sucrose: A highly reactive system for the oxidation of organic contaminants in water. *Chem. Eng. J.* 166, 962–969 (2011).

Pinto, I.S.X., Pacheco, P.H.V.V., Coelho, J.V., Lorencon, E., Ardisson, J.D., Fabris, J.D., Souza, P.P. de, Krambrock, K.W.H., Oliveira, L.C.A., Márcio C. Pereira: Nanostructured δ -FeOOH: An efficient Fenton-like catalyst for the oxidation of organics in water. *Appl. Catal. B Environ.* 119–120, 175–182 (2012).

Pirdashti, M., Curteanu, S., Kamangar, M.H., Hassim, M.H., Khatami, M.A.: Artificial neural networks: Applications in chemical engineering. *Rev. Chem. Eng.* 29, 205–239 (2013).

Porter, J.F., McKay, G., Choy, K.H.: The prediction of sorption from a binary mixture of acidic dyes using single- and mixed-isotherm variants of the ideal adsorbed solute theory. *Chem. Eng. Sci.* 54, 5863–5885 (1999).

Postai, D.L., Demarchi, C.A., Zanatta, F., Melo, D.C.C., Rodrigues, C.A.: Adsorption of rhodamine B and methylene blue dyes using waste of seeds of *Aleurites Moluccana*, a low cost adsorbent. *Alexandria Eng. J.* (2016).

El Qada, E.N., Allen, S.J., Walker, G.M.: Adsorption of Basic Dyes onto Activated Carbon Using Microcolumns. *Ind. Eng. Chem. Res.* 45, 6044–6049 (2006).

Radke, C., Prausnitz, J.: Adsorption of organic solutes from dilute aqueous solution of activated

carbon. *Ind. Eng. Chem. Fundam.* 11, 445–451 (1972).

Rafatullah, M., Sulaiman, O., Hashim, R., Ahmad, A.: Adsorption of methylene blue on low-cost adsorbents: A review. *J. Hazard. Mater.* 177, 70–80 (2010).

Rajoriya, S., Bargole, S., Saharan, V.K.: Degradation of a cationic dye (Rhodamine 6G) using hydrodynamic cavitation coupled with other oxidative agents: Reaction mechanism and pathway. *Ultrason. Sonochem.* 34, 183–194 (2017).

Rauf, M.A., Meetani, M.A., Khaleel, A., Ahmed, A.: Photocatalytic degradation of Methylene Blue using a mixed catalyst and product analysis by LC/MS. *Chem. Eng. J.* 157, 373–378 (2010).

Rivera-Utrilla, J., Sánchez-Polo, M., Gómez-Serrano, V., Alvarez, P.M., Alvim-Ferraz, M.C.M., Dias, J.M.: Activated carbon modifications to enhance its water treatment applications. An overview. *J. Hazard. Mater.* 187, 1–23 (2011).

Rodríguez, A., García, J., Ovejero, G., Mestanza, M.: Adsorption of anionic and cationic dyes on activated carbon from aqueous solutions: Equilibrium and kinetics. *J. Hazard. Mater.* 172, 1311–1320 (2009).

Rotte, N.K., Yerramala, S., Boniface, J., Srikanth, V.V.S.S.: Equilibrium and kinetics of Safranin O dye adsorption on MgO decorated multi-layered graphene. *Chem. Eng. J.* 258, 412–419 (2014).

Ruthven, D.M., Farooq, S., Knaebel, K.S.: *Pressure swing adsorption* Vol. 480. New York: VCH publishers (1994).

Şahin, Ö., Kaya, M., Saka, C.: Plasma-surface modification on bentonite clay to improve the performance of adsorption of methylene blue. *Appl. Clay Sci.* 116–117, 46–53 (2015).

Salleh, M.A.M., Mahmoud, D.K., Karim, W.A.W.A., Idris, A.: Cationic and anionic dye adsorption by agricultural solid wastes: A comprehensive review. *Desalination.* 280, 1–13 (2011).

Schay, G.: *Theory of the Langmuir Type of Physical Adsorption of Gas.* *Chim. Phys. Hungary.*

53, 691 (1956).

Shafeeyan, M.S., Daud, W.M.A.W., Houshmand, A., Shamiri, A.: A review on surface modification of activated carbon for carbon dioxide adsorption. *J. Anal. Appl. Pyrolysis*. 89, 143–151 (2010).

Shams-Nateri, A.: Dye concentrations determination in ternary mixture solution by using colorimetric algorithm. *Iran. J. Chem. Chem. Eng.* 30, 51–61 (2011).

Sharma, K., Dalai, A.K., Vyas, R.K.: Removal of synthetic dyes from multicomponent industrial wastewaters. *Rev. Chem. Eng.* (2018).

Sharma, K., Vyas, R.K.: Adsorption of multicomponent dye mixture: a brief review. In: *Chemcon* (2015).

Sharma, K., Vyas, R.K., Dalai, A.K.: Comparison of reactive adsorption and adsorption: Kinetic, thermodynamic, and desorption studies. *Manuscr. Submitt. elsewhere Publ.* (2017)(a).

Sharma, K., Vyas, R.K., Dalai, A.K.: Degradation of binary dye mixture using reactive adsorption: Kinetic and thermodynamic studies. *Manuscr. Submitt. elsewhere Publ.* (2017)(b).

Sharma, K., Vyas, R.K., Singh, K., Dalai, A.K., Gupta, V.K.: Reactive adsorption of Safranin O: Modeling, batch experimental, and degradation studies. *Manuscr. Submitt. elsewhere Publ.* (2017)(c).

Sharma, M., Vyas, R.K., Singh, K.: Theoretical and Experimental Analysis of Reactive Adsorption in a Packed Bed: Parallel and Branched Pore-Diffusion Model Approach. *Ind. Eng. Chem. Res.* 55, 5945–5954 (2016).

Sheindorf, C., Rebhun, M., Sheintuch, M.: A Freundlich-type multicomponent isotherm. *J. Colloid Interface Sci.* 79, 136–142 (1981).

Sheindorf, C., Rebhun, M., Sheintuch, M.: Organic pollutants adsorption from multicomponent systems modeled by Freundlich type isotherm. *Water Res.* 16, 357–362 (1982).

Shen, D., Fan, J., Zhou, W., Gao, B., Yue, Q., Kang, Q.: Adsorption kinetics and isotherm of

anionic dyes onto organo-bentonite from single and multisolute systems. *J. Hazard. Mater.* 172, 99–107 (2009).

Shen, W., Li, Z., Liu, Y.: Surface Chemical Functional Groups Modification of Porous Carbon. *Recent Patents Chem. Eng.* 1, 27–40 (2008).

Shukla, P., Wang, S., Sun, H., Ang, H., M Tadó: Activated carbon supported cobalt catalysts for advanced oxidation of organic contaminants in aqueous solution. *Appl. Catal. B Environ.* 100, 529–534 (2010).

Sirianuntapiboon, S., Srisornsak, P.: Removal of disperse dyes from textile wastewater using bio-sludge. *Bioresour. Technol.* 98, 1057–1066 (2007).

Sismanoglu, T., Kismir, Y., Karakus, S.: Single and binary adsorption of reactive dyes from aqueous solutions onto clinoptilolite. *J. Hazard. Mater.* 184, 164–169 (2010).

Smith, E.H., Tseng, S., Weber, W.J.: Modeling the Adsorption of Target Compounds by GAC in the Presence of Background Dissolved Organic Matter. *Environ. Prog.* 6, 18–25 (1987).

Souza, W.F. de, Guimarães, I.R., Oliveira, L.C.A., Guerreiro, M.C., Guarieiro, A.L.N., Carvalho, K.T.G.: Natural and H₂-reduced limonite for organic oxidation by a Fenton-like system: Mechanism study via ESI-MS and theoretical calculations. *J. Mol. Catal. A Chem.* 278, 145–151 (2007).

Srivastava, V.C., Mall, I.D., Mishra, I.M.: Equilibrium modelling of single and binary adsorption of cadmium and nickel onto bagasse fly ash. *Chem. Eng. J.* 117, 79–91 (2006).

Suykens, J.A., Vandewalle, J.: Least Squares Support Vector Machine Classifier. *Neural Process. Lett.* 9, 293–300 (1999).

Tan, I.A.W., Hameed, B.H., Ahmad, A.L.: Equilibrium and kinetic studies on basic dye adsorption by oil palm fibre activated carbon. *Chem. Eng. J.* 127, 111–119 (2007).

Tovar-Gómez, R., Moreno-Virgen, M. del R., Moreno-Pérez, J., Bonilla-Petriciolet, A., Hernández-Montoya, V., Durán-Valle, C.J.: Analysis of synergistic and antagonistic adsorption of heavy metals and acid blue 25 on activated carbon from ternary systems. *Chem. Eng. Res.*

Des. 93, 755–772 (2015).

Tressaud, A.: Fluorine and the Environment: Agrochemicals, Archaeology, Green Chemistry vol. (2). Elsevier (2006).

Trojanowicz, M.: Analytical applications of carbon nanotubes: a review. TrAC - Trends Anal. Chem. 25, 480–489 (2006).

Turabik, M.: Adsorption of basic dyes from single and binary component systems onto bentonite: simultaneous analysis of Basic Red 46 and Basic Yellow 28 by first order derivative spectrophotometric analysis method. J. Hazard. Mater. 158, 52–64 (2008).

Vapnik, V.N.: The nature of statistical learning theory. Statistics for engineering and information science. Springer (2000).

Verma, A.K., Dash, R.R., Bhunia, P.: A review on chemical coagulation/flocculation technologies for removal of colour from textile wastewaters. J. Environ. Manage. 93, 154–68 (2012).

Verma, Y.: Acute toxicity assessment of textile dyes and textile and dye industrial effluents using *Daphnia magna* bioassay. Toxicol. Ind. Health. 24, 491–500 (2008).

Vijayaraghavan, K., Yun, Y.S.: Chemical modification and immobilization of *Corynebacterium glutamicum* for biosorption of reactive black 5 from aqueous solution. Ind. Eng. Chem. Res. 46, 608–617 (2007).

Vijayaraghavan, K., Yun, Y.-S.: Competition of Reactive red 4, Reactive orange 16 and Basic blue 3 during biosorption of Reactive blue 4 by polysulfone-immobilized *Corynebacterium glutamicum*. J. Hazard. Mater. 153, 478–86 (2008).

Wang, H., Hu, D.: Comparison of SVM and LS-SVM for regression. Neural Networks and Brain. 1, 279–283 (2005).

Wang, S., Ng, C.W., Wang, W., Li, Q., Hao, Z.: Synergistic and competitive adsorption of organic dyes on multiwalled carbon nanotubes. Chem. Eng. J. 197, 34–40 (2012)(a).

Wang, S., Ng, C.W., Wang, W., Li, Q., Li, L.: A comparative study on the adsorption of acid and reactive dyes on multiwall carbon nanotubes in single and binary dye systems. *J. Chem. Eng. Data.* 57, 1563–1569 (2012)(b).

Wang, X., Mei, L., Xing, X., Liao, L., Lv, G., Li, Z.: Mechanism and process of methylene blue degradation by manganese oxides under microwave irradiation. *Appl. Catal. B Environ.* 160-161, 211–216 (2014).

Weber, T.W., Chakravorti, R.K.: Pore and solid diffusion models for fixed-bed adsorbers. *AIChE J.* 20, 228–238 (1974).

Won, S.W., Choi, S.B., Yun, Y.-S.: Interaction between protonated waste biomass of *Corynebacterium glutamicum* and anionic dye Reactive Red 4. *Colloids Surfaces A Physicochem. Eng. Asp.* 262, 175–180 (2005).

Wong, Y.C., Szeto, Y.S., Cheung, W.H., McKay, G.: Adsorption of acid dyes on chitosan - Equilibrium isotherm analyses. *Process Biochem.* 39, 693–702 (2004).

Wu, F.C., Tseng, R.L., Juang, R.S.: Initial behavior of intraparticle diffusion model used in the description of adsorption kinetics. *Chem. Eng. J.* 153, 1–8 (2009).

Xu, J. hong, Gao, N. yun, Zhao, D. ye, Zhang, W. xian, Xu, Q. kun, Xiao, A. hong: Efficient reduction of bromate in water by nano-iron hydroxide impregnated granular activated carbon (Fe-GAC). *Chem. Eng. J.* 275, 189–197 (2015).

Yacout, D.M.M., Abd El-Kawi, M.A., Hassouna, M.S.: Cradle to gate environmental impact assessment of acrylic fiber manufacturing. *Int. J. Life Cycle Assess.* 21, 326–336 (2016).

Yagub, M.T., Sen, T.K., Afroze, S., Ang, H.M.: Dye and its removal from aqueous solution by adsorption: A review. *Adv. Colloid Interface Sci.* 209, 172–184 (2014).

Yahyaei, B., Azizian, S.: Rapid adsorption of binary dye pollutants onto the nanostructured mesoporous alumina. *J. Mol. Liq.* 199, 88–95 (2014).

Yan, B., Chen, Z., Cai, L., Chen, Z., Fu, J., Xu, Q.: Fabrication of polyaniline hydrogel: Synthesis, characterization and adsorption of methylene blue. *Appl. Surf. Sci.* 356, 39–47

(2015).

Yan, D., Gang, D.D., Asce, M., Zhang, N., Lin, L.: Adsorptive Selenite Removal Using Iron-Coated GAC : Modeling Selenite Breakthrough with the Pore Surface Diffusion Model. 139, 213–219 (2013).

Yang, L., Zhang, Y., Liu, X., Jiang, X., Zhang, Z., Zhang, T., Zhang, L.: The investigation of synergistic and competitive interaction between dye Congo red and methyl blue on magnetic MnFe₂O₄. Chem. Eng. J. 246, 88–96 (2014).

Yang, Y., Jin, D., Wang, G., Wang, S., Jia, X., Zhao, Y.: Competitive biosorption of Acid Blue 25 and Acid Red 337 onto unmodified and CDAB-modified biomass of *Aspergillus oryzae*. Bioresour. Technol. 102, 7429–36 (2011).

Yin, C., Aroua, M., Daud, W.: Review of modifications of activated carbon for enhancing contaminant uptakes from aqueous solutions. Sep. Purif. Technol. 52, 403–415 (2007).

Yogi, C., Kojima, K., Wada, N., Tokumoto, H., Takai, T.: Photocatalytic degradation of methylene blue by TiO₂ film and Au particles-TiO₂ composite film. Thin Solid Films. 516, 5881–5884 (2008).

Yola, M.L., Eren, T., Atar, N., Wang, S.: Adsorptive and photocatalytic removal of reactive dyes by silver nanoparticle-colemanite ore waste. Chem. Eng. J. 242, 333–340 (2014).

Yu, J., Zhu, J., Feng, L., Cai, X., Zhang, Y., Chi, R.: Removal of cationic dyes by modified waste biosorbent under continuous model: Competitive adsorption and kinetics. Arab. J. Chem. (2015).

Zaghbani, N., Hafiane, A., Dhahbi, M.: Removal of Safranin T from wastewater using micellar enhanced ultrafiltration. Desalination. 222, 348–356 (2008).

Zahrim, a. Y., Hilal, N.: Treatment of highly concentrated dye solution by coagulation/flocculation-sand filtration and nanofiltration. Water Resour. Ind. 3, 23–34 (2013).

Zazo, J.A., Casas, J.A., Mohedano, A.F., Rodríguez, J.J.: Catalytic wet peroxide oxidation of phenol with a Fe/active carbon catalyst. Appl. Catal. B Environ. 65, 261–268 (2006).

Zeinali, N., Ghaedi, M., Shafie, G.: Competitive adsorption of methylene blue and brilliant green onto graphite oxide nano particle following: Derivative spectrophotometric and principal component-artificial neural network model methods for their simultaneous determination. *J. Ind. Eng. Chem.* 20, 3550–3558 (2014).

Zeldowitsch, J.: Adsorption site energy distribution. *Acta Phys. Chim. URSS.* 1, 961–973 (1934).

Zhao, X., Bu, X., Wu, T., Zheng, S.-T., Wang, L., Feng, P.: Selective anion exchange with nanogated isorecticular positive metal-organic frameworks. *Nat. Commun.* 4, 2344 (2013).

Zhao, X., Huang, J., Wang, B., Bi, Q., Dong, L., Liu, X.: Preparation of titanium peroxide and its selective adsorption property on cationic dyes. *Appl. Surf. Sci.* 292, 576–582 (2014).

Zolgharnein, J., Asanjrani, N., Bagtash, M., Azimi, G.: Multi-response optimization using Taguchi design and principle component analysis for removing binary mixture of alizarin red and alizarin yellow from aqueous solution by nano γ -alumina. *Spectrochim. Acta Part A Mol. Biomol. Spectrosc.* 126, 291–300 (2014)(a).

Zolgharnein, J., Bagtash, M., Asanjarani, N.: Hybrid central composite design approach for simultaneous optimization of removal of alizarin red S and indigo carmine dyes using cetyltrimethylammonium bromide-modified TiO₂ nanoparticles. *J. Environ. Chem. Eng.* 2, 988–1000 (2014)(b).

Zolgharnein, J., Bagtash, M., Shariatmanesh, T.: Simultaneous removal of binary mixture of Brilliant Green and Crystal Violet using derivative spectrophotometric determination, multivariate optimization and adsorption characterization of dyes on surfactant modified nano- γ -alumina. *Spectrochim. Acta. A. Mol. Biomol. Spectrosc.* 137, 1016–28 (2015).

Appendices

I. Calibration curves

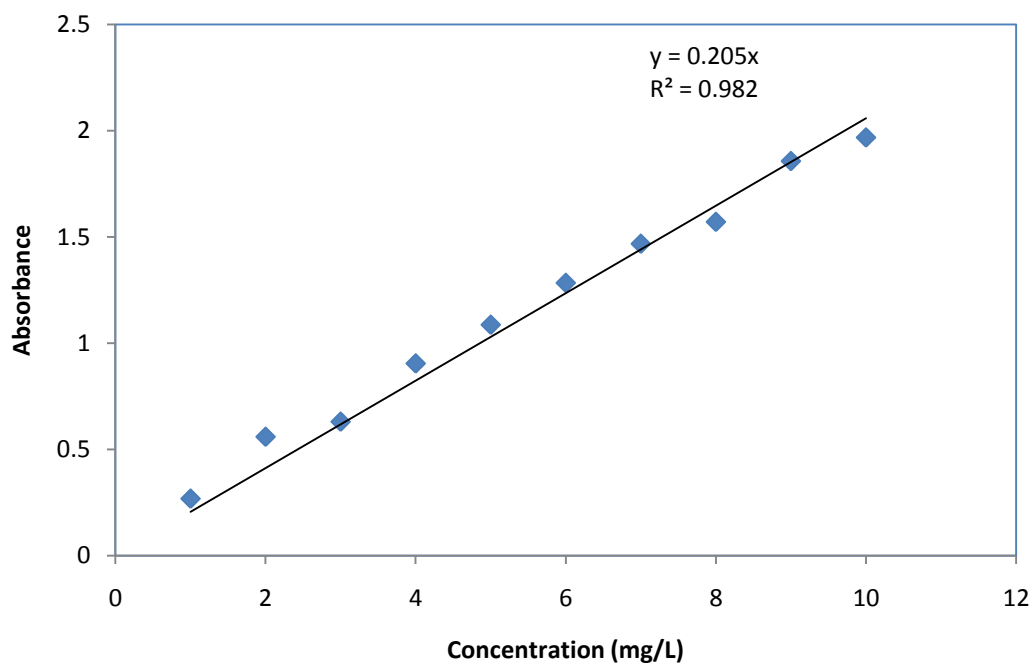


Table I.1: Calibration curve of MB in single dye system

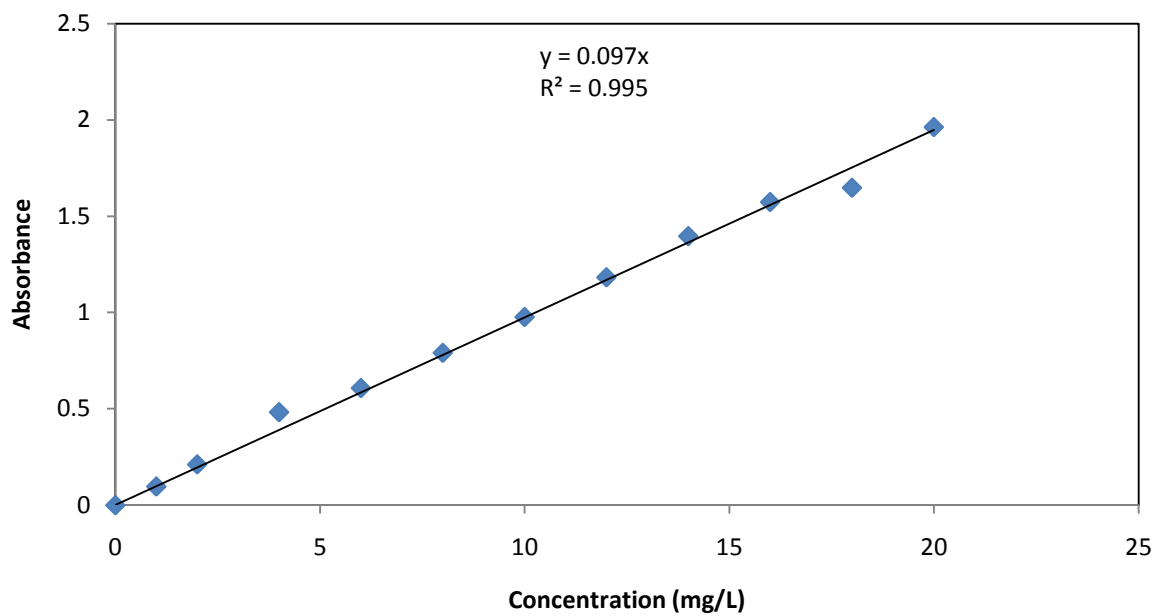


Table I.2: Calibration curve of SO in single dye system

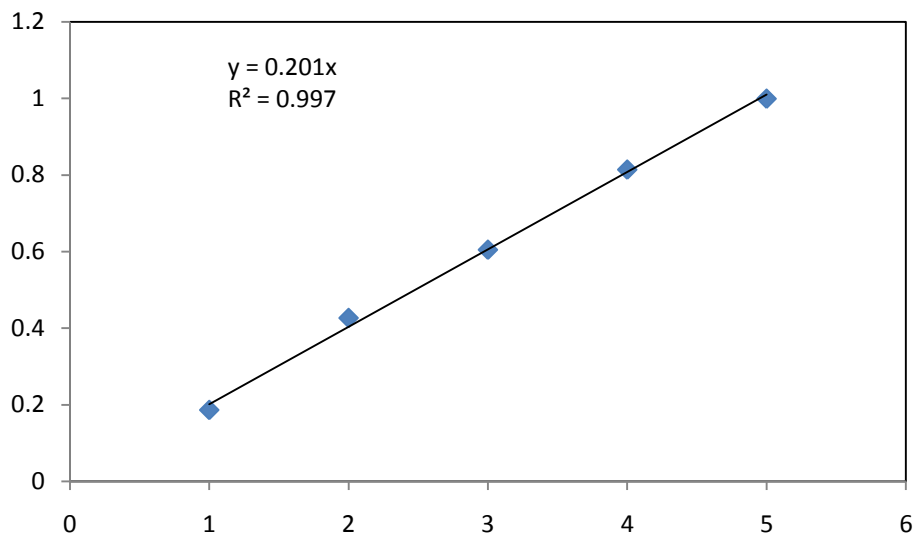


Table I.3: Calibration curve of MB in binary dye system

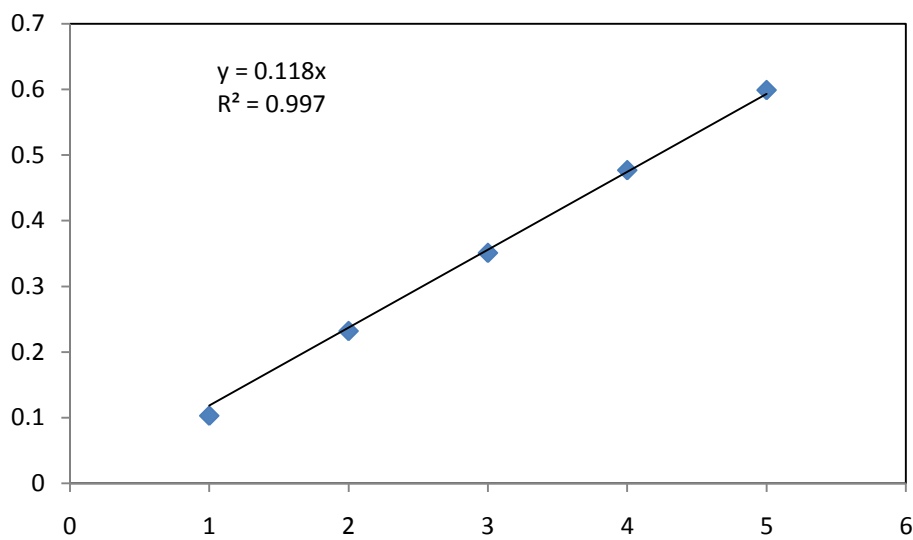


Table I.4: Calibration curve of SO in binary dye system

II. Experimental data on Methylene Blue removal

Table II.1: Data of MB reactive adsorption

Time (min)	Concentration (mg/L)	$-\ln(C_t/C_0)$	$1/C_t$												
Temperature	20°C			30°C			40°C			50°C			60°C		
0	10	0.000	0.100	10	0.000	0.10	10	0.000	0.100	10	0.000	0.100	10	0.000	0.100
30	8.473	0.166	0.118	7.498	0.288	0.13	6.985	0.359	0.143	6.483	0.433	0.154	6.273	0.466	0.159
60	5.488	0.600	0.182	4.976	0.698	0.20	4.907	0.712	0.203	4.176	0.873	0.239	3.717	0.990	0.269
90	3.556	1.034	0.281	2.556	1.364	0.39	2.346	1.450	0.426	2.010	1.605	0.498	1.605	1.830	0.623
120	2.502	1.385	0.399	1.390	1.973	0.72	1.341	2.009	0.745	1.098	2.209	0.911	0.624	2.774	1.602
150	1.298	2.042	0.770	0.917	2.389	1.09	0.888	2.422	1.126	0.512	2.972	1.952	0.268	3.618	3.727
180	0.951	2.353	1.051	0.605	2.805	1.65	0.493	3.010	2.029	0.249	3.694	4.020	0.122	4.407	8.200

Table II.2: Kinetics data of MB reactive adsorption at 30°C

Reaction kinetic models	Parameters	Values
Pseudo-first-order	k_{app} (min^{-1})	0.015
	R^2	0.985
Pseudo-second-order	k_{app} ($\text{mg}^{-1} \text{min}^{-1}$)	0.008
	R^2	0.883

Table II.3: Effect of temperature on the apparent rate constant on reactive adsorption of MB.

T (°C)	k_{app} (min ⁻¹)
20	0.012
30	0.015
40	0.016
50	0.019
60	0.023

Table II.4: Equilibrium data for adsorption of MB onto Fe-GAC.

Temperature	C_e	q_e	C_e/q_e	$\ln C_e$	$\ln q_e$
20°C	4.9	25.3	0.195	1.597	3.231
	11.5	42.5	0.270	2.442	3.750
	18.8	55.9	0.336	2.934	4.024
	28.0	59.9	0.468	3.333	4.092
	36.3	68.5	0.530	3.592	4.227
30°C	3.8	30.7	0.125	1.349	3.425
	9.7	51.6	0.187	2.269	3.944
	16.9	65.7	0.257	2.825	4.185
	25.4	72.8	0.349	3.236	4.288
	34.5	77.5	0.445	3.541	4.350
40°C	3.1	34.3	0.092	1.145	3.535
	7.1	64.7	0.109	1.954	4.170
	14.6	76.9	0.190	2.683	4.342
	22.2	88.9	0.250	3.101	4.487
	31.9	90.5	0.352	3.463	4.505
50°C	2.4	37.8	0.065	0.894	3.632
	6.1	69.6	0.088	1.806	4.242
	12.7	86.7	0.146	2.539	4.462
	20.8	96.0	0.217	3.035	4.564
	30.1	99.3	0.303	3.406	4.599
60°C	1.9	40.5	0.047	0.643	3.701
	4.2	79.1	0.053	1.428	4.371
	11.4	93.1	0.122	2.431	4.534
	18.3	108.7	0.168	2.904	4.689
	27.1	114.6	0.236	3.299	4.742

Table II.5: Kinetics data for adsorption of MB onto Fe-GAC at 30°C.

Time (min)	C_e	$\log(q_e - q_t)$	t/q_t	q_t
30	9.9	1.481	61.5	0.49
60	9.5	1.453	25.6	2.34
90	8.8	1.395	15.2	5.90
120	8.2	1.337	13.2	9.02
150	7.7	1.281	12.8	11.63
180	7.5	1.257	14.2	12.66
210	7.1	1.213	14.5	14.39
240	6.6	1.136	14.0	17.05
300	5.8	0.996	14.4	20.83
420	4.9	0.707	16.3	25.63
480	4.7	0.643	18.2	26.34
600	4.4	0.428	21.3	28.05
720	4.2	0.179	24.6	29.22
840	4.1	0.039	28.3	29.63
1080	4.0	-	36.0	30.00
1200	3.8	-	39.0	30.7
1440	3.9	-	46.8	30.7

III. Experimental data on Safranin O removal

Table III.1: Adsorption equilibrium data for removal of SO onto Fe-GAC at 30 °C.

C_e	q_e	C_e/q_e	$\ln C_e$	$\ln q_e$
0.15	9.8	0.016	-1.867	2.287
3.08	16.9	0.182	1.126	2.828
9.11	20.9	0.436	2.210	3.039
17.05	22.9	0.743	2.836	3.133
25.61	24.4	1.050	3.243	3.194

Table III.2: SO removal time versus concentration data onto Fe-GAC

Time (h)	Concentration (mg/L)
0	10
1	7.969
2	6.289
3	5.753
4	4.794
5	4.165

Table III.3: Data of SO reactive adsorption at 30°C

Time (min)	Concentration (mg/L)	$-\ln (C_t/C_0)$	$1/C_t$
0	10	0.000	0.100
30	6.722	0.397	0.148
60	3.113	1.167	0.321
90	1.948	1.636	0.513
120	0.938	2.366	1.065
150	0.392	3.240	2.552

Table III.4: Kinetics data of SO reactive adsorption at 30°C

Kinetic models	Parameters	Values
Pseudo first order	k_{app} (min^{-1})	0.010
	R^2	0.982
Pseudo second order	k_{app} ($\text{mg}^{-1}\text{min}^{-1}$)	0.007
	R^2	0.756

IV. Experimental data on simultaneous removal of Methylene Blue and Safranin O

Table IV.1: Data of MB in binary dye reactive adsorption.

Time (min)	Concentration (mg/L)	$-\ln(C_t/C_0)$	$1/C_t$												
Temperature	15 °C			20 °C			25 °C			30 °C			35 °C		
0	5.0	0.000	0.2	5.0	0.000	0.2	5.0	0.000	0.2	5.0	0.000	0.2	5.0	0.000	0.2
60	3.403	0.320	0.294	3.348	0.336	0.299	3.662	0.247	0.273	3.294	0.353	0.303	3.289	0.354	0.304
120	2.776	0.524	0.360	2.726	0.542	0.367	2.500	0.628	0.400	2.430	0.657	0.411	1.751	0.984	0.571
180	2.159	0.775	0.463	1.881	0.913	0.532	1.562	1.099	0.640	1.403	1.206	0.712	0.771	1.805	1.297
240	1.726	0.999	0.579	1.428	1.189	0.700	1.095	1.454	0.914	0.687	1.921	1.456	0.547	2.148	1.827
300	1.373	1.228	0.728	1.010	1.535	0.990	0.597	2.061	1.675	0.468	2.305	2.138	0.306	2.729	3.268
360	1.057	1.489	0.946	0.677	1.935	1.478	0.448	2.348	2.233	0.341	2.621	2.934	0.147	3.464	6.814
420	0.878	1.675	1.139	0.398	2.466	2.513	0.259	2.897	3.865	0.189	3.210	5.289	0.127	3.609	7.882

Table IV.2: Kinetics data of MB in binary dye reactive adsorption at 30°C.

Kinetic models	Parameters	Values
Pseudo first order	k_{app} (min^{-1})	0.007
	R^2	0.987
Pseudo second order	k_{app} ($\text{mg}^{-1}\text{min}^{-1}$)	0.010
	R^2	0.827

Table IV.3. Effect of temperature on the apparent rate constant of MB in binary dye reactive adsorption system.

T (°C)	k_{app} (10^{-2} min^{-1})
15	0.41
20	0.54
25	0.65
30	0.74
35	0.90

Table IV.4: Data of SO in binary dye reactive adsorption.

Time (min)	Concentration (mg/L)	$-\ln(C_t/C_0)$	$1/C_t$												
Temperature	15 °C			20 °C			25 °C			30 °C			35 °C		
0	5.0	0.0	0.2	5.0	0.0	0.2	5.0	0.0	0.2	5.0	0.0	0.2	5.0	0.0	0.2
60	3.763	0.209	0.266	3.627	0.245	0.276	3.686	0.229	0.271	3.746	0.213	0.267	3.619	0.248	0.276
120	3.263	0.351	0.306	3.297	0.341	0.303	2.881	0.476	0.347	2.996	0.437	0.334	2.301	0.700	0.435
180	2.746	0.524	0.364	2.695	0.542	0.371	2.068	0.807	0.484	2.097	0.793	0.477	1.297	1.274	0.771
240	2.326	0.689	0.430	2.089	0.797	0.479	1.648	1.034	0.607	1.331	1.248	0.752	0.797	1.761	1.255
300	2.025	0.828	0.494	1.771	0.962	0.565	1.339	1.242	0.747	0.987	1.547	1.013	0.521	2.185	1.919
360	1.703	1.001	0.587	1.364	1.223	0.733	0.797	1.761	1.255	0.763	1.805	1.311	0.386	2.487	2.593
420	1.500	1.128	0.667	0.975	1.560	1.026	0.636	1.987	1.573	0.500	2.227	2.000	0.326	2.654	3.065

Table IV.5: Kinetics data of SO in binary dye reactive adsorption at 30°C.

Kinetic models	Parameters	
Pseudo first order	k_{app} (min^{-1})	0.005
	R^2	0.985
Pseudo second order	k_{app} ($\text{mg}^{-1}\text{min}^{-1}$)	0.004
	R^2	0.885

Table IV.6. Effect of temperature on the apparent rate constant of SO in binary dye reactive adsorption system.

T (°C)	k_{app} (10^{-2}min^{-1})
15	0.27
20	0.34
25	0.45
30	0.50
35	0.67

Table IV.7: Equilibrium data for binary dye adsorption of MB and SO onto Fe-GAC at 30°C.

MB					SO				
C_e	q_e	C_e/q_e	$\ln C_e$	$\ln q_e$	C_e	q_e	C_e/q_e	$\ln C_e$	$\ln q_e$
0.458	5.4	0.084	-0.782	1.691	0.492	5.1	0.097	-0.710	1.626
1.100	9.0	0.122	0.095	2.198	1.186	8.1	0.146	0.171	2.096
1.851	11.5	0.161	0.616	2.442	1.983	10.2	0.195	0.685	2.319
2.701	13.0	0.208	0.994	2.564	2.915	10.8	0.269	1.070	2.384
3.458	15.4	0.224	1.241	2.736	3.737	12.6	0.296	1.318	2.536

Table IV.8: Kinetic data of MB in binary dye adsorption system.

Time (min)	C_e	$\log(q_e - q_t)$	t/q_t	$t^{0.5}$
30	3.7	0.839	9.46	5.477
60	3.3	0.765	14.11	7.746
90	3.1	0.726	18.94	9.487
120	2.8	0.651	21.44	10.954
150	2.4	0.548	22.93	12.247
180	2.3	0.508	26.26	13.416
210	2.1	0.447	28.86	14.491
240	2.0	0.402	31.79	15.492
270	1.7	0.259	32.69	16.432
300	1.6	0.192	35.21	17.321
330	1.3	-0.079	35.71	18.166
360	1.0	-0.864	36.23	18.974
390	1.0	-1.206	38.95	19.748
420	1.0	-	41.69	20.494

Table IV.9: Kinetic data of SO in binary dye adsorption system.

Time (min)	C_e	$\log(q_e - q_t)$	t/q_t	$t^{0.5}$
30	4.7	0.866	39.33	5.477
60	4.4	0.820	39.89	7.746
90	4.0	0.744	35.11	9.487
120	3.7	0.692	37.51	10.954
150	3.5	0.636	39.55	12.247
180	3.3	0.598	43.35	13.416
210	3.1	0.533	44.65	14.491
240	3.0	0.484	47.40	15.492
270	2.7	0.379	47.20	16.432
300	2.6	0.322	49.86	17.321
330	2.2	0.082	47.78	18.166
360	2.0	-0.183	48.27	18.974
390	1.9	-0.395	50.57	19.748
420	1.8	-	51.76	20.494

V. MATLAB programs

V.1 Safranin O surface – parallel pore diffusion mathematical modeling

```
function [t qma qmi c]=fun()
global a b Dma Dmi KLa A V kr phi NFD R dr r rho
NFD = 50;
qma(1:NFD+1) = 0;
qmi(1:NFD+1) = 0;
c = 0.01; %kg/m3
tspan = [0, 5*3600];
%Without reaction...
%texpt=[0 1 2 3 4 5];
%yexpt=0.001 * [10, 7.969, 6.289, 5.753, 4.794, 4.165];

%With reaction...
texpt=[0 1 2 3 4 5];
yexpt=0.001*[10, 6.722, 3.113, 1.948, 0.938, 0.392];
%kg/m3

yinit = [qma qmi c];
sol= odel5s(@gac,tspan,yinit);
t=0:tspan(2)/100:tspan(2);
y=deval(sol,t); y=y';

tRSQ=texpt*3600;
yRSQ=deval(sol,tRSQ); yRSQ=yRSQ';

qma= y(:,1:NFD+1);
for i=1:length(t)
for j=1:NFD+1
qmi(i,j) = y(i,j+NFD+1);
end
end
c= y(:,2*NFD+3);
cRSQ=yRSQ(:,2*NFD+3);
R2=rsq(yexpt,cRSQ)
figure(1), plot(texpt,yexpt./0.001,'o',t/3600,c./0.001),
title('Adsorption Only'), xlabel('Time, h'), ylabel('SO
concentration, mg/L');
```

```

figure(2)
surf(r*1000,t/3600,qma/0.001)
title('qma(r,t)')
colormap(hsv)
xlabel('Radial distance, mm')
ylabel('Time, h')
zlabel('q_m_a, mg/g')

```

```

figure(3)
surf(r*1000,t/3600,qmi/0.001)
title('qmi(r,t)')
colormap(hsv)
xlabel('Radial distance, mm')
ylabel('Time, h')
zlabel('q_m_i, mg/g')

```

```

figure(4)
plot(r*1000,qma/0.001)

```

```

figure(5)
plot(t/3600,qma/0.001)

```

```

figure(6)
plot(r*1000,qmi/0.001)

```

```

figure(7)
plot(t/3600,qmi/0.001)

```

```

function f= gac(t,y)
global a b Dma Dmi KLa A V kr phi NFD R dr r rho
a = 23;%m3/kg
b = 909;%m3/kg
rho =930;%kg/m3
Dma = 0.8*1.38e-12;%m2/sec
Dmi = 5.0*1.38e-13;%m2/sec
KLa=8.15e-5;%m/sec
A=0.0003687;%m2
V=0.0001;%m3

```

```

kr=5*0.00017; %/sec; %with reaction
%kr=0; %without reaction
phi = 0.66;
R = 0.001;%m
dr = (R/NFD);
r = 0:dr:R;

qma = y(1:NFD+1);
qmi(1:NFD+1) = y (NFD+2:2*NFD+2);
c= y(2*NFD+3);
for i=2:NFD
dqmadr(i) = (qma(i+1)-qma(i-1))/(2*dr);
dqmidr(i) = (qmi(i+1)-qmi(i-1))/(2*dr);
d2qmadr2(i) = (qma(i+1)-2*qma(i)+qma(i-1))/(dr^2);
d2qmadr2(i) = (qmi(i+1)-2*qmi(i)+qmi(i-1))/(dr^2);
end
i=1;
d2qmadr2(1)=2*(qma(2)-qma(1))/(dr)^2;
d2qmadr2(1)=2*(qmi(2)-qmi(1))/(dr)^2;

i=NFD+1;

csma = langmuir(qma(NFD+1));
csmi = langmuir(qmi(NFD+1));
dqmadr(NFD+1)= (KLa/(rho*Dma))*(c-csma);
d2qmadr2(NFD+1)= (2*qma(NFD) -
2*qma(NFD+1)+2*dr*(KLa/(rho*Dma))*(c-csma))/dr^2;
dqmidr(NFD+1)= (KLa/(rho*Dmi))*(c-csmi);
d2qmadr2(NFD+1)= (2*qmi(NFD) -
2*qmi(NFD+1)+2*dr*(KLa/(rho*Dmi))*(c-csmi))/dr^2;

i=1;
dqmadt(i)=Dma*(3*d2qmadr2(1))-kr*qma(i);
dqmidt(i)=Dmi*(3*d2qmadr2(1));

for i=2:NFD+1
dqmadt(i) = Dma*(d2qmadr2(i) + (2/r(i))*dqmadr(i))-
kr*qma(i);
dqmidt(i) = Dmi*(d2qmadr2(i) + (2/r(i))*dqmidr(i));
end

```

```

cs= phi*csma+(1-phi)*csmi;
dcdt = -(KLa/V)*(c-cs)*A;
f(1:NFD+1)= dqmadt(1:NFD+1);
f(NFD+2:2*NFD+2)= dqmidt(1:NFD+1);
f(2*NFD+3)= dcdt;
f=f';

```

```

function cs = langmuir(qs)
global a b Dma Dmi KLa A V kr phi NFD R dr r rho
cs =qs/(a-b*qs);

```

```

function R2 = rsq(X,Y)
mX=mean(X);
mY=mean(Y);
R2num=sum((X-mX).*(Y'-mY));
R2den=sum((X-mX).^2)*sum((Y'-mY).^2);
R2=R2num/sqrt(R2den);

```

V.2 MB and SO binary adsorption surface – pore diffusion mathematical modeling

```
function [t q c]=fun()
global D1 D2 KLa1 KLa2 A V NFD R dr r rho cinit1 cinit2
NFD = 50;
q1(1:NFD+1)= 0;
q2(1:NFD+1)= 0;
cinit1= 0.005;%kg/m3
cinit2= 0.005;%kg/m3
tspan = [0,7*3600];
%Without reaction...
texpt=[0 1 2 3 4 5 6 7];
c1expt=0.001 * [5,3.3,2.8,2.3,2.0,1.6,1.0,1.0];
c2expt=0.001*[5,4.4,3.7,3.3,3.0,2.6,2.0,1.8];

yinit = [q1 q2 cinit1 cinit2];
sol= ode15s(@gac,tspan,yinit);
t=0:tspan(2)/100:tspan(2);
y=deval(sol,t);y=y';

tRSQ=texpt*3600;
yRSQ=deval(sol,tRSQ);yRSQ=yRSQ';

q1= y(:,1:NFD+1);
q2= y(:,NFD+2:2*NFD+2);
c1= y(:,2*NFD+3);
c2=y(:,2*NFD+4);
c1RSQ=yRSQ(:,2*NFD+3);
c2RSQ=yRSQ(:,2*NFD+4);
R2FORc1=rsq(c1expt,c1RSQ)
R2FORc2=rsq(c2expt,c2RSQ)

figure(1),plot(texpt,c1expt./0.001,'o',t/3600,c1./0.001
),title('Adsorption of MB'),xlabel('Time,
h'),ylabel('MB concentration, mg/L');
figure(2),plot(texpt,c2expt./0.001,'o',t/3600,c2./0.001
),title('Adsorption of SO'),xlabel('Time,
h'),ylabel('SO concentration, mg/L');

figure(3),surf(r*1000,t/3600,q1/0.001)
```

```

title('q1(r,t)')
colormap(hsv)
xlabel('Radial distance, mm')
ylabel('Time, h')
zlabel('q1, mg/g')

figure(4), surf(r*1000,t/3600,q2/0.001)
title('q2(r,t)')
colormap(hsv)
xlabel('Radial distance, mm')
ylabel('Time, h')
zlabel('q2, mg/g')

figure(5)
plot(r*1000,q1/0.001),ylabel('q1, mg/g'),xlabel('Radial
distance, mm')

figure(6)
plot(r*1000,q2/0.001),ylabel('q2, mg/g'),xlabel('Radial
distance, mm')

figure(7)
plot(t/3600,q1/0.001),ylabel('q1, mg/g'),xlabel('Time,
h')

figure(8)
plot(t/3600,q2/0.001),ylabel('q2, mg/g'),xlabel('Time,
h')

function f= gac(t,y)
global D1 D2 KLa1 KLa2 A V NFD R dr r rho cinit1 cinit2
rho =930;%kg/m3

D1 = 2.2e-11;%m2/sec
D2 = 1.9e-11;%m2/sec;
KLa1 = 5.9e-5;%m/sec
KLa2 = 3.0e-5;%m/sec

A=0.0003687*40/100;%m2
V=0.0001;%m3
R = 0.001;%m

```

```

m=40*1e-6; %kg
dr = (R/NFD);
r = 0:dr:R;
qlavginit=0;

q1(1:NFD+1) = y(1:NFD+1);
q2=y(NFD+2:2*NFD+2);
c1=y(2*NFD+3);
c2=y(2*NFD+4);

for i=2:NFD
dq1dr(i) = (q1(i+1)-q1(i-1))/(2*dr);
dq2dr(i) = (q2(i+1)-q2(i-1))/(2*dr);
d2q1dr2(i) = (q1(i+1)-2*q1(i)+q1(i-1))/(dr^2);
d2q2dr2(i) = (q2(i+1)-2*q2(i)+q2(i-1))/(dr^2);
end
i=1;
d2q1dr2(1)=2*(q1(2)-q1(1))/(dr)^2;
d2q2dr2(1)=2*(q2(2)-q2(1))/(dr)^2;

i=NFD+1;

cs = NewtonRaphson([q1(NFD+1), q2(NFD+1)], [c1,c2]);
dq1dr(NFD+1)= (KLa1/(rho*D1))* (c1-cs(1));
dq2dr(NFD+1)= (KLa2/(rho*D2))* (c2-cs(2));
d2q1dr2(NFD+1)= (2*q1(NFD) -
2*q1(NFD+1)+2*dr*(KLa1/(rho*D1))* (c1-cs(1)))/dr^2;
d2q2dr2(NFD+1)= (2*q2(NFD) -
2*q2(NFD+1)+2*dr*(KLa2/(rho*D2))* (c2-cs(2)))/dr^2;

i=1;
dq1dt(i)=D1*(3*d2q1dr2(1));
dq2dt(i)=D2*(3*d2q2dr2(1));

for i=2:NFD+1
dq1dt(i) = D1*(d2q1dr2(i) + (2/r(i))*dq1dr(i));
dq2dt(i) = D2*(d2q2dr2(i) + (2/r(i))*dq2dr(i));
end

dc1dt = -(KLa1/V)*(c1-cs(1))*A;
dc2dt = -(KLa2/V)*(c2-cs(2))*A;

```

```

f(1:NFD+1)= dq1dt(1:NFD+1);
for i=1:NFD+1
    f(NFD+1+i)=dq2dt(i);
end

f(2*NFD+3)= dc1dt;
f(2*NFD+4)=dc2dt;
f=f';

function cs=NewtonRaphson(qsgiven,csguess)
cs=csguess;
Niter=50;
for i=1:Niter
qs = Freundlich(cs);
dqsdcs = DerivFreundlich(cs);
F=qs-qsgiven;
Jac=[dqsdcs(1,1), dqsdcs(1,2);dqsdcs(2,1),dqsdcs(2,2)];
dcs=-0.1*inv(Jac)*F';
csnew=cs+dcs';
csnew(1)=max(0,csnew(1));
csnew(2)=max(0,csnew(2));
cs=csnew;
end

function dqsdcs = DerivFreundlich(cs)
change=1e-7;
csnew(1)=cs(1)+change;
csnew(2)=cs(2);
qs=Freundlich(cs);
qsnew=Freundlich(csnew);
dqsdcs(1,1) = (qsnew(1)-qs(1))/change;
dqsdcs(2,1) = (qsnew(2)-qs(2))/change;
csnew(1)=cs(1);
csnew(2)=cs(2)+change;
qsnew=Freundlich(csnew);
dqsdcs(1,2)=(qsnew(1)-qs(1))/change;
dqsdcs(2,2)=(qsnew(2)-qs(2))/change;

function qs = Freundlich(cs)
%For binary system
cs=1000*cs; %To convert kg/m3 to mg/L

```

```

KF1=18.34;
KF2=13.805;
n1=0.43;
n2=0.18;
x1=1.666;
x2=-0.318;
y1=1.071;
y2=0.815;
z1=1.553;
z2=-0.901;
qs(1)=KF1*cs(1)^(n1+x1)/(cs(1)^x1 + y1*cs(2)^z1);
qs(2)=KF2*cs(2)^(n2+x2)/(cs(2)^x2 + y2*cs(1)^z2);
qs=qs*0.001;%To convert mg/g to kg/kg

```

```

function R2 = rsq(X,Y)
mX=mean(X);
mY=mean(Y);
R2num=sum((X-mX).*(Y'-mY));
R2den=sum(((X-mX).^2))*sum(((Y'-mY).^2));
R2=R2num/sqrt(R2den);

```

V.3 MB and SO binary reactive adsorption surface – pore diffusion mathematical modeling

```

function [t q1 q2 c1 c2]=fun_binary_RA()
global D1 D2 KLa1 KLa2 A V kr NFD R dr r rho cinit1
cinit2
NFD = 50;
q1(1:NFD+1)= 0;
q2(1:NFD+1)= 0;
cinit1= 0.005;%kg/m3
cinit2= 0.005;%kg/m3
tspan = [0,7*3600];

%With reaction...
texpt=[0 1 2 3 4 5 6 7];
clexpt=0.001*[5,3.294,2.430,1.403,0.687,0.468,0.341,0.189];

```

```
c2expt=0.001*[5,3.746,2.996,2.097,1.331,0.987,0.763,0.500];
```

```
yinit = [q1 q2 cinit1 cinit2];  
sol= ode15s(@gac,tspan,yinit);  
t=0:tspan(2)/100:tspan(2);  
y=deval(sol,t);y=y';
```

```
tRSQ=texpt*3600;  
yRSQ=deval(sol,tRSQ);yRSQ=yRSQ';
```

```
q1= y(:,1:NFD+1);  
q2= y(:,NFD+2:2*NFD+2);  
c1= y(:,2*NFD+3);  
c2=y(:,2*NFD+4);  
c1RSQ=yRSQ(:,2*NFD+3);  
c2RSQ=yRSQ(:,2*NFD+4);  
R2FORc1=rsq(c1expt,c1RSQ)  
R2FORc2=rsq(c2expt,c2RSQ)
```

```
figure(1),plot(texpt,c1expt./0.001,'o',t/3600,c1./0.001),  
title('Reactive adsorption of MB'),xlabel('Time, h'),  
ylabel('MB concentration, mg/L');  
figure(2),plot(texpt,c2expt./0.001,'o',t/3600,c2./0.001),  
title('Reactive adsorption of SO'),xlabel('Time, h'),  
ylabel('SO concentration, mg/L');
```

```
figure(3),surf(r*1000,t/3600,q1/0.001)  
title('q1(r,t)')  
colormap(hsv)  
xlabel('Radial distance, mm')  
ylabel('Time, h')  
zlabel('q1, mg/g')
```

```
figure(4),surf(r*1000,t/3600,q2/0.001)  
title('q2(r,t)')  
colormap(hsv)  
xlabel('Radial distance, mm')  
ylabel('Time, h')  
zlabel('q2, mg/g')
```

```

function f= gac(t,y)
global D1 D2 KLa1 KLa2 A V kr NFD R dr r rho cinit1
cinit2
rho =930;%kg/m3

D1 = 2.2e-11;%m2/sec
D2 = 1.9e-11;%m2/sec;
KLa1 = 1.5*5.9e-5;%m/sec
KLa2 = 2*3.0e-5;%m/sec
kr1 = 5*0.000123; %/sec, with reaction
kr2 = 5*0.000083; %/sec, with reaction

A=0.0003687*40/100;%m2
V=0.0001;%m3
R = 0.001;%m
m=40*1e-6; %kg
dr = (R/NFD);
r = 0:dr:R;
qlavginit=0;

q1(1:NFD+1) = y(1:NFD+1);
q2=y(NFD+2:2*NFD+2);
c1=y(2*NFD+3);
c2=y(2*NFD+4);

for i=2:NFD
dq1dr(i) = (q1(i+1)-q1(i-1))/(2*dr);
dq2dr(i) = (q2(i+1)-q2(i-1))/(2*dr);
d2q1dr2(i) = (q1(i+1)-2*q1(i)+q1(i-1))/(dr^2);
d2q2dr2(i) = (q2(i+1)-2*q2(i)+q2(i-1))/(dr^2);
end
i=1;
d2q1dr2(1)=2*(q1(2)-q1(1))/(dr)^2;
d2q2dr2(1)=2*(q2(2)-q2(1))/(dr)^2;

i=NFD+1;

cs = NewtonRaphson([q1(NFD+1), q2(NFD+1)], [c1,c2]);

dq1dr(NFD+1)= (KLa1/(rho*D1))*(c1-cs(1));
dq2dr(NFD+1)= (KLa2/(rho*D2))*(c2-cs(2));

```

```

d2q1dr2(NFD+1) = (2*q1(NFD) -
2*q1(NFD+1) + 2*dr*(KLa1/(rho*D1))*(c1-cs(1)))/dr^2;
d2q2dr2(NFD+1) = (2*q2(NFD) -
2*q2(NFD+1) + 2*dr*(KLa2/(rho*D2))*(c2-cs(2)))/dr^2;

```

```

i=1;
dq1dt(i)=D1*(3*d2q1dr2(1))-kr1*q1(i);
dq2dt(i)=D2*(3*d2q2dr2(1))-kr2*q2(i);

```

```

for i=2:NFD+1
dq1dt(i) = D1*(d2q1dr2(i) + (2/r(i))*dq1dr(i)) -
kr1*q1(i);%with reaction
dq2dt(i) = D2*(d2q2dr2(i) + (2/r(i))*dq2dr(i)) -
kr2*q2(i);%with reaction
end

```

```

dc1dt = -(KLa1/V)*(c1-cs(1))*A;
dc2dt = -(KLa2/V)*(c2-cs(2))*A;
f(1:NFD+1) = dq1dt(1:NFD+1);
for i=1:NFD+1
    f(NFD+1+i) = dq2dt(i);
end

```

```

f(2*NFD+3) = dc1dt;
f(2*NFD+4) = dc2dt;
f=f';

```

```

function cs=NewtonRaphson(qsgiven,csguess)
cs=csguess;
Niter=100;
for i=1:Niter
qs = Freundlich(cs);
dqsdcs = DerivFreundlich(cs);
F=qs-qsgiven;
Jac=[dqsdcs(1,1), dqsdcs(1,2);dqsdcs(2,1),dqsdcs(2,2)];
dcs=-0.1*inv(Jac)*F';
csnew=cs+dcs';
csnew(1)=max(0,csnew(1));
csnew(2)=max(0,csnew(2));
cs=csnew;

```

end

```
function dqsdcs = DerivFreundlich(cs)
change=1e-7;
csnew(1)=cs(1)+change;
csnew(2)=cs(2);
qs=Freundlich(cs);
qsnew=Freundlich(csnew);
dqsdcs(1,1) = (qsnew(1)-qs(1))/change;
dqsdcs(2,1) = (qsnew(2)-qs(2))/change;
csnew(1)=cs(1);
csnew(2)=cs(2)+change;
qsnew=Freundlich(csnew);
dqsdcs(1,2)=(qsnew(1)-qs(1))/change;
dqsdcs(2,2)=(qsnew(2)-qs(2))/change;
```

```
function qs = Freundlich(cs)
%For binary system
cs=1000*cs; %To convert kg/m3 to mg/L
KF1=18.34;
KF2=13.805;
n1=0.43;
n2=0.18;
x1=1.666;
x2=-0.318;
y1=1.071;
y2=0.815;
z1=1.553;
z2=-0.901;
qs(1)=KF1*cs(1)^(n1+x1)/(cs(1)^x1 + y1*cs(2)^z1);
qs(2)=KF2*cs(2)^(n2+x2)/(cs(2)^x2 + y2*cs(1)^z2);
qs=qs*0.001;%To convert mg/g to kg/kg
```

```
function R2 = rsq(X,Y)
mX=mean(X);
mY=mean(Y);
R2num=sum((X-mX).*(Y'-mY));
R2den=sum(((X-mX).^2))*sum(((Y'-mY).^2));
R2=R2num/sqrt(R2den);
```

Publications

Article(s) published in journal

- *Sharma, K., Dalai, A.K., Vyas, R. K. (2017). Removal of synthetic dyes from multicomponent industrial wastewaters, Reviews in Chemical Engineering, 34 (1), 107 – 134.*
- *Sharma, K., Vyas, R. K., Dalai, A.K. (2017). Thermodynamic and kinetic studies of Methylene Blue degradation using reactive adsorption and its comparison with adsorption, Journal of Chemical & Engineering Data, 62 (11), 3651-3662.*

Article(s) in conference(s)

- *Sharma, K., Vyas, R. K. (2015). Adsorption of multicomponent dye mixture: a brief review, accepted for oral presentation, CHEMCON-2015, December 27-30, 2015, held at India institute of technology Guwahati, India.*

Allied article(s) in conference(s)

- *Sharma, K., Vyas, R. K., Vyas, A., Singh, S. K. (2015). Conversion of waste PVC into fuel: a brief review, accepted for oral presentation, CHEMCON-2015, December 27-30, 2015, held at India institute of technology Guwahati, India.*
- *Sharma, K., Vyas, A., Vyas, R. K. (2016). Conversion of Lignocellulosic Biomass (Water Hyacinth) into Levulinic Acid, accepted for oral presentation, CHEMCON-2016, December 27-30, 2016, held at Chennai Regional Centre of IChE, Chennai, India.*
- *Kumar, P., Sharma, K., Vyas, R. K. (2016). Adsorptive Removal of Lamivudine From Its Aqueous Solution Using Granular Activated Carbon, accepted for poster presentation, CHEMCON-2016, December 27-30, 2016, held at Chennai Regional Centre of IChE, Chennai, India.*

Article(s) to be communicated to journals shortly

- *Sharma, K., Vyas, R. K., Singh, K., Dalai, A.K., Gupta, V. K. (2017). Reactive adsorption of Safranin O: Modeling, batch experimental, and degradation studies, to be communicated.*
- *Sharma, K., Vyas, R. K., Dalai, A.K. (2017). Degradation of binary dye mixture using reactive adsorption: Kinetic and thermodynamic studies, to be communicated.*
- *Sharma, K., Vyas, R. K., Singh, K., Dalai, A.K. (2017). Surface pore diffusion modeling of binary dye mixture using adsorption and reactive adsorption onto metal oxide coated GAC, to be communicated.*

Komal Sharma, Ajay K. Dalai and Raj K. Vyas*

Removal of synthetic dyes from multicomponent industrial wastewaters

DOI 10.1515/revce-2016-0042

Received September 23, 2016; accepted December 23, 2016

Abstract: Colored effluents containing dyes from various industries pollute the environment and pose problems in municipal wastewater treatment systems. Industrial effluents consist of a mixture of dyes and require study of the simultaneous removal of dyes. Simultaneous quantification of dyes in the solution is a common problem while using a spectrophotometric method due to overlapping of their absorption spectra. Derivative spectroscopy and chemometric methods in spectrophotometric analysis facilitate simultaneous quantification of dyes. Adsorption is a widely used treatment method for the removal of a mixture of recalcitrant dyes in industrial wastewaters. Confirming the assertion, this paper presents a state-of-the-art review on methods used for simultaneous quantification of dyes and the effects of various parameters on their adsorptive removal. This paper also reviews the adsorption equilibrium, modeling, mechanisms of dyes adsorption, and adsorbent regeneration techniques in multicomponent dye systems. It has been observed that chemometric techniques provide accuracy, repeatability, and high speed in processing and helps in better operability in real wastewater treatment plants. The conclusions include the need for the development of thermodynamic models that can predict simultaneous physisorption and chemisorption exhibited by different dyes and to develop isotherm models that can describe chemisorption of a mixture of dyes. The paper delves into inadequately researched gray areas of adsorption of a mixture of dyes which require the development of modified adsorption methods that serves process intensification for complete degradation/mineralization.

Keywords: chemometric methods in spectrophotometric analysis; mathematical modeling; mechanism; multicomponent dye mixture adsorption; parameters.

*Corresponding author: **Raj K. Vyas**, Department of Chemical Engineering, Malaviya National Institute of Technology, Jaipur 302017, India, e-mail: rkvyas2@gmail.com

Komal Sharma: Department of Chemical Engineering, Malaviya National Institute of Technology, Jaipur 302017, India

Ajay K. Dalai: Department of Chemical and Biological Engineering, University of Saskatchewan, Saskatoon, Canada

1 Introduction

Dyes are chemicals that, on binding with a material, give color to the material. Dyes are ionic, aromatic organic molecules with structures including aryl rings that have delocalized electron systems (Allen et al. 2004). They have been extensively used in many industries, such as textile, leather tanning, paper production, food industry, hair colorings, etc. (Gürses et al. 2016). It has been predicted that the global textile market was of US\$1557.1 billion with a production of more than 88.5 million tons per year until the end of 2015. The share of developing countries in the global textile market has risen to account for 58.6% in terms of cost within last decade (Yacout et al. 2016). Most of the dyes used in textile processing are lacking in complete fixation of dyes to fabrics, and thus, 20% of dyes enter the environment, which produces dye-containing colored effluents (Nadejde et al. 2015). Of current world production of dyestuffs of about 10 million kg per year, approximately 2 million kg of active dye per year enter the biosphere, either in the dissolved or suspended form in water (Allen et al. 2003). Even at very low concentration, the presence of dye in water is highly visible. The intensity of the color of a dye depends upon the number of functional groups present as its chromophore (Verma et al. 2012). The dye-polluted wastewater is characterized by high biochemical and chemical oxygen demands (Liu et al. 2014, Ghaedi et al. 2015). The presence of dyes in wastewater reduces sunlight penetration and resists photochemical action, which creates problems in maintaining ecological balance. Their carcinogenic and toxic nature causes damage to living organisms (Wong et al. 2004, Sharma and Vyas 2015). Due to large-scale production, extensive application, and uncontrolled discharge into water bodies, synthetic dyes cause considerable environmental pollution and may impact serious health-risk factors. The inflow of dye industrial effluents into the natural water bodies results in acute toxicity to aquatic life (Verma 2008). Hitherto, various methods like adsorption, hydrodynamic cavitation, photocatalytic decolorization, microbiological decomposition, etc., for the treatment of dye containing wastewater have been practiced (Slokar and Majcen Le Marechal 1998, Forgacs

et al. 2004, Chakraborty and Gupta 2013, Gupta et al. 2015b, Rajoriya et al. 2017). Among these, adsorption is one of the most powerful and extensively used techniques for the removal of various forms of wastewater contaminants, due to simplicity of operation and cost together with availability of a wide variety of adsorbents (Chan et al. 2012b, Sharma et al. 2013).

A number of studies have focused on the sorption behavior of dyes in single component dye system by various sorbents (Isa et al. 2007, Olgun and Atar 2009), though industrial dye effluents usually contain a number of dyes. In a mixture of dyes, quantification of one dye is interfered by the presence of the other. Thus, simultaneous quantification of dyes in an aqueous solution has remained a challenge. Several studies are available in the literature dealing with quantification of dyes in a mixture elucidating different aspects (Zeinali et al. 2014, Zolgharnein et al. 2014a, 2015). Multisolute sorption systems have received scarce attention compared to single solute systems due to complex behavior and competitive and/or synergic effect of solutes present in the system. First experimental results on the removal of the binary mixture were presented by Kolthoff and van der Goot (1929) and treatment of ternary system was reported by McKay and Al-Duri (1987).

Several other studies are available on the simultaneous removal of dyes and heavy metals from a mixture (Kyzas et al. 2013, 2015). Adsorption in fixed beds (Walker and Weatherley 1997), membrane systems (Khani et al. 2015), and photocatalytic degradation (Gupta et al. 2006, Gözmen et al. 2009, Andronic and Duta 2012) are a few methods for the simultaneous removal of a mixture of dyes.

Reviews on various techniques used for decolorization of the mixture of dyes (Gupta et al. 2015a) and applicable isotherm models for multicomponent adsorption of dyes (Noroozi and Sorial 2013) are available. To our knowledge, to date, there is a lack of a detailed review on adsorption of multicomponent dye mixture from wastewater. Similarly, simultaneous quantitative detection of dyes in a mixture and the effect of parameters during adsorptive removal of dyes have not been reviewed.

In the present review, derivative spectrophotometric and chemometric-based methods used for simultaneous quantitative analysis of a multicomponent mixture of dyes present in the aqueous solution have been presented. This review is an attempt to summarize the significant contributions made so far in this area with particular reference to batch adsorptive treatment. This article also covers various isotherm models that represent equilibrium data for a specific adsorbate-adsorbent

system of a dye mixture and discusses the effects of parameters on selective adsorption in multicomponent dye mixtures. Besides, it also focuses on studies on the mechanism of simultaneous adsorption of a binary mixture of dyes and adsorbent regeneration. It further critically analyzes gray areas that need to be studied in order to make this treatment technology commercially attractive. The review will help researchers to access a comprehensive literature on techniques being used for quantification of dyes, adsorption of multicomponent dye mixture, and future perspectives on quantification, isotherms, modeling and degradation/mineralization for adsorptive removal.

2 Quantitative determination of dyes in a multicomponent mixture

Quantitative methods for a multicomponent mixture are based on the principle that the absorbance at any wavelength of a multicomponent mixture is equal to the sum of the absorbance of each component in the mixture at that wavelength. The simple approach for the analysis of solutes present in a multicomponent mixture is based on the measurements at a number of wavelengths equal to the number of components in the mixture. Usually, the selected wavelengths are those of the absorbance maximum of each component (Nateri and Ekrami 2009).

Measurements of dye concentrations present in binary and ternary aqueous systems using spectrophotometry are reported in the literature. Equations obtained with absorbance values and calibration constants at respective wavelengths of solutes can be solved easily in MATLAB by converting them into matrices (Mahmoodi et al. 2010, 2011a, Mahmoodi 2014a). Nevertheless, spectrophotometry is not selective and requires the solutes present in a sample to have different absorption spectrum with low overlapping (An et al. 2010, Issa et al. 2014).

Derivative techniques and multivariate methods in chemometrics play an important role in the analysis of solutes present in mixtures using UV-vis molecular absorption spectrophotometry. These approaches are useful in the resolution of band overlapping in quantitative analysis. It has been proved that derivative technique is very useful in the resolution of sample binary mixtures of dyes whereas multivariate calibration (MVC) has been found to be the method of choice for more complex mixtures (Nevado et al. 1999).

2.1 Derivative spectroscopy

UV-vis absorption spectrophotometry is a widely used analytical method for quantitative analysis due to its low cost, speed, and simplicity of measurements. In addition, this method requires the analytes present in a given sample to have different absorption spectrum with low overlapping; thus, its applications in a multicomponent system are limited (An et al. 2010, Hemmateenejad et al. 2014). A number of studies are available in the literature for measuring the concentration of dyes present in multicomponent mixtures with simple (Al-Degs et al. 2007) to more advanced (Gao et al. 2011) spectrophotometric techniques. The selection of the analytical method is dependent on the extent of spectral overlap between solutes or the presence of a complex matrix. It is important to use a suitable method for accurate solute quantification in multisolute systems due to the complexity of real matrices or high spectral/chromatographic overlap (Issa et al. 2014). Figure 1 shows the spectral overlap of Acid Blue 25 and Direct Blue 86 (Douissa et al. 2014).

Derivative spectrophotometry resolves the problem of quantification of solutes present in a mixture due to overlapping. This advanced modern spectrophotometric technique is based on derivative spectra, which are generated from parent zero-order spectrum. The derivatization

of zero-order spectra enhances the selectivity for a compound and reduces the disturbance caused by the presence of other compounds in a sample. Hence, concentrations of dye present in mixtures can be determined by measuring the absorbance signal at the first-order derivative wavelength. This method does not require any prior separation or purification step before carrying out quantification of analytes (Karpińska 2004).

The derivative form of Beer's law is as follows:

$$D^n = \frac{d^n A}{d\lambda^n}, \quad (1)$$

where D is the value of derivative of n -order at wavelength λ .

The derivative spectrum of a mixture is the sum of derivative spectra of each individual component as per the additivity law:

$$D_{\text{mix}}^n = D_1^n + D_2^n + \dots + D_x^n, \quad (2)$$

where the value of n -order derivative of a mixture at analytical wavelength $D_1^n, D_2^n, \dots, D_x^n$ are the values of n -order derivative at analytical wavelength of 1st, 2nd, ..., x th elements of mixture. This allows the determination of several components (x) in a mixture by measuring the amplitude of derivative spectrum of a mixture at several (minimum x) wavelengths (Karpińska 2004).

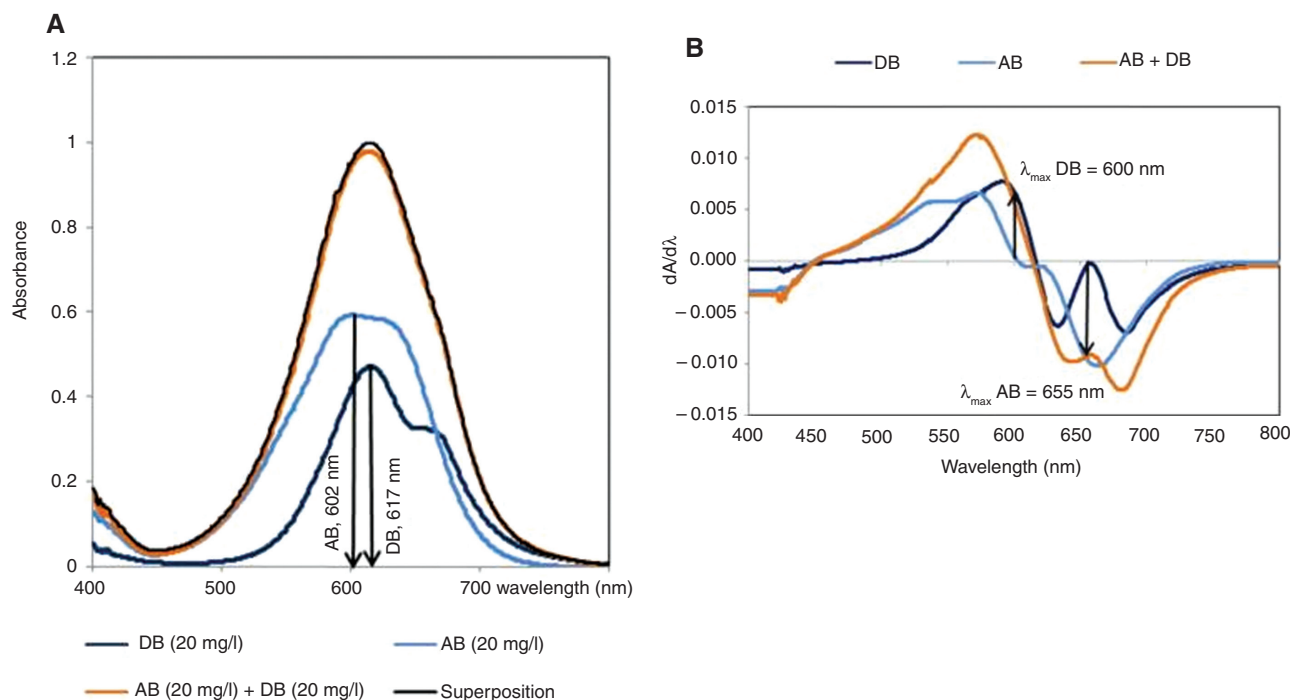


Figure 1: Spectral overlap of Acid Blue 25 (AB) and Direct Blue 86 (DB) in single and binary solutions.

(A) Zero order absorption spectra and (B) First order derivative spectra. Reprinted from Douissa et al. (2014), with permission from Elsevier.

According to the “zero-crossing technique” for simultaneous determination of analytes present in a sample, the measurement height of the derivative peak of an analyte is performed at those wavelengths at which spectra of other components has a zero or near-zero value; the measured amplitude is proportional only to a concentration of assayed compounds (Turabik 2008). It is necessary that zero-crossing wavelengths do not change with the varied concentrations of related species (Zolgharnein et al. 2015). The best linear responses are obtained using zero-crossing technique and the calibration graphs are less affected by the concentration of other components (Gao et al. 2010). Andronic and Duta (2012) developed a simple, sensitive, and selective model for simultaneous analysis of two dyes in solutions using a first-order derivative spectrophotometric method that used to overcome the spectral overlapping.

Dependence on instrumental parameters, nonrobust properties of the derivatization parameters, and lack of homogeneous protocol of optimization the parameters of the method and presentation of results are disadvantages of derivative spectroscopy (Karpińska 2004).

2.2 Spectrophotometry using chemometric methods

The introduction of computer and statistical techniques into chemistry helps to resolve analytical problems for much more complex samples. Chemometrics combine chemistry with the computer, which facilitates workers to resolve the constituents of a complex system without using a pre-separation step (An et al. 2010, Hemmateenejad et al. 2014). Chemometric methods provide analysis and quantification of analytes in complex matrices even without any prior knowledge about their chemical substances (Gholami et al. 2016). Figure 2 shows the flowchart of a quantitative chemometric method. For applying these techniques, absorbance data matrix and concentration data matrix for prediction of the unknown concentrations of solutes in their mixture can be obtained using zero-to-fourth-order derivative absorption spectra.

Chemometrics employ the multivariate curve resolution–alternating least square technique to analyze

spectroscopic data of evolutionary processes in order to extract information about a number of chemical species involved in the system along with their concentration profiles and pure spectra of species. This provides a platform to perform adsorption of multi solutes from wastewater systems (An et al. 2010, Hemmateenejad et al. 2014). Multivariate quantification methods like multilinear regression (MLR), principal component regression (PCR), and partial least squares (PLS1) can resolve the problem of spectrum overlapping or complex matrices which is normally observed in analytical chemistry (Al-Degs et al. 2008, Al-Degs and Sweileh 2012, Gholami et al. 2016). Issa et al. (2014) presented the algorithms for MLR, PCR, and PLS. Details on algorithms of MLR, PCR, and PLS1 could be found from literature (Brereton 2003). MVC methods minimize/eliminate sample preparation and avoid application of tedious chromatographic or electrochemical methods (Al-Degs et al. 2008, Al-Degs and Sweileh 2012). PLS is preferable to conventional PCR for data processing as the information from the calibration solution is better used as it reflects a criterion of the similarity of the sample to the calibration set. PLS uses both spectral and concentration data, unlike PCR, in which the data decomposition is conducted only using the spectral information (An et al. 2010).

PLS can provide a robust regression model, which requires a large number of calibration and test sets and all analytes and interferences have to be in the calibration set at the appropriate concentration level. PLS and related chemometric methods require previous knowledge of all components in the samples, but identification of all components in complex matrices is impractical and time-consuming. Second-order or higher-order data analysis is used for quantification of analytes even in the presence of unmodeled or uncalibrated interferences. Second-order MVC methods were successfully applied for three-way array of data that is obtained by stacking the data matrices of different samples under each other (Gholami et al. 2016). Al-Degs and Sweileh (2012) developed a simple and sensitive spectrophotometric method for the simultaneous determination of five dyes using solid-phase extraction. They developed a model by using calibration set, while the effectiveness of the proposed model for prediction was tested in the validation set. A large number of calibration



Figure 2: Quantitative chemometric methods (Nevado et al. 1999).

samples are necessarily required due to the high spectral overlap between the dyes present in a mixture (Al-Degs and Sweileh 2012). The PLS, PCR, and MLS methods often suffer in much more complex practice during a calibration process.

Artificial neural network (ANN) is able to solve complex structure consists of highly nonlinear process. ANN is a flexible model and often robust with respect to input noise (Himmelblau 2008, Pirdashti et al. 2013). Zeinali et al. (2014) combined second-order derivative spectrophotometry and principal component analysis-ANN model (PCA-ANN) for accurate and reproducible determination of competitive nature of a binary dye mixture during the adsorption process. The PCA-ANN model was used to minimize the dimensionality of large data sets by reducing the number of spectral data, which enables it to predict the concentrations of both dyes in the mixtures (Zeinali et al. 2014). ANN models suffer with some problems, like overfitting of data, requirements for selecting the number of hidden nodes hidden layers, adjustment of parameters containing weights and biases, etc., which may lead to unreliability of the method. Support vector machine (SVM), a novel neural network algorithm, has distinct advantages when compared to ANN (Abdi et al. 2014). The problem of overfitting is unlikely to occur with SVM as it provides a global optimum solution rather than local as in other neural network models (Kim 2003). The concept of SVM was introduced by Vapnik in 2000 as a supervised learning algorithm.

Although SVM has an outstanding performance for solving static function approximation problems, it has a higher computational load (Wang and Hu 2005). In an effort to minimize the complexity of SVM and also to enhance its speed of convergence, Suykens and Vandewalle (1999) proposed a modified version of SVM, called least squares SVM (LS-SVM). Abdi et al. (2014) compared SVM and LS-SVM. Table 1 shows some good features of LS-SVM over SVM. They found the LS-SVM more reliable and applied it to predict dye removal efficiency in a ternary mixture of dyes. It is reported that the novel intelligent model (LS-SVM) was capable of simulating the actual physical trend of the dye removal efficiency with variation

of adsorbent dosage and initial dye concentration in single and ternary mixture systems (Abdi et al. 2014).

SVM-based methods also have some drawbacks. The limitation of an SVM-based method is that it is largely characterized by the choice of its kernel. Discrete data presentation and reduced speed and size, both in training and testing, are also additional limitations (Borges 1998). Table 2 summarizes the methods used by various researchers for simultaneous quantification of a mixture of dyes present in the wastewater system.

Derivative techniques under computer-controlled instrumentation and MVC methods using chemometrics both play a very useful role in the resolution of band overlapping in quantitative analysis of multicomponent mixtures by UV-vis molecular absorption spectrophotometry (Nevado et al. 1999, Andronic and Duta 2012). The derivative spectrophotometric method has been used due to its economic, facile, and simple approach, whereas chemometric methods simultaneously determine components present in a mixture with speed, precision, and accuracy. Chemometrics avoid preliminary separation step (Nevado et al. 1999, Ghaedi et al. 2014, Zolgharnein et al. 2015).

A method impending should provide accuracy and precision to estimated experimental values in order to achieve the definite concentration of the solutes present in the mixtures. It has indicated that the method used for quantification of dyes should has minimum discrepancy (between the known and predicted concentration data) to propagate toward accurate experimental outcome (Zeinali et al. 2014). Apart from discrepancy, the availability of a compatible system and its thorough knowledge are also necessary criteria of selection of a suitable method.

3 Effects of various parameters on adsorptive removal of dyes from multicomponent systems

In practice, normally, the wastewater is a mixture of several dyes rather than a single one and during adsorption; the solutes compete with each other for adsorption.

Table 1: Comparison between SVM and LS-SVM techniques (Abdi et al. 2014).

Particulars	SVM	LS-SVM
Static function approximation problem solving	Higher computational burden, owing to required constraint optimization programming	Good speed of convergence
Formulation	Equality constraints	Inequality constraints
Optimum solution	Linear equations (linear programming)	Quadratic programming problem
Function approximation	Uses all samples	Selects some sparse support vectors

Table 2: Method used for simultaneous quantification of dyes.

Dyes	Methods	Remark(s)	Reference
Methylene blue and malachite green	PLS as a MVC	Minimize/eliminate sample preparation and to avoid applying tedious chromatographic or electrochemical methods	Issa et al. (2014)
Methylene blue and brilliant green	1. Second order derivative spectrophotometric	Results displayed that the performance of derivative spectrophotometric method was better than the PCA-ANN model	Zeinali et al. (2014)
Acid Blue 25 and Direct Blue 86	2. ANN and PCA First order derivative spectrophotometric	–	Douissa et al. (2014)
Acid Red 14 and Reactive Red 15	PLS regression as a MVC	PLS uses both spectral and concentration data, but in PCR, the data decomposition is conducted using only the spectral information	Gao et al. (2011)
Direct Blue 78, Direct Red 79, and Direct Yellow 106	Colorimetric algorithm	Colorimetric algorithm achieves the lowest average ternary relative error when compared with Beer's law. Colorimetric algorithm decreases the effect of wavelength shifting on recipe prediction performance	Shams-Nateri (2011)
Brilliant green and methylene blue	Fifth and fourth order derivative spectrophotometric	–	Ghaedi et al. (2013)
Basic Yellow 28 and Basic Red 46	First order derivative spectrophotometric	–	Turabik (2008)

The interactions among these compounds may mutually enhance or mutually inhibit adsorption capacity (Ho and McKay 1999). Generally, a mixture of different adsorbates present in wastewater may exhibit three possible types of adsorption behavior: synergism (the effects of the mixture is to enhance the adsorption capacity than that of each of the individual adsorbates in the mixture), antagonism (the effect of the mixture is to reduce the adsorption capacity than that of each of the individual adsorbates in the mixture), and noninteraction (the mixture has no effect on the adsorption of each of the adsorbates in the mixture) (Srivastava et al. 2006). Knowledge of the magnitude of such competitive interactions among the dyes needs to model adsorbate migration toward the adsorbent surface in aqueous systems (Gutierrez and Fuentes 1993). A selected list of a mixture of dyes and adsorbents studied are summarized in Table 3.

A reduction in individual dye adsorption capacity in multisolite mixtures is common with the presence of another solute, although the extent of reduction varies with the type of dyes investigated (Al-Degs et al. 2007). Factors that affect the adsorption preference of a sorbent for different kinds of adsorbates may be related to the characteristics of the adsorption sites (e.g. functional groups, structure, surface properties, etc.), the properties of the adsorbates (e.g. ionic size, ionic weight, molecular structure, ionic nature or standard reduction potential, etc.), parameters of experimental conditions, and solution

chemistry (e.g. pH, ionic strength, etc.) (Allen et al. 1988, Turabik 2008).

To measure the extent of competition between dyes, El-Barghouthi et al. (2007) presented a parameter, known as competition factor (CF). CF is the ratio of the adsorption capacity for one dye in the presence of the other dye to the adsorption capacity for the same dye from single solute solution. CF can be used to evaluate the extent of competition between solutes (El-Barghouthi et al. 2007). Yang et al. (2011) introduced the concept of inhibition percentage to describe the competitiveness of the two dyes in a binary system. It is given as the difference between adsorption capacities in single and that in binary systems (Yang et al. 2011).

On the contrary, some adsorbates show a synergistic effect on the used adsorbent, electronic interactions, the formation of any specific bond between dye, and adsorbent surface, and the size of individual dye molecule may be responsible for such phenomenon (Wang et al. 2012a). Various factors affecting the dye adsorption in multisolite mixture systems are discussed in detail below.

3.1 Adsorbent dose

The adsorbent dose is an important parameter as it determines the capacity of an adsorbent for a given initial concentration of dye solution and in turn shows whether the process is cost-effective or not (Hajati et al.

Table 3: Dyes and adsorbents studied in multicomponent adsorption systems.

Dyes	Adsorbent (s)	Reference
Acid Yellow 117 and Acid Blue 25	Bamboo-derived activated carbon	Chan et al. (2012a)
Cibacron Black B and Cibacron Red RB	Phosphoric acid modified sawdust	Chakraborty et al. (2006)
Polar blue and polar yellow	Activated carbon	Choy et al. (1999)
Methylene blue and malachite green	Rarasaponin-bentonite	Kurniawan et al. (2012)
Methylene blue and Acid Orange 7	Methylene blue and Acid Orange 7	Liao et al. (2012)
C.I. Basic Blue 41 and C.I. Basic Red 18	Granular activated carbon and SWP	Noroozi et al. (2008)
Acid Blue 80 and Acid Yellow 117	Activated carbon	Porter et al. (1999)
Levafix Brilliant Red E-4BA and Levafix Brilliant Blue E-4BA	Microporous H-type activated carbon	El-Barghouthi et al. (2007)
Methylene blue and Safranin-O	Nickel sulfide nanoparticles loaded on activated carbon	Ghaedi et al. (2014)
Reactive Blue 4 and Acid Red 183	Multiwall carbon nanotubes	Wang et al. (2012b)
Congo red and methyl blue	Magnetic MnFe ₂ O ₄	Yang et al. (2014)
Methyl orange and bromothymol blue	Nanostructured mesoporous alumina	Yahyaie and Azizian (2014)
Methyl orange and Reactive Yellow 17		
Methyl orange and methyl violet		
Direct Green 6 and Direct Red 31	Core-shell magnetic adsorbent nanoparticle	Mahmoodi (2014b)
Direct Green 6 and Acid Red 18		
Acid Blue 80 and Acid Red 114	Activated carbon, Filtrasorb 400	Choy et al. (2000)
Acid Blue 80 and Acid Yellow 117		
Acid Red 114 and Acid Yellow 117		
Congo red and Acid Violet, and rhodamine B	Waste banana pith	Namasivayam and Kanchana (1992)
Acid Scarlet GR, Acid Turquoise Blue 2G, and Indigo Carmine	Poly-diallyldimethylammonium modified bentonite	Shen et al. (2009)
Remazol Reactive Yellow, Remazol Reactive Black, and Remazol Reactive Red	Filtrisorb 400 activated carbon (FS400)	Al-Degs et al. (2007)
Acid Green 25, Acid Black 26, and Acid Blue 7	Date stones	Mahmoodi et al. (2010)
Direct Red 31, Direct Green 6, and Acid Blue	Gemini polymeric nanoarchitecture	Abdi et al. (2014)
Methylene blue and rhodamine B	Modified waste sugarcane bagasse	Yu et al. (2015)
Methylene blue and brilliant green	Graphite oxide nanoparticle	Zeinali et al. (2014)
Methyl orange and methylene blue	Polyacrylonitrile fiber hydrothermally treated with hyperbranched polyethylenimine	Fan et al. (2015)
Direct Blue 78 and Direct Red 31	Activated carbon	Mahmoodi et al. (2011a)
Acid Blue 93 and methylene blue	Cellulose-based biosorbent	Liu et al. (2015a)
Acid Red 183 and Reactive Blue 4	Boron industry waste	Atar et al. (2011)
Disperse Red 60 and Disperse Blue 60	GAC	Sirianuntapiboon and Srisornsak (2007)
Reactive Blue 21 and Reactive Red 195	Clinoptilolite-type natural zeolite	Sismanoglu et al. (2010)
Basic Red 46 and Basic Yellow 28	Bentonite	Turabik (2008)
Methylene blue and Acid Red 183	Multiwalled carbon nanotube	Wang et al. (2012a)
Reactive Yellow 86 and Reactive Red 2	Novel composite containing silver nanoparticles (AgNPs) and COW	Yola et al. (2014)
Reactive Blue 4 and Reactive Red 4	PIPC	Vijayaraghavan and Yun (2008)
Reactive Blue 4 and Reactive Orange 16		
Reactive Blue 4 and Basic Blue 3		
Acid Orange 10 and Acid Blue 80	Husk of the mango seed	Dávila-Jiménez et al. (2009)
Acid Orange 7 and Acid Blue 324		
Acid Orange 8 and Acid Green 25		
Acid Red 1 and Acid Green 27		
Methylene orange, rhodamine B, and methylene blue	Mesoporous Cu ₂ O submicro-spheres	Liu et al. (2012)
Remazol Reactive Yellow, Remazol Reactive Black, and Remazol Reactive Red	Activated carbon Filtrasorb 400	Al-Degs et al. (2000)
Direct Fast Scarlet, Eosin Y, and Reactive Violet K-3R	Poly-(epichlorohydrin dimethylamine) modified bentonite	Kang et al. (2009)
Acid Blue 92, Direct Green 6, and Direct Red 31	Gemini polymeric nanoarchitecture	Mahmoodi et al. (2013)
Alizarin Red and Alizarin Yellow	γ-alumina	Zolgharnein et al. (2014a)
Basic Blue 3, Basic Red 22, and Basic Yellow 21	Peat	Al-Duri and McKay (1991)

2014). The increase in adsorption with the dose can be attributed to increased surface area leading to the increased rate of mass transfer, the availability of more adsorption sites for dye adsorption up to a certain limit, and then it reaches a constant value. A decrease in adsorption capacity of adsorbent may be attributed to overlapping or aggregation of adsorption sites, resulting in a decrease in the total adsorbent surface area available to the dye (Mahmoodi et al. 2011b). The dye with a higher affinity would be preferentially removed by adsorption in case of limited dose of adsorbent (Shen et al. 2009). There is a critical adsorbent amount for which the removal percentage of dyes approaches a constant value (Ghaedi et al. 2013). Table 4 shows surface area of various adsorbents used in the removal of a mixture of dyes from wastewater.

3.2 Initial dye concentration

Percentage dye adsorption decreases with an increase in initial dye concentration in the dye solution as adsorption sites would be saturated, and as a result, the adsorbent would give a lower yield for the adsorption at higher concentrations of dyes. But the adsorbed amount per unit mass of adsorbent is increased if the amount of adsorbent dose is kept constant. This can be explained by the increase in the driving force due to larger concentration

gradient at the higher initial dye concentration. Reduced percent adsorption at high dye concentrations may sometimes be attributed to repulsion occurring between adsorbed dye molecules on the surface of adsorbent and residual dye molecules in the solution (Hajati et al. 2014, Almasian et al. 2015, An et al. 2015). Figure 3 shows a comparative result of initial dye concentration on dye removal from single and binary systems using PAN25%w/w EDA (polyacrylonitrile 25% w/w ethylenediamine) nanofiber (Almasian et al. 2015).

A study using dyes Metanil Yellow and Reactive Blue also indicated that an increase in initial dye concentration led to an increase in the adsorption trend of dye on the adsorbent (Chiou and Chuang 2006).

It is reported that the equilibrium uptake amounts of dyes in binary mixture onto sorbent decreased considerably with increasing concentrations of the other dye, indicating their antagonistic effect. The binary solution exhibited inhibitory (antagonistic) adsorption for each dye showing lower adsorption yield. At lower concentrations of moieties in the solution, all dye molecules present in the solution could interact with the binding sites, and thus, the percent adsorption was higher than those at higher initial concentrations of the binary mixture. At higher dye concentrations, lower adsorption yield is due to the saturation of adsorption sites. The presence of the other dye in the solution develops a competition for adsorption sites on the surface of sorbent and some sites

Table 4: Surface area of various adsorbents used in removal of mixture of dyes from wastewater.

Adsorbent	Surface area (m ² /g)	Reference
CaFe ₂ O ₄ magnetic nanoparticles	42	Liu et al. (2015b)
Clay	117	Issa et al. (2014)
Zeolite	173	
Filtrisorb 400 activated carbon	1100	Al-Degs et al. (2007)
Peat	32	Allen et al. (2004)
Silica/chitosan hybrid	8	Cestari et al. (2005)
Charred sawdust	559	Chakraborty et al. (2006)
Bamboo derived activated carbon	2471	Chan et al. (2012a)
Acid treated okara	1	Gao et al. (2011)
Cadmium hydroxide nanowires loaded on activated carbon	1271	Ghaedi and Mosallanejad (2014)
Hydroxy-aluminum pillared bentonite	200	Hao et al. (2014)
Poly(epichlorohydrin dimethylamine) modified bentonite	27	Kang et al. (2009)
Bamboo charcoal modified by microwave radiation	255	Liao et al. (2012)
Mesoporous Cu ₂ O submicro-spheres	58	Liu et al. (2012)
Cellulose-based Bioadsorbent	364	Liu et al. (2015a)
Multiwall carbon nanotube	217	Wang et al. (2012b)
Bentonite	72	Turabik (2008)
Magnetic MnFe ₂ O ₄	156	Yang et al. (2014)
Titanium peroxide	48	Zhao et al. (2014)
Na-Bentonite and organoclay	36 and 28	Anirudhan and Ramachandran (2015)
Alumina nanoparticles	110	Zolgharnein et al. (2015)

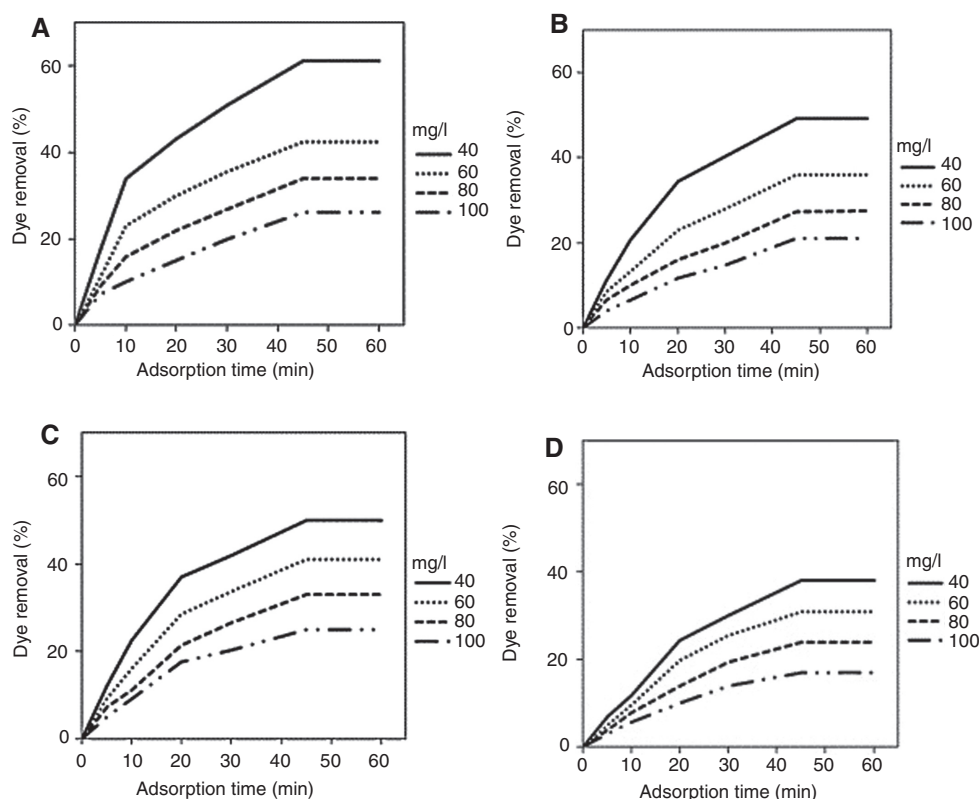


Figure 3: Effect of initial dye concentration on dye removal from single and binary systems by PAN25%w/w EDA nanofiber. (A) Direct Red 80 (single), (B) Direct Red 23 (single), (C) Direct Red 80 (binary), (D) Direct Red 23 (binary). Reprinted from Almasian et al. (2015), with permission from Elsevier.

are occupied by the second component, especially at a relatively higher concentration (Turabik 2008).

3.3 Molecular dimension of dye

Ghaedi and Mosallanejad (2014) showed the kinetics of the competitive adsorption of Malachite Green and Sunset Yellow at their equal initial concentrations in mixture. It is reported that the initial adsorption rate of Sunset Yellow onto cadmium hydroxide nanowires loaded on activated carbon ($\text{Cd}(\text{OH})_2\text{-NW-AC}$) was found faster than that of the Malachite Green, and the time for Sunset Yellow to reach the adsorption equilibrium was shorter than for Malachite Green. The reason for this might be the unequal size of molecules of the two dyes. Sunset Yellow molecule is much smaller than dye Malachite Green molecule and it is easier for the molecule of Sunset Yellow to diffuse into ($\text{Cd}(\text{OH})_2\text{-NW-AC}$) (Ghaedi and Mosallanejad 2014).

Pelekani and Snoeyink (2000) selected adsorbates of similar size and they investigated the effect of pore size distribution on competitive adsorption mechanism between Atrazine and Methylene Blue on a series of

phenolic resin-based microporous activated carbon fibers. The adsorptive competition mechanism of a particular pore is controlled by the size of the adsorbate relative to both the pore size and the size of the competing species. Primary micropores have an ability of adsorption selectivity or molecular sieve ability, which get reduced rapidly with increasing pore size and characteristics of selectivity is almost absent for the secondary micropore region. The competitive effect was more dominant in micropore region for the same adsorption sites and the magnitude of the competition decreases with increase in the pore volume. This enables transfer of adsorbates from primary micropore region to the secondary micropores (8–20 Å) (Pelekani and Snoeyink 2000).

Chan et al. (2012b) demonstrated the difficulty of using single component parameters to predict multicomponent systems. The correlative extended Freundlich model was best fitted to the experimental data of system, which suggests that the significant nonideal effects because of the properties of the adsorbate and heterogeneous surface of the tyre demineralized activated carbon. The multicomponent model based on the extended Langmuir and the ideal adsorbed solution theory (IAST) models provided

a good prediction of sorption behavior only if two dyes with similar sizes and properties are used in the binary system, since the adsorbate-adsorbate interaction is greatly reduced as they have similar sorption behavior. However, models on the removal of Acid Blue 25 and Acid Yellow 117 using tyre demineralized activated carbon were not a good fit compared to the empirical models, since the adsorption behavior is so different in the single-component system, as the systems are nonideal adsorbed solute systems particularly at high solution concentrations, which mean that the general assumption of the ideal system is not applicable (Chan et al. 2012b). The efficiency and the kinetic results obtained in a study (Duta and Visa 2015) showed that the dye structure, molecular flexibility, and dimension differently influence the competition for the adsorption sites. Bemacid Blue dye molecule showed fast diffusion at the easily accessible sites, although it has large molecular size as the molecule consists of aromatic rings linked only by σ flexible bonds. The more rigid azo-bond containing Bemacid Red molecule has a slower diffusion, thus slower adsorption, but is able to use a larger amount of adsorption sites (e.g. inside the small micropores) (Duta and Visa 2015). So, molecular dimensions play an important role in describing the behavior of an adsorption system that contains a mixture of dyes. Physical properties pertinent to the adsorption of few dyes are listed in Table 5, which can be used in future research to study the adsorption behavior of combinations of dyes in an aqueous solution.

The adsorption behavior of the dyes in binary mixtures was investigated by Dávila-Jiménez et al. (2009)

based on the relative molecular volume of the constituents and the amount of sulfonic groups present in the dye. They reported that the amount of solute adsorption is directly proportional to the molecular volume difference. Large molecular volume difference produces a negligible diminution in the adsorption of the large molecule Acid Blue 80 from mixture and a considerable decrease in the adsorption of the small dye Acid Orange 10 from mixture vis-a-vis single component solutions. A great reduction in the removal capacity was observed for Acid Green 25 in the presence of Acid Orange 8 and it amounts to 23%. Large molecular volume difference produces a negligible diminution of the adsorption of the large-molecule Acid Green 27 in a mixture and a considerable decrease in the adsorption of the small dye Acid Red 1 in mixture with respect to single-component solutions. Table 6 shows the effects of relative molecular volume of the constituents and the amount of sulfonic groups present in the dye (Dávila-Jiménez et al. 2009).

3.4 Temperature

Issa et al. (2014) reported that the sorption of methylene blue and malachite green dyes was decreased with an increase in temperature, and this was evident from the maximum sorption values of solute, C_{sm} , or equilibrium constants (K_L) for solutes as obtained from Langmuir equation. For both Methylene Blue and Malachite Green dyes, K_L values have been reduced by 60% and 40%, respectively, on increasing solution temperature by 20°C.

Table 5: General characteristics of various dyes.

Dye	Chromophore	Mol. wt. in ionized form (g mol ⁻¹)	λ_{max} (nm)	Electrical charges	Length (Å)	Width (Å)	Depth (Å)	Reference
Methylene Blue	Thiazine	284.4	665	+1	16.34	7.93	4.00	Zhao et al. (2013)
Sudan I	Azo	248.28	476	0	13.55	9.74	3.68	Zhao et al. (2013)
Acid Orange 7	Azo	327.33	507.5	-1	15.67	10.03	5.44	Zhao et al. (2013)
Orange G	Azo	406.33	512	-2	15.64	10.14	5.44	Zhao et al. (2013)
New Cocaine	Azo	535.49	536	-3	17.38	10.48	5.44	Zhao et al. (2013)
Acid Red 88	Azo	377.39	503	-1	15.66	10.27	5.44	Zhao et al. (2013)
Tropaeolin OO	Azo	352.39	529	-1	17.52	7.70	6.48	Zhao et al. (2013)
Ponceau 6R	Azo	456.44	518	-2	17.09	10.41	5.44	Zhao et al. (2013)
Croscsein Scarlet 3B	Disazo	510.50	510	-2	21.81	10.61	5.44	Zhao et al. (2013)
Croscsein Scarlet 7B	Disazo	538.55	-	-2	22.17	10.24	5.44	Zhao et al. (2013)
Acid Black 1	Disazo	570.51	330	-2	22.93	11.15	5.44	Zhao et al. (2013)
Methyl Blue	Triarylmethane	753.82	602	-2	24.49	14.35	13.89	Zhao et al. (2013)
Acid Blue 25	Anthraquinone	393.39	600	-1	15.518	12.573	5.413	Aguayo-Villarreal et al. (2013)
Acid Green 25	Anthraquinone	576.60	642	-2	15	14.9	11.6	Dávila-Jiménez et al. (2009)
Acid Yellow 117	Disazo	802.84	438	-2	29.1	20.2	4.01	Chan et al. (2012b)
Malachite Green	Triarylaminethane	329.46	618	+1	12	11	10	Castellini et al. (2008)

Table 6: Effect of relative molecular volume of the constituents and the amount of sulfonic groups present in dye (Dávila-Jiménez et al. 2009).

Dyes in binary mixture	Relative molecular volume, ΔV (\AA^3)	Number of sulfonic groups on the dye moieties	Comparison of dye adsorption in individual and in binary mixtures solutions (suffix "m")	Effect
Acid Orange 10 + Acid Blue 80	214	2 and 2		The relative diminutions of the adsorbed amount are higher for the small molecules
Acid Orange 7 + Acid Blue 324	90	1 and 1		Removal of both dyes decreases in the mixture as compared to the single component solution
Acid Orange 8 + Acid Green 25	173	1 and 2		For this pair, competition of molecules with different bulkiness and different number of sulfonic functionalities play an important role

Table 6 (continued)

Dyes in binary mixture	Relative molecular volume, ΔV (\AA^3)	Number of sulfonic groups on the dye moieties	Comparison of dye adsorption in individual and in binary mixtures solutions (suffix "m")	Effect
Acid Red 1 + Acid Green 27	199	2 and 2		Relative diminutions of the adsorbed amount are higher for the small molecules. Large molecular volume difference produces a negligible diminution of the adsorption of the large molecules.

This observation indicated that sorption of both dyes is sensitive to temperature and the sorption process is physically controlled (Issa et al. 2014).

The higher temperature is needed to obtain a better dye removal by ZnS:Mn nanoparticles loaded on activated carbon (ZnS:Mn-NP-AC) (Hajati et al. 2014). More adsorption at higher temperature in this case shows that large dye ion mobility was enhanced at higher temperature (Turabik 2008, Mahmoodi et al. 2010, Hajati et al. 2014), probably due to that an increasing number of molecules having sufficient energy at higher temperature interact with surface active sites (Mahmoodi et al. 2010).

3.5 pH

pH may play an important role in the removal efficiency of the target analytes by influencing the present state of analytes in solution. The dye adsorption capacity can be determined by the strength of ionic interaction between the adsorbent and the dyes (Ghaedi et al. 2012). Generally, high adsorption capacity is observed when anionic dyes are adsorbed on the adsorbent surface at acidic pH and cationic dyes at basic pH. This is by virtue of the strong electrostatic interaction between opposite charges that reside on the adsorbent surface and dye molecules (Mahmoodi et al. 2011b, Kurniawan et al. 2012).

Turabik (2008) studied the effects of pH (2–8) for the adsorption of Basic Yellow 28 and Basic Red 46 dyes from aqueous solution onto bentonite. It was found that the adsorption of Basic Yellow 28 and Basic Red 46 dyes on bentonite is controlled by a pH-independent adsorption

mechanism that occurs partly by ion exchange releasing exchangeable cations in the interlayer and basal plane surfaces and partly via non-coulombic interactions between an adsorbed cation and a neutralized site for the removal of basic dye onto bentonite (Turabik 2008). Similarly, Zeinali et al. (2014) and An et al. (2015) also found that adsorption of dyes on the adsorbent is controlled by a pH-independent adsorption mechanism.

It is reported that free biomass of *Corynebacterium glutamicum* possesses excellent reactive dye-binding capacity (Vijayaraghavan and Yun 2007). This specific characteristic of polysulfone-immobilized protonated *C. glutamicum* (PIPC) is used for biosorption of reactive dyes. Among different initial pH values in the range of 2–12, maximum 94% Reactive Blue 4 biosorption is reported between pH 2 and 3. In acidic pH, the biomass has a net positive charge due to protonation of carboxyl, phosphate, and amine functional groups (Won et al. 2005). Furthermore, reactive dyes release anions (ROSO_3^-) in the solution, which exhibits electrostatic attraction toward the positively charged biomass cell surface. In particular, the amino groups present in *C. glutamicum* were mainly responsible for reactive dye biosorption and the hydrogen ion acts as a bridging ligand between the bacterial cell wall and the dye molecule (Vijayaraghavan and Yun 2008). At acidic pH, increased uptake of the anionic dyes due to electrostatic interactions between the positive surface of a composite containing silver nanoparticles and colemanite ore waste (Ag-COW) was proclaimed as the surface charge of Ag-COW became more positive (Yola et al. 2014). Table 7 represents a list of dyes and their suitable pH for maximum adsorption.

Table 7: Favorable pH for dyes of different characteristics.

Dyes mixture	Nature of dye	Adsorbent	pH range	Favorable pH	Remarks	Reference
Brilliant green and methylene blue	Cationic	<i>Saccharomyces cerevisiae</i>	1.0–8.0	6	Practically applicable for dye removal from natural aqueous dye solutions	Ghaedi et al. (2013)
Direct Yellow 12 and Reactive Orange 12	Anionic	ZnS:Mn nanoparticles loaded on activated carbon	1.0–7.0	2	–	Hajati et al. (2014)
Methylene blue and brilliant green	Cationic	Graphite oxide nanoparticles	2.0–10.0	NA	Adsorption of dyes is controlled by a pH-independent adsorption mechanism	Zeinali et al. (2014)
Basic Yellow 28 and Basic Red 46	Cationic	Bentonite	2.0–8.0	NA	pH-independent adsorption occurs by ion exchange and non-coulombic interactions	Turabik (2008)
Direct Red 80 and Direct Red 23	Anionic	PAN-EDA nanofibers	2.1, 2.5, 3, 3.5, 6.5, and 9.1	3.5	–	Almasian et al. (2015)
Crystal Violet and Congo red	Cationic and anionic	CaFe ₂ O ₄ magnetic nanoparticles	4.0–10.0	NA	pH was not a critical limiting factor in a high efficiency of the dye removal using CaFe ₂ O ₄	An et al. (2015)
Metanil Yellow and Reactive Blue 15	Anionic	Cross-linked chitosan beads	3.0–8.0	Metanil Yellow-4 Reactive Blue 15-3	Uptakes were much higher in acidic solutions than those in neutral and alkaline conditions	Chiou and Chuang (2006)
Direct Fast Scarlet, Eosin Y and Reactive Violet K-3R	Anionic	Poly-(epichlorohydrin dimethylamine) modified bentonite (EPIDMA/bentonite)	3.0–11.0	5	–	Kang et al. (2009)
Reactive Yellow 86 and Reactive Red2	Anionic	Ag-COW	2.0–9.0	2	Surface charge of Ag-COW became more positive that increased dye uptake	Yola et al. (2014)
Methylene blue and malachite green	Cationic	Rarasaponin-bentonite	3.0–10.0	8	–	Kurniawan et al. (2012)
Reactive Red and Basic Red	Anionic and cationic	Water-compatible molecularly imprinted polymer	2.0–12.0	Reactive Red-2 Basic Red-10	–	Kyzas et al. (2009)
Direct Red 23 and Acid Green 25	Anionic	Chitosan	2.0–10.0	2	High adsorption capacity due to the strong electrostatic interaction between-NH ⁺ ₃ of chitosan and dye anions	Mahmoodi et al. (2011b)
Alizarin Red S and Indigo Carmine	Anionic	Cetyltrimethylammonium bromide-modified TiO ₂	2.0–10.0	2.0	–	Zolgharnein et al. (2014b)

Fan et al. (2015) demonstrated that PANF-g-HPEIs (hydrothermally treated polyacrylonitrile fiber with hyperbranched polyethylenimine) adsorbent activated with different pH solutions effectively adsorb cationic and anionic dyes by applying a proper treatment. HPEI is a cationic polyelectrolyte; therefore, PANF-g-HPEIs may adsorb methyl orange, an anionic dye, from the water. The capability of adsorbing cationic dye, methylene blue is due to the presence of COOH group on PANF-g-HPEIs. Figure 4 shows that PANF-g-HPEI pretreated with pH=5 solution can selectively adsorb the anionic methyl orange molecules from the methyl orange/methylene blue mixture, while PANF-g-HPEI pretreated with pH=10 solution can selectively adsorb the cationic methylene blue molecules from the methyl orange/methylene blue mixture. The entire phenomena were studied using UV-vis spectra of a binary mixture as shown in Figure 4 (Fan et al. 2015).

The pH influence of pretreatment solution on the fiber's adsorption performance can be explained by two ways for the interaction of methyl orange with an adsorbent at pH=5. One is the increase in the number of protonated amines via hydrogen-bonding interaction and the other is the transformation of anionic COO⁻ groups back into the neutral COOH groups, which produce ionic attraction between the anionic sulfonate group of methyl orange and some protonated amines of HPEI. The quaternized ammoniums repel the same-charged methylene blue to access COO⁻ groups, which hinder the adsorption of the cationic dye, when a neutral solution of methylene blue mixed with HPEI moieties of PANF-g-HPEIs without any pretreatment. Methylene blue adsorption disfavors the pretreatment with a solution of pH=5 as it increases the number of protonated amines and partially or completely transforms COO⁻ groups back into COOH groups. When the fiber is pretreated by a solution of pH=10, a majority of

the protonated amines are turned into the neutral amines, resulting in that the repelling force between PANF-g-HPEIs and methylene blue molecules diminishes, and the attraction force between COO⁻ groups and methylene blue molecules becomes dominant (Fan et al. 2015).

3.6 Salt content

Dye industrial wastewater commonly contains dissolved inorganic ions. These ions may compete for the active sites on the adsorbent surface because these salts have small molecular sizes and thus reduce the dye removal efficiency (Mahmoodi et al. 2010, 2011a,b). A major drawback resulting from the reactivity and nonselectivity of active sites on the adsorbent is their reaction with nontarget compounds, leading to dye auxiliaries in the exhausted dye bath present in the background water matrix. Thus, an increased amount of adsorbent is needed to accomplish the desired degree of dye removal (Mahmoodi et al. 2010).

3.7 Presence of major cations and anions

Liu et al. (2015b) investigated the effects of common existing ions of inorganic salts on the selective adsorption of dyes from industrial wastewater. In a ternary mixture system containing Congo red, methyl orange, and rhodamine B, an impact of coexisting ions on the uptake of Congo red in the presence of anions and cations viz. K⁺, NH₄⁺, Ni²⁺, Mg²⁺, Cu²⁺, Pb²⁺, Zn²⁺, NO₃⁻, CO₃²⁻, PO₄³⁻, and SO₄²⁻ was studied. PO₄³⁻ and SO₄²⁻ caused a significant decrease in the adsorption of Congo red. This was probably due to the formation of inner-sphere surface complexes on

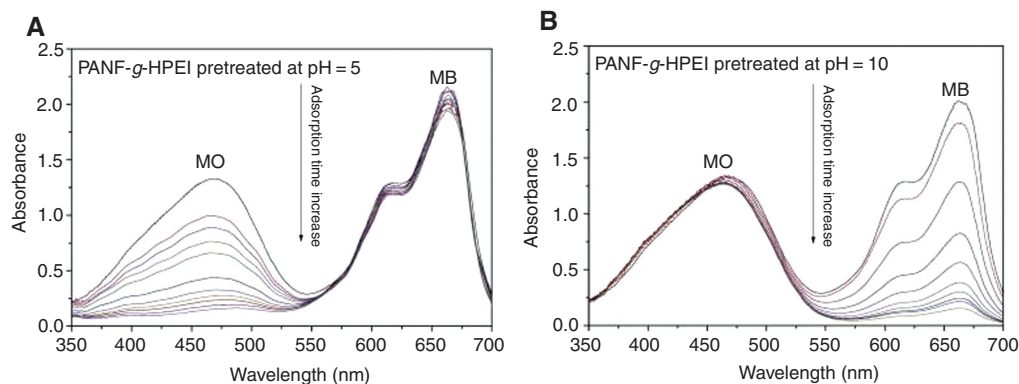


Figure 4: Time-dependent UV-vis spectra of mixture of methyl orange (MO)/methylene blue (MB) in the presence of PANF-g-HPEI pretreated at pH (A) 5 and (B) 10.

Reprinted from Fan et al. (2015), with permission from Elsevier.

the adsorbent CaFe_2O_4 magnetic nanoparticles (MNPs). But the complex composition of heavy metal ions and many other ionic species had no obvious negative effect on the adsorption of Congo red from wastewater (Liu et al. 2015b).

Apart from the molecular dimension of dye, the effect of different parameters like adsorbent dose, initial dye concentration, temperature, pH, salt content, and the presence of major cations and anions on synergistic and antagonistic behavior of dyes during adsorption are extensively studied in a multicomponent dye system. It is reported that molecular dimension of each component differently influence the competition for the adsorption sites and subsequently affect its rate and extent of adsorption during the treatment of a mixture of dyes.

4 Equilibrium relationship for dyes in multicomponent adsorption system

Isotherms show the equilibrium relationship of a particular adsorbate-adsorbent system, and these are the basic requirements for any adsorption system design. Real industrial wastewater effluent contains a mixture of several synthetic dyes; hence, it is necessary to use isotherms that can express multicomponent adsorption, and competitive interaction among the participating adsorbates is taken into account. However, single solute isotherms would provide convenience to predict equilibrium of mixtures both from theoretical and practical applications of adsorption (Noroozi and Sorial 2013).

The presence of more than one solute in a system shows nonideality. Multicomponent systems demonstrate many deviations from “ideal” adsorption due to sorbate-sorbate interactions in the solution. At sorption sites, generally alteration occurs in sorbent affinity (or capacity) for one sorbate in the presence of the other due to nonequal competition among sorbates and heterogeneity of the adsorbent surface that implies to have nonequal chances to be adsorbed for species (Al-Duri and McKay 1991).

Isotherm models that have been modified for the multicomponent mixture of dyes are as follows.

4.1 Extended Langmuir isotherm

Butler and Ockrent (1930) extended the Langmuir model to describe the sorption equilibrium in competitive adsorption systems. This empirical model assumes

homogeneous adsorbent surface with respect to the energy of adsorption, no interaction between adsorbed species, and adsorption sites are equally available to all adsorbed species.

This model is applicable for ideal solutions. It is essential for applying extended Langmuir isotherm to an adsorption system that each solute obeys Langmuir behavior in a single solute system.

$$q_{e,i} = \frac{q_{m,i} K_{L,i} C_{e,i}}{1 + \sum_{i=1}^n K_{L,i} C_{e,i}} \quad (3)$$

Kurniawan et al. (2012) proposed a revisited mathematical equation for K_L and q_m parameters for binary adsorption system because competitions (total or partial) between adsorbate species for the adsorption sites on the solid surface occur and may act as the sorption-controlling factor. Adsorption potential is also affected by the lateral interaction or competitive behavior of dyes. So it could be remarked that both K_L and q_m parameters from single Langmuir model cannot be used to describe adsorption behaviors in binary system adequately (Kurniawan et al. 2012).

The mathematical relationship between q_m and θ (fractional loading of each adsorbate species on the adsorbent surface) shows that the surface of the adsorbent was occupied by both adsorbates with certain fractional loadings. The mathematical relationship between K_L and θ explains the adsorption potential for the adsorbate species which compete with each other for the adsorption sites. Since the competition between adsorbate species occurs in binary system, the values of adsorption affinity for each adsorbate should be lower than in single system (Kurniawan et al. 2012).

4.2 Jain and Snoeyink modified extended Langmuir model

Jain and Snoeyink (1973) developed a model to predict adsorption equilibrium for nonideal systems. They extended the Langmuir theory of multicomponent mixtures of binary adsorbates that is thermodynamically consistent only if $q_{e,1} = q_{e,2}$. The Jain-Snoeyink (JS) model proposed an additional term to the extended Langmuir equation that incorporates the competitive sorption behavior of binary organic sorbates on activated carbon from aqueous solutions (Jain and Snoeyink 1973).

Sorption occurs without competition for different types of sites of sorbent along with adsorption with an

equal competition of solutes for sites in a binary organic system. In addition, the effects of competitive sorption became more significant with the increase in the number of solutes in solution (Martin and Al-Bahrani 1977). Choy et al. (2000) applied the JS model to predict adsorption equilibrium of a binary dye system and found that this model cannot be used to predict multicomponent acid dye sorption on activated carbon. They found poor correlations between the predicted and experimental data (Choy et al. 2000).

4.3 Extended Freundlich isotherm

Extended Freundlich isotherm describes the nonideal and reversible adsorption. This empirical isotherm model can be applied to multilayer adsorption, where the heat of adsorption and affinities are nonuniformly distributed over the heterogeneous surface (Adamson and Gast 1997). The total amount of adsorbed solute on the adsorbent is the summation of adsorption on all sites (each having bond energy), with the stronger binding sites occupied first, until adsorption energy is exponentially decreased upon the completion of the adsorption process (Zeldowitsch 1934).

The equilibrium adsorption from binary mixtures can also be estimated by the extended Freundlich equation as given below (Fritz and Schlueder 1974):

$$q_{e,1} = \frac{K_{F,1} C_{e,1}^{n_1+x_1}}{C_{e,1}^{x_1} + y_1 C_{e,2}^{z_1}} \quad (4)$$

and

$$q_{e,2} = \frac{K_{F,2} C_{e,2}^{n_2+x_2}}{C_{e,2}^{x_2} + y_2 C_{e,1}^{z_2}}, \quad (5)$$

where $K_{F,1}$, $K_{F,2}$, n_1 , and n_2 can be estimated from the corresponding individual Freundlich isotherm equations and the other six parameters (x_1 , y_1 , z_1 and x_2 , y_2 , z_2) are the multicomponent Freundlich adsorption constants of the first and the second components (McKay and Al-Duri 1989).

4.4 Sheindorf-Rebuhn-Sheintuch equation

Sheindorf et al. (1981) proposed the Sheindorf-Rebuhn-Sheintuch (SRS) equation, which is a Freundlich-type multicomponent adsorption isotherm. They employed Freundlich-type multicomponent adsorption isotherm

and employed it successfully to describe the adsorption data of various binary systems. In deriving the SRS equation, the empirical model assumes that each component individually obeys Freundlich isotherm equation, exponential distribution of adsorption energies of sites exists for each component in a multicomponent adsorption, and competitive Langmuir isotherm determines the coverage by each sorbate at each energy level.

According to the SRS equation, the isotherm coefficients can be determined from the monocomponent isotherm except for the adsorption competition coefficients, which have to be determined experimentally for a multicomponent system. The adsorption isotherm for component i in a k -component system expressed in terms of weight of sorbate can be written as (Sheindorf et al. 1981)

$$q_i = K_{Fi} C_i \left(\sum_{j=1}^k \alpha_{ij} C_j \right)^{n_i-1}, \quad (6)$$

where α_{ij} is the competition coefficient for the adsorption of component i in the presence of component j .

Sheindorf et al. (1982) applied the SRS equation to the adsorption of organic pollutants on activated carbon from the binary and ternary component aqueous solutions. They reported that the SRS equation is superior to competitive Langmuir isotherm when the components obey the Freundlich isotherm; however, some parameters are required for the Freundlich isotherm than for the multisection Langmuir isotherm. The competition coefficients are obtained experimentally and these coefficients can be used in more complex systems ($k \geq 3$) (Sheindorf et al. 1982).

The competition coefficients are determined from experimental data of multicomponent systems and depend on the nature of a particular system. One of the major advantages of the SRS equation is that the adsorption equilibrium of mixtures of three or more components can be predicted by substituting values obtained for a bicomponent mixture in Eq. (6). This avoids performing a tiresome experimental work with three or more solute mixtures. Values for α_{ij} range from zero (complete lack of competition) to values greater than zero (normally < 10) for a high degree of competition (Gutierrez and Fuentes 1993).

4.5 Ideal adsorbed solution theory

IAST is the most thermodynamically accepted model. It is originally proposed by Myers and Prausnitz (1965) for gas mixtures and later developed by Radke and Prausnitz (1972) for dilute liquid solutions. The IAST model

predicts the adsorption equilibrium of ideal mixture from corresponding single solute isotherms as it assumes that the adsorbed mixture forms an ideal solution (Myers and Prausnitz 1965).

Noroozi et al. (2008) applied the IAST model on the basis of the theory that was demonstrated by Lu and Sorial (2004) for the binary adsorption of dyes on granular activated carbon (GAC) and silkworm pupa (SWP). They found that IAST gave reasonable predictions of the binary systems of the dyes on GAC but it failed to predict the binary system on SWP. IAST model can be applied only to adsorption systems governed by physisorption, and adsorption of the dye by SWP was suspected to occur by chemisorptions. The tendency for physisorption to occur in a case of SWP was limited due to its nonporosity (Noroozi et al. 2008). Ho and McKay (1999) summarized the probable reasons for not getting satisfactory correlations of experimental data on the application of the ideal adsorbed solution (IAS) model. No model has yet been proposed to predict chemisorption occurring because of chemical nature of dyes in multicomponent systems (Noroozi and Sorial 2013).

Porter et al. (1999) proposed the mixed-isotherm variants of the IAS theory. The IAS model described the binary experimental data that did not use the same isotherm model as the single-component data for one dye. In order to find out which isotherm model best represents the experimental data, they applied IAS theory using four different dye-isotherm pairings. The binary equilibrium data were provided by a mixed isotherm IAS model in which one dye was represented by Freundlich isotherm and another dye by Langmuir isotherm using single-component parameters derived based on the new error function (Porter et al. 1999).

4.6 P-factor

This is a correlative technique that has been developed by McKay and Al-Duri (1987) and applied to dye/carbon systems. It is an easy-to-use method based on a “lumped” capacity factor P_i , defined as follows (McKay and Al-Duri 1987):

$$P_i = \frac{q_{i,\max,\text{single}}}{q_{i,\max,\text{multi}}} \quad (7)$$

Dimensionless capacity factor P correlates the single component equilibrium data with the multicomponent equilibrium data. The P -factor model is a simplified method that uses a ratio of monolayer capacity $q_{i,\max}$ for

the correlation. The method involved modifying the single-component solid-phase concentration $q_{i,\max,\text{single}}$ and correlating it with the $q_{i,\max,\text{multi}}$ values of the mixtures.

This model assumes a Langmuir isotherm; hence, for each component i , the multicomponent isotherm equation is described as

$$q_{e,i,\text{multi}} = \frac{1}{P_i} \frac{q_{m,i} K_{L,i} C_{e,i}}{1 + \sum_{i=1}^n K_{L,i} C_{e,i}} \quad (8)$$

Interaction and competition affect the value of factor P , and it likely depends on the relative concentrations of the dyes that vary throughout the adsorption isotherm, the extent of surface coverage of the adsorbent, the relative rates of each dye component to reach equilibrium, and changes in affinity and interactions throughout the equilibrium isotherm. Overall, it provides a major improvement over the data predicted by the extended Langmuir isotherm equation. Choy et al. (2004) gave the values of the capacity factor P for different acid dye systems.

4.7 Interaction factor

Schay (1956) first proposed interaction factor η_i for the i th component in a system of N components. η is specific to each component i and is a function of all other components in the solution. It is difficult to predict the altered sorption capacity due to sorbent-sorbate interactions and competition of each component during sorption process. Various interactions in solution and on the surface of the sorbent lead to a different loading; to incorporate these effects into a correlative model, an interaction term η has been introduced (Choy et al. 2000). It assumes that the value of the interaction factor cannot be negative. It is based on minimizing the variance between measured and calculated multicomponent equilibrium data. The calculation of η is based on minimizing the hybrid fractional error function (HYBRID). It also includes the number of degrees of freedom of the systems – the number of data points r minus the number of parameters p of the isotherm equations – as a divisor (Choy et al. 2000).

$$\eta = \frac{100}{r-p} \sum_{i=1}^r \left[\frac{(q_{e,\text{meas}} - q_{e,\text{calc}})^2}{q_{e,\text{meas}}} \right]_i \quad (9)$$

It has been reported that the incorporation of an interaction factor to extended Langmuir equation provides good results for systems whose components have similar

sorbent affinities (McKay and Al-Duri 1989, Al-Duri and McKay 1991). Hence for the Langmuir isotherm:

$$q_{e,i} = \frac{q_{m,i} K_{L,i} (C_{e,i} / \eta_i)}{1 + \sum_{j=1}^r K_{L,i} (C_{e,i} / \eta_j)} \quad (10)$$

Ho and McKay (1999) applied the concept of interaction factor to extended Langmuir equation to predict equilibrium data of copper and nickel ions in a competitive sorption system from aqueous solution using Peat. Furthermore, McKay and Al-Duri (1989) and Al-Duri and McKay (1991) found this model suitable for getting equilibrium isotherm data for a multicomponent mixture of dyes with extended Langmuir equation. Chakraborty et al. (2006) studied the extended Langmuir isotherm modified with the interaction factors for adsorption of Reactive Red and Reactive Black on sawdust. They reported that it agrees well with the equilibrium data of dye mixtures.

Being a simpler and relatively accurate approach, Choy et al. (2000) found that the application of the interaction factor does not provide a satisfactory correlation for their experimental data. The reason might be this isotherm model neglects constant K for other components present in a system. They summarized the reasons for not getting satisfactory correlation using interaction factor. Table 8 summarizes adsorption equilibrium isotherms found suitable by various researchers for different systems consisting of binary dye mixture.

5 Mathematical modeling of multicomponent batch sorption

Knowledge of the process behavior is needed before implementing it on a large scale. Mathematical modeling and simulation provide a complete knowledge of the process under different circumstances and enable a researcher to design a process without any prior experimental analysis. The literature is found rich with mathematical modeling of continuous systems (Liapis and Rippin 1979, Ruthven et al. 1994, Fernandez et al. 2015) for removal of mixture of dyes due to their direct industrial application, whereas batch studies are helpful to estimate necessary parameters to facilitate necessary parameters in mathematical modeling (Al-Duri and McKay 1991). Only a limited number of batch studies on sorption of a mixture of dyes to sorption have been reported in the literature (Al-Duri and McKay 1991, 1992, McKay and Al-Duri 1991). Chen et al. (2001)

studied film-pore diffusion modeling for the sorption of metal ions from aqueous effluents onto peat in an agitated batch sorber.

Literature reveals that film-solid diffusion is appropriate to describe the adsorption of dyes (McKay and Al-Duri 1990). Film-solid diffusion can describe a widest range of multicomponent solute systems and it is a widely used model as it provides accurate results with a similar diffusional behavior of solutes (Liapis and Rippin 1977, Smith et al. 1987). The Freundlich extended empirical isotherm (Al-Duri and McKay 1991) and the modified extended Redlich-Peterson isotherm (McKay and Al-Duri 1991) were used for solid solute equilibrium. The fundamental equations of a single solute system were extended to binary (Al-Duri and McKay 1991, McKay and Al-Duri 1991) and ternary (McKay and Al-Duri 1991) dye systems. The following equations were developed based on nonidealities in the adsorbed phase, constant intraparticle diffusivity, an absence of counterdiffusion, and independent diffusion of components (Al-Duri and McKay 1991). The governing equations of batch modeling for multicomponent system of dyes are as follows:

$$\frac{\delta u_j}{\delta t_j} = \frac{\delta^2 u_j}{\delta x^2} D_{sj}, \quad (11)$$

$$\frac{\delta u_j}{\delta t_j} x dx = \frac{k_f R}{1000 \rho_s D_{sj} (1 - \varepsilon_p)} (C_{tj} - C_{sj}), \quad (12)$$

$$q(t)_j = 3 \int_0^1 u_j x dx, \quad (13)$$

and

$$-V \frac{dC(t)_j}{dt} = m \frac{dq_j}{dt}, \quad (14)$$

where dimensionless terms are

$$u_j = q(r, t)_j \cdot x, \quad (15)$$

$$\gamma_j = \frac{t D_{sj}}{R^2}, \quad (16)$$

and

$$x = r / R \quad (17)$$

Initial and boundary conditions are as follows:

$$u_j(0, \gamma_j) = 0 = u_j(x, 0) \quad (18)$$

and

$$u_j = (R, \gamma_j) = u_{sj}(\gamma_j) \quad (19)$$

Table 8: Adsorption mechanism of some dyes on various adsorbents.

Adsorbent	Adsorbates	Adsorption isotherm	Reference
Activated carbon	Direct Blue 78 and Direct Red 31	Langmuir	Mahmoodi et al. (2011a)
Chitosan	Direct Red 23 and Acid Green 25	Temkin	Mahmoodi et al. (2011b)
Cellulose extracted from <i>Posidonia oceanica</i>	Acid Blue 25 and Direct Blue 86	Extended Langmuir	Douissa et al. (2014)
GAC	C.I. Basic Blue 41 and C.I. Basic Red 18	IAST	Noroozi et al. (2008)
Natural kaolinitic-clay and philipsite-rich-zeolite tuff	Methylene Blue and Malachite Green	Langmuir and competitive Langmuir	Issa et al. (2014)
H-type activated carbon	Levafix Brilliant Red E-4BA and Levafix Brilliant Blue E-4BA	Competitive-Langmuir model	El-Barghouthi et al. (2007)
Filtrisorb 400 activated carbon	Remazol Reactive Yellow, Remazol Reactive Black, and Remazol Reactive Red	Langmuir	Al-Degs et al. (2007)
Peat	Basic Blue 3, Basic Yellow 21, and Basic Red 22	Extended Langmuir	Allen et al. (2004)
Cationic surfactant (hexadecyltrimethylammonium chloride) modified bentonite clay	Methylene blue, crystal violet, and rhodamine B	Extended Freundlich	Anirudhan and Ramachandran (2015)
Activated carbon from sawdust	Cibacron Red RB and Cibacron Black B	Langmuir isotherm modified with an interaction factor	Chakraborty et al. (2006)
Activated carbon from waste bamboo	Acid Yellow 117 and Acid Blue 25	Redlich-Peterson	Chan et al. (2008)
Activated carbon	Acid Blue and Acid Yellow	Extended Langmuir	Choy et al. (1999)
Activated carbon	Acid Blue 80 and Acid Red 114	Langmuir isotherm modified with a P-factor	Choy et al. (2004)
	Acid Blue 80 and Acid Yellow 117 Acid Red 114 and Acid Yellow 117 Acid Blue 80, Acid Red 114, and Acid Yellow 117		
Acid treated okara	Acid Red 14 and Reactive Red 15	Partial competitive Langmuir, Langmuir-Freundlich, and extended Freundlich	Gao et al. (2011)
Clinoptilolite type natural zeolite	Reactive Blue 21 and Reactive Red 195	Extended Langmuir	Sismanoglu et al. (2010)

These equations can be solved numerically for t and analytically for x (McKay et al. 1984). Solid diffusivity is an increasing function of the initial solute concentration of each solute in a multicomponent system, and a single value of k_j described each component for specified conditions (Al-Duri and McKay 1991, McKay and Al-Duri 1991). However, D_{eff} was reduced with C_0 for multicomponent systems due to increased internal resistance and competitive effects. Overall, it is reported that enhanced relative diffusion rate was found for the originally slower component and that inhibited the diffusion rate of the faster one in a case of multisolite systems (Al-Duri and McKay 1992).

6 Mechanism of dye adsorption

A suitable mechanism for adsorption of a mixture of dyes on an adsorbent surface can thoroughly explain

the effects of competition and synergism in a multi-component dye mixture. Wang et al. (2012a) studied the interaction between cationic and anionic dyes, i.e. methylene blue-Acid Red 183, in a binary system on the positively charged multiwalled carbon nanotubes (MWCNT). Figure 5 shows the proposed molecular arrangements of adsorption of methylene blue-Acid Red 183 on the multiwalled carbon nanotubes. They investigated the effects of varying one dye concentration on the other dye adsorption. A synergistic effect was observed for both dyes, with increased Methylene Blue concentration at a fixed initial Acid Red 183 concentration. In the above binary dye systems, methylene blue showed favorite adsorption on multiwalled carbon nanotubes due to hydrophobic effect and π - π bonds. A higher concentration of methylene blue molecules resulted in increased methylene blue adsorption on the MWCNT due to small molecular size and less space hindrance. Perhaps, the increased adsorption of

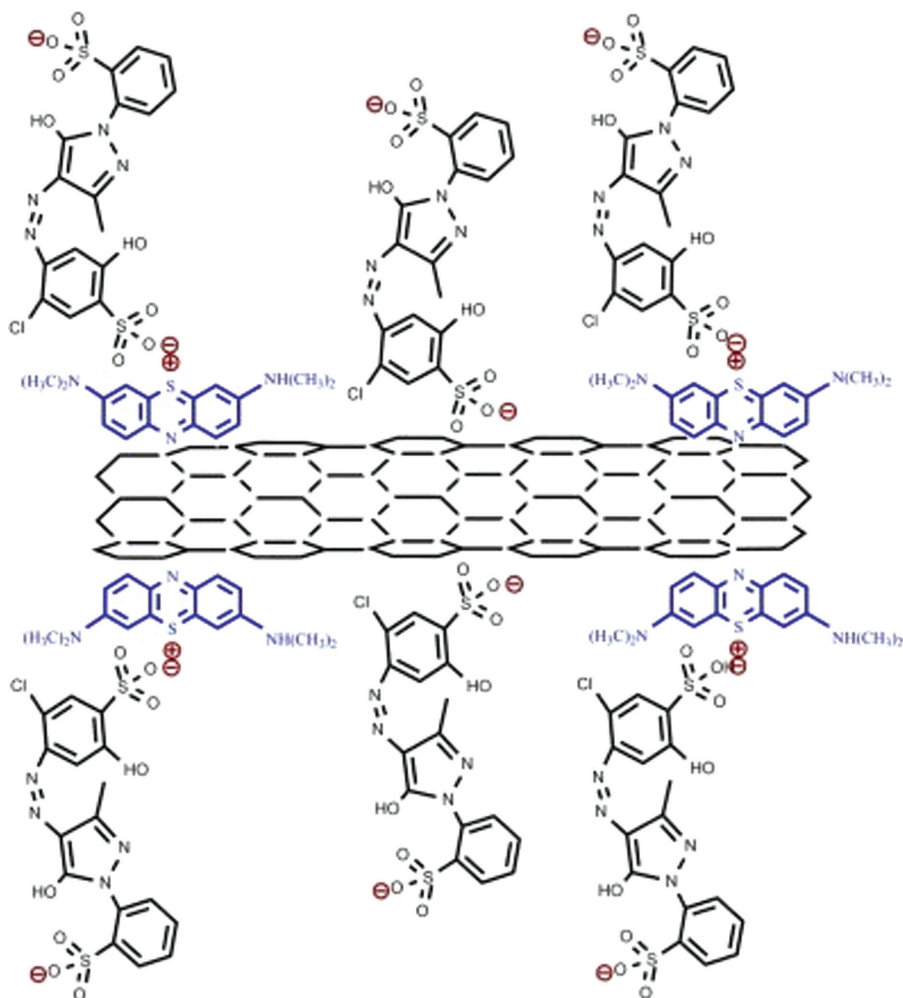


Figure 5: Dye adsorption mechanism on MWCNT in binary-dye solutions. Reprinted from Wang et al. (2012a) with permission from Elsevier.

Acid Red 183 was ascribed to these reasons: first, the surface adsorbed methylene blue has a positive charge, which served as the sites for electrostatic attraction to negatively charge Acid Red 183. Second, Acid Red 183 presents two electronic charges, so it adsorbed on the multi-walled carbon nanotubes due to electrostatic interactions (Wang et al. 2012a).

Furthermore, the authors found that increased Acid Red 183 concentration showed an antagonistic effect for methylene blue dye. It may be due to the hindrance that occurred during methylene blue adsorption at a much high concentration of Acid Red 183. Acid Red 183 in the binary solution showed stronger affinity to the MWCNT due to electrostatic interactions. Methylene blue adsorption was reduced because anionic dye has a larger molecule size and is likely to orient itself vertically against the CNT wall (Wang et al. 2012a).

Yang et al. (2014) studied the interaction mechanism of two anionic dyes, i.e. Congo red-methyl blue, in a binary system on magnetic MnFe_2O_4 . Fluorescence spectroscopy was used to inspect the interactions between Congo red and methyl blue. The sorption process of dyes was not mainly controlled by the electrostatic interaction among Congo red-methyl blue molecules and adsorbent surface. The presence of positive and negative charges on the adsorbent surface arising due to the changes in pH had no significant effect on the adsorptive affinity. The hydrogen bond interaction was the major driving force involved in dye adsorption on to MnFe_2O_4 (Yang et al. 2014). Similar results were also reported by Liu et al. (2015b) for Congo red in the presence of methyl orange and rhodamine B. The negative values of ΔH° and ΔS° confirmed that the main binding forces between the dyes were hydrogen bond and van der Waals interactions. The negative ΔG°

values indicated the spontaneous nature of the binding process (Yang et al. 2014).

Yang et al. (2014) interpreted the phenomenon of Congo red-methyl blue adsorption based on the results obtained from fluorescence spectroscopy, which showed that the fluorescence intensity of methyl blue regularly decreased with the increasing concentration of Congo red. In binary dye system, methyl blue presented favorable adsorption on the MnFe_2O_4 due to relatively higher adsorption rate and larger adsorption capacity than Congo red. The enhanced adsorption of Congo red could be attributed to the concurrent adsorption on the MnFe_2O_4 due to hydrogen bonding interactions and the surface adsorbed methyl blue served as a site to bind Congo red to form a 1:1 complex via hydrogen bonds and van der Waals forces as shown in Figure 6. Synergism promoted the adsorption of Congo red dye, while methyl blue removal was inhibited by competitive adsorption due to increasing concentration of Congo red (Yang et al. 2014).

7 Regeneration studies

Desorption and regeneration enable reuse of the same adsorbent for multiple cycles to make a process more economical, and a few studies illustrated this process (El-Barghouthi et al. 2007, Liu et al. 2015b). Theoretically, the adsorption process is completely reversible if all adsorbed dye molecules were desorbed during the course of desorption; however, this is not likely to happen due to the heterogeneity of the carbon surface (El-Barghouthi et al. 2007).

El-Barghouthi et al. (2007) demonstrated that the fraction of reversible adsorption of dyes depends on a degree of interaction between some dye molecules and some of

higher-energy sites of the adsorbent. This results in strong attachment of some dye molecules to the surface, which do not desorb. In this study, it has been reported that the system represented a low extent of desorption of dyes. It was found that 30% of the adsorbed blue dye was desorbed using water at a considerably higher initial surface concentration and desorption was insignificant for the lower surface concentrations. Poor desorption of the reactive dyes from the activated carbon indicated that a significant fraction of the adsorbed dyes was strongly attached to the carbon surface (El-Barghouthi et al. 2007).

Liu et al. (2015b) illustrated a method for magnetic adsorbent regeneration to desorb a selective anionic dye. They found that regenerated adsorbent showed highly selective adsorption capacity for one of the anionic dye from anionic-cationic dye mixture after five regeneration-removal cycles and a strong anti-interference ability that confirmed the potential of magnetic adsorbent as a practical selective adsorbent for treatments of dye containing effluents (Liu et al. 2015b).

8 Potential research areas

Knowledge of the characteristics of a multicomponent mixture of dyes in the effluent stream is essential for understanding and predicting the behavior of real wastewater systems. Removal of a multicomponent mixture of dyes present in wastewater using adsorption is becoming increasingly common. Although a number of studies have been carried out on decolorization of textile wastewater containing multiple dyes of different classes using various adsorbents, it is still a potential area for further research. Some areas that are yet to be established and require the attention of researchers are summarized below.

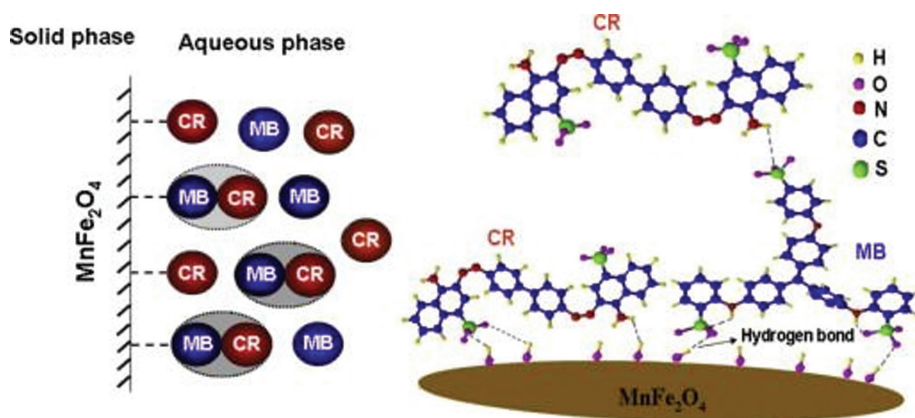


Figure 6: The molecular arrangements of adsorption of methyl blue, Congo red, and methyl blue-Congo red on MnFe_2O_4 . Reprinted from Yang et al. (2014), with permission from Elsevier.

8.1 Simultaneous quantification methods

Even with the availability of spectrophotometric and chemometric techniques used for simultaneous quantification of dyes, this field still has potential opportunities to develop methods that are easy and reliable and can be used to operate in real wastewater treatment plants.

8.2 Search of mechanism

A relevant adsorption mechanism can explain the process of adsorption of multicomponent dye mixture. The adsorption mechanism has hardly been understood for multicomponent systems. The development of a most suitable mechanism for adsorption of a mixture of dyes on an adsorbent surface can thoroughly explain the effects of competition and synergism.

Synergism, antagonism, and noninteraction are the three possible behaviors that a mixture of solutes may exhibit in a wastewater system. An intense understanding of the magnitude of such competitive interactions among the dyes needs modeling of adsorbates migration toward the adsorbent surface in aqueous systems.

8.3 Modeling

Several dyes present in multicomponent systems are chemically different in nature due to the presence of their inherent chromophore groups. The process of adsorption depends on interaction and competition among different dyes to reach the adsorbent surface. Suitable thermodynamic models need to be proposed to predict simultaneous physisorption and chemisorptions exhibited by different dyes with the adsorbent.

Although a number of isotherms are available to represent the adsorption equilibrium in multicomponent systems, the prediction and evaluation of multicomponent chemisorption equilibrium have not been attempted. Hence, it is imperative to study equilibrium of multiple dyes that exhibit chemisorption and propose simpler models of appropriate isotherms to describe the phenomenon effectively.

Not much attention has been paid toward modeling and simulation studies in this area. Mathematical modeling and simulation are a prerequisite for designing adsorption systems and minimizing the efforts needed for implementation of the process on a large scale. It provides complete knowledge of the process under different circumstances and enables the designer to easily decide

the fate of the technology even in the absence of real experimental data. Modeling studies may help in designing processes such as adsorption/desorption of mixture of solutes and unfold complexity of the process.

Desorption/regeneration enables the use of the same adsorbent for multiple cycles, making the process economical. Desorption/regeneration studies of adsorbent used in a multicomponent mixture of dyes are scarcely reported in the literature. Evaluation of the performance of an adsorbent in multiple regeneration cycles needs to be explained in detail covering experimental and modeling studies.

8.4 Novel separation techniques and process intensification

Complete degradation and mineralization of dye moieties are needed in order to avoid/reduce regeneration requirements and further treatment to dispose of the adsorbed dye in an environmentally compatible manner. Dye degradation and removal require process intensification in order to combine adsorption with other processes such as chemical reaction to avoid subsequent separation steps. Therefore, further research is required to combine adsorption with the chemical reaction to enhance removal significantly and examine newer pathways for producing valuable chemicals through newer routes. A mixture of dyes on reactive adsorption shall yield myriads of degradation products that may be of commercial significance.

A dye can be recycled after separation and recovery from a mixture. A mixture of adsorbents with distinct nature may be used for separation/removal of a mixture of dyes, where dyes preferentially migrate towards the surface of a compatible adsorbent.

Dyes from a mixture can be recovered by a combination of processes, which are compatible and complementary in nature. For example, dyes can be removed by a combination of plain and reactive adsorbents through adsorption and reactive adsorption processes. In such a case, one dye can be conserved/recovered while the other may be degraded to form desirable product(s) or may be completely mineralized.

9 Conclusions

Dyeing effluents contain a mixture of dyes. The present review covers a wide range of studies on adsorptive removal of a multicomponent mixture of dyes from

wastewater. Quantification of individual dyes present in a mixture can be accomplished by simple spectrophotometric methods. Derivative spectroscopy and multivariate methods in chemometrics quantify dyes simultaneously when their absorption spectra overlap. The basis of selection of a method used for quantification of dyes should have minimum divergence from true values to propagate toward an accurate experimental outcome. These established methods require sophisticated instrumentation and profound knowledge in statistics. Therefore, this field still has the potential opportunity to develop a new integrated method that is easy and reliable and needed to assess quantitative detection of dyes in the real wastewater system.

Apart from various parameters, the molecular dimensions of each component differently influence the competition for the adsorption sites and therefore affect its rate and extent of adsorption during the treatment of a mixture of dyes. A variety of equilibrium isotherms is available that are able to describe the equilibrium performance of physisorption in aqueous solution. None of the isotherms is yet available that efficiently describes the process of chemical binding of dyes with an adsorbent.

There is growing interest in the development of multicomponent dye system at pilot plant scale. Mathematical modeling and simulation studies for adsorption of dye mixture are essential for the design of treatment systems and their scale up. Dyes present in a mixture behave on the basis of their interaction with other dyes. Limited studies have described underlying adsorption mechanisms. Regeneration studies for high-capacity adsorbents used in multicomponent systems of dyes are required in order to make adsorption process economical. Further study on modeling of adsorbate migration, complete degradation/mineralization of dyes, and regeneration of adsorbent used in a multicomponent mixture of dyes are recommended.

Nomenclature

λ	wavelength, nm
A	absorbance, Au
C_e	equilibrium concentration of dye in the solution, mg/l
C_i	concentration of i th component in the solution, mg/l
q_e	adsorption capacities at equilibrium, mg/g
q_i	adsorption capacities of i th component in solution, mg/g
q_m	Langmuir constant for maximum adsorption capacity of the adsorbent, mg/g
K_L	Langmuir constant for maximum adsorption capacity of the adsorbent, l/mg
θ	constant representing fractional loading of adsorbate on adsorbent surface, dimensionless

K_f	capacity of the adsorbent constant for Freundlich, dimensionless
n	intensity of adsorption constant for Freundlich, dimensionless
x, y, z	multicomponent Freundlich adsorption constants, dimensionless
C_{sj}	equilibrium concentrations of dye for the j th component in the solution, mg/l
C_{ij}	equilibrium concentrations of dye for the j th component in the solution at any time t , mg/l
D_{sj}	solid intraparticle diffusion coefficient (or diffusivity), cm^2/s
k_{ff}	external mass transfer coefficient for the j th component, cm/s
q_j	average solid phase concentration of the j th component, mg/g
r	radial position in the adsorbent particle, cm
R	radius of the adsorbent particle, cm
t	time, s
u_j	q_j/x , dimensionless solid phase concentration of j th component, dimensionless
V	volume of solution, L
x	r/R , dimensionless distance across the particle, dimensionless
ϵ_p	adsorbent particle voidage, dimensionless
ρ_s	adsorbent solid density, g/cm^3

References

- Abdi J, Bastani D, Abdi J, Mahmoodi NM, Shokrollahi A, Mohammadi AH. Assessment of competitive dye removal using a reliable method. *J Environ Chem Eng* 2014; 2: 1672–1683.
- Adamson AW, Gast AP. *Physical chemistry of surfaces*, New York: Wiley Interscience, 1997.
- Aguayo-Villarreal IA, Hernández-Montoya V, Bonilla-Petriciolet A, Tovar-Gómez R, Ramírez-López EM, Montes-Morán MA. Role of acid blue 25 dye as active site for the adsorption of Cd 2+ and Zn2+ using activated carbons. *Dye Pigment* 2013; 96: 459–466.
- Al-Degs YS, Sweileh JA. Simultaneous determination of five commercial cationic dyes in stream waters using diatomite solid-phase extractant and multivariate calibration. *Arab J Chem* 2012; 5: 219–224.
- Al-Degs Y, Khraisheh MAM, Allen SJ, Ahmad MN. Effect of carbon surface chemistry on the removal of reactive dyes from textile effluent. *Water Res* 2000; 34: 927–935.
- Al-Degs Y, Khraisheh MAM, Allen SJ, Ahmad MN, Walker GM. Competitive adsorption of reactive dyes from solution: equilibrium isotherm studies in single and multisolute systems. *Chem Eng J* 2007; 128: 163–167.
- Al-Degs YS, El-Sheikh AH, Al-Ghouti MA, Hemmateenejad B, Walker GM. Solid-phase extraction and simultaneous determination of trace amounts of sulphonated and azo sulphonated dyes using microemulsion-modified-zeolite and multivariate calibration. *Talanta* 2008; 75: 904–915.
- Al-Duri B, McKay G. Prediction of binary systems for kinetics of batch adsorption using basic dyes onto activated carbon. *Chem Eng Sci* 1991; 46: 193–204.

- Al-Duri B, McKay G. Pore diffusion: dependence of the effective diffusivity on the initial sorbate concentration in single and multisolute batch adsorption systems. *J Chem Technol Biotechnol* 1992; 55: 245–250.
- Allen SJ, McKay G, Khader KYH. Multi-component sorption isotherms of basic dyes onto peat. *Environ Pollut* 1988; 52: 39–53.
- Allen SJ, Gan Q, Matthews R, Johnson PA. Comparison of optimised isotherm models for basic dye adsorption by kudzu. *Bioresour Technol* 2003; 88: 143–152.
- Allen SJ, McKay G, Porter JF. Adsorption isotherm models for basic dye adsorption by peat in single and binary component systems. *J Colloid Interface Sci* 2004; 280: 322–333.
- Almasian A, Mahmoodi NM, Olya ME. Tectomer grafted nanofiber: synthesis, characterization and dye removal ability from multicomponent system. *J Ind Eng Chem* 2015; 32: 85–98.
- An L, Deng J, Zhou L, Li H, Chen F, Wang H, Liu Y. Simultaneous spectrophotometric determination of trace amount of malachite green and crystal violet in water after cloud point extraction using partial least squares regression. *J Hazard Mater* 2010; 175: 883–888.
- An S, Liu X, Yang L, Zhang L. Enhancement removal of crystal violet dye using magnetic calcium ferrite nanoparticle: study in single- and binary-solute systems. *Chem Eng Res Des* 2015; 94: 726–735.
- Andronic L, Duta A. Photodegradation processes in two-dyes systems – simultaneous analysis by first-order spectra derivative method. *Chem Eng J* 2012; 198–199: 468–475.
- Anirudhan TS, Ramachandran M. Adsorptive removal of basic dyes from aqueous solutions by surfactant modified bentonite clay (organoclay): kinetic and competitive adsorption isotherm. *Process Saf Environ Prot* 2015; 95: 215–225.
- Atar N, Olgun A, Wang S, Liu S. Adsorption of anionic dyes on boron industry waste in single and binary solutions using batch and fixed-bed systems. *J Chem Eng Data* 2011; 56: 508–516.
- Brereton RG. *Chemometrics: data analysis for the laboratory and chemical plant*, England: John Wiley & Sons, 2003.
- Burges CJ. A tutorial on support vector machines for pattern recognition. *Data Min Knowl Discov* 1998; 2: 121–167.
- Butler JAV, Ockrent C. Studies in electrocapillarity. III. *J Phys Chem* 1930; 34: 2841–2859.
- Castellini E, Andreoli R, Malavasi G, Pedone A. Deflocculant effects on the surface properties of kaolinite investigated through malachite green adsorption. *Colloids Surf A Physicochem Eng Asp* 2008; 329: 31–37.
- Cestari AR, Vieira EFS, Pinto AA, Lopes ECN. Multistep adsorption of anionic dyes on silica/chitosan hybrid: 1. Comparative kinetic data from liquid- and solid-phase models. *J Colloid Interface Sci* 2005; 292: 363–372.
- Chakraborty D, Gupta SS. Photo-catalytic decolourisation of toxic dye with N-doped titania: a case study with Acid Blue 25. *J Environ Sci (China)* 2013; 25: 1034–1043.
- Chakraborty S, Basu JK, De S, DasGupta S. Adsorption of reactive dyes from a textile effluent using sawdust as the adsorbent. *Ind Eng Chem Res* 2006; 45: 4732–4741.
- Chan LS, Cheung WH, McKay G. Adsorption of acid dyes by bamboo derived activated carbon. *Desalination* 2008; 218: 304–312.
- Chan LS, Cheung WH, Allen SJ, McKay G. Error analysis of adsorption isotherm models for acid dyes onto bamboo derived activated carbon. *Chin J Chem Eng* 2012a; 20: 535–542.
- Chan OS, Cheung WH, McKay G. Single and multicomponent acid dye adsorption equilibrium studies on tyre demineralised activated carbon. *Chem Eng J* 2012b; 191: 162–170.
- Chen B, Hui CW, McKay G. Film-pore diffusion modeling for the sorption of metal ions from aqueous effluents onto peat. *Water Res* 2001; 35: 3345–3356.
- Chiou MS, Chuang GS. Competitive adsorption of dye Metanil Yellow and RB15 in acid solutions on chemically cross-linked chitosan beads. *Chemosphere* 2006; 62: 731–40.
- Choy KKH, McKay G, Porter JF. Sorption of acid dyes from effluents using activated carbon. *Resour Conserv Recycl* 1999; 27: 57–71.
- Choy KKH, Porter JF, McKay G. Langmuir isotherm models applied to the multicomponent sorption of acid dyes from effluent onto activated carbon. *J Chem Eng Data* 2000; 45: 575–584.
- Choy KKH, Porter JF, McKay G. Intraparticle diffusion in single and multicomponent acid dye adsorption from wastewater onto carbon. *Chem Eng J* 2004; 103: 133–145.
- Dávila-Jiménez MM, Elizalde-González MP, Hernández-Montoya V. Performance of mango seed adsorbents in the adsorption of anthraquinone and azo acid dyes in single and binary aqueous solutions. *Bioresour Technol* 2009; 100: 6199–6206.
- Douissa NB, Dridi-Dhaouadi S, Mhenni MF. Study of antagonistic effect in the simultaneous removal of two textile dyes onto cellulose extracted from *Posidonia oceanica* using derivative spectrophotometric method. *J Water Process Eng* 2014; 2: 1–9.
- Duta A, Visa M. Simultaneous removal of two industrial dyes by adsorption and photocatalysis on a fly-ash-TiO₂ composite. *J Photochem Photobiol A Chem* 2015; 306: 21–30.
- El-Barghouthi MI, El-Sheikh AH, Al-Degs YS, Walker GM. Adsorption behavior of anionic reactive dyes on h-type activated carbon: competitive adsorption and desorption studies. *Sep Sci Technol* 2007; 42: 2195–2220.
- Fan Y, Liu HJ, Zhang Y, Chen Y. Adsorption of anionic MO or cationic MB from MO/MB mixture using polyacrylonitrile fiber hydrothermally treated with hyperbranched polyethylenimine. *J Hazard Mater* 2015; 283: 321–328.
- Fernandez ME, Bonelli PR, Cukierman AL, Lemcoff NO. Modeling the biosorption of basic dyes from binary mixtures. *Adsorption* 2015; 21: 177–183.
- Forgacs E, Cserhâti T, Oros G. Removal of synthetic dyes from wastewaters: a review. *Environ Int* 2004; 30: 953–971.
- Fritz W, Schluender EU. Simultaneous adsorption equilibria of organic solutes in dilute aqueous solutions on activated carbon. *Chem Eng Sci* 1974; 29: 1279–1282.
- Gao JF, Zhang Q, Su K, Wang JH. Competitive biosorption of Yellow 2G and Reactive Brilliant Red K-2G onto inactive aerobic granules: simultaneous determination of two dyes by first-order derivative spectrophotometry and isotherm studies. *Bioresour Technol* 2010; 101: 5793–5801.
- Gao JF, Wang JH, Yang C, Wang SY, Peng YZ. Binary biosorption of Acid Red 14 and Reactive Red 15 onto acid treated okara: simultaneous spectrophotometric determination of two dyes using partial least squares regression. *Chem Eng J* 2011; 171: 967–975.
- Ghaedi M, Mosallanejad N. Study of competitive adsorption of malachite green and Sunset Yellow dyes on cadmium hydroxide nanowires loaded on activated carbon. *J Ind Eng Chem* 2014; 20: 1085–1096.
- Ghaedi M, Montazerzohori M, Biyareh MN, Mortazavi K, Soylak M. Chemically bonded multiwalled carbon nanotubes as efficient material for solid phase extraction of some metal ions in food samples. *Int J Environ Anal Chem* 2012; 93: 528–542.
- Ghaedi M, Hajati S, Barazesh B, Karimi F, Ghezelbash G. *Saccharomyces cerevisiae* for the biosorption of basic dyes

- from binary component systems and the high order derivative spectrophotometric method for simultaneous analysis of brilliant green and methylene blue. *J Ind Eng Chem* 2013; 19: 227–233.
- Ghaedi M, Pakniat M, Mahmoudi Z, Hajati S, Sahraei R, Daneshfar A. Synthesis of nickel sulfide nanoparticles loaded on activated carbon as a novel adsorbent for the competitive removal of methylene blue and safranin-O. *Spectrochim Acta Part A Mol Biomol Spectrosc* 2014; 123: 402–409.
- Ghaedi M, Hajjati S, Mahmudi Z, Tyagi I, Agarwal S, Maity A, Gupta VK. Modeling of competitive ultrasonic assisted removal of the dyes – methylene blue and safranin-O using Fe₃O₄ nanoparticles. *Chem Eng J* 2015; 268: 28–37.
- Gholami A, Masoum S, Mohsenikia A, Abbasi S. Chemometrics-assisted excitation-emission fluorescence analytical data for rapid and selective determination of optical brighteners in the presence of uncalibrated interferences. *Spectrochim Acta Part A Mol Biomol Spectrosc* 2016; 153: 108–117.
- Gözmen B, Turabik M, Hesenov A. Photocatalytic degradation of Basic Red 46 and Basic Yellow 28 in single and binary mixture by UV/TiO₂/periodate system. *J Hazard Mater* 2009; 164: 1487–1495.
- Gupta AK, Pal A, Sahoo C. Photocatalytic degradation of a mixture of crystal violet (Basic Violet 3) and methyl red dye in aqueous suspensions using Ag⁺ doped TiO₂. *Dye Pigment* 2006; 69: 224–232.
- Gupta VK, Khamparia S, Tyagi I, Jaspal D, Malviya A. Decolorization of mixture of dyes: a critical review. *Global J Environ Sci Manage* 2015a; 1: 71–94.
- Gupta VK, Sharma M, Vyas RK. Hydrothermal modification and characterization of bentonite for reactive adsorption of methylene blue: an ESI-MS study. *J Environ Chem Eng* 2015b; 3: 2172–2179.
- Gürses A, Açıkyıldız M, Güneş K, Gürses MS. Dyes and pigments: their structure and properties. In: *Dyes and pigments*. Springer, 2016: 13–29.
- Gutierrez M, Fuentes HR. Modeling adsorption in multicomponent systems using a Freundlich-type isotherm. *J Contam Hydrol* 1993; 14: 247–260.
- Hajati S, Ghaedi M, Karimi F, Barazesh B, Sahraei R, Daneshfar A. Competitive adsorption of Direct Yellow 12 and Reactive Orange 12 on ZnS:Mn nanoparticles loaded on activated carbon as novel adsorbent. *J Ind Eng Chem* 2014; 20: 564–571.
- Hao Y, Yan L, Yu H, Yang K, Yu S, Shan R, Du B. Comparative study on adsorption of basic and acid dyes by hydroxy-aluminum pillared bentonite. *J Mol Liq* 2014; 199: 202–207.
- Hemmateenejad B, Shadabipour P, Khosousi T, Shamsipur M. Chemometrics investigation of the light-free degradation of methyl green and malachite green by starch-coated CdSe quantum dots. *J Ind Eng Chem* 2014; 27: 384–390.
- Himmelblau DM. Accounts of experiences in the application of artificial neural networks in chemical engineering. *Ind Eng Chem Res* 2008; 47: 5782–5796.
- Ho YS, McKay G. Competitive sorption of copper and nickel ions from aqueous solution using peat. *Adsorption* 1999; 5: 409–417.
- Isa MH, Lang LS, Asaari FAH, Aziz HA, Ramli NA, Dhas JPA. Low cost removal of disperse dyes from aqueous solution using palm ash. *Dye Pigment* 2007; 74: 446–453.
- Issa AA, Al-Degs YS, Al-Ghouti MA, Olimat AAM. Studying competitive sorption behavior of methylene blue and malachite green using multivariate calibration. *Chem Eng J* 2014; 240: 554–564.
- Jain JS, Snoeyink VL. Adsorption from bisolute systems on active carbon. *J Water Pollut Control Fed* 1973; 45: 2463–2479.
- Kang Q, Zhou W, Li Q, Gao B, Fan J, Shen D. Adsorption of anionic dyes on poly(epichlorohydrin dimethylamine) modified bentonite in single and mixed dye solutions. *Appl Clay Sci* 2009; 45: 280–287.
- Karpińska J. Derivative spectrophotometry – recent applications and directions of developments. *Talanta* 2004; 64: 801–822.
- Khani R, Ghasemi JB, Shemirani F, Rahmanian R. Application of bilinear least squares/residual bilinearization in bulk liquid membrane system for simultaneous multicomponent quantification of two synthetic dyes. *Chemom Intell Lab Syst* 2015; 144: 48–55.
- Kim K. Financial time series forecasting using support vector machines. *Neurocomputing* 2003; 55: 307–319.
- Kolthoff IM, van der Goot E. The adsorption of hydroxybenzenes and other aromatic compounds and their replacing action upon each other at the interface water-charcoal. *Recl Des Trav Chim des Pays-Bas* 1929; 48: 265–287.
- Kurniawan A, Sutiono H, Indraswati N, Ismadji S. Removal of basic dyes in binary system by adsorption using rarasaponin-bentonite: revisited of extended Langmuir model. *Chem Eng J* 2012; 189–190: 264–274.
- Kyzas GZ, Bikiaris DN, Lazaridis NK. Selective separation of basic and reactive dyes by molecularly imprinted polymers (MIPs). *Chem Eng J* 2009; 149: 263–272.
- Kyzas GZ, Lazaridis NK, Kostoglou M. On the simultaneous adsorption of a reactive dye and hexavalent chromium from aqueous solutions onto grafted chitosan. *J Colloid Interface Sci* 2013; 407: 432–441.
- Kyzas GZ, Sifaka PI, Pavlidou EG, Chrissafis KJ, Bikiaris DN. Synthesis and adsorption application of succinyl-grafted chitosan for the simultaneous removal of zinc and cationic dye from binary hazardous mixtures. *Chem Eng J* 2015; 259: 438–448.
- Liao P, Malik Ismael Z, Zhang W, Yuan S, Tong M, Wang K, Bao J. Adsorption of dyes from aqueous solutions by microwave modified bamboo charcoal. *Chem Eng J* 2012; 195–196: 339–346.
- Liapis AI, Rippin DWT. A general model for the simulation of multi-component adsorption from a finite bath. *Chem Eng Sci* 1977; 32: 619–627.
- Liapis AI, Rippin DWT. The simulation of binary adsorption in continuous countercurrent operation and a comparison with other operating modes. *AIChE J* 1979; 25L: 455–460.
- Liu J, Gao Z, Han H, Wu D, Xu F, Wang H, Jiang K. Mesoporous Cu₂O submicro-spheres, facile synthesis and the selective adsorption properties. *Chem Eng J* 2012; 185–186: 151–159.
- Liu S, Ding Y, Li P, Diao K, Tan X, Lei F, Zhan Y, Li Q, Huang B, Huang Z. Adsorption of the anionic dye Congo red from aqueous solution onto natural zeolites modified with *N,N*-dimethyl dehydrobiethylamine oxide. *Chem Eng J* 2014; 248: 135–144.
- Liu L, Gao ZY, Su XP, Chen X, Jiang L, Yao JM. Adsorption removal of dyes from single and binary solutions using a cellulose-based bioadsorbent. *ACS Sustain Chem Eng* 2015a; 3: 432–442.
- Liu X, An S, Wang Y, Yang Q, Zhang L. Rapid selective separation and recovery of a specific target dye from mixture consisted of

- different dyes by magnetic Ca-ferrites nanoparticles. *Chem Eng J* 2015b; 262: 517–526.
- Lu Q, Sorial GA. Adsorption of phenolics on activated carbon – impact of pore size and molecular oxygen. *Chemosphere* 2004; 55: 671–679.
- Mahmoodi NM. Dendrimer functionalized nanoarchitecture: synthesis and binary system dye removal. *J Taiwan Inst Chem Eng* 2014a; 45: 2008–2020.
- Mahmoodi NM. Synthesis of core–shell magnetic adsorbent nanoparticle and selectivity analysis for binary system dye removal. *J Ind Eng Chem* 2014b; 20: 2050–2058.
- Mahmoodi NM, Hayati B, Arami M. Textile dye removal from single and ternary systems using date stones: kinetic, isotherm, and thermodynamic studies. *J Chem Eng Data* 2010; 55: 4638–4649.
- Mahmoodi NM, Salehi R, Arami M. Binary system dye removal from colored textile wastewater using activated carbon: kinetic and isotherm studies. *Desalination* 2011a; 272: 187–195.
- Mahmoodi NM, Salehi R, Arami M, Bahrami H. Dye removal from colored textile wastewater using chitosan in binary systems. *Desalination* 2011b; 267: 64–72.
- Mahmoodi NM, Abdi J, Najafi F. Gemini polymeric nanoarchitecture as a novel adsorbent: synthesis and dye removal from multicomponent system. *J Colloid Interface Sci* 2013; 400: 88–96.
- Martin RJ, Al-Bahrani KS. Adsorption studies using gas-liquid chromatography – II. Competitive adsorption. *Water Res* 1977; 11: 991–999.
- McKay G, Al-Duri B. Simplified model for the equilibrium adsorption of dyes from mixtures using activated carbon. *Chem Eng Process Process Intensif* 1987; 22: 145–156.
- McKay G, Al-Duri B. Prediction of multicomponent adsorption equilibrium data using empirical correlations. *Chem Eng J* 1989; 41: 9–23.
- McKay G, Al-Duri B. Study of the mechanism of pore diffusion in batch adsorption systems. *J Chem Technol Biotechnol* 1990; 48: 269–285.
- McKay G, Al-Duri B. Multicomponent dye adsorption onto carbon using a solid diffusion mass-transfer model. *Ind Eng Chem Res* 1991; 30: 385–395.
- McKay G, Allen SJ, McConvey IF, Walters JHR. External mass transfer and homogeneous solid-phase diffusion effects during the adsorption of dyestuffs. *Ind Eng Chem Process Des Dev* 1984; 23: 221–226.
- Myers AL, Prausnitz JM. Thermodynamics of mixed-gas adsorption. *AIChE J* 1965; 11: 121–127.
- Nadejde C, Neamtu M, Schneider RJ, Hodoroaba VD, Ababei G, Panne U. Catalytic degradation of relevant pollutants from waters using magnetic nanocatalysts. *Appl Surf Sci* 2015; 352: 42–48.
- Namasivayam C, Kanchana N. Waste banana pith as adsorbent for color removal from wastewaters. *Chemosphere* 1992; 25: 1691–1705.
- Nateri AS, Ekrami E. Quantitative analysis of bicomponent dye solutions by derivative spectrophotometry. *Pigment Resin Technol* 2009; 38: 43–48.
- Navado JJB, Flores JR, Llerena MJV, Fariñas NR. Simultaneous spectrophotometric determination of tartrazine, patent blue V, and indigo carmine in commercial products by partial least squares and principal component regression methods. *Talanta* 1999; 48: 895–903.
- Noroozi B, Sorial GA, Bahrami H, Arami M. Adsorption of binary mixtures of cationic dyes. *Dye Pigment* 2008; 76: 784–791.
- Noroozi B, Sorial GA. Applicable models for multi-component adsorption of dyes: a review. *J Environ Sci* 2013; 25: 419–429.
- Olgun A, Atar N. Equilibrium and kinetic adsorption study of Basic Yellow 28 and Basic Red 46 by a boron industry waste. *J Hazard Mater* 2009; 161: 148–156.
- Pelekani C, Snoeyink VL. Competitive adsorption between atrazine and methylene blue on activated carbon: the importance of pore size distribution. *Carbon N Y* 2000; 38: 1423–1436.
- Pirdashti M, Curteanu S, Kamangar MH, Hassim MH, Khatami MA. Artificial neural networks: applications in chemical engineering. *Rev Chem Eng* 2013; 29: 205–239.
- Porter JF, McKay G, Choy KH. The prediction of sorption from a binary mixture of acidic dyes using single- and mixed-isotherm variants of the ideal adsorbed solute theory. *Chem Eng Sci* 1999; 54: 5863–5885.
- Radke C, Prausnitz J. Adsorption of organic solutes from dilute aqueous solution of activated carbon. *Ind Eng Chem Fundam* 1972; 11: 445–451.
- Rajoriya S, Bargole S, Saharan VK. Degradation of a cationic dye (rhodamine 6G) using hydrodynamic cavitation coupled with other oxidative agents: reaction mechanism and pathway. *Ultrason Sonochem* 2017; 34: 183–194.
- Ruthven DM, Farooq S, Knaebel KS. *Pressure swing adsorption*, Vol. 480, New York: VCH publishers, 1994.
- Schay, G. Theory of the Langmuir type of physical adsorption of gas. *Chim Phys Hungary* 1956; 53: 691.
- Shams-Nateri A. Dye concentrations determination in ternary mixture solution by using colorimetric algorithm. *Iran J Chem Chem Eng* 2011; 30: 51–61.
- Sharma K, Vyas RK. Adsorption of multicomponent dye mixture: a brief review. In: *Chemcon*, 2015.
- Sharma M, Vyas RK, Singh K. A review on reactive adsorption for potential environmental applications. *Adsorption* 2013; 19: 161–188.
- Sheindorf C, Rebhun M, Sheintuch M. A Freundlich-type multicomponent isotherm. *J Colloid Interface Sci* 1981; 79: 136–142.
- Sheindorf C, Rebhun M, Sheintuch M. Organic pollutants adsorption from multicomponent systems modeled by Freundlich type isotherm. *Water Res* 1982; 16: 357–362.
- Shen D, Fan J, Zhou W, Gao B, Yue Q, Kang Q. Adsorption kinetics and isotherm of anionic dyes onto organo-bentonite from single and multisolute systems. *J Hazard Mater* 2009; 172: 99–107.
- Sirianuntapiboon S, Srisornsak P. Removal of disperse dyes from textile wastewater using bio-sludge. *Bioresour Technol* 2007; 98: 1057–1066.
- Sismanoglu T, Kismir Y, Karakus S. Single and binary adsorption of reactive dyes from aqueous solutions onto clinoptilolite. *J Hazard Mater* 2010; 184: 164–169.
- Slokar YM, Majcen Le Marechal A. Methods of decoloration of textile wastewaters. *Dye Pigment* 1998; 37: 335–356.
- Smith EH, Tseng S, Weber WJ. Modeling the adsorption of target compounds by GAC in the presence of background dissolved organic matter. *Environ Prog* 1987; 6: 18–25.

- Srivastava VC, Mall ID, Mishra IM. Equilibrium modelling of single and binary adsorption of cadmium and nickel onto bagasse fly ash. *Chem Eng J* 2006; 117: 79–91.
- Suykens JA, Vandewalle J. Least squares support vector machine classifier. *Neural Process Lett* 1999; 9: 293–300.
- Turabik M. Adsorption of basic dyes from single and binary component systems onto bentonite: simultaneous analysis of Basic Red 46 and Basic Yellow 28 by first order derivative spectrophotometric analysis method. *J Hazard Mater* 2008; 158: 52–64.
- Vapnik VN. The nature of statistical learning theory. *Statistics for engineering and information science*, New York: Springer, 2000.
- Verma Y. Acute toxicity assessment of textile dyes and textile and dye industrial effluents using *Daphnia magna* bioassay. *Toxicol Ind Health* 2008; 24: 491–500.
- Verma AK, Dash RR, Bhunia P. A review on chemical coagulation/flocculation technologies for removal of colour from textile wastewaters. *J Environ Manage* 2012; 93: 154–168.
- Vijayaraghavan K, Yun YS. Chemical modification and immobilization of *Corynebacterium glutamicum* for biosorption of Reactive Black 5 from aqueous solution. *Ind Eng Chem Res* 2007; 46: 608–617.
- Vijayaraghavan K, Yun YS. Competition of Reactive red 4, Reactive orange 16 and Basic blue 3 during biosorption of Reactive Blue 4 by polysulfone-immobilized *Corynebacterium glutamicum*. *J Hazard Mater* 2008; 153: 478–86.
- Walker GM, Weatherley LR. Adsorption of acid dyes on to granular activated carbon in fixed beds. *Water Res* 1997; 31: 2093–2101.
- Wang H, Hu D. Comparison of SVM and LS-SVM for regression. *Neural Netw Brain* 2005; 1: 279–283.
- Wang S, Ng CW, Wang W, Li Q, Hao Z. Synergistic and competitive adsorption of organic dyes on multiwalled carbon nanotubes. *Chem Eng J* 2012a; 197: 34–40.
- Wang S, Ng CW, Wang W, Li Q, Li L. A comparative study on the adsorption of acid and reactive dyes on multiwall carbon nanotubes in single and binary dye systems. *J Chem Eng Data* 2012b; 57: 1563–1569.
- Won SW, Choi SB, Yun YS. Interaction between protonated waste biomass of *Corynebacterium glutamicum* and anionic dye Reactive Red 4. *Colloids Surf A Physicochem Eng Asp* 2005; 262: 175–180.
- Wong YC, Szeto YS, Cheung WH, McKay G. Adsorption of acid dyes on chitosan – equilibrium isotherm analyses. *Process Biochem* 2004; 39: 693–702.
- Yacout DMM, Abd El-Kawi MA, Hassouna MS. Cradle to gate environmental impact assessment of acrylic fiber manufacturing. *Int J Life Cycle Assess* 2016; 21: 326–336.
- Yahyaei B, Azizian S. Rapid adsorption of binary dye pollutants onto the nanostructured mesoporous alumina. *J Mol Liq* 2014; 199: 88–95.
- Yang Y, Jin D, Wang G, Wang S, Jia X, Zhao Y. Competitive biosorption of Acid Blue 25 and Acid Red 337 onto unmodified and CDAB-modified biomass of *Aspergillus oryzae*. *Bioresour Technol* 2011; 102: 7429–36.
- Yang L, Zhang Y, Liu X, Jiang X, Zhang Z, Zhang T, Zhang L. The investigation of synergistic and competitive interaction between dye Congo red and methyl blue on magnetic $MnFe_2O_4$. *Chem Eng J* 2014; 246: 88–96.
- Yola ML, Eren T, Atar N, Wang S. Adsorptive and photocatalytic removal of reactive dyes by silver nanoparticle-colemanite ore waste. *Chem Eng J* 2014; 242: 333–340.
- Yu J, Zhu J, Feng L, Cai X, Zhang Y, Chi R. Removal of cationic dyes by modified waste biosorbent under continuous model: competitive adsorption and kinetics. *Arab J Chem* 2015 (In press).
- Zeinali N, Ghaedi M, Shafie G. Competitive adsorption of methylene blue and brilliant green onto graphite oxide nano particle following: derivative spectrophotometric and principal component-artificial neural network model methods for their simultaneous determination. *J Ind Eng Chem* 2014; 20: 3550–3558.
- Zeldowitsch J. Adsorption site energy distribution. *Acta Phys Chim URSS* 1934; 1: 961–973.
- Zhao X, Bu X, Wu T, Zheng ST, Wang L, Feng P. Selective anion exchange with nanogated isorecticular positive metal-organic frameworks. *Nat Commun* 2013; 4: 2344.
- Zhao X, Huang J, Wang B, Bi Q, Dong L, Liu X. Preparation of titanium peroxide and its selective adsorption property on cationic dyes. *Appl Surf Sci* 2014; 292: 576–582.
- Zolgharnein J, Asanjani N, Bagtash M, Azimi G. Multi-response optimization using Taguchi design and principle component analysis for removing binary mixture of alizarin red and alizarin yellow from aqueous solution by nano γ -alumina. *Spectrochim Acta Part A Mol Biomol Spectrosc* 2014a; 126: 291–300.
- Zolgharnein J, Bagtash M, Asanjarani N. Hybrid central composite design approach for simultaneous optimization of removal of alizarin red S and indigo carmine dyes using cetyltrimethylammonium bromide-modified TiO₂ nanoparticles. *J Environ Chem Eng* 2014b; 2: 988–1000.
- Zolgharnein J, Bagtash M, Shariatmanesh T. Simultaneous removal of binary mixture of Brilliant Green and Crystal Violet using derivative spectrophotometric determination, multivariate optimization and adsorption characterization of dyes on surfactant modified nano- γ -alumina. *Spectrochim. Acta A. Mol Biomol Spectrosc* 2015; 137: 1016–1028.

Bionotes



Komal Sharma

Department of Chemical Engineering,
Malaviya National Institute of Technology,
Jaipur 302017, India

Komal Sharma is currently a PhD scholar under the supervision of Dr. Raj K. Vyas, Chemical Engineering Department, MNIT Jaipur, India, and under the cosupervision of Dr. Ajay K. Dalai, University of Saskatchewan, Canada. She completed her master's degree at MBM Engineering College, Jodhpur, India. She has worked on conversion of waste plastic into fuel. At present she is working on the removal of textile dyes from its aqueous mixture using reactive adsorption. She has published two research articles in international journals, one in a national journal, and presented a number of articles at national and international conferences.

**Ajay K. Dalai**

Department of Chemical and Biological Engineering, University of Saskatchewan, Saskatoon, Canada

Dalai holds a PhD in Chemical Engineering from the University of Saskatchewan, where he is currently employed as a full Professor and Canada Research Chair in Bioenergy and Environmentally Friendly Chemical Processing. His research focus is the novel catalyst development for gas to liquid technologies, development of carbon adsorbents for CO₂ capture, biodiesel production, hydrogen/syngas production, hydroprocessing of gas oil, and value added products from biomass. Prof. Dalai holds several patents and has published over 300 research papers mostly on heterogeneous catalysis and catalytic processes in international journals and conference proceedings. He is a fellow of Canadian Academy of Engineering, Chemical Institute of Canada, Engineering Institute of Canada, American Institute of Chemical Engineers, Indian Institute of Chemical Engineers, Royal Society of Canada, and Royal Society of Chemistry (UK).

**Raj K. Vyas**

Department of Chemical Engineering, Malaviya National Institute of Technology, Jaipur 302017, India
rkvyas2@gmail.com

Raj K. Vyas is an Associate Professor at the Chemical Engineering Department, MNIT Jaipur, India. He obtained his PhD from the erstwhile University of Roorkee, Roorkee (now IIT Roorkee). The major areas of his research are separation processes, environmental engineering, and catalysis and biotechnology. He has published/presented over 60 research papers in various international/national journals/conferences of repute, guided five PhDs, and over a dozen master's theses. He has received several academic awards, including a "Khosla Commendation Certificate" from University of Roorkee, Roorkee, in 1996.

Graphical abstract

Komal Sharma, Ajay K. Dalai and Raj K. Vyas

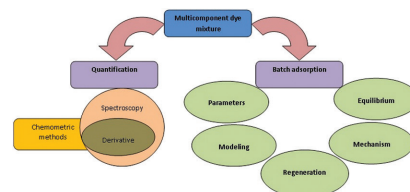
Removal of synthetic dyes from multicomponent industrial wastewaters

DOI 10.1515/revce-2016-0042

Rev Chem Eng 2017; x(x): xxx–xxx

Review: An outline of studies on quantification and batch adsorption of multicomponent dye mixtures.

Keywords: chemometric methods in spectrophotometric analysis; mathematical modeling; mechanism; multicomponent dye mixture adsorption; parameters.



Thermodynamic and Kinetic Studies of Methylene Blue Degradation Using Reactive Adsorption and Its Comparison with Adsorption

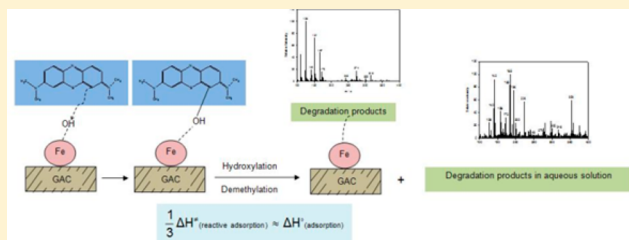
Komal Sharma,[†] Raj K. Vyas,^{*,†} and Ajay K. Dalai[‡]

[†]Department of Chemical Engineering, Malaviya National Institute of Technology, Jaipur 302017, India

[‡]Department of Chemical and Biological Engineering, University of Saskatchewan, Saskatoon, Canada

Supporting Information

ABSTRACT: Granular activated carbon doped with iron (Fe-GAC) was prepared and methylene blue (MB) removal efficiency was tested using reactive adsorption (Fe-GAC/H₂O₂) and adsorption (Fe-GAC). The color removal efficiencies of Fe-GAC/H₂O₂ and Fe-GAC were found to be 94% and 25%, respectively, in 3 h at 30 °C. The higher MB removal was achieved because of hydroxyl radical-induced oxidative degradation in the presence of Fe-GAC/H₂O₂ at natural pH. MB removal rate using reactive adsorption (0.015 min⁻¹) was much faster than adsorption (0.004 min⁻¹). Thermodynamic parameters revealed that enthalpy change was approximately one-third for reactive adsorption as that for adsorption, indicating reactive adsorption to be superior. Electrospray ionization-mass spectrometry (ESI-MS) analysis showed that reactive degradation of MB molecule followed demethylation and hydroxylation processes. The process of reactive adsorption was further investigated by identifying compounds using desorption from spent Fe-GAC through ESI-MS. Recovery and identification of such degraded compounds may be commercially attractive. An oxidative degradation pathway and a reactive adsorption scheme have been proposed.



1. INTRODUCTION

Dye contaminants present in aqueous media pose serious environmental hazards. Cationic dyes are very difficult to remove through traditional and available protocols. Highly colored wastewaters from textile industries enter natural water sources deteriorating their quality and subsequently intensifying toxicity.^{1,2} Therefore, degradation and subsequent removal of these moieties have a great role in minimizing pollution of the environment. Reactive adsorption comprises concurrent reaction and separation of the solute during adsorption in a single unit operation.³ Reactive adsorption has great potential to replace adsorption as it increases the rate of degradation by a significant proportion and requires less frequent sorbent regeneration.⁴ It overcomes various complications of adsorption such as cumbersome removal and disposal of sorbed harmful species, nonattainment of complete contaminant removal, and slow removal rate.⁵ The major component of organic pollutants consists of highly toxic colored dyes.⁶ Reactive degradation may completely eradicate the color via degradation of dye molecules and may render the wastewater much less harmful.⁷

Granular activated carbon (GAC) has excellent adsorption capacity, chemical stability, mechanical strength, and economic promise for the removal of dissolved organic matter.^{8–10} Fe³⁺ or Fe²⁺ loading on GAC serve as catalyst in the removal of organic compounds through oxidation.¹¹ The catalytic effect of Fe³⁺ and GAC as the electron donor¹¹ played a significant role in the formation of a hydroxyl radical from hydrogen peroxide which breaks large molecules into smaller fragments.¹²

Furthermore, impregnation of iron oxide on GAC (Fe-GAC) eradicates the limitation of sludge production in the Fenton process.¹³

Methylene blue (MB) is an intensely colored greenish crystalline compound, mostly used in dyeing and printing of textiles.^{14–16} MB is a common water pollutant which is a subject of hazardous environmental concerns.^{17–19} Therefore, it is of great interest to study degradation and removal of MB to reduce its lateral impacts. MB degradation in the presence of H₂O₂ using a composite of Fe-rich soil and sucrose-based charcoal²⁰ and δ -FeOOH nanoparticles²¹ is well documented in the literature. Studies on the reactive adsorption of MB using clays^{3,7} have been reported earlier. The paucity of literature on kinetic and thermodynamic aspects of dye degradation using reactive adsorption motivates further research. Furthermore, formation of some deposits on the surface of the reactive adsorbent during reactive adsorption has been reported earlier.^{22,23} Ania et al. (2011) studied the existence of the variety of species adsorbed in the activated carbons after its exposure to an antibiotic using thermal analysis.²⁴ However, studies on identification of degraded deposited species have been scarcely reported. No study is available in the literature identifying dye reactive adsorption products that are adsorbed on the spent adsorbent. Recovery and identification of such degraded compounds may be commercially attractive obtained

Received: April 23, 2017

Accepted: October 3, 2017

from dyes and other organic pollutants. These moieties can be applied as precursors for the production of valuable industrially important fine-chemicals after recovery and proper separation. Such an exercise would open up newer routes for remediation of unseawater created by hazardous pollutants. As a future research, it is imperative to carry out detailed studies on separation schemes, utilization, and production pathways for useful chemicals using degraded products of reactive adsorption.

In this study, the kinetic and thermodynamic parameters of MB dye removal using reactive adsorption were investigated. Furthermore, desorption studies were carried out on the spent Fe-GAC to confirm the degradation of the MB molecule via reactive adsorption, and the degraded products adsorbed on the surface were identified. To obtain deeper knowledge of the removal of MB dye using Fe-GAC/H₂O₂, the reaction intermediates of the oxidative degradation process were identified along with the possible degradation pathways in this research. Fe-GAC was used as an adsorbent to compare the MB removal performance with reactive adsorption. λ_{max} (663 nm) was used for MB decoloration study during reactive adsorption and adsorption.²⁵

2. EXPERIMENTAL SECTION

2.1. Materials. MB (AR grade) was obtained from Fisher Scientific (India) and used as an adsorbate without further purification. Granular activated carbon was procured from CDH (India), and hydrogen peroxide and ferric chloride were procured from Merck (India).

2.2. Instruments. A UV–vis spectrophotometer (Shimadzu corporation analytical instruments, Japan; UV 1800) was used to analyze the absorbance at 663 nm (λ_{max} of MB) before and after each experiment to measure respective concentrations of aqueous solution. A pH meter (Hanna Instruments, USA) was used to determine the pH of aqueous solutions.

2.3. Synthesis of Fe-GAC. Fe-GAC was prepared using 2.5% Fe³⁺ solution using FeCl₃.^{26,27} Mondal et al. (2007) discussed the net positive charge of Fe-GAC that depends on the concentration of Fe³⁺ ions in the impregnating solution. The change in net positive charge of Fe-GAC was found negligible at 2.5% Fe³⁺ concentration in the impregnating solution.²⁶ GAC was washed multiple times followed by drying at 105 °C until a constant weight was obtained. Afterward, 10 g of GAC was used and further treated with 24 mL of FeCl₃ solution (2.5% Fe³⁺) at its natural pH (2–4). Iron impregnation was carried out in an oven at 70 °C until complete drying of the solution. Unbound iron of the Fe-impregnated GAC was removed by multiple washings using deionized water. Finally, Fe-GAC was dried at 110° until no change in weight loss was found, and then it was stored for further use.

2.4. Methods and Techniques. Images of GAC and Fe impregnated GAC particles were captured using a TecnaiG² 20 (FEI) S-Twin 200 kV transmission electron microscope (TEM) coupled with energy dispersive spectroscopy (EDS). The surface areas of virgin GAC and Fe-GAC were measured using the BET surface area method. A QuadraSorb Station 2 BET surface area analyzer was used to conduct the nitrogen adsorption–desorption process at 77.35 K. The multilayer Brunauer–Emmett–Teller (BET) equation was used to obtain the surface area. The structure of GAC and Fe-GAC was recorded by X'Pert Pro X-ray diffractometer (PAN analytical BV, The Netherlands) operated at a voltage of 45 kV and current of 40 mA with Cu K α radiation of wavelength 1.54059

Å, at a grazing angle X-ray diffraction. Scanning was done in the region of 2 θ from 10° to 50°. A Xevo G2-S Q TOF (Waters, USA) mass spectrometer is used to carry out electrospray ionization-mass spectrometry (ESI-MS) analyses in the positive ion mode.

2.5. Batch Reactive Adsorption Studies. Fe-GAC exhibits catalytic activity in the presence of H₂O₂, and this characteristic was used for the study of degradation of MB present in an aqueous solution. An Erlenmeyer flask was charged with 100 mL of aqueous solution of MB (10 mg/L), and 0.2 g·L⁻¹ of catalyst was added. H₂O₂ (1.0 mM) was added to the flask and the reaction mixture was continuously agitated using a shaker at 30 ± 1 °C at pH 6.5 (natural pH of the MB solution). For a defined time interval, a sample was pipetted into a quartz cell, and the UV–visible spectrophotometer was used to measure its absorption spectrum. Batch experiments of reactive adsorption were carried out at different temperatures (20–60 °C) for kinetic and thermodynamic studies. An ESI-MS analysis was carried out to identify the degradation intermediates during the reactive adsorption of MB at different time intervals.

2.6. Batch Adsorption Studies. Batch equilibrium experiments were conducted using equal masses of 0.2 g·L⁻¹ of Fe-GAC in 100 mL of MB (10–50 mg·L⁻¹). Batch kinetics of MB removal was studied with initial MB concentration of 10 mg·L⁻¹ and a dose of 0.2 g·L⁻¹ of Fe-GAC. The aqueous solution was kept in an isothermal incubator shaker for 24 h at 30 ± 1 °C and 150 rpm to reach the equilibrium of the mixture of dye solution and adsorbent. Thermodynamic parameters (ΔG° , ΔH° , ΔS°), for the adsorption process were obtained from the experiments carried out at different temperatures (20–60 °C).

3. RESULTS AND DISCUSSION

3.1. Adsorbent Characterization. Figure 1a shows the TEM image of virgin GAC. Clusters of iron on GAC are visible

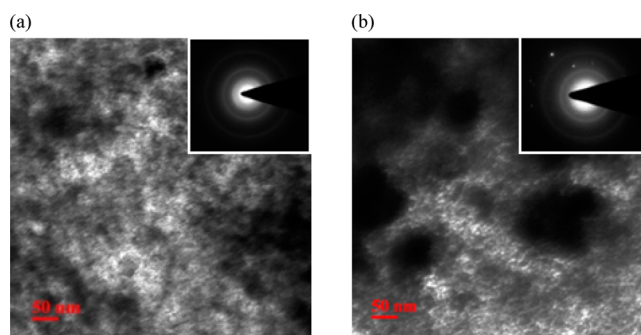


Figure 1. TEM images of (a) GAC and (b) Fe-GAC.

in the TEM image (Figure 1b). Figure 1b demonstrates that Fe has been embedded into the GAC particles. Figure 1a shows the amorphous nature of GAC while Figure 1b indicates the crystalline nature of the synthesized reactive adsorbent. Elemental analysis of GAC by EDS was used for further confirmation of presence of Fe on the GAC surface (Figure 2a,b); a significant amount of iron has been impregnated on the GAC surface (Table 1). It can be interpreted from Table 1 that the GAC surface primarily consists of carbon and oxygen only, whereas Fe-GAC has iron and chloride ion traces in addition to C and O elements. TEM analysis of Fe-GAC verified the presence of nanosized iron particle clusters in GAC. This size of

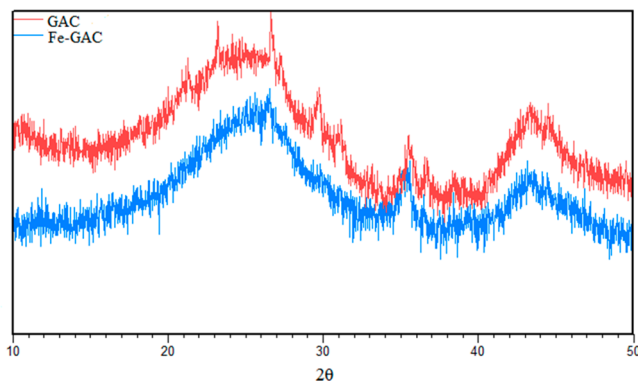


Figure 2. XRD patterns of GAC and iron-impregnated GAC.

Table 1. Elemental Analysis of GAC and Fe-GAC Using EDS

elemental analysis	GAC (wt %)	Fe-GAC (wt %)
C	99.60	96.56
O	0.40	1.06
Fe		2.17
Cl		0.21

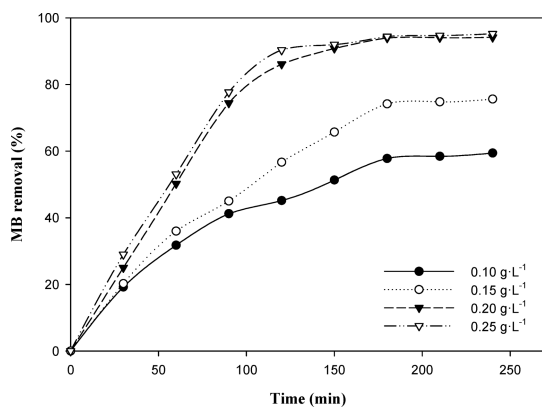


Figure 3. Effect of adsorbent dose on dye removal using Fe-GAC/ H_2O_2 at different time intervals (temp, 30 °C; C_0 , 10 $mg\cdot L^{-1}$; pH, 6.5; H_2O_2 , 1.0 mM).

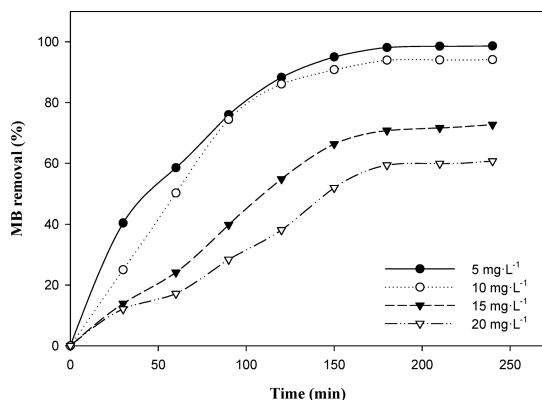


Figure 4. Effect of initial dye concentration on dye removal using Fe-GAC/ H_2O_2 at different time intervals (temp, 30 °C; dose of Fe-GAC, 0.2 $g\cdot L^{-1}$; pH, 6.5; H_2O_2 , 1.0 mM).

iron particles deposited in GAC was found consistent with literature values.^{28,29}

The BET surface areas of GAC and Fe-GAC were found to be 657 and 450 $m^2\cdot g^{-1}$, respectively. Reduction in specific

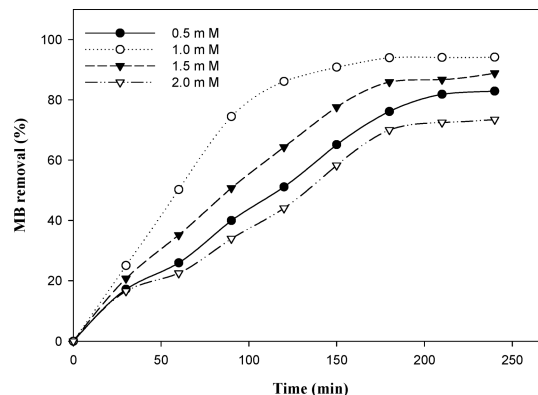


Figure 5. Effect of H_2O_2 dose on dye removal using Fe-GAC/ H_2O_2 at different time intervals (temp, 30 °C; C_0 , 10 $mg\cdot L^{-1}$; pH, 6.5; dose of Fe-GAC, 0.2 $g\cdot L^{-1}$).

surface area of Fe-GAC indicates that iron is impregnated inside the GAC particle during modification.

No significant difference could be marked between the XRD patterns of GAC and iron-doped GAC apart from a peak in the Fe-GAC sample at $2\theta = 26^\circ$ which was a broad halo for GAC (Figure 2). The XRD pattern of Fe-GAC showed a reflection corresponding to the crystalline phases, such as akaganeite (β -FeOOH).²⁹ The XRD pattern of Fe-GAC showed the presence of crystallinity, as its preparation involved drying at 70–80 °C for 8 h, during this period amorphous iron (hydr)oxides gradually converted to crystalline iron(III) oxides.³⁰ The presence of crystalline phases in Fe-GAC could be confirmed using TEM diffraction patterns (see Figure 1).

The almost similar pattern was obtained after impregnation, which may occur because the deposited Fe particles were really too small to diffract, or may be because of the too low concentration of adsorbed iron. It has already been reported earlier that XRD patterns of activated carbon did not change either by oxidation or impregnation with iron(III) or (II) chloride solutions.³¹ Adsorbent characterization using TEM-EDS, BET surface area, and XRD confirms that GAC was fairly doped with Fe particles. The loading of these Fe particles on carbon materials produce free radicals using oxidizing agents which play an important role in the removal of organic impurity (see section 3.2.3).

3.2. Batch Reactive Adsorption Studies. 3.2.1. *Optimization of Reactive Adsorption Conditions.* The effect of variation of adsorbent dose on the removal of MB by Fe-GAC/ H_2O_2 is shown in Figure 3. The amount of Fe-GAC was varied from 0.10 $g\cdot L^{-1}$ to 0.25 $g\cdot L^{-1}$ for 240 min at an initial MB dye concentration of 10 $mg\cdot L^{-1}$. It is apparent that the dye concentration in solution decreases significantly up to 180 min with increasing Fe-GAC amount due to the availability of a higher amount of Fe^{3+} which further helps in producing a larger amount of hydroxyl radicals.¹² A further increase in adsorbent dose (0.20 $g\cdot L^{-1}$ to 0.25 $g\cdot L^{-1}$) did not improve the dye removal significantly. This may be due to the limitation of hydrogen peroxide availability.

Figure 4 shows the effect of initial dyes concentration on the removal percentage. During the study, it was found that at lower concentration of MB, a higher percent removal was observed because of the low ratio of solute concentrations to adsorbent sites³² and availability of ample amount of hydroxyl radicals. However, at higher dye concentrations lower removal was found due to the saturation of adsorption sites and

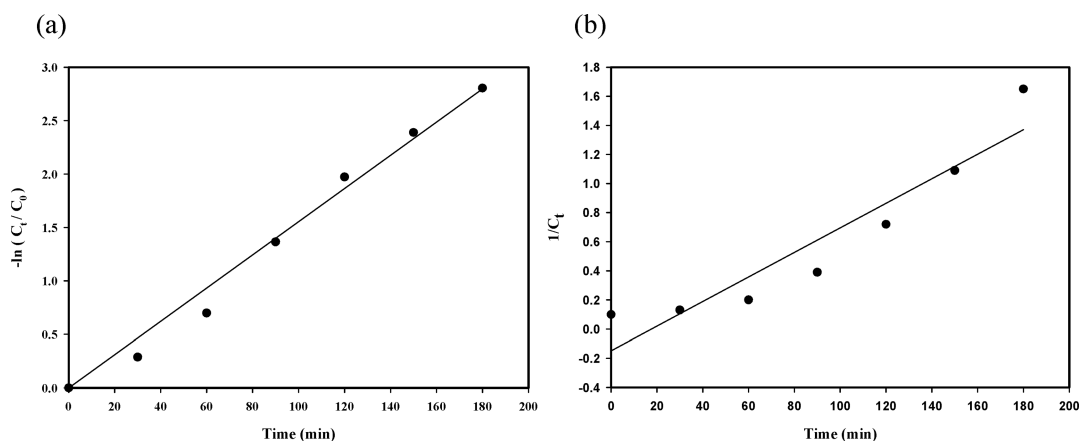


Figure 6. (a) Pseudo-first-order and (b) pseudo-second-order plot for reactive adsorption kinetics of MB (temp, 30 °C; C_0 , 10 mg·L⁻¹; pH, 6.5; H₂O₂, 1.0 mM; dose of Fe-GAC, 0.2 g·L⁻¹).

Table 2. Effect of Temperature on the Apparent Rate Constant for Reactive Adsorption of MB

T (°C)	k_{app} (min ⁻¹)
20	0.012
30	0.015
40	0.016
50	0.019
60	0.023

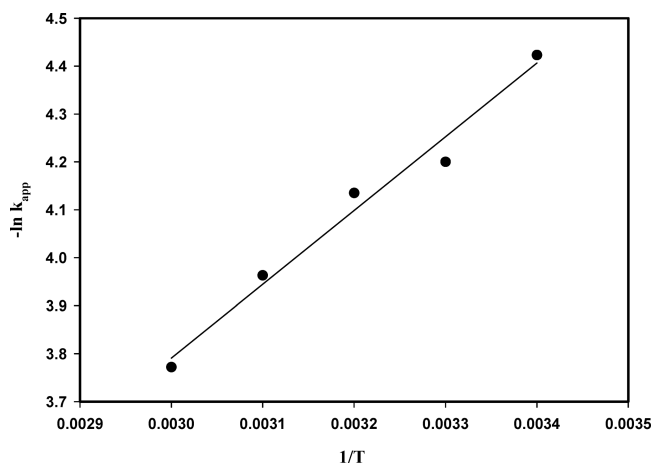


Figure 7. Effect of temperature on the apparent rate constant of MB (temp, 30 °C; C_0 , 10 mg·L⁻¹; pH, 6.5; H₂O₂, 1.0 mM; dose of Fe-GAC, 0.2 g·L⁻¹).

shortage of hydroxyl radicals.³³ There was no significant difference observed in dye removal for initial concentrations of 5 mg·L⁻¹ and 10 mg·L⁻¹. This may be due to the availability of sufficient hydroxyl radicals for removal of MB at 10 mg·L⁻¹

concentration also. Therefore, 10 mg·L⁻¹ dye concentration was chosen for further experiments.

The increase in hydrogen peroxide concentration from 0.5 to 1.0 mM accelerated the MB decolorization (Figure 5) due to the availability of a higher amount of hydroxyl radicals for oxidative degradation of MB. However, when the hydrogen peroxide concentration was increased from 1.0 to 2.0 mM, at the same operating conditions, the dye removal efficiency decreased. This could be because of the production of hydroperoxyl radicals (HO₂•) by hydroxyl radicals in the presence of a local excess of H₂O₂ that contributes to •OH-scavenging.^{12,33} The hydroperoxyl radicals are much less reactive than •OH with reaction rate constants lower than 2×10^4 M⁻¹ s⁻¹ in the presence of organic matter.³³ Oxidative degradation of dye only takes place due to reaction with •OH, and HO₂• does not take part into this process.¹² Therefore, a 1.0 mM H₂O₂ dose was considered optimum.

3.2.2. Kinetics of Reactive Adsorption Decoloration. The kinetics analysis of the decoloration of the dye solutions was carried out. First-order kinetics can be expressed as

$$-\ln \frac{C_t}{C_0} = k_{app} t \quad (1)$$

The experimental data fits linearly between $-\ln \frac{C_t}{C_0}$ and t for MB to the above equation, confirming the applicability of the pseudo-first-order kinetics model with an R^2 value of 0.985 as shown in Figure 6a. k_{app} values obtained at different temperatures are listed in Table 2. Second-order reaction systems can be represented by

$$\frac{1}{C_t} = \frac{1}{C_0} + k_{app} \times t \quad (2)$$

Table 3. Thermodynamic Parameters for Reactive Adsorption of MB

T (°C)	E_a (kJ·mol ⁻¹)	ΔG^\ddagger (kJ·mol ⁻¹)	ΔH^\ddagger (kJ·mol ⁻¹)	ΔS^\ddagger (kJ·mol ⁻¹ ·K ⁻¹)
20	12.46	82.53	10.03	-0.25
30		84.87	9.94	
40		87.59	9.86	
50		90.01	9.78	
60		92.35	9.69	

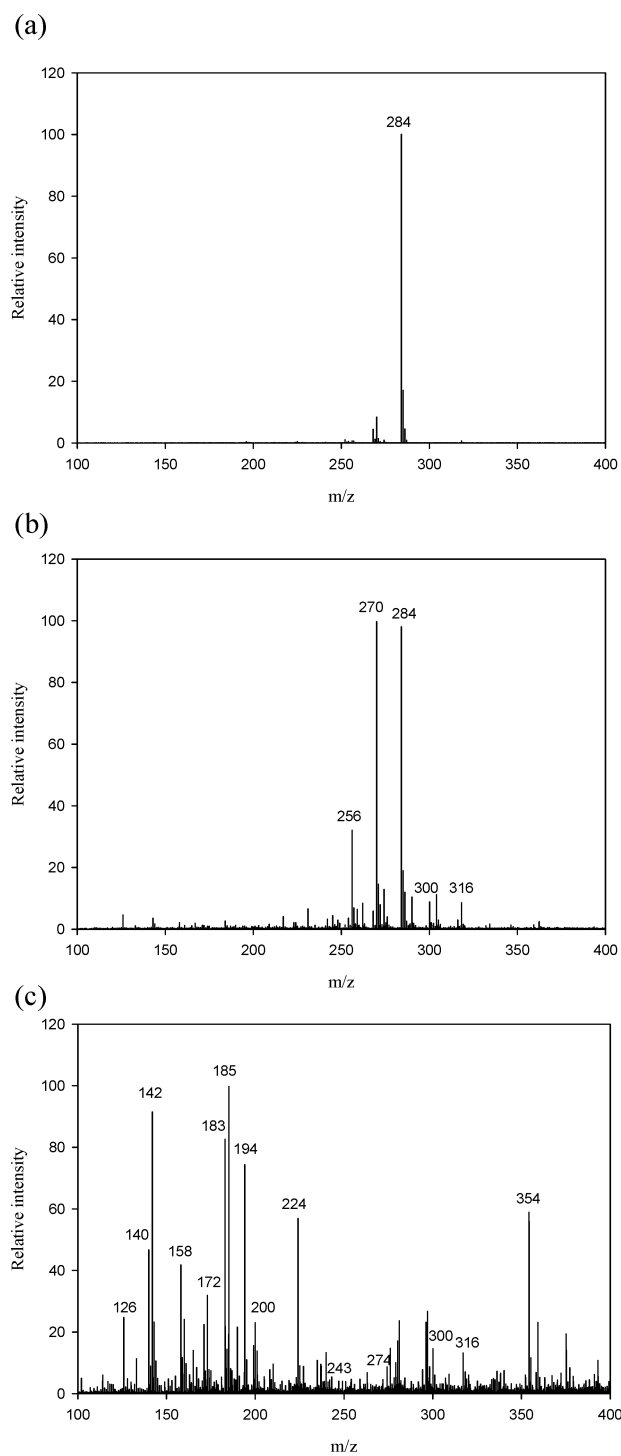


Figure 8. ESI-MS of (a) aqueous solution of MB before reaction; (b) degradation products of MB using Fe-GAC/H₂O₂ after 1 h; and (c) degradation products of MB using Fe-GAC/H₂O₂ after 3 h of reaction.

A plot of $1/C_t$ versus t was plotted as shown in Figure 6b. The plot shows an upward concave curvature and it indicates that pseudo-second-order kinetics can be neglected.

3.2.3. Thermodynamics of Reactive Adsorption. The effect of temperature on reactive adsorption was studied in the range of 20 to 60 °C. Table 2 lists k_{app} values of MB at different temperatures. MB degradation was increased with increasing temperature. The dependence of apparent rate constant on temperature can be expressed by Arrhenius relation as follows:

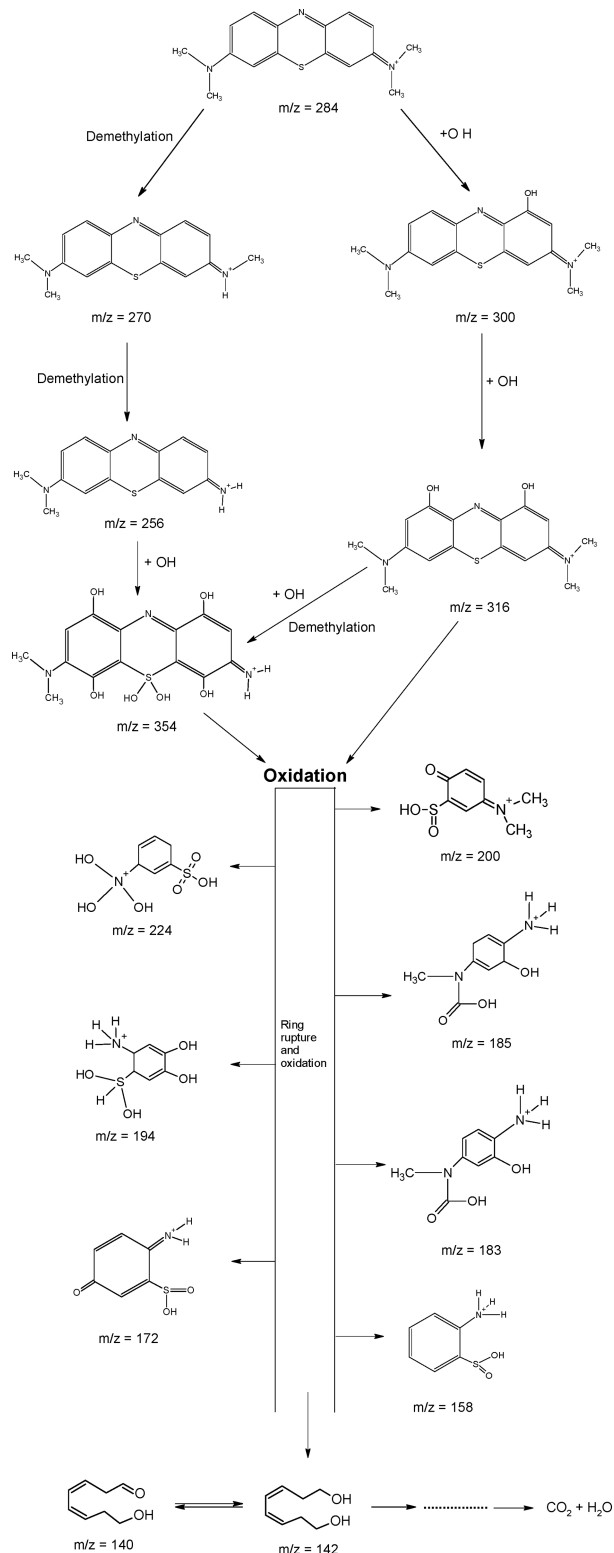


Figure 9. Proposed oxidative degradation pathway of MB during reactive adsorption using the Fe-GAC/H₂O₂ system.

$$k_{app} = A e^{-E_a/RT} \quad (3)$$

Simplified,

$$\ln k_{app} = \ln A - \frac{E_a}{RT} \quad (4)$$

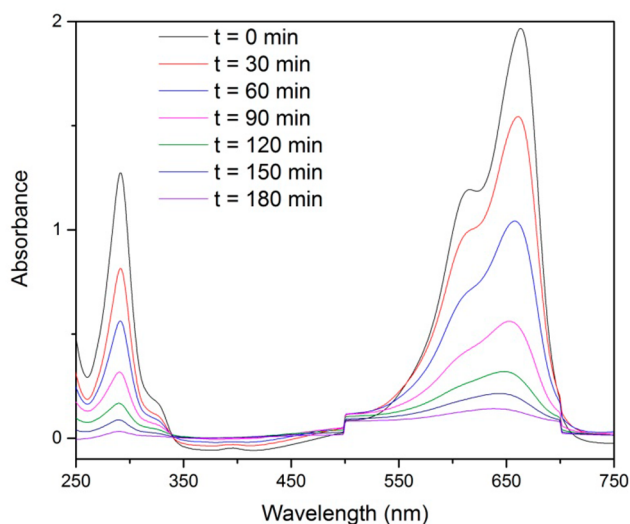


Figure 10. Spectral changes during reactive adsorption of MB dye using Fe-GAC/H₂O₂.

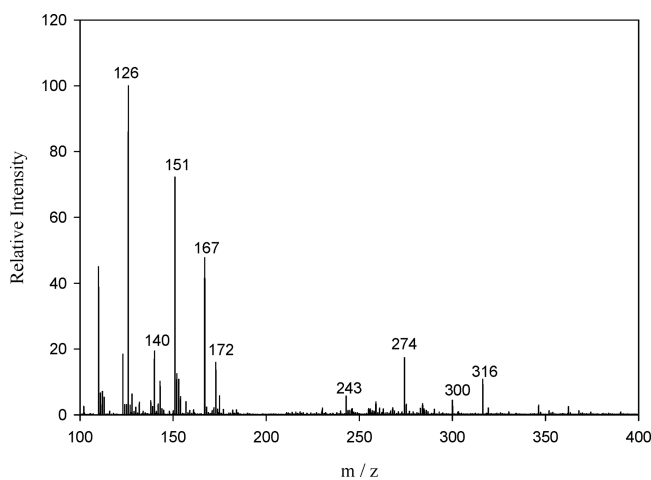


Figure 11. ESI-MS of leached aqueous solution of spent Fe-GAC.

A linear plot between $\ln k_{\text{app}}$ and $1/T$ shows a straight line (Figure 7). The activation energy was estimated from eq 4 and the value is given in Table 3. Higher MB degradation was achieved with increasing temperature as elevated temperatures enhanced the formation of $\bullet\text{OH}$ radicals in the Fe-GAC/H₂O₂ system.³⁴ Table 3 presents the thermodynamic properties (ΔG^\ddagger , ΔH^\ddagger , and ΔS^\ddagger) of MB oxidative degradation using

reactive adsorption which were determined using activation energy and apparent rate constant.³⁵

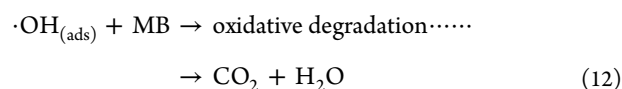
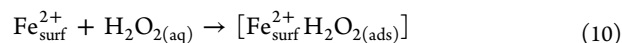
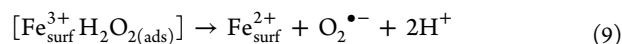
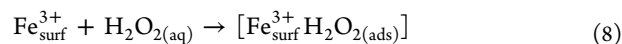
$$\Delta G^\ddagger = RT(23.76 + \ln T - \ln k_{\text{app}}) \quad (5)$$

$$\Delta H^\ddagger = E_a - RT \quad (6)$$

$$\Delta S^\ddagger = \frac{\Delta H^\ddagger - \Delta G^\ddagger}{T} \quad (7)$$

From Table 3, it can be seen that reactive adsorption of MB is not a temperature dependent process. However, an increase in temperature facilitates enhanced formation of $\bullet\text{OH}$ radicals that effectively degrade the dye. Similar results were reported for photodegradation of phenolics.³⁶

3.2.4. Reaction Mechanism. The Fe³⁺ or Fe²⁺ loading on carbon materials for oxidation have played a significant role in the removal of organic compounds.¹¹ Degradation of MB using the Fe-GAC/H₂O₂ system occurs through several parallel reactions. The presence of hydroxylated products ($m/z = 300, 316$ in Figure 8) shows that the reaction with Fe-GAC is initiated by the activation of H₂O₂ in the presence of Fe³⁺ to produce an $\bullet\text{OH}$ radical via a Haber–Weiss mechanism.²⁰ During the reaction, $\bullet\text{OH}$ radicals are produced through a reaction between H₂O₂ and Fe³⁺. The $\bullet\text{OH}$ radical serves as reactive species for MB molecule oxidation, and it contributes to regenerate the Fe surface to its original form through a number of reactions.^{20,21} The half-life of the hydroxyl radical is very short (10^{-9} s).³⁷ Therefore, degradation of the MB molecule takes place when it travels through the $\bullet\text{OH}$ radical that attached to the Fe-GAC active surface. A number of steps likely to represent the possible mechanism of MB oxidative degradation are shown in eqs 8–12:



The $\bullet\text{OH}$ radical has the ability to attack the aromatic ring of the organic substrate electrophilically. The generated hydroxyl radicals can diffuse to the external surface from the inner

Table 4. Related Adsorption Equilibrium Parameters for the Adsorption of MB on Fe-GAC at Different Temperatures

adsorption isotherms constants	temp (°C)				
	20	30	40	50	60
Langmuir Adsorption Isotherm					
q_m (mg·g ⁻¹)	90.91	100.00	111.11	125.00	142.86
K_L (L·mg ⁻¹)	0.08	0.12	0.17	0.21	0.25
R^2	0.991	0.999	0.994	0.998	0.995
R_L	0.56	0.46	0.37	0.32	0.29
Freundlich Adsorption Isotherm					
K_F (mg·g ⁻¹) (L·mg ⁻¹) ^{1/n}	12.13	18.34	24.48	30.36	37.79
$1/n$	0.49	0.43	0.41	0.38	0.36
R^2	0.974	0.968	0.903	0.915	0.881

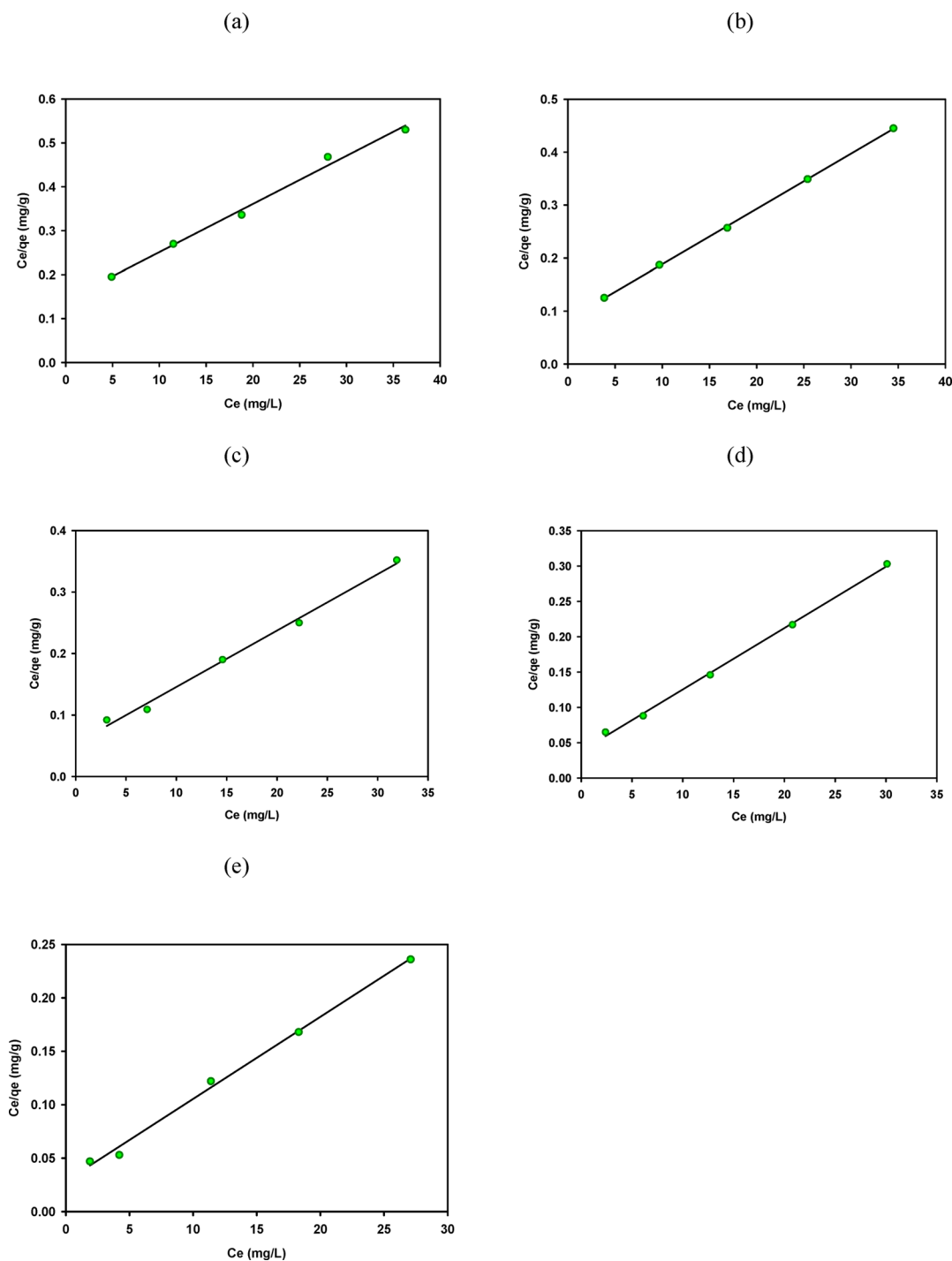


Figure 12. Langmuir isotherm plots at temperatures (a) 20 °C, (b) 30 °C, (c) 40 °C, (d) 50 °C, and (e) 60 °C (adsorption conditions: C_0 , 10–50 $\text{mg}\cdot\text{L}^{-1}$; dose of Fe-GAC, 0.2 $\text{g}\cdot\text{L}^{-1}$).

surface of the microporous material to break the large organic molecule into smaller fragments that can further diffuse into the microporous material.¹² Therefore, formation of deposits on the surface of the sorbent during reactive adsorption^{22,23} was further confirmed by desorption studies of spent Fe-GAC.

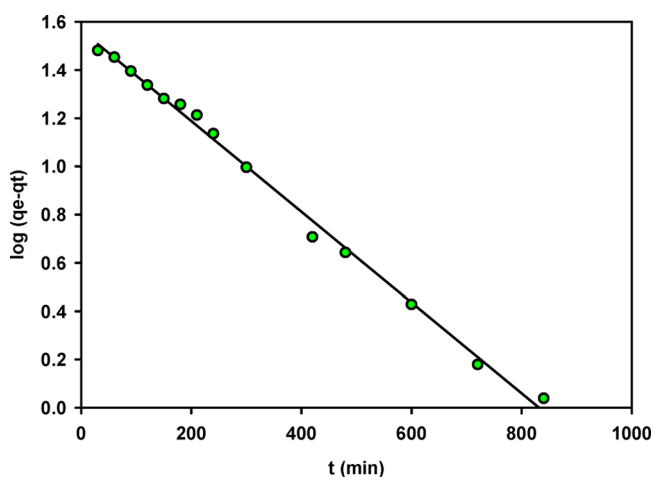
3.2.5. MB Oxidative Degradation Study Using ESI-MS. The results obtained from ESI-MS study suggest that use of Fe-GAC as reactive adsorbent catalyzes the generation of hydroxyl radicals from H_2O_2 decomposition and promotes oxidative degradation of MB. The analysis of an aqueous solution containing MB (Figure 8a–c) during the batch study of

reactive adsorption using ESI-MS showed oxidative degradation of MB in the solution due to an occurrence of chemical reactions on Fe-GAC surface. A degradation pathway for MB removal by reactive adsorption (Figure 9) with the formation of different intermediate products corresponding to their individual m/z values has been proposed.

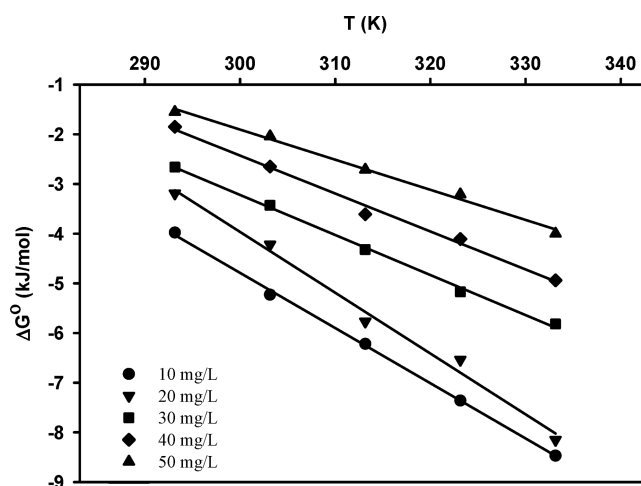
Initially at $t = 0$, single peak at $m/z = 284$ shown in Figure 8a indicates the presence of MB solely in the solution. Figure 10 shows UV–vis spectra of MB with one main band in the visible region.

Table 5. Kinetic Parameters for the Adsorption of MB onto the Fe-GAC at 30 °C

parameters	value
Pseudo-first-order Kinetic Model	
$q_{e, \text{exp}}$ ($\text{mg}\cdot\text{g}^{-1}$)	34.8
$q_{e, \text{calc}}$ ($\text{mg}\cdot\text{g}^{-1}$)	36.56
k_1 (min^{-1})	0.004
R^2	0.995
Pseudo-second-order Kinetic Model	
$q_{e, \text{calc}}$ ($\text{mg}\cdot\text{g}^{-1}$)	45.46
k_2 ($\text{g}\cdot\text{mg}^{-1}\cdot\text{min}$)	4.44×10^{-5}
R^2	0.841
Weber–Morris Intraparticle Diffusion	
k_{id} ($\text{mg}\cdot\text{g}^{-1}\cdot\text{min}^{-1/2}$)	1.0
C ($\text{mg}\cdot\text{g}^{-1}$)	-0.72
R^2	0.877

Figure 13. Pseudo-first-order kinetics (adsorption conditions: temp, 30 °C; C_0 , 10 $\text{mg}\cdot\text{L}^{-1}$; dose of Fe-GAC, 0.2 $\text{g}\cdot\text{L}^{-1}$).

ESI-MS analysis for MB degradation using Fe-GAC/ H_2O_2 system revealed that with the reaction period of 1 h, the intensity of signal at $m/z = 284$ decreased with the formation of intermediates (Figure 8b). It is reported that hydroxyl radicals facilitate demethylation of organic compounds.^{13,38,39} The shift of the absorption band, in the demethylation process, is a characteristic phenomenon.^{25,40} The absorbance peak due to formation of intermediate products of MB was shifted to 657 nm from 663 nm as the degradation time prolonged (Figure 10). Moreover, ESI-MS results obtained at 1 h of reaction period showed that the MB molecule degradation is initiated by demethylation. In reactive adsorption process, the generated $\bullet\text{OH}$ radicals may prefer to attack the alkyl branch of MB to destroy the molecule structure which is further degraded by the N-demethylation process. The ESI-MS spectrum showed

Figure 14. Plot of Gibbs free energy change, ΔG° versus temperature, T (adsorption conditions: temp, 20–60 °C; C_0 , 10–50 $\text{mg}\cdot\text{L}^{-1}$; dose of Fe-GAC, 0.2 $\text{g}\cdot\text{L}^{-1}$).

manifolds of peaks at $m/z = 270$ and 256 along with the parent peak $m/z = 284$, corresponding probably to the replacement of methyl groups with protons. These are likely due to fragmentation of the parent molecule, and the new peaks that emerged in the spectra are the well-known homologues of MB such as Azure B ($m/z = 270$) and Azure A ($m/z = 256$).^{41,42}

After 3 h (Figure 8c) of reaction, the signal corresponding to MB ($m/z = 284$) completely disappeared with the formation of different degradation products. MB absorbance peaks shifted to 652, 648, 639, and 637 nm as the reaction time proceeds (Figure 10). By observing shift in absorbance in the visible region of each MB spectra, it may be concluded that N-demethylation occurred throughout the reaction. Many peaks of different intensities were observed after 3 h in the mass spectra indicating that composition and concentration of the degradation products changes with time. Furthermore, new compounds found at $m/z = 300$, 316, and 354 were probably due to hydroxylation of the aromatic ring. These results indicated that the reactive degradation of the MB molecule was initiated by demethylation which was facilitated by the hydroxyl radicals, followed by hydroxylation. The inclusion of one, two, and six hydroxylation stages to the MB molecule, due to the addition of the $\bullet\text{OH}$ to the aromatic ring of MB, produces three signal fragments at $m/z = 300$, 316, and 354.^{3,43} Additionally, after 180 min of reaction, the formation of intermediates with $m/z = 224$, $m/z = 200$, $m/z = 194$, $m/z = 185$, $m/z = 183$, $m/z = 172$, and $m/z = 158$ occurred because of overoxidation of the hydroxylated intermediates.⁴⁴ Finally, the signal of $m/z = 142$ and $m/z = 140$ were indicative of the ring rupture.⁴⁵ Therefore, reactive adsorption of dye solutions

Table 6. Thermodynamic Parameters for Adsorption of MB onto Fe-GAC

dye concn ($\text{mg}\cdot\text{L}^{-1}$)	ΔG° ($\text{kJ}\cdot\text{mol}^{-1}$)					ΔH° ($\text{kJ}\cdot\text{mol}^{-1}$)	ΔS° ($\text{kJ}\cdot\text{mol}^{-1}\cdot\text{K}^{-1}$)	R^2
	20 °C	30 °C	40 °C	50 °C	60 °C			
10	-4.12	-5.23	-6.02	-6.90	-7.71	28.53	0.11	0.999
20	-3.30	-4.22	-5.58	-6.14	-7.42	32.75	0.12	0.991
30	-2.75	-3.43	-4.18	-4.85	-5.30	20.96	0.08	0.998
40	-1.91	-2.65	-3.49	-3.86	-4.50	20.49	0.07	0.993
50	-1.60	-2.04	-2.63	-3.01	-3.64	16.30	0.06	0.994

imparted their discoloration (Figure 10), and a significant degree of destruction of the dye molecule (Figure 8c).

Reactive adsorption of MB using Fe-GAC/H₂O₂ renders the aqueous solution almost colorless. After 3 h of operation, the color changed from bluish to light purple probably due to the presence of oxidative degradation products. The color removal efficiencies of Fe-GAC/H₂O₂ and Fe-GAC were observed to be 94% and 25% in 3 h at 30 °C. Figure 10 shows changes in absorption spectra when the aqueous solution of MB was degraded with the Fe-GAC/H₂O₂ for 180 min. The intensity of the maximum absorption peak at 663 nm decreased due to the degradation of MB. It has been postulated that MB removal occurred due to oxidative degradation. The MB spectra show the maximum absorption in the UV region at 291 nm due to the presence of polyatomic rings. It can be seen that almost complete mineralization of the polyaromatic rings occurred after 3 h of oxidative degradation of MB (see Figure 10).

According to reactive adsorption, one fragment of H₂O₂ gets attached to the adsorbate^{7,46} and results in a hydroxylated and demethylated product of MB. It has been already shown previously in the literature that there is the possible formation of some deposits on the surface of the adsorbent which occurs in the reactive adsorption process.^{22,23} In the present study, it was found that the degradation products of MB reactive adsorption are adsorbed on the reactive adsorbent surface, which was evident from the desorption study of the spent Fe-GAC carried out by using a boiling process in distilled water for 15 min. The leachate was subsequently analyzed using ESI-MS analysis. ESI-MS spectra indicated the presence of degradation products at *m/z* = 316, 300, 274, 243, 172, 167, 151, 140, and 126, etc. (see Figure 11). The structures of these compounds were given in Figure 9. Ania et al. (2011) studied the existence of degraded compounds adsorbed on an activated carbons surface after its exposure to antibiotics using thermal analysis.²⁴

MB retention on Fe-GAC seems to be taking place due to reactive adsorption only. ESI-MS analysis showed the absence of MB (*m/z* = 284) adsorption on the carbon surface (see Figure 11). MB reactive adsorption relies on the chemical nature of either the carbon or the target probe (MB), and may provoke incomplete irreversible transformations of the adsorbate.²⁴ The deposition of degradation products during the process of reactive adsorption was found in line with the results reported earlier in the literature.²³ MB solely was found on the Fe-GAC surface in the case of adsorption.

3.3. Batch Adsorption Studies. **3.3.1. Equilibrium.** Adsorption equilibrium is a dynamic equilibrium state where both adsorption and desorption rates are equal.⁴⁷ The experimental data were analyzed using Langmuir and Freundlich isotherms to describe the nature of the adsorption equilibrium.

Langmuir isotherm

$$\frac{C_e}{q_e} = \frac{1}{q_m K_L} + \frac{C_e}{q_m} \quad (13)$$

Freundlich isotherm

$$\ln(q_e) = \frac{1}{n} \ln(C_e) + \ln(K_F) \quad (14)$$

The essential characteristic (separation factor) of the Langmuir equation R_L , indicates the nature of the adsorption process. The characteristic parameters of the Langmuir and Freundlich isotherms models at different temperatures along with the R^2 values are listed in Table 4.

Figure 12 shows the Langmuir equilibrium isotherm of MB adsorption onto Fe-GAC. The applicability of the isotherm model was decided by comparing R^2 values (correlation coefficients). The results show that the Langmuir isotherm fits better than the Freundlich isotherm as R^2 is higher for the Langmuir isotherm. The monolayer capacity increased with increasing temperature due to the endothermic nature of adsorption, and it was further confirmed by the thermodynamic study. In the present study, R_L values were in the range of 0–1 which confirms that the Fe-GAC is found to be a suitable sorbent for MB dye adsorption under prescribed experimental conditions. The equilibrium study was not carried out for reactive adsorption, as the MB molecule degrades during the process. Therefore, there is no possibility that the MB equilibrium becomes established during reactive adsorption.

3.3.2. Kinetics. To investigate the adsorption kinetics of MB on Fe-GAC, pseudo-first-order, pseudo-second-order, and Weber–Morris intraparticle diffusion models were used. The results of the kinetic parameters are shown in Table 5.

It is reported that the pseudo-first-order model explains well the kinetics of the removal of the solute that is present in lower concentrations in solution and is represented as follows:³²

$$\log(q_e - q_t) = \log(q_e) - \frac{k_1 t}{2.303} \quad (15)$$

The pseudo-second-order kinetic model can be expressed as follows:⁴⁸

$$\frac{t}{q_t} = \frac{1}{k_2 q_e^2} + \frac{1}{q_e} t \quad (16)$$

The Weber–Morris intraparticle diffusion model is³²

$$q_t = k_{id} t^{1/2} + C \quad (17)$$

Figure 13 shows the pseudo-first-order kinetic model fits for MB adsorption onto the Fe-GAC. In the present work, a higher value of correlation coefficients for the pseudo-first-order compared to the second-order kinetic and intraparticle diffusion models (see Table 5) indicates that the experimental data of the MB adsorption onto the Fe-GAC adsorbent well followed the pseudo-first-order rate model. Rate constant values indicated that the removal efficiency of MB decreased significantly for adsorption ($k_1 = 0.004 \text{ min}^{-1}$, see Table 5) when compared with reactive adsorption ($k_{app} = 0.015 \text{ min}^{-1}$, see Table 2). Therefore, the MB removal rate constant was found almost four times for reactive adsorption than adsorption.

The Weber–Morris theory was employed to identify the rate controlling steps that occurred during the sorption process.⁴⁹ The intraparticle diffusion model accounted for the initial surface adsorption and subsequent intraparticle diffusion phenomena. The intercept of the linear plot suggests that the intraparticle diffusion is not the only rate-controlling step⁹ and the sorption process is rather complex and involves more than one diffusion resistance.⁵⁰ Therefore, it could be stated that surface adsorption was operated in parallel to the intraparticle diffusion during MB and Fe-GAC interactions.⁵¹

3.3.3. Thermodynamics. Table 6 shows thermodynamic parameters (ΔG° , ΔH° , ΔS°) for the adsorption process. Thermodynamic parameters, namely, Gibbs free energy change (ΔG°), enthalpy change (ΔH°) and entropy change (ΔS°) were calculated as per the following equations;^{52,53}

$$\Delta G^\circ = -RT \ln K_e \quad (18)$$

$$K_e = \frac{q_e}{C_e} \quad (19)$$

$$\Delta G^\circ = \Delta H^\circ - T\Delta S^\circ \quad (20)$$

The negative values of Gibbs free energy change (ΔG°) confirm the feasibility of the process and the spontaneous nature. Thermodynamic parameters estimated using the plot of ΔG° versus T for the sorption of MB onto Fe-GAC is shown in Figure 14. The positive value of ΔH° suggests the endothermic nature of MB adsorption onto Fe-GAC. The positive value of ΔS° reflects the affinity of the Fe-GAC for MB.⁵¹

Monolayer adsorption is the predominant mechanism for dye accumulation on the adsorbent surface. Kinetic and equilibrium isotherm parameters explain that the main contribution source of dye sorption on an adsorbent surface is an electrostatic force along with other pathways such as hydrogen bonding.⁵⁴ Thermodynamic data confirm that the interaction is through van der Waals forces as ΔH° values show physical adsorption.^{51,55,56} The binding of dye on to the adsorbent surface can be explained by the electrostatic interaction. The presence of akaganeite (β -FeOOH) may produce negative charge (OOH^-) on the surface of GAC that attracts cationic dye MB toward the adsorbent surface and gives high monolayer adsorption capacity.

On comparing enthalpy values of MB removal obtained for reactive adsorption (Table 3) with adsorption (Table 6), it can be found that the enthalpy value is almost one-third for MB removal using reactive adsorption. Hence, reactive adsorption for dye removal is an efficient method that completely removes the dye by degrading its molecule while consuming less energy. Reactive adsorption was found to be a more efficient method for dye removal than adsorption which may occur because reactive adsorption involves oxidative reaction of hydroxyl radicals and dye molecule.⁵⁷ As fast as a hydroxyl radical is formed, it reacts with a dye molecule as this radical has a very short half-life. Gupta et al. (2016) reported that the oxidative reaction took place on the external macropore surface only. The concentration of adsorbed organic moiety on the macroporous surface was degraded rapidly due to the generation of $\bullet\text{OH}$ radicals. These generated hydroxyl free radicals are highly reactive and give a high rate of the reaction. It was also reported that the overall resistance offered for dye sorption during reactive adsorption was much less as compared to pure adsorption. High pore diffusivity is the main force for rapid reactive sorption of MB into Fe-GAC.⁵

4. CONCLUSIONS

The synthesized reactive adsorbent (Fe-GAC) performed effectively with H_2O_2 for the degradation of MB in aqueous solution. Complete degradation of MB was attained after 3 h of oxidative reaction. MB removal was almost four times faster for reactive adsorption than adsorption. Reactive adsorption was found as an efficient method for MB removal as it consumes much less energy when compared with adsorption and it mineralizes the dye for safer release to the water bodies. The ESI-MS technique using (Fe-GAC/ H_2O_2) revealed that reactive degradation of the MB molecule was initiated by demethylation which was facilitated by hydroxyl radicals, followed by hydroxylation. Desorption studies of spent Fe-GAC further confirmed that the MB molecule was degraded using reactive adsorption. As a future research, it would be imperative to carry out detailed studies on separation schemes,

utilization, and production pathways for useful chemicals using degraded products of reactive adsorption. A scheme for the removal of MB using reactive adsorption has been proposed. The iron oxide loaded on GAC/ H_2O_2 may serve as an effective and promising system for the efficient removal and mineralization of organic compounds from wastewater.

■ ASSOCIATED CONTENT

Supporting Information

The Supporting Information is available free of charge on the ACS Publications website at DOI: 10.1021/acs.jced.7b00379.

Equilibrium data for adsorption of MB onto Fe-GAC (PDF)

■ AUTHOR INFORMATION

Corresponding Author

*Tel: +91 9414214146. E-mail: rkvyas2@gmail.com.

ORCID

Raj K. Vyas: 0000-0001-9330-1539

Ajay K. Dalai: 0000-0002-3083-2217

Notes

The authors declare no competing financial interest.

■ ACKNOWLEDGMENTS

The authors acknowledge Dr. K. S. Rama Rao, Indian Institute of Chemical Technology (IICT), Hyderabad, for BET surface area analysis of GAC and Fe-GAC. The authors also thank the Material Research Centre (MRC); Malaviya National Institute of Technology (MNIT), Jaipur, for the characterization of GAC and Fe-GAC using TEM coupled EDS and XRD. K.S. thanks Dr. Sumanta Kumar Meher, Department of Chemistry, MNIT, Jaipur, for the useful discussion for deriving the proposed scheme for the oxidative degradation of MB dye.

■ ABBREVIATIONS

k_{app}	apparent rate constant, min^{-1}
A	pre-exponential factor
E_a	activation energy of reaction, $\text{kJ}\cdot\text{mol}^{-1}$
ΔG^\ddagger	Gibbs energy of reactive adsorption, $\text{kJ}\cdot\text{mol}^{-1}$
ΔH^\ddagger	enthalpy of reactive adsorption, $\text{kJ}\cdot\text{mol}^{-1}$
ΔS^\ddagger	entropy of reactive adsorption, $\text{kJ}\cdot\text{mol}^{-1}\cdot\text{K}^{-1}$
C_0	initial concentration of dye in liquid-phase, $\text{mg}\cdot\text{L}^{-1}$
C_e	liquid-phase equilibrium concentration of dye, $\text{mg}\cdot\text{L}^{-1}$
q_e	solid phase equilibrium concentration, $\text{mg}\cdot\text{g}^{-1}$
C_t	liquid-phase concentration of dye at time t , $\text{mg}\cdot\text{L}^{-1}$
q_t	solid phase concentration at time t , $\text{mg}\cdot\text{g}^{-1}$
q_m	maximum amount of dye per unit weight of adsorbent for complete monolayer coverage, $\text{mg}\cdot\text{g}^{-1}$
K_L	equilibrium adsorption constant related to the affinity of binding sites, $\text{L}\cdot\text{mg}^{-1}$
K_F	adsorption capacity of the adsorbent, $(\text{mg}\cdot\text{g}^{-1}) (\text{L}\cdot\text{mg}^{-1})^{1/n}$
k_1	first order rate constant, min^{-1}
k_2	second order rate constant, $\text{g}\cdot\text{mg}^{-1}\cdot\text{min}$
k_{id}	intraparticle diffusion rate constant, $(\text{mg}\cdot\text{g}^{-1}\cdot\text{min}^{-1/2})$
C	constant
n	constant
R_L	separation factor
ΔG°	Gibbs energy of adsorption, $\text{kJ}\cdot\text{mol}^{-1}$
ΔH°	enthalpy of adsorption, $\text{kJ}\cdot\text{mol}^{-1}$
ΔS°	entropy of adsorption, $\text{kJ}\cdot\text{mol}^{-1}\cdot\text{K}^{-1}$

K_c adsorption equilibrium constant

REFERENCES

- (1) Asfaram, A.; Fathi, M. R.; Khodadoust, S.; Naraki, M. Removal of Direct Red 12B by garlic peel as a cheap adsorbent: Kinetics, thermodynamic and equilibrium isotherms study of removal. *Spectrochim. Acta, Part A* **2014**, *127*, 415–421.
- (2) Bagheri, A. R.; Ghaedi, M.; Asfaram, A.; Bazrafshan, A. A.; Jannesar, R. Comparative study on ultrasonic assisted adsorption of dyes from single system onto Fe₃O₄ magnetite nanoparticles loaded on activated carbon: Experimental design methodology. *Ultrason. Sonochem.* **2017**, *34*, 294–304.
- (3) Gupta, V. K.; Sharma, M.; Vyas, R. K. Hydrothermal modification and characterization of bentonite for reactive adsorption of methylene blue: An ESI-MS study. *J. Environ. Chem. Eng.* **2015**, *3*, 2172–2179.
- (4) Shukla, P.; Wang, S.; Sun, H.; Ang, H.; Tadé, M. Activated carbon supported cobalt catalysts for advanced oxidation of organic contaminants in aqueous solution. *Appl. Catal., B* **2010**, *100*, 529–534.
- (5) Gupta, V. K.; Sharma, M.; Singh, K.; Vyas, R. K. Reactive adsorption of phenol onto Fe-GAC: Parallel pore batch modeling and experimental studies. *J. Taiwan Inst. Chem. Eng.* **2016**, *63*, 116–124.
- (6) Sharma, K.; Dalai, A. K.; Vyas, R. K. Removal of synthetic dyes from multicomponent industrial wastewaters. *Rev. Chem. Eng.* **2018**, DOI: 10.1515/revce-2016-0042.
- (7) Nogueira, F. G. E.; Lopes, J. H.; Silva, A. C.; Gonçalves, M.; Anastácio, A. S.; Sapag, K.; Oliveira, L. C. A. Reactive adsorption of methylene blue on montmorillonite via an ESI-MS study. *Appl. Clay Sci.* **2009**, *43*, 190–195.
- (8) Rafatullah, M.; Sulaiman, O.; Hashim, R.; Ahmad, A. Adsorption of methylene blue on low-cost adsorbents: A review. *J. Hazard. Mater.* **2010**, *177*, 70–80.
- (9) Chang, J.; Ma, J.; Ma, Q.; Zhang, D.; Qiao, N.; Hu, M.; Ma, H. Adsorption of methylene blue onto Fe₃O₄/activated montmorillonite nanocomposite. *Appl. Clay Sci.* **2015**, *119*, 132–140.
- (10) Asfaram, A.; Ghaedi, M.; Azghandi, M. A.; Goudarzi, A.; Dastkhoon, M. Statistical experimental design, least squares-support vector machine (LS-SVM) and artificial neural network (ANN) methods for modeling the facilitated adsorption of methylene blue dye. *RSC Adv.* **2016**, *6*, 40502–40516.
- (11) Xu, J.; Gao, N.; Zhao, D.; Zhang, W.; Xu, Q.; Xiao, A. Efficient reduction of bromate in water by nano-iron hydroxide impregnated granular activated carbon (Fe-GAC). *Chem. Eng. J.* **2015**, *275*, 189–197.
- (12) Neamu, M.; Catrinescu, C.; Kettrup, A. Effect of dealumination of iron(III)—exchanged Y zeolites on oxidation of Reactive Yellow 84 azo dye in the presence of hydrogen peroxide. *Appl. Catal., B* **2004**, *51*, 149–157.
- (13) Chen, C. C.; Chen, W. C.; Chiou, M. R.; Chen, S. W.; Chen, Y. Y.; Fan, H. J. Degradation of crystal violet by an FeGAC/H₂O₂ process. *J. Hazard. Mater.* **2011**, *196*, 420–425.
- (14) Hajjaji, M.; El Arfaoui, H. Adsorption of methylene blue and zinc ions on raw and acid-activated bentonite from Morocco. *Appl. Clay Sci.* **2009**, *46*, 418–421.
- (15) Asfaram, A.; Ghaedi, M.; Hajati, S.; Rezaeinejad, M.; Goudarzi, A.; Purkait, M. K. Rapid removal of Auramine-O and Methylene blue by ZnS: Cu nanoparticles loaded on activated carbon: A response surface methodology approach. *J. Taiwan Inst. Chem. Eng.* **2015**, *53*, 80–91.
- (16) Agarwal, S.; Tyagi, I.; Gupta, V. K.; Bagheri, A. R.; Ghaedi, M.; Asfaram, A.; Hajati, S.; Bazrafshan, A. A. Rapid adsorption of ternary dye pollutants onto copper (I) oxide nanoparticle loaded on activated carbon: Experimental optimization via response surface methodology. *J. Environ. Chem. Eng.* **2016**, *4*, 1769–1779.
- (17) Anirudhan, T. S.; Ramachandran, M. Adsorptive removal of basic dyes from aqueous solutions by surfactant modified bentonite clay (organoclay): Kinetic and competitive adsorption isotherm. *Process Saf. Environ. Prot.* **2015**, *95*, 215–225.
- (18) Ghosh, D.; Bhattacharyya, K. G. Adsorption of methylene blue on kaolinite. *Appl. Clay Sci.* **2002**, *20*, 295–300.
- (19) Mazaheri, H.; Ghaedi, M.; Asfaram, A.; Hajati, S. Performance of CuS nanoparticle loaded on activated carbon in the adsorption of methylene blue and bromophenol blue dyes in binary aqueous solutions: Using ultrasound power and optimization by central composite design. *J. Mol. Liq.* **2016**, *219*, 667–676.
- (20) Pereira, M. C.; Cavalcante, L. C. D.; Magalhães, F.; Fabris, J. D.; Stucki, J. W.; Oliveira, L. C. A.; Murad, E. Composites prepared from natural iron oxides and sucrose: A highly reactive system for the oxidation of organic contaminants in water. *Chem. Eng. J.* **2011**, *166*, 962–969.
- (21) Pinto, I. S. X.; Pacheco, P. H. V. V.; Coelho, J. V.; Lorencon, E.; Ardisson, J. D.; Fabris, J. D.; de Souza, P. P.; Krambrock, K. W. H.; Oliveira, L. C. A.; Pereira, M. C. Nanostructured δ -FeOOH: An efficient Fenton-like catalyst for the oxidation of organics in water. *Appl. Catal., B* **2012**, *119–120*, 175–182.
- (22) Abecassis-Wolfovich, M.; Landau, M. V.; Brenner, A.; Herskowitz, M. Catalytic Wet Oxidation of Phenol with Mn–Ce-Based Oxide Catalysts: Impact of Reactive Adsorption on TOC Removal. *Ind. Eng. Chem. Res.* **2004**, *43*, 5089–5097.
- (23) Zazo, J. A.; Casas, J. A.; Mohedano, A. F.; Rodríguez, J. J. Catalytic wet peroxide oxidation of phenol with a Fe/active carbon catalyst. *Appl. Catal., B* **2006**, *65*, 261–268.
- (24) Ania, C.; Pelayo, J.; Bandosz, T. J. Reactive adsorption of penicillin on activated carbons. *Adsorption* **2011**, *17*, 421–429.
- (25) Rauf, M. A.; Meetani, M. A.; Khaleel, A.; Ahmed, A. Photocatalytic degradation of Methylene Blue using a mixed catalyst and product analysis by LC/MS. *Chem. Eng. J.* **2010**, *157*, 373–378.
- (26) Mondal, P.; Balomajumder, C.; Mohanty, B. A laboratory study for the treatment of arsenic, iron, and manganese bearing ground water using Fe³⁺ impregnated activated carbon: Effects of shaking time, pH and temperature. *J. Hazard. Mater.* **2007**, *144*, 420–426.
- (27) Mondal, P.; Majumder, C. B.; Mohanty, B. Effects of adsorbent dose, its particle size and initial arsenic concentration on the removal of arsenic, iron and manganese from simulated ground water by Fe³⁺ impregnated activated carbon. *J. Hazard. Mater.* **2008**, *150*, 695–702.
- (28) Hristovski, K. D.; Westerhoff, P. K.; Möller, T.; Sylvester, P. Effect of synthesis conditions on nano-iron (hydr)oxide impregnated granulated activated carbon. *Chem. Eng. J.* **2009**, *146*, 237–243.
- (29) Chang, Q.; Lin, W.; Ying, W. Preparation of iron-impregnated granular activated carbon for arsenic removal from drinking water. *J. Hazard. Mater.* **2010**, *184*, 515–522.
- (30) Gu, Z.; Fang, J.; Deng, B. Preparation and evaluation of GAC-based iron-containing adsorbents for arsenic removal. *Environ. Sci. Technol.* **2005**, *39*, 3833–3843.
- (31) Muñoz, G.; Fierro, V.; Celzard, A.; Furdin, G.; Gonzalez-Sánchez, G.; Ballinas, M. L. Synthesis, characterization and performance in arsenic removal of iron-doped activated carbons prepared by impregnation with Fe(III) and Fe(II). *J. Hazard. Mater.* **2009**, *165*, 893–902.
- (32) Bagheri, A. R.; Ghaedi, M.; Asfaram, A.; Hajati, S.; Ghaedi, A. M.; Bazrafshan, A.; Rahimi, M. R. Modeling and optimization of simultaneous removal of ternary dyes onto copper sulfide nanoparticles loaded on activated carbon using second-derivative spectrophotometry. *J. Taiwan Inst. Chem. Eng.* **2016**, *65*, 212–224.
- (33) Kasiri, M. B.; Aleboeyh, H.; Aleboeyh, A. Degradation of Acid Blue 74 using Fe-ZSM5 zeolite as a heterogeneous photo-Fenton catalyst. *Appl. Catal., B* **2008**, *84*, 9–15.
- (34) Lee, C.; Yoon, J. Temperature dependence of hydroxyl radical formation in the hv/Fe³⁺/H₂O₂ and Fe³⁺/H₂O₂ systems. *Chemosphere* **2004**, *56*, 923–934.
- (35) Lonhienne, T.; Gerday, C.; Feller, G. Psychrophilic enzymes: Revisiting the thermodynamic parameters of activation may explain local flexibility. *Biochim. Biophys. Acta, Protein Struct. Mol. Enzymol.* **2000**, *1543*, 1–10.
- (36) Naeem, K.; Weiqian, P.; Ouyang, F. Thermodynamic parameters of activation for photodegradation of phenolics. *Chem. Eng. J.* **2010**, *156*, 505–509.
- (37) Sies, H. Strategies of antioxidant defense. *Eur. J. Biochem.* **1993**, *215*, 213–219.

- (38) Behnajady, M. A.; Modirshahla, N.; Shokri, M.; Vahid, B. Effect of operational parameters on degradation of Malachite Green by ultrasonic irradiation. *Ultrason. Sonochem.* **2008**, *15*, 1009–1014.
- (39) Rajoriya, S.; Bargole, S.; Saharan, V. K. Degradation of a cationic dye (Rhodamine 6G) using hydrodynamic cavitation coupled with other oxidative agents: Reaction mechanism and pathway. *Ultrason. Sonochem.* **2017**, *34*, 183–194.
- (40) Wang, X.; Mei, L.; Xing, X.; Liao, L.; Lv, G.; Li, Z. Mechanism and process of methylene blue degradation by manganese oxides under microwave irradiation. *Appl. Catal., B* **2014**, *160–161*, 211–216.
- (41) Orendorz, A.; Ziegler, C.; Gnaser, H. Photocatalytic decomposition of methylene blue and 4-chlorophenol on nanocrystalline TiO₂ films under UV illumination: A ToF-SIMS study. *Appl. Surf. Sci.* **2008**, *255*, 1011–1014.
- (42) Yogi, C.; Kojima, K.; Wada, N.; Tokumoto, H.; Takai, T. Photocatalytic degradation of methylene blue by TiO₂ film and Au particles-TiO₂ composite film. *Thin Solid Films* **2008**, *516*, 5881–5884.
- (43) Oliveira, L. C. A.; Ramalho, T. C.; Goncalves, M.; Cereda, F.; Carvalho, K. T.; Nazzarro, M. S.; Sapag, K. Pure niobia as catalyst for the oxidation of organic contaminants: Mechanism study via ESI-MS and theoretical calculations. *Chem. Phys. Lett.* **2007**, *446*, 133–137.
- (44) Mesquita, A. M.; Guimarães, I. R.; Castro, G. M. M. d.; Goncalves, M. A.; Ramalho, T. C.; Guerreiro, M. C. Boron as a promoter in the goethite (α -FeOOH) phase: Organic compound degradation by Fenton reaction. *Appl. Catal., B* **2016**, *192*, 286–295.
- (45) de Souza, W. F.; Guimarães, I. R.; Oliveira, L. C. A.; Guerreiro, M. C.; Guarieiro, A. L. N.; Carvalho, K. T. G. Natural and H₂-reduced limonite for organic oxidation by a Fenton-like system: Mechanism study via ESI-MS and theoretical calculations. *J. Mol. Catal. A: Chem.* **2007**, *278*, 145–151.
- (46) *Compendium of Chemical Terminology (Gold Book)*, 2nd ed.; McNaught, A., Wilkinson, D. A., Eds.; IUPAC, 2017; <https://doi.org/10.1351/goldbook>.
- (47) Foo, K. Y.; Hameed, B. H. Insights into the modeling of adsorption isotherm systems. *Chem. Eng. J.* **2010**, *156*, 2–10.
- (48) Dil, E. A.; Ghaedi, M.; Asfaram, A. The performance of nanorods material as adsorbent for removal of azo dyes and heavy metal ions: Application of ultrasound wave, optimization and modeling. *Ultrason. Sonochem.* **2017**, *34*, 792–802.
- (49) McKay, G.; Otterburn, M. S.; Sweeney, A. G. The removal of colour from effluent using various adsorbents-III. Silica: Rate processes. *Water Res.* **1980**, *14*, 15–20.
- (50) Rodríguez, A.; García, J.; Ovejero, G.; Mestanza, M. Adsorption of anionic and cationic dyes on activated carbon from aqueous solutions: Equilibrium and kinetics. *J. Hazard. Mater.* **2009**, *172*, 1311–1320.
- (51) Bhattacharyya, K. G.; Sharma, A. Kinetics and thermodynamics of Methylene Blue adsorption on Neem (*Azadirachta indica*) leaf powder. *Dyes Pigm.* **2005**, *65*, 51–59.
- (52) Hong, S.; Wen, C.; He, J.; Gan, F.; Ho, Y. S. Adsorption thermodynamics of Methylene Blue onto bentonite. *J. Hazard. Mater.* **2009**, *167*, 630–633.
- (53) Karagoz, S.; Tay, T.; Ucar, S.; Erdem, M. Activated carbons from waste biomass by sulfuric acid activation and their use on methylene blue adsorption. *Bioresour. Technol.* **2008**, *99*, 6214–6222.
- (54) Ansari, F.; Ghaedi, M.; Taghdiri, M.; Asfaram, A. Application of ZnO nanorods loaded on activated carbon for ultrasonic assisted dyes removal: Experimental design and derivative spectrophotometry method. *Ultrason. Sonochem.* **2016**, *33*, 197–209.
- (55) Postai, D. L.; Demarchi, C. A.; Zanatta, F.; Melo, D. C. C.; Rodrigues, C. A. Adsorption of rhodamine B and methylene blue dyes using waste of seeds of *Aleurites Moluccana*, a low cost adsorbent. *Alexandria Eng. J.* **2016**, *55*, 1713–1723.
- (56) Dil, E. A.; Ghaedi, M.; Ghaedi, A.; Asfaram, A.; Jamshidi, M.; Purkait, M. K. Application of artificial neural network and response surface methodology for the removal of crystal violet by zinc oxide nanorods loaded on activate carbon: Kinetics and equilibrium study. *J. Taiwan Inst. Chem. Eng.* **2016**, *59*, 210–220.
- (57) Sharma, K. Removal of textile dyes from aqueous solution using reactive adsorption. Ph.D. Thesis, Malaviya National Institute of Technology, Jaipur. To be submitted. 2017.